UNIVERSITAT POLITÈCNICA DE VALÈNCIA

Universitat Politècnica de València

Doctoral Thesis

Doctoral Programme in Technologies for Health and Well-Being

Biomimetic injectable hydrogels of gelatin and hyaluronic acid for hepatic cell culture.

Julio Rodríguez Fernández

July, 2024. Valencia

Supervised by:

Prof. Gloria Gallego Ferrer

PhD. Laia Tolosa Pardo

Prof. Manuel Salmerón Sánchez

Siempre nos hemos definido por la capacidad de superar lo imposible. Y contamos estos momentos. Estos momentos cuando nos atrevemos a apuntar más alto, a romper barreras, a dar a conocer lo desconocido. Contamos estos momentos como nuestros logros más orgullosos. Pero perdimos todo eso. O tal vez nos hemos olvidado de que todavía somos pioneros. Y apenas hemos comenzado. Y que nuestros mayores logros no pueden quedar atrás, que nuestro destino está por encima de nosotros.

Interstellar.

Acknowledgments

¡Por fin! Quien le iba a decir a mi yo del pasado que acabaría donde estoy ahora. Un chico de 17 años que descubrió el mundo de la ingeniería de tejidos gracias a una operación de rodilla y que marcaría el rumbo de estos últimos años. Quiero creer que todo tiene su motivo y su razón de ser. Al igual que todas las personas que he tenido el placer de conocer durante este largo, duro y costoso pero gratificante proceso. Pensaba que el paso más duro sería escribir lo que es la tesis, pero estas palabras suponen una descarga emocional difícil de describir.

Para mí esta tesis, a pesar de que sobre el papel han sido 3 años y medio, llevo en lo que considero mis casas ya casi 6 años. Este proceso empezó hace un poco más de 5 años con mi trabajo fin de grado y no quiero olvidarme de agradecer y reconocer a todas las personas que me han acompañado desde entonces.

Primero agradecer a quienes me brindaron la primera oportunidad que ha durado hasta hoy. Gracias **Gloria** y **Laia**, ha sido un camino que hemos compartido desde hace ya 5 años y no podré agradecer lo suficiente. **Gloria**, gracias por tu dedicación conmigo, por elegir a un chico con más motivación que currículum, por guiarle en el mundo de los biomateriales y contar con él para los problemas informáticos. Ha sido un verdadero placer ser dirigido por una Catedrática de tu nivel, lo pongo en mayúsculas porque lo merece. **Laia**, tengo que reconocer que al principio no pensaba ser capaz de mantener unas células vivas, pero conseguiste que un ingeniero fuese capaz de ello. Gracias por tu paciencia y trato cercano, por enseñarme que las células hay que pasarlas con medio limpio y sobre todo creer en mí. A pesar de que tengas dos hijas y no quieras más hijos, me has cuidado como al que más. En definitiva, gracias por crear el entorno perfecto para crecer tanto en mi faceta investigadora como humana. También agradecer a **Manolo** por su guía científica durante estos años y confiar en mí para este proyecto. Casi acabo haciendo la tesis en Glasgow, pero tocaba esta vez en Valencia.

Continuar por el que he considerado mi hogar durante 5 años, el **CBIT**. Me atrevería a decir que aquí he conocido a personas que me han marcado para siempre. La primera persona la cual creo que tiene mención especial por aguantarme, aconsejarme, ayudarme y sobre todo quererme con todo lo que

eso conlleva eres tú, **Estela**. Aún recuerdo aquella época en la que no nos conocíamos, pero sabíamos quiénes éramos "esa persona que trabaja por la mañana y hace hidrogeles". Quizá no he sido una persona fácil de tratar según qué momentos, soy terco, orgulloso y me cuesta dar abrazos. Gracias por asustarte siempre, por hacerme las cejas y pintarme un eyeliner azul que luego no había dios quien lo limpiase. Pero eso no quita el cariño que te tengo y te guardaré. Albacete siempre estará conmigo (aunque para mí fuese un pueblo sin El Corte Inglés). **Ana,** mi querida primita. Has estado desde el primer momento de este camino, hemos compartido momentos pasando de estar en el zulo a tener nuestro propio despacho. Nos hemos comido olas de calor en Víver, sorpresas y salseo en Pamplona, cantar por las calles de Castellón con una charanga, escuchar un "Primito, quítame el brazo que me pesas" en Pedralba y un largo etcétera de momentos que atesoraré. **Jose**, mi compañero de cabezazos, memes y risas. Ya lo dije en su momento, quién nos iba a decir que ambos estaríamos en el camino de ser doctores. Las calles de Pamplona siempre agradecerán una limpieza con pasta de dientes, una pena que no vieran ese kit de costura tan mono. Ha sido un placer compartir laboratorio contigo, esos "buenos días" no los cambio por nada y los echo de menos. Una pena que ahora que acaba mi etapa, vuelvas sin yo estar. William siempre estará con nosotros. **María**, por fin Julito se hace mayor. Sin duda todo lo pueda decir de ti son cosas bonitas, no cambies nunca la gente es muy afortunada de tenerte. Creo que las palabras que más te he podido repetir son "Por favor" y "Gracias", has sido un apoyo fundamental durante estos años. Siempre he dicho que eres una gran científica (aunque hayas cambiado de faceta) y he disfrutado mucho tu lado más investigador y sobre todo la creación de cuentas de Twitter aleatorias. ¡Primitos, os quiero mucho!

No me voy a olvidar del terremoto de energía y piparras, **Arantxa.** Llegaste a punto para el último año de mi tesis, pero qué año. Voy a echar de menos tus "dime mi siela" y buscarte a las 11:00 y 14:00 para almorzar y comer, pero claro yo sin decir una palabra, un gesto de cabeza era suficiente para que nos entendieses a mí y mi puntual estómago. Ahora le toca a mi querida compañera de despacho **Irene**, gracias por esa autenticidad. Admiro la fuerza de voluntad y resiliencia que has tenido durante este tiempo, si hay alguien que merece terminar la tesis y con buen pie eres tú más que nadie. Ya no voy a tener a quien robarle chicles y quien se meta conmigo en los almuerzos. Ay, **Paco** si pensabas que te librabas de los agradecimientos estabas equivocado. Si hubiera un departamento de recursos humanos…creo que ya sabes el resto. Gracias por compartir este sentido de humor que dudo nos lleve al cielo después de todo. **Sandra F**, siento comunicar que gofrito ya no come más gofres, es triste lo sé, pero todo ha sido para bien. Me alegro de haber compartido

laboratorio contigo, no desistas con este proceso, todo pasa y todo termina. **Inma**, parece que los ingenieros biomédicos si podemos ser importantes en la investigación y sabemos más de lo que piensa mucha gente. No pierdas el inconformismo que te caracteriza y ese punto de revolución. Gracias por estar siempre. **Nadia**, quien iba a decir que las tazas podían llenarse de agua por dos partes eh... Gracias por poner siempre las risas, el buen rollo y ser tan auténtica. Espero en el futuro trabajar contigo, de corazón.

Por último, al resto de compañeros y excompañeros del CBIT. **Sandra C, Ximo, Pachi, Sandra I, Laura T, Sofía y Teresa.** Gracias por todo. Y mención especial a las dos últimas personas de la lista por dejarme dirigir sus TFG y TFM, respectivamente. Ha sido un verdadero placer compartir esta experiencia con vosotras.

Claro, no puedo dejarme a mis compañeros de **Hepatología experimental** del **IISLAFE**. Sin duda habéis hecho que tener experimentos allí se hiciera ameno. Primero de todo **Estela V y Quique**, sois unos compañeros de laboratorio geniales y trabajar con vosotros ha sido un verdadero placer. No creo que sea **capaz de olvidar tan cultivado y barroco lenguaje que tantas risas nos ha sacado** o los almuerzos en la escalera. ¡Los siguientes sois vosotros, ánimo! Mis queridas **Nuri y Anabel**, creo que sin vosotras no sería la mitad de científico que soy. Gracias por siempre estar cuando he necesitado de vuestra ayuda, el laboratorio os necesita tanto o más que a los estudiantes. Os voy a echar mucho de menos, los "xiquet" de Anabel y los "Dime cari" de Nuri. Por último, **Patri**, llegaste la última y aun así no veas lo que voy a echar de menos a Belce, ser el punching ball de este laboratorio ha sido algo nuestro, pero "tristemente" te cedo el puesto a jornada completa.

Por supuesto a mi familia crossfit, quien nos iba a decir que personas tan diferentes podían llegar a formar un grupo tan genial. **Ana** y **Alejandro**, os lo dije en su momento, pero sois la perfecta definición de amor, gracias por estar siempre para Julsito. Ñeh. **Irene**, siempre serás la pelirroja del grupo, el pegamento que no deja que nadie se quede colgado y que Jaén es bonito cuando tú estás. Eres auténtica. **Daniel**, por más fiestas de primavera, pasitos prohibidos y "wi wi". Pensar que de pequeños teníamos los pueblos al lado, pero ha sido en Valencia donde nos hemos hecho grandes sosios. No cambies. **Neus** y **Rubén**, bueno claro y vuestro hijo perruno Rodri. ¿Qué bonito es ver que uno se levanta a las 5 de la mañana a trabajar y otras a las 10 no? Cuando necesitamos alegría, vosotros sabéis como darnos ese toque de diversión. Gracias por tantas resacas y buenos momentos. **Genki,** todo queda entre

barras, snatch y clean verdad? Gracias por empujarme a darle amor a la barra y ser la persona que mejor baila bachata en el grupo.

Jorge, Noelia, Guzmán y Miguel, lo que Cheste ha unido jamás lo separa nada. Después de casi ya 13 años seguimos unidos, quizá nos vemos poco para lo que nos queremos, pero nada cambia. Gracias a todos por haber estado en una etapa muy complicada para mí y sobre todo saber apreciarme como persona a pesar de todo. Ahora quería aprovechar para dar las gracias a otra persona que también formaba parte de este querido grupo, pero por desgracia ya no está con nosotros y quería agradecer en particular su gran corazón. **Damián**, allá donde estés amigo, por fin lo he conseguido. Espero que estés orgulloso de mi, no olvidaré todo lo que hemos compartido. ¡Siempre fuertes!

¿Parece que estos agradecimientos se están alargando no? Eso significa que he sido afortunado de tener a muchas personas importantes a lo largo de este camino. Pero me falta quienes han estado desde el principio de todo, mi familia. **Mamá,** ya está, tu niño se hace doctor. Creo que ahora entiendo aquello que dicen que el amor de una madre es el primero, el que es para siempre y el más sincero. Gracias por ser y estar. Solo nosotros sabemos lo que hemos pasado hasta llegar aquí y más estos tres últimos años. Nunca podré agradecerte por todo lo que has hecho para educar y hacer crecer a este niño. Y a mi querida hermana **Eri**, siempre has sido un espejo en donde mirarme, una persona inteligente, buena, dedicada y trabajadora. Desde pequeño mi ilusión era que estuvieras orgulloso de tu tete, que el día de mañana pudieras alardear de lo bueno que es tu hermanito. Espero haber cumplido con creces.

Por último, pero no menos importante. **Aurora,** llegaste al final de esta etapa y yo sin querer complicarme, pero que bonita complicación. Como he dicho al principio de los agradecimientos, las cosas tienen su motivo y razón. Tenía que ser en ese momento y desde entonces me has hecho sentirme muy afortunado, a pesar de que ya no vivieses en Beicon. Lo que nos separa ahora mismo será lo que nos una en el futuro. ¿Esto al final va a durar 83 años no? ¡Te quiero!

En definitiva. **¡Gracias a todos!**

This work has been supported by the Institute of Health Carlos III (Plan Estatal de I+D+i 2013-2016) and co-financed by the European Regional Development Fund "A way to achieve Europe" (FEDER) through grants PI18/00993, PI21/00223 and CP16/00097; by the Spanish Ministry of Science and Innovation MCIN/AEI/10.13039/501100011033 through the PID2019-106000RB-C21 and PID2019-106000RB-C22 Grants and by the Generalitat Valenciana (PROMETEO/2019/060). Laia Tolosa was supported by ISCIII CP16/00097 and MV21/00044. Manuel Salmerón Sánchez was supported by an EPSRC Programme Grant (EP/P001114/1).

In addition, thanks for the technical support received from the Cytomics Unit, Analytical Unit and Animal Facilities from the Instituto de Investigación Sanitaria La Fe, and the Microscopy Service of the Universitat Politècnica de València.

Index

List of figures

List of tables

List of equations

Abstract

Liver tissue engineering offers an advantageous toxicological screening and disease-modelling tool and could also provide an alternative therapy to liver transplantation to treat end-stage liver diseases. Several cell-based models have been proposed to study liver physiology and disease development. The classical *in vitro* systems rely on monolayer cultures of primary human hepatocytes or hepatoma cell lines, although the use of more complex systems that also consider the three-dimensional organization has been encouraged in the last years. The main objective of this PhD Thesis is to develop a three-dimensional hepatic system that recapitulates the three-dimensional organization of the liver using hydrogels and scaffolds based on liver's extracellular matrix composition, and their application for the study and treatment of liver diseases.

To this purpose, we first optimized the composition using gelatin-hyaluronic acid hydrogels, looking for the mechanical properties closer to the human liver. In order to determine the suitability of the developed hydrogels for hepatic cell culture, *in situ* crosslinking of HepG2 cells, a hepatoma cell line widely used in Hepatology, was used and both viability and functionality of the cells were analyzed. Mechanical characterization of hydrogels and the evaluation of HepG2 cells functionality, led us to select the 20-80 gelatin-hyaluronic acid composition as the optimal for hepatic cell culture.

Secondly, gelatin-hyaluronic acid scaffolds with interconnected porosity were prepared and used for the culture of primary human hepatocytes and the evaluation of key hepatic functions. Primary human hepatocytes cultured in gelatin-hyaluronic acid scaffolds exhibited increased albumin and urea secretion and metabolic capacity (cytochrome P450 and UDP-glucuronosyltransferase activity levels) compared to standard monolayer cultures. The transplant of the scaffold containing human hepatocytes led to an improvement in liver function (transaminase levels, necrosis) and ameliorated damage in a mouse model of acetaminophen-induced liver failure. Additionally, the *in vivo* study also provided a mechanistic understanding of acetaminophen-induced liver injury and the impact of transplantation by analyzing cytokine production and oxidative stress induction to find suitable biomarkers of cell therapy’s effectiveness.

Finally, in the last part of this doctoral thesis we have explored the use of bioprinting as a method for increasing the throughput of the test systems that best mimic the environment and complexity of liver tissue. To transform the

developed hydrogels into bioinks, the molecular weight of hyaluronic acid was increased. Then, the suitability of hybrid gelatin and hyaluronic acid as bioinks was studied by determining viscosity, uniformity, and pore factor. Bioprinting of HepG2 cells demonstrated the fitness of the selected bioinks for culturing hepatic cells and improving their performance, suggesting the suitability for automatising and scaling-up hydrogel's manufacturing.

Resumen

La ingeniería tisular hepática ofrece una herramienta propicia de cribado toxicológico y modelización de enfermedades, que también podría proporcionar una terapia alternativa al trasplante de hígado para tratar enfermedades hepáticas en fase terminal. Se han propuesto varios modelos celulares para estudiar la fisiología hepática y el desarrollo de enfermedades. Los sistemas *in vitro* clásicos se basan en cultivos en monocapa de hepatocitos humanos primarios o líneas celulares de hepatoma, aunque en los últimos años se ha fomentado el uso de sistemas más complejos que también tienen en cuenta la organización tridimensional. El objetivo principal de esta Tesis Doctoral es desarrollar un sistema hepático tridimensional que recapitule la organización tridimensional del hígado utilizando hidrogeles y constructos porosos basados en la matriz extracelular hepática, y su aplicación para el estudio y tratamiento de enfermedades hepáticas.

Para ello, primero optimizamos la composición utilizando hidrogeles de gelatina y ácido hialurónico, buscando las propiedades mecánicas más parecidas a las del hígado humano. Para determinar la idoneidad de los hidrogeles desarrollados para el cultivo de células hepáticas, se utilizó la reticulación *in situ* de células HepG2, una línea celular de hepatoma ampliamente utilizada en Hepatología, y se analizó tanto la viabilidad como la funcionalidad de las células. La caracterización mecánica de los hidrogeles y la evaluación de la funcionalidad de las células HepG2, nos llevaron a seleccionar la composición 20-80 gelatina-ácido hialurónico como la óptima para el cultivo de células hepáticas.

En segundo lugar, se prepararon constructos porosos de gelatina-ácido hialurónico con porosidad interconectada y se utilizaron para el cultivo de hepatocitos humanos primarios y la evaluación de las funciones hepáticas clave. Los hepatocitos humanos primarios cultivados en constructos porosos de gelatina-ácido hialurónico mostraron una mayor secreción de albúmina y urea, y una mayor capacidad metabólica (niveles de actividad citocromo P450 y UDP-glucuronosiltransferasa) en comparación con los cultivos en monocapa estándar. El trasplante del constructo poroso con hepatocitos humanos produjo una mejora de la función hepática (niveles de transaminasas, necrosis) y mejoró el daño en un modelo de ratón de insuficiencia hepática inducida por acetaminofeno. Además, el estudio *in vivo* también proporcionó una comprensión mecanicista de la lesión hepática inducida por acetaminofeno y el impacto del trasplante mediante el análisis de la producción de citoquinas y la inducción de estrés oxidativo para encontrar biomarcadores adecuados de la eficacia de la terapia celular.

Finalmente, en la última parte de esta tesis doctoral hemos explorado el uso de la bioimpresión como método para aumentar el rendimiento de los sistemas de ensayo que mejor imitan el entorno y la complejidad del tejido hepático. Para transformar los hidrogeles desarrollados en biotintas, se aumentó el peso molecular del ácido hialurónico. A continuación, se estudió la idoneidad de biotintas híbridas de gelatina y ácido hialurónico mediante la determinación de la viscosidad, la uniformidad y el factor de poros. La bioimpresión de células HepG2 demostró la idoneidad de las biotintas seleccionadas para el cultivo de células hepáticas y la mejora de su producción, lo que sugiere la conveniencia de automatizar y escalar la fabricación de hidrogeles.

Resum

L'enginyeria tissular hepàtica ofereix una ferramenta propícia de cribratge toxicològic i modelització de malalties, que també podria proporcionar una teràpia alternativa al trasplantament de fetge per a tractar malalties hepàtiques en fase terminal. S'han proposat diversos models cel·lulars per a estudiar la fisiologia hepàtica i el desenvolupament de malalties. Els sistemes *in vitro* clàssics es basen en cultius en monocapa d'hepatòcits humans primaris o línies cel·lulars d'hepatoma, encara que en els últims anys s'ha fomentat l'ús de sistemes més complexos que també tenen en compte l'organització tridimensional. L'objectiu principal d'esta Tesi Doctoral és desenvolupar un sistema hepàtic tridimensional que recapitula l'organització tridimensional del fetge utilitzant hidrogels i suports porosos basats en la matriu extracel·lular hepàtica, i la seua aplicació per a l'estudi i tractament de malalties hepàtiques.

Per a això, primer vam optimitzar la composició utilitzant hidrogels de gelatina i àcid hialurònic, buscant les propietats mecàniques més semblants a les del fetge humà. Per a determinar la idoneïtat dels hidrogels desenvolupats per al cultiu de cèl·lules hepàtiques, es va utilitzar la reticulació in situ de cèl·lules HepG2, una línia cel·lular de hepatoma àmpliament utilitzada en Hepatologia, i es va analitzar tant la viabilitat com la funcionalitat de les cèl·lules. La caracterització mecànica dels hidrogels i l'avaluació de la funcionalitat de les cèl·lules HepG2, ens van portar a seleccionar la composició 20-80 gelatina-àcid hialurònic com l'òptima per al cultiu de cèl·lules hepàtiques.

En segon lloc, es van preparar suports porosos de gelatina-àcid hialurònic amb porositat interconnectada i es van utilitzar per al cultiu d'hepatòcits humans primaris i l'avaluació de les funcions hepàtiques clau. Els hepatòcits humans primaris cultivats en suports porosos de gelatina-àcid hialurònic van mostrar una major secreció d'albúmina i urea, i una major capacitat metabòlica (nivells d'activitat citocrom P450 i UDP-glucuronosiltransferasa) en comparació amb els cultius en monocapa estàndard. El trasplantament del suport porós amb hepatòcits humans va produir una millora de la funció hepàtica (nivells de transaminases, necrosis) i va millorar el mal en un model de ratolí d'insuficiència hepàtica induïda per acetaminofèn. A més, l'estudi *in vivo* també va proporcionar una comprensió mecanicista de la lesió hepàtica induïda per acetaminofèn i l'impacte del trasplantament mitjançant l'anàlisi de la producció de citocines i la inducció d'estrès oxidatiu per a trobar biomarcadors adequats de l'eficàcia de la teràpia cel·lular.

Finalment, en l'última part d'esta tesi doctoral hem explorat l'ús de la bioimpresió com a mètode per a augmentar el rendiment dels sistemes d'assaig que millor

imiten l'entorn i la complexitat del teixit hepàtic. Per a transformar els hidrogels desenvolupats en biotintes, es va augmentar el pes molecular de l'àcid hialurònic. A continuació, es va estudiar la idoneïtat de biotintes híbrides de gelatina híbrida i l'àcid hialurònic mitjançant la determinació de la viscositat, la uniformitat i el factor de porus. La bioimpresió de cèl·lules HepG2 va demostrar la idoneïtat de les biotintes seleccionades per al cultiu de cèl·lules hepàtiques i la millora de la seua producció, la qual cosa suggereix la conveniència d'automatitzar i escalar la fabricació d'hidrogels.

Glossary

2D: Two-dimensional

3D: Three-dimensional

AFP: Alfa-fetoprotein

ALF: Acute liver failure

Alg: Alginate

ALT: Alanine aminotransferase

APAP: Acetaminophen

AST: Aspartate aminotransferase

ATR-FTIR: Attenuated total reflectance - Fourier Transformed Infrared

BSA: Bovine serum albumin

CXCL-1: Chemokine ligand 1

CYP: Cytochrome P450

dECM: decellularized Extracellular matrix

DILI: Drug-induced liver injury

DLP: Digital light processing

dPBS: Dulbecco's phosphate buffered saline

EBB: Extrusion-based bioprinting

ECM: Extracellular matrix

EDC: N-(3-Dimethylaminopropyl)-N'-ethylcarbodiimide

EDTA: Ethylenediaminetetraacetic acid

ELISA: Enzyme-linked-immunosorbent assay

EMD: Electro-magnetic droplet

GAG: Glycosaminoglycan

Gel: Gelatin

GelMA: Gelatin Methacryloyl

GSH: Glutathione

HA: Hyaluronic acid

HCC: Hepatocellular carcinoma

HLC: Hepatocyte-like cells

HPLC/MS: High-performance liquid chromatography/mass spectrometry

HRP: Horseradish peroxidase

HSC: Hepatic stellate cells

HUVEC: Human umbilical vein endotelial cells

H_2O_2: Hydrogen Peroxide

ICO: Intrahepatic cholangiocyte organoid

IF-γ: Interferon gamma

IL-6: Interleukin-6

iPSC: induced pluripotent stem cells

KC: Kupffer cells

LSEC: Liver sinusoidal endothelial cells

MASLD: Metabolic associated steatotic liver disease

MES: 2-(N-morpholino) ethanesulfonic acid

MMP: Metalloproteinase

MSC: Mesenchymal stem cells

MWCO: Molecular weight cut off

NEM: N-ethylmaleimide

NHS: N-Hydroxysuccinimide

OA: Ophthalmic acid

PEG: Polyethylene glycol

PF: Pore factor

PHH: Primary human hepatocyte

PI: Propidium iodide

SCID: Severe combined immunodeficient

SLA: Stereolitography

TNF-α: Tumour necrosis factor alpha

U: Uniformity

UGT: UDP-glucuronosyltransferase

ULPC-MS/MS: Ultra-performance liquid chromatography – mass spectrometry

UV: Ultraviolet

VP: Volumetric (bio)printing

State of the art

1. Liver structure and functionality

The liver is the major internal organ in the human body and plays a key role in more than 500 different functions that include protein synthesis (i.e., albumin, transferrin), metabolism of carbohydrates, proteins and lipids and detoxification of endogenous and foreign compounds. These functions can be altered by different disorders such as congenital metabolic diseases, viral infections, metabolic associated steatotic liver disease (MASLD, formerly known as non-alcoholic fatty liver disease) or hepatocellular carcinoma (HCC).

The liver presents a uniform anatomical structure (Gebhardt et al., 2014). The structural unit of the liver is the hepatic lobule, which is hexagonal and consists of hepatocyte plates that radiate from the central vein located in the center of the hexagon following a honeycomb-like pattern (Godoy et al., 2013). The portal triad is composed by a vein, an artery, and a bile duct, and it is located at each vertex of the hexagon (Figure 1) (Godoy et al., 2013).The blood rich in oxygen and different soluble factors enters through the portal vein and hepatic artery and runs concentrically toward the center of the lobule, whereas the bile flows outward from the center to the bile duct located in the vertex of the lobule (Gebhardt et al., 2014). The areas surrounding the central vein are known as pericentral, whereas the ones close to the portal triad are called periportal. Thus, there is a dynamic and functional diversity known as liver zonation that allows performing multiple functions in parallel (Gebhardt et al., 2014; Panday et al., 2022). Liver zonation has been also implicated in the initiation and progression of liver disease (Panday et al., 2022). For this reason, some new cell-based models have also tried to simulate liver zonation for instance modulating oxygen tension (Panday et al., 2022).

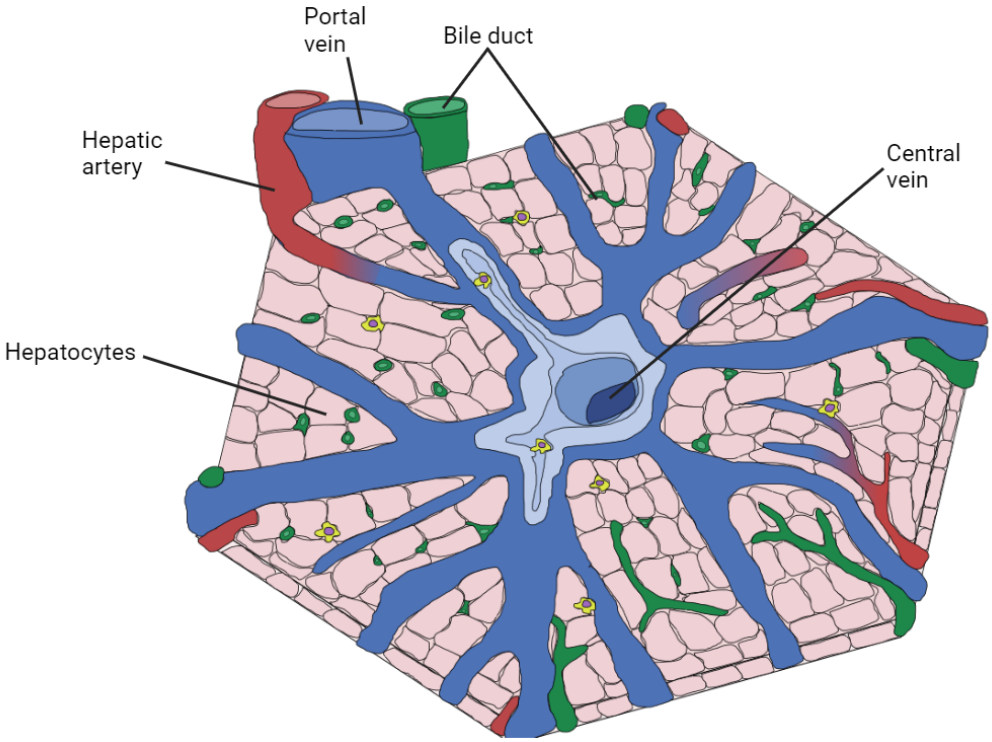

Figure 1. Representation of the liver structural unit, the hepatic lobule. *The hepatic artery, portal vein, and bile duct comprise the portal triad, with the hepatocytes arranged in a cordon that connects them to the central vein. Adapted from (Lemos et al., 2019)*

1.1. Liver cells

The liver is formed by several cell types with different embryological origins that display unique functions (Trefts et al., 2017). Hepatocytes are the major cell type in the liver and perform most of the secretory and metabolic functions of the liver. Cholangiocytes are epithelial cells that line the bile duct. Non-parenchymal cells include Kupffer cells that are liver resident macrophages, hepatic stellate cells, and liver sinusoidal endothelial cells (Trefts et al., 2017). Figure 2 exemplifies the distribution of the different cell types in the hepatic lobule.

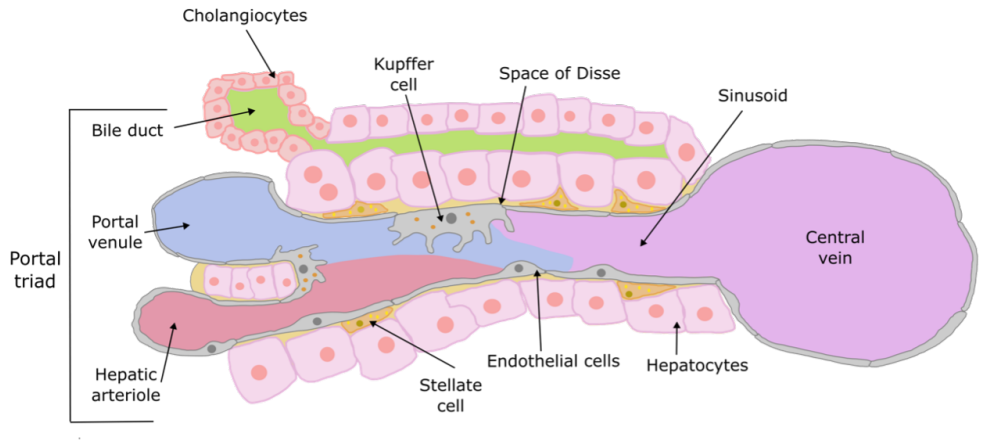

Figure 2. Schematic overview of the distribution of cells in the hepatic cord. *Numerous sinusoids, which are discontinuous vessels made of specialized fenestrated endothelial cells, are seen within each lobule. Between the sinusoids and the hepatocyte cords lies the space of Disse, which is home to stellate cells. The liver's specialized macrophages, known as Kupffer cells, are also located within the sinusoids. Bile salts are secreted into the bile canaliculi, which connect to the bile duct, by hepatocytes. The epithelial cells that line the bile ducts are called cholangiocytes. Image created with Inkscape.*

Hepatocytes account for approximately 80% of the total cell volume mass. They are responsible for most of the liver functions. Hepatocytes express the greater part of circulating plasma proteins like albumin, transporters, blood clotting factors and immune modulators. They synthesize different proteins such as albumin that is implicated in the maintenance of the transport of different molecules in the blood. They are also implicated in the metabolism of ammonia and endogenous and exogenous substances and manage the homeostasis of bile acids, cholesterol, triglycerides, and glucose/glycogen (Godoy et al., 2013). They are polygonal epithelial cells that possess apical (canalicular) and basolateral (sinusoidal) domains (Schulze et al., 2019). This polarity and the fact that simultaneously receive venous and arterial blood permits to combine the main functions in the liver: production of plasma proteins and endocytic uptake of lipids and other substances, which also makes them susceptible to damage induced by drugs or other toxins (Schulze et al., 2019). Functional zonation of hepatocytes has been deeply studied and it is mostly endorsed to oxygen gradients and WNT signaling (Ramachandran et al., 2020). Functions that are energetically demanding (i.e. gluconeogenesis) are performed by periportal hepatocytes, while pericentral hepatocytes are more implicated in drug metabolism and glycolysis that require less energy (Aizarani et al., 2019).

Cholangiocytes, also known as biliary epithelial cells, account for approximately 3% of the liver mass. They modify the bile composition produced by the hepatocytes and participate in the detoxification of foreign compounds (Dianat et al., 2014). As hepatocytes, cholangiocytes are polarized with basolateral and apical membranes that express different receptors and channels (Salas-Silva et al., 2021). Additionally, cholangiocytes help to regulate the bile flow, guaranteeing the appropriate release for digestion.

Kupffer cells (KC) are localized in the hepatic sinusoid and have been described to play a major role in the systemic and hepatic response to pathogens (Dixon et al., 2013). They are also critical mediators in liver injury and repair and show high plasticity that depends on the microenvironment. The activation of KC is key in injury or infection since their inflammatory response has a protective role and limits the injury (Ulevitch et al., 2005). However, in some conditions, such as MASLD, there is an uncontrolled activation of these cells that may lead to chronic inflammation (Dixon et al., 2013).

Liver sinusoidal endothelial cells (LSEC) are very specialized endothelial cells that establish the wall of the hepatic sinusoid. Due to their location, they control the transfer of substances between blood and liver parenchyma and exhibit a great endocytic activity (Sørensen et al., 2015). LSEC display unique immune functions (Jenne et al., 2013) and play an important role in regeneration and liver disease like fibrosis (Ding et al., 2014). On the other hand, RNAseq technology has also shown a significant zonation in LSEC (Aizarani et al., 2019; Halpern et al., 2018).

Hepatic stellate cells (HSC) are located in the space of Disse and one of their major functions is vitamin A metabolism and lipid storage (Senoo, 2004). The space of Disse is a thin perisinusoidal area that separates hepatocytes and endothelial cells that allows the bidirectional exchange between cells (Sanz-García et al., 2021). Another important role of HSC is the production of ECM. Under pathological conditions such as fibrosis or cirrhosis, HSC proliferate and activate into myofibroblasts, which produce and secrete high amounts of different liver ECM components, mainly collagen type I or glycoproteins, and increase inflammation and immunoregulation (Puche et al., 2013). On the other hand, it has been demonstrated that modifications in the stiffness and constituents of liver ECM also impact HSC responses (Puche et al., 2013).

1.2. Liver extracellular matrix

The extracellular matrix (ECM) is the non-cellular part of a tissue that acts as a scaffold for the cells, which is critical in providing the biochemical signals needed for morphogenesis, homeostasis, and survival (Frantz et al., 2010). In normal conditions, liver ECM comprises less than 3% of the relative area and is mainly composed by collagens (being types I, III, IV and V the most abundant), glycoproteins such as fibronectin, laminin or nestin, and glycosaminoglycans (GAGs) such as hyaluronic acid (HA), chondroitin, heparan and dermatan sulfates (Figure 3) (Baiocchini et al., 2016; Bedossa et al., 2003).

Liver ECM is composed by two different structures (basement membrane and intersticial matrix) that differ in both morphology and biochemistry. The interstitial matrix is composed by collagen (types I and III) and fibronectin. The basement membrane is mainly composed by laminin, heparan sulfate and collagen IV and forms a thin acellular layer that facilitates diffusion. However, it is not present in the sinusoids and parenchyma of healthy livers (Allu et al., 2023).

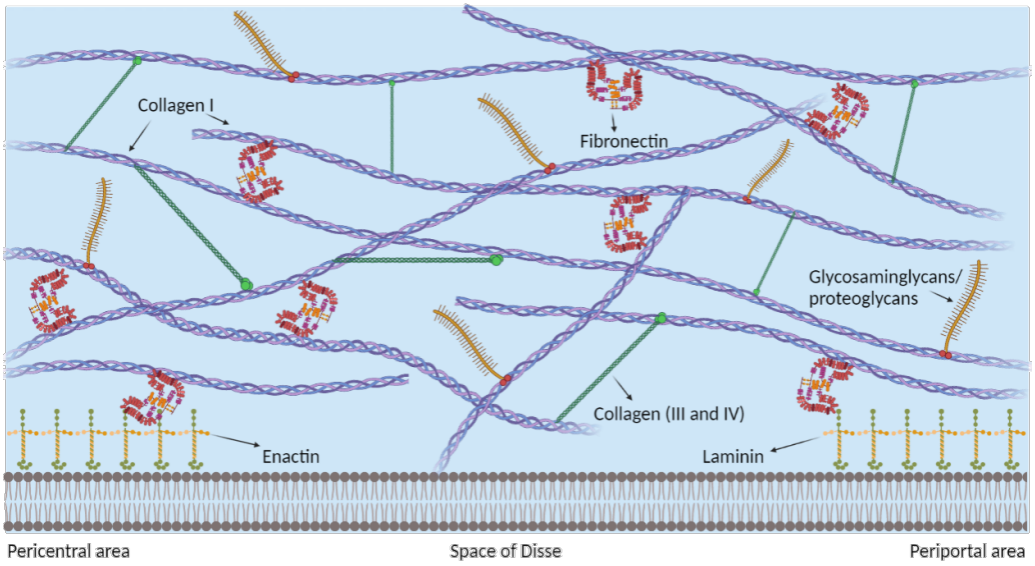

Figure 3. Schematic representation of molecules presents in the liver ECM matrix. *Image created with biorender. Adapted from* (Ye et al., 2019)

Collagen is a structural protein typically found in its triple helix form (90%) (Ricard-Blum, 2011), and represents between 20-30% of the proteins of the human body (Harkness, 1961). As the main component of the liver ECM, it is found in a variety of types and different locations, which led to hypothesize that plays different functions along the tissue (Bissell et al., 1988). LSEC, HSC, hepatocytes and lipocytes secrete this protein naturally to the ECM (Bissell et

al., 1988). The space of Disse reflects the forementioned heterogeneity, for example collagen type IV can be found in the portal triad zone, whereas central vein zone with abundant fibrillar collagen (type I) is related to mature cells like hepatocytes (Reid et al., 1992). Collagen not only plays a supportive role on the connective tissue, biologically had correlation with the expression of some hepatic markers such as albumin (Bissell et al., 1988) and the development of certain pathologies like fibrosis/cirrhosis which is based on the accumulation of fibrillar collagens over physio-pathological levels. Being a major component of liver ECM, collagen has been used in different tissue engineering approaches such drug delivery systems thanks to its non-antigenicity and controlled degradability by crosslinking; wound healing applications, which benefit from its hemostatic properties or forming hydrogels/scaffolds for liver tissue engineering because its biocompatibility and cell adhesion properties (Lee et al., 2001).

Proteins monopolize the liver ECM, but other molecules also play relevant roles on the tissue. GAGs are molecules composed by a carbohydrate chain covalently bonded to a protein (Lamberg et al., 1974) and they are also unevenly distributed as the collagen. HA, heparan sulfate, dermatan sulfate, keratan sulfate and chondroitin sulfate, are the GAGs present in the liver ECM, but their distribution and function is uneven along the liver (Bedossa et al., 2003). The little amount of GAGs found in the liver ECM made difficult to unravel the specific functions they play. Even though, GAGs are believed to help with tissue hydration by retaining water molecules and support hepatic cell functions (Yada et al., 2003). The potential of HA also is extended to liver tissue engineering with applications such as non-invasive biomarker for liver fibrosis (Neuman et al., 2016), drug delivery on cancer targeted therapy (Xu et al., 2013) and as a scaffold to support the hepatic functionality of human hepatocytes (Deegan et al., 2016).

Liver ECM has a critical role in the regulation of cell behavior, phenotype, migration, and proliferation (Ford et al., 2018). The remodeling of liver ECM can both help to maintain viability and functionality of the tissue and lead to disease (Ford et al., 2018). For instance, in liver fibrosis different chemicals or viruses can induce cell death, and, thus, the liberation of different mediators that can trigger the activation of HSC (Mejias et al., 2020). Activated HSC depose elastin and collagen resulting in an augment of stiffness (Ford & Rajagopalan, 2018).

The modification of the ECM is an extremely coordinated process that involves synthesis, secretion, degradation, and reorganization of the different components (Arriazu et al., 2014). When there is an injury or malfunction of the

enzymes implicated in the modification of ECM such as the matrix metalloproteinases (MMPs), there is a pathological deposition of ECM (Arriazu et al., 2014; Leroy et al., 2004).

On the other hand, several cell types are implicated in the modifications of liver ECM. In fact, the crosstalk between HSC, portal fibroblasts, LSEC and KC has been extensively discussed (Arriazu et al., 2014). In this sense, Ramachandran et al. (2019) using RNAseq technology identified pathogenic subpopulations of endothelial cells, macrophages (KC, mononuclear phagocytes, and scar-associated macrophages) and myofibroblasts in fibrotic human tissues (Ramachandran et al., 2019).

2. Liver disease

The liver has an extraordinary ability to restore its mass after loss or injury (Michalopoulos et al., 1997) and liver regeneration has been shown to combine both hepatocyte proliferation (hyperplasia) and hypertrophy (Kholodenko et al., 2017), although certain conditions such as chronic liver injury can impair its regenerative properties (Chawla et al., 2023). Acute and chronic liver disease are the major reasons of mortality worldwide (approximately 2 million deaths per year) and poses a considerable economic problem. The main causes of liver disease are viral hepatitis, MASLD and alcoholic liver disease (Asrani et al., 2019; Pimpin et al., 2018). Others include primary cholangitis, autoimmune hepatitis and inherited metabolic disorders such as alpha-1-antitrypsin deficiency (Asrani et al., 2019). These trends are constantly changing, and viral liver disease will probably be reduced in the future thanks to vaccination and new treatments, while drug-induced liver injury (DILI) and MASLD are expected to increase in Western countries (Asrani et al., 2019).

Alcohol consumption is a risk factor associated with multiple diseases, including cirrhosis and cancer (Pimpin et al., 2018). There is an exponential correlation between alcohol consumption and the development of cirrhosis (Burton et al., 2017; Pimpin et al., 2018), but it is also important to take into account the synergic effect of alcohol and other factors such as obesity or infection in developing disease (Hart et al., 2010). Alcoholic liver disease includes the development of steatosis, liver injury and inflammatory infiltrate. These damages usually appear associated to fibrosis and can progress to HCC (Bataller et al., 2019). Histologically, cirrhosis, which can also be produced by other diseases, e.g. hepatitis, presents an expansion of the ECM and the capillarization of the endothelium (Bhatia et al., 2014).

MASLD is characterized by excessive lipid accumulation in the liver and can range from simple steatosis to steatohepatitis, also characterized by inflammation and necrosis of hepatocytes and fibrosis (Pelechá et al., 2021). Hepatic fibrosis can be defined as the accumulation of ECM proteins in the space of Disse that can even block the blood flow (Ströbel et al., 2021). In liver fibrosis, in response to chronic liver injury, HSC are activated into proliferative fibrogenic fibroblasts and upregulate several inflammatory mediators that finally results in ECM accumulation and progressive fibrosis (Tsuchida et al., 2017). The progression of steatohepatitis underlies cirrhosis and even HCC (EASL, 2016; Pelechá et al., 2021). Different genetic, dietary, metabolic, and immunological factors have been implicated in MASLD (EASL, 2016; Pelechá et al., 2021). Currently, there is no pharmacological therapy available and the variation in lifestyle is the commonest therapeutic indication (Diehl et al., 2017).

Hepatitis B and C infection is one of the major reasons for liver disease in Europe (Pimpin et al., 2018). The pathogenesis of virus B and C infections is generally mediated by the immune system, even though both viruses can avoid immune removal and continue to replicate in the infected host for years. Chronic infection can result in oxidative stress induction and inflammation (Arzumanyan et al., 2013). Advanced liver disease due to virus B has been reduced, thanks to vaccination, although its complete disappearance is complex (Ray, 2022). On the other hand, hepatitis C is the leading cause of HCC, although antiviral therapies have reduced the burden of virus C infection (Ray, 2022).

HCC is the most common type of primary liver cancer that is often linked to other chronic liver diseases such as MASLD or hepatitis. There seems to be a final pathway in the pathogenesis of HCC, regardless the cause, wherein repetitive hepatocyte injury begins a vicious cycle of cell death and regeneration that eventually results in genomic instability and onset of HCC (Dhanasekaran et al., 2016). Different treatments are available for HCC, including surgical resection, liver transplantation, chemotherapy, and immunotherapy (Ruff et al., 2023), although HCC patients are frequently at an advanced stage or with compromised liver function, thus limiting the therapeutic options.

DILI is one of the principal reasons for acute liver failure (ALF) and a major cause of drug attrition in the preclinical and clinical phases of drug development or withdrawals after they have been commercialized (Kaplowitz, 2005). It involves high costs to both the pharmaceutical companies working on the drug development process and healthcare organizations due to its associated morbidities and mortality (Björnsson et al., 2015; EASL, 2019). DILI reactions

are frequently intricate processes that involve multiple interactions between hepatocytes and non-parenchymal cells. Furthermore, drugs can induce DILI by different mechanisms such as immune-mediated responses, mitochondrial damage, oxidative stress induction, steatosis, or cholestasis.

Inherited metabolic liver diseases are a heterogenous group of rare disorders mostly characterized by a defect in a single enzyme or protein with metabolic functions, e.g. receptors or transporters (Anand et al., 2022; Pareja et al., 2020). Some examples of these disorders include urea cycle disorders due to defects of urea synthesis and related metabolic pathways; Crigler-Najjar syndrome type 1 caused by mutations of the UDP glucuronosyltransferase 1A1 that produce severe hyperbilirubinemia; Wilson disease due to mutations of the *ATP7B* gene, involved in copper transport; and glycogen storage diseases produced by mutations that alter the accumulation of glycogen (Anand et al., 2022). As these diseases do not normally present changes in the liver architecture, although their primary treatment is organ transplantation, the characteristics of these disorders are an ideal scenario for cell therapy treatment (Bhatia et al., 2014).

2.1. Liver disease treatment

Liver transplantation is the only effective treatment for end-stage liver disease, and although it has a high survival rate (85% after 1 year) (Adam et al., 2012), there is a worldwide scarcity of organs, and many patients worsen or may even die while they are on the waiting list (Dutkowski et al., 2015). New strategies have been explored to amplify the number of available organs or improve their quality (i.e. dynamic preservation, living donors) (Dutkowski et al., 2015). Despite these efforts, the next-generation treatments such as cell transplantation or other bioengineering approaches have also been explored for the treatment of liver disease (Bizzaro et al., 2019).

Liver cell transplantation using hepatocytes, macrophages or stem cells has been suggested as an alternative or bridging technique to reduce liver disease mortality and morbidity. The first attempts at liver cell-based therapies focused on inherited metabolic disorders since they are produced by the lack or dysfunction of a single enzyme, although cell transplantation has been also applied in different liver diseases (Lysy et al., 2008; Smets et al., 2008).

It emerged as an alternative to organ transplantation and as an option for patients with different kind of liver disease, including inborn errors of metabolism and end-stage liver disease (Dhawan et al., 2004; Meyburg et al., 2009). However, the low engraftment and repopulation of transplanted hepatocytes has

prompted the use of alternative based on tissue engineering principles. Liver cell therapy through tissue engineering implicates creating functional liver tissue for regenerating diseased organs. In order to restore the hepatic functions of the disease liver, different strategies to produce liver tissue such as the use of decellularized-recellularized tissue (Mazza et al., 2015), scaffolds (Hammond et al., 2006) or hydrogels (Ye et al., 2019) have been described.

3. Current *in vitro* models for liver tissue engineering

Animal models have helped us to understand the mechanisms involved in liver disease and to decipher the mechanisms implicated in liver regeneration. However, different human *in vitro* models are now used to fully recapitulate human liver disease and develop safer and more efficacious treatments (Yuan et al., 2023). Table 1 summarizes major advantages and disadvantages of most commonly used liver *in vitro* models, including two-dimensional (2D) and three-dimensional (3D) models.

Table 1. *Advantages and disadvantages of the current in vitro liver tissue engineering models.*

Models	Advantages	Disadvantages	Refs
2D cell culture			
HepG2 cells	High availability, easy handling, low cost and standardized culture conditions Stable hepatic phenotype, Experimental reproducibility and suitable to high-throughput screenings	Lack of cell-matrix interaction Undifferentiated phenotype characteristic of highly proliferating tumor cells Low expression of certain drug-metabolizing enzymes (depending on the cell line) Absence on non-parenchymal cells Difficult transferability of data to normal (non-malignant) human liver	(Donato et al., 2015)
PHH	High liver-specific activity: phase I and II enzyme activity, glycogen storage, bile secretion, urea synthesis, etc. High differentiated phenotype Good reproducibility of liver drug metabolism Good transferability of human data Show variability in humans	Lack of cell-matrix interaction Lack of non-parenchymal cell types Loss of cell viability and quality in short time Scarce availability and poor plateability of some lots of cryopreserved hepatocytes Short-term expression of CYP enzymes Loss of cell polarity	(Donato et al., 2020)
Hepatic co-culture with non-parenchymal cells	Improved hepatic functionality compared to monocultures Improved longevity/functionality of all cell types Higher expression of CYP and Phase II isoforms than in monotypic culture Inducibility of CYP enzymes by xenobiotics Good correlation with *in vivo* and human data (human hepatocytes) Retention of morphology, bile canaliculi and cell-cell contacts	Lack of cell-matrix interaction Contribution of each cell type cannot be distinguished on gene expression. Methods vary greatly among protocols No standard as to which other cell type to use	(Takebe et al., 2013)

3D cell culture			
HepG2 cells in hydrogels/scaffolds	Hepatic functionality improved compared to 2D cell culture 3D cell organisation Ability to reproduce pathologies through variable matrix stiffness	Difficult cell and RNA retrieval for gene expression analysis No expression of CYP activity Polymer autofluorescence difficult cell imaging	(Lan et al., 2010)
PHH in hydrogels/scaffolds	High liver-specific activity: phase I and II enzyme activity, glycogen storage, bile secretion, urea synthesis, etc. 3D cell organisation Sustained long-term hepatic functionality and cell survival Ability to reproduce pathologies through variable matrix stiffness	Difficult cell and RNA retrieval for gene expression analysis Formation of necrotic regions due to poor oxygen diffusion Low cell culture longevity Polymer autofluorescence difficult cell imaging	(Lee et al., 2020)
Co-culture of hepatic cells with non-parenchymal cells in hydrogels/scaffolds	3D cell organisation Improved hepatic functionality compared to monocultures Recapitulation of cell variety found in the liver niche Ability to reproduce pathologies through variable matrix stiffness	Difficult RNA extraction for gene expression analysis Polymer autofluorescence difficult cell imaging Contribution of each cell type cannot be distinguished on gene expression	(Thanapirom et al., 2021)
Other approaches			
Microfluidic devices	Flow mimicking cell conditions (shear flow) Chemical gradient Promote round cell aggregates more similar to *in vivo* morphology Increase and maintain liver-specific functions. Precisely adjust flow rates and metabolite or drug concentrations in the medium Better correlation with *in vivo* data compared with static hepatocyte cultures and this correlation further improved when co-cultures are used	Lack of 3D cell organisation Emerging technology Variability of viability and differentiation status depending on culture conditions Does not maintain viability or functionality longer than other 3D methods Currently unsuitable for throughput	(Ju et al., 2015)

Microfluidic devices with hydrogel	Flow mimicking cell conditions Tissue specific response 3D cell organisation	Challenging hydrogel addition inside devices Difficult cell and RNA retrieval from the hydrogels and devices Complex approaches to employ microscopy techniques	(Messelmani et al., 2022)
Sandwich cell culture	Higher survival and expression of CYP and phase II enzymes than monolayer cultures Cell polarity and functional bile canaliculi	Lack of non-parenchymal cell types No native 3D cell organisation Several days are required to re-establish functional cell transport systems Relative high variability depending on culture conditions (extracellular matrix proteins)	(Schyschka et al., 2013)
Hepatic organoids	Cell-cell contact Cell-matrix interaction due to production of own ECM Long term cell culture longevity Long-term CYP/UGT acitivity	No optimised spheroid size and cell type to use Currently not suitable for high-throughput analysis Size spheroid influences necrotic cores due to oxygen diffusion	(Ohkura et al., 2014)

3.1. Monoculture

Traditionally*, in vitro* models have relied on monolayer 2D cultures; however, these systems do not accurately reproduce the spatial organization of the liver or cell-matrix interactions that have been described to improve and stabilize hepatocyte's functionality (Bell et al., 2018; Lee et al., 2020).

Primary human hepatocytes (PHH) are the gold standard for liver cell-based assays (Gómez-Lechón et al., 2004; Hewitt et al., 2007; Gómez-Lechón et al., 2008; O'Brien et al., 2004, 2006; Soldatow et al., 2013; Tolosa et al., 2014). They can be isolated and cultured, although a significant loss of functionality and reduction of quality over long periods of culture in monolayer configuration has been extensively described (Godoy et al., 2013; Gómez-Lechón et al., 2004; Hewitt et al., 2007; Gómez-Lechón et al., 2008; Soldatow et al., 2013). One of the major advantages of cultured PHH is the fact that they can reflect inter-individual variability (Chowdhary et al., 2017), although they present other major limitations as the scarcity of liver tissue for isolating them and vulnerability to freezing and thawing procedures (Fox, 2004; Hansel et al., 2014; Iansante et al., 2018).

Human liver cell lines (HepG2, Huh7, HepaRG) are an alternative to PHH that present high availability and easy handling (Donato et al., 2015; Gómez-Lechón et al., 2014), although their metabolic performance is reduced and they do not reflect inter-individual differences (Gómez-Lechón et al., 2014). HepG2 cells, isolated from an HCC, were the first cultured cells that showed key hepatic functions (Aden et al., 1979). Morphologically, they appear to have a half-way resemblance between hepatocytes and cells with hepatocarcinoma. HepG2 cells are polygonal with size between 12-19 μm and large nuclei and present a high-volume ratio nuclei/cytoplasm (Arzumanian et al., 2021). Biologically, they are an immortalized cell line that display specific hepatic functions such as albumin synthesis, glycogen storage, and cellular metabolism (Donato et al., 2015; Tai et al., 2018; Westerink et al., 2007; Wiśniewski et al., 2016). However, their principal drawback is lack of biotransformation enzymes, particularly cytochrome P450 (CYP) enzymes, which means that they are unable to be susceptible to metabolism-mediated hepatotoxicity (Guengerich, 2019). Nevertheless, it is the most used cell line for drug screening and toxicity assays, since they are derived from human liver and retain the expression of some enzymes relevant for human metabolism, including phase II enzymes. In 2021

data extracted from PubMed, 76% of the manuscripts using human hepatic cell lines selected HepG2 cells as their cell model (Arzumanian et al., 2021).

Induced pluripotent stem cells (iPSC) have been known as a promising cell supply. Its potential to be differentiated towards different phenotypes, including hepatic lineage, would solve the cell scarcity problem and in particular PHH (Forbes et al., 2015; Hannan et al., 2013). One of the major advantages is the fact that these iPSC models could reflect inter-individual variability (Takayama et al., 2014) and could be a therapeutic option alternative to organ transplantation, although most advantageous protocols that permit the differentiation of iPSC into a more mature stage are urgently needed. Recently, researchers have focused on new culture systems (3D cultures, co-culture systems, microfluidic devices) that allow to keep the cultures over longer periods and maintain or even improve their functionality (Godoy et al., 2013).

3.2. Co-Culture of hepatic cells

Although traditional *in vitro* models have relied on the use of a single cell type, recently other models that consider liver's multicellularity have been also proposed. For instance, the co-culture of HepG2 cells with KC, showed cell-cell contact between both cell types and a better response to a lipopolysaccharide-induced inflammatory response (Hoebe et al., 2001). Additionally, it was described that the distance between both cell types could be key to modulate this response due to the existence of short-life/small molecules, manifesting the relevance of the co-culture and cell-cell contact (Hoebe et al., 2001). Co-culture is not limited to two cell types, the necessity of complex models can be answered by culturing as many cell types as technically possible. Suurmond *et al.* created a microfluidic platform to culture HepG2, human umbilical vein endothelial cells (HUVEC) and KC spheroids to improve the MASLD modelling outcome. The spheroid system demonstrated to improve the activation of the KC as well as increased levels of proinflammatory cytokines and cell stress markers.

On the other hand, the expression of hepatic markers, such as alfa-fetoprotein (AFP), albumin, transthyretin, and retinol-binding protein 4, was sustained by the co-culture of hepatic endoderm cells from iPSC with HUVEC and mesenchymal stem cells (MSC) (Takebe et al., 2013). Finally, the co-culture with other non-hepatic cells has also demonstrated to improve the stability of the cell culture along hepatic functionality. For instance, co-culture of PHH and 3T3-J2 murine embryonic fibroblasts displayed stable cell culture and improved urea production and CYP3A4 activity (Davidson et al., 2021). The authors mentioned that the molecular mechanism that promotes this effect remain unknown, besides the different origin of both cell lines.

3.3. Hepatic organoids

Alternatively, 3D environments not only can be defined by the use of an external matrix like scaffolds or hydrogels. Cell organoids have been defined by different authors, but the most accepted description was coined by Lancaster, Knoblich, Huch, and Koo. Depicted as a group of cells with tissue-derived origins such as stem cells, embryonic stem cells, or iPSC, which can self-organize and self-renew resembling the native behaviour of the tissue (Huch et al., 2015; Lancaster et al., 2014).

Hepatic organoids have been widely used as a 3D alternative to monolayer cultures for different applications more prominently used for drug toxicity and disease modelling (Prior et al., 2019; Sun et al., 2020; Tostões et al., 2012). In 2016, Leite et al. found a huge increase in collagen secretion (100-fold) and an upregulation of COL1A1 and COL1A3 genes in HepaRG/HSC organoids, which led to recreate liver fibrosis through methotrexate and allyl alcohol repeated exposure (Leite et al., 2016). Congenital liver fibrosis was also modelled by differentiated genome-edited iPSC into different hepatic lineage cells such as hepatoblasts, cholangiocytes, and HSC. Through the activation of the PDGFRB-STAT3 pathway, dilation of bile ducts, and accumulation of assembled collagen, they confirmed a liver organoid model able to display key features of liver fibrosis which could help to discover new anti-fibrotic treatments (Guan et al., 2021). Hepatic cancer has been another application for liver organoids, which helped to reveal unknown events such as the trigger of contact between mitochondria and endoplasmic reticulum membranes once c-MYC (oncogene) was introduced in hepatocyte organoids (Sun et al., 2019). The culture of tumour organoids derived from HCC, cholangiocarcinoma, and its combination, kept the expression profile as well as the genetic mutations of the original tumours. Altogether, they discovered patient-specific drug sensitivities which could lead into new personalised therapies for liver cancer (Broutier et al., 2017).

Moreover, disease modelling it is not limited to cancer or chronic liver pathologies, inborn metabolic disorders can also be mimicked by organoids. Liver organoids derived from liver biopsies reflected the diversity of genotypes in alpha-1 antitrypsin deficiency, improved specific downregulations or upregulations were found and associated to each genotype (Gómez-Mariano et al., 2020). In addition, drug screening has always been undermined by the limited and non-precise outcomes from 2D platforms or monoculture. Liver organoids had demonstrated better outcomes by offering 3D organisation and multi-cell type culture. Organoids based on the co-culture of HepG2 and NIH-

3T3 fibroblasts along a microfluidic device, created a platform that demonstrated better drug detoxification through CYP enzymatic activity as well as improved hepatic functionality based on albumin synthesis compared to 2D cell culture (Au et al., 2014).

3.4. Microfluidic devices

The advances to recreate more accurate platforms to recapitulate the native idiosyncratic behaviour of the liver, not only have been focused on tridimensionality. Traditional models always asked for alternatives on cell organisation, but also to improve the static condition of the culture. Human organism it is not a static entity, blood and oxygen flow, and in particular for liver tissue, bile is produced and secreted. Microfluidic devices focus on tailored small platforms formed by narrow channels and patterned surfaces to mimic dynamic *in vivo* conditions and creating high-throughput devices.

Drug metabolism and toxicity has been widely studied by the culture of HepG2 cells in microfluidic devices because of the possibility to create chemical gradients easily. Ye *et al.* tailored a device which created drug gradients to expose several cell cultures to different concentrations at the same time. In this system, doxorubicin exhibited a dose-dependent effect in HepG2 cells, inducing apoptosis and mitochondrial dysfunction (Ye et al., 2007). Other drugs (i.e. APAP, diclofenac, cyclosporine A) have been also tested using these platforms in HepG2 cells (Ju et al., 2015; Mao et al., 2012), or in PHH (Deguchi et al., 2021; Yeon et al., 2010).

Microfluidic devices had not been limited to monoculture and drug toxicity testing. Co-culture of parenchymal and non-parenchymal cells has been possible with more complex microchips that simulate the configuration of a liver sinusoid, achieving better albumin and urea production compared to a static culture and keeping them functional for 28 days (Prodanov et al., 2016). Gori *et al.* induced lipid accumulation to HepG2 by exposure of palmitic and oleic acid, modelling steatosis. In addition, the device allowed to have a progressive accumulation instead of an acute lipid intake, simulating better a slow chronic steatosis episode (Gori et al., 2016). As microfluidics always missed the tridimensionality offered by hydrogels or scaffolds, some authors have described methods to merge both techniques to recapitulate the advantages of both (Clancy et al., 2022; Messelmani et al., 2022)

4. Hydrogels

Hydrogels are polymeric hydrophilic networks able to absorb large amounts of water without dissolving. They maintain their integrity in the presence of an aqueous environment due to the crosslinking points between the polymeric chains (Peters et al., 2021). These crosslinks can be chemical, formed by covalent bonds, or physical, which imply non-covalent bonds such as hydrophobic interactions, hydrogen bonding, chains entanglements, crystallites of semi-crystalline polymers or ionic interactions (Annabi et al., 2014). They can even form dual networks consisting of physical and chemical crosslinks that can sometimes result mechanically advantageous (Jiang et al., 2021). Chemical hydrogels are more stable than physical hydrogels in physiological environments in which the pH or ionic strength can suffer changes. They are good candidates for liver tissue engineering due to their water sorption capacity and softness in mimicking the liver's mechanical properties, they can be combined to mimic the composition of the liver ECM and have the capacity to deliver biomolecules (Tong et al., 2018).

One of the hydrogel's disadvantages is that many crosslinking reactions are cytotoxic and cannot take place in the presence of cells (Lai, 2010), although mild reactions have been explored; these can take place together with the cells to form *in situ* gelling or injectable hydrogels (Tan et al., 2010). They are advantageous because the precursor solution can be mixed with cells and bioactive components and be injected into the body where they become solid, homogeneously entrapping the cells, completely filling a tissue defect and being implantable by minimally invasive procedures. In this thesis we optimized a family of enzymatically gellable hydrogels of gelatin (Gel) and HA for the 3D culture of hepatic cells (Rodriguez-Fernandez et al., 2023). These types of hydrogels can be used to form 3D construct structures by bioprinting through the development of bioinks (a solution of the precursor molecules of the hydrogel together with a suspension of cells) (Ramiah et al., 2020).

The main physical properties of hydrogels, their swelling capacity and mechanical properties depend on different parameters, including crosslinking density, the chemical nature of the polymeric chains (through the Flory-Huggins interaction parameter), the activity of water in the environment, the concentration of polymers, the porosity of the hydrogel, etc. The network structure, characterized by its mesh size (Raghuwanshi et al., 2019), determines the diffusivity of water or other soluble species (growth factors or drugs) through the hydrogel. The rubber elasticity theory describes the mechanical behaviour of

hydrogels, and the Flory-Huggins equation describes their equilibrium swelling (Richbourg et al., 2020). The elastic modulus of hydrogels increases with the crosslinking density, while the water sorption capacity and diffusivity of biomolecules decreases with it. The lower the interaction parameter, the more water is absorbed by the hydrogel. The higher the water activity in the environment, the more water is retained by the hydrogel.

4.1. Polymers for hydrogels

4.1.1. Natural polymers

Liver-derived hydrogels can be created with liver dECM since they preserve many of the components of the natural matrix that can be beneficial for 3D liver cell culture. Willemse *et al.* used liver dECM hydrogels to culture and expand intrahepatic cholangiocyte organoids (ICO) as alternatives to tumour-derived basement membrane extracts (Willemse et al., 2022). Liver dECM allowed successfully culturing ICO in dynamic spinner flasks, which was more efficient and faster than the classical culture in basement membrane extracts. Despite the promising results, as the liver ECM varies in different parts of the organ, the composition of the resulting hydrogels is difficult to control, so that chemically defined hydrogels are preferred in liver tissue engineering (S. Ye et al., 2019), as in the case of Alg, which has been explored in many tissue engineering applications. In general, Alg has a bad interaction with cells, and when it is directly crosslinked with $CaCl_2$ salt it becomes a non-injectable hydrogel due to the rapid crosslinking reaction. To make it injectable for liver tissue engineering, Tong *et al*. (Tong et al., 2018) developed a two-step method to ionically crosslink the hydrogel with Ca^{2+} through an insoluble calcium salt that progressively released the crosslinking ions. To improve the interaction with cells, the study used glycyrrhizin triterpene glycoside (GL) which provided the hydrogel with specific binding sites for hepatic cells. The authors demonstrated that the new GL-Alg-Ca hydrogel had suitable viscoelastic properties for the cell culture of hepatic cells (HepG2) with enhanced hepatic functionality and CYP expression in 3D rather than 2D.

Of the chemically defined hydrogels, collagen is probably the best for liver tissue engineering because it is one of the main components of the liver ECM (Baiocchini et al., 2016). It forms a viscous solution in acetic acid and forms a physical hydrogel when neutralized with NaOH (Desimone et al., 2010). Col bioinks and the resulting hydrogels possess very low mechanical properties to their use alone in liver tissue engineering, so they are usually combined with other more rigid polymers, as for example polycaprolactone grids in the form of

scaffolds (Lee et al., 2016) for the heterotypic culture of rat hepatocytes, HUVEC, and human lung fibroblasts encapsulated into collagen filaments. The authors described a vascular formation and an enhanced functionality of hepatocytes (albumin secretion and urea synthesis) in the case of the heterotypic interaction among hepatocytes and non-parenchymal cells compared to hepatocytes monoculture. Gel, the denaturalized version of Col, is an alternative hydrogel widely used in tissue engineering because it is cheaper and possesses some of the advantages of Col. It is soluble in physiological buffers (not needing acetic acid) and forms a physical hydrogel by reducing the temperature. The problem is that the sol-gel transition is situated below 37 ˚C, forming liquid solutions in cell culture conditions. This has led to a search for alternative ways to crosslink Gel for use in tissue engineering. One of the most frequently used methods is ultraviolet (UV) light crosslinking of gelatin methacryloyl (GelMA), which has been tested in building 3D lobule-like microtissues for the co-culture of hepatocytes and fibroblasts (Cui et al., 2019). The study showed that urea synthesis and albumin secretion by HepG2 were significantly higher in co-culture than in monoculture.

In the group of GAGs present in liver ECM, HA has been proposed as a suitable hydrogel for its high hydration capacity and mechanical stiffness, as well as the ability to interact with cells through the binding domains for the cell surface receptors CD44 and RHAMM (An et al., 2021). An example of its use in liver tissue engineering can be found in (Christoffersson et al., 2019), in which HA was crosslinked using an 8-arm polyethylene glycol (PEG) by click chemistry giving rise to hydrogels with a shear storage modulus that ranged from 100 Pa to 1 kPa. HepG2 cells and HLC derived from human iPSC were successfully cultured within the hydrogels after grafting arginine-glycine-aspartic acid (RGD) adhesion motifs to HA, which secreted more albumin than non-functionalized HA hydrogels. Heparin is another abundant GAG in liver ECM, with the advantage that it binds ECM proteins such as the hepatic growth factor (HGF) thanks to the presence of the sulfated group in its structure. For instance, heparin hydrogels can be obtained by Michael-type addition reaction of thiolated heparin and diacrylated PEG crosslinker (Kim et al., 2010). By the inclusion of HGF in heparin, single hepatocytes and hepatocyte spheroids showed excellent hepatic functions up to 20 days in culture.

Not only pure hydrogels are interesting for *in vitro* systems in liver tissue engineering, combining different components of the ECM can often give rise to hydrogels with improved characteristics, as in the case of the study in (Chen et al., 2021), in which the authors established a biomimetic difunctional HA-Col

hydrogel matrix which can recapitulate the inherent characteristics of natural ECM, such as fast relaxation, a nanofibrillar structure, as well as abundant adhesion domains. The same authors propose this hydrogel mixture to build a viscoelastic matrix system with native adhesion domains and fibrillary architecture to provide a mimetic microenvironment for the cell culture of HepG2 cells, as an *in vitro* artificial liver model to study alcohol-induced liver disease (Jiang et al., 2021). HA has also been combined with Gel (Malinen et al., 2014) for the culture of HepaRG cells.

4.1.2. Synthetic polymers

PEG hydrogels are the most frequently used synthetic hydrogels in tissue engineering due to their biocompatibility, neutral charge, and precise control of the crosslinking density, giving rise to networks with reproducible mechanical properties. PEG's disadvantages against natural origin hydrogels are their non-biodegradability and lack of recognition sites to interact with cells. These drawbacks have been solved, on one hand by providing PEG with matrix-MMP sensitive peptides (as crosslinking agents or in the polymer backbone), allowing PEG degradation in cell microenvironment (Stevens et al., 2015). On the other hand, the chemical modification of PEG including bioactive factors, such as the adhesion sequence RGD, has permitted the interaction with cells, in general, and with hepatic cells, in particular, for the improvement of the hepatic functionality of hepatocytes (in co-culture with fibroblasts) (Underhill et al., 2007). Orthogonally cross-linked thiol-ene hydrogel PEG systems were synthesized in (Lin et al., 2014) as a cytocompatible niche for culturing Huh7 and HepG2 cells in 3D. When these hydrogels contained bioactive matrix MMP-sensitive peptide linkers they could better upregulate the expression of several hepatocyte-specific genes and enhanced hepatocyte functions than bioinert hydrogels of the same nature. Including RGD motifs was also positive for upregulated hepatic functionality.

Hydrogels have achieved progress in the *in vitro* culture of hepatic cells since hepatic functionality and the culture time of hepatocytes has improved in 3D in comparison to the traditional monolayer culture. However, hydrogels have also posed new challenges related to the construction of more physiologically relevant *in vitro* models. For instance, there is a need to recreate the native liver microarchitecture, with a heterogeneous ECM that can be recreated by building micropatterned hydrogels (Agarwal et al., 2019; Huang et al., 2020). Although the hydrogels described here have a good affinity for hepatic cells or have been decorated with biomolecules that provide cell-matrix interactions, the inclusion of growth factors presented by the hydrogel in synergy with the interaction

domains can represent a step forward in hepatic functionality (Trujillo et al., 2019). New hydrogel formulations that more accurately reproduce the viscoelastic behaviour of the native tissue are expected in the future (Cantini et al., 2020; Rizwan et al., 2022) to adequately mimic the *in vivo* situation in order to improve the current outcomes.

4.2. Hydrogels for liver tissue engineering

Regarding the use of hydrogels for liver tissue engineering strategies, different types of polymers, including chitosan, alginate (Alg), or natural-derived ECM molecules, have been used as hydrogels for liver tissue engineering. For instance, rat hepatocytes encapsulated in Alg microbeads gave metabolic support in an animal liver failure model (Jitraruch et al., 2014) and has been suggested as a promising approach for the treatment of children with ALF (Dhawan et al., 2020). The authors used cryopreserved PHH encapsulated into Alg microbeads, obtaining encouraging results, since 4 of the 8 children tested avoided organ transplants (Dhawan et al., 2020). Despite the promising results, the safety of the procedure continues to be uncertain since Alg is non-biodegradable in mammals and its lasting effects have not been thoroughly analysed (McKiernan et al., 2020). For this reason, other authors have used other approaches like Col-based hydrogels (Shagidulin et al., 2023; Zhao et al., 2019; Zhong et al., 2016). Zhao *et al*. used Col hydrogels seeded with neonatal and adult hepatocytes for the treatment of liver fibrosis in a multi-site injection strategy that enabled transplanting a huge number of liver cells into liver parenchyma in a single intervention and observed a reduction in fibrosis (Zhao et al., 2019). Interestingly, Chiang *et al*. used HGF-releasing hydrogels for the transplantation of iPSC-derived hepatocyte-like cells (HLC), obtaining increased antioxidant and anti-apoptotic potential of the cells and improving the results in treating ALF (Chiang et al., 2015).

4.3. Scaffolds for liver tissue engineering.

Decellularized liver tissue is an ideal scaffold since it retains the natural vascular network as well as the microarchitecture and components of liver ECM (Zhang et al., 2021). Decellularized ECM (dECM) can be used directly as a scaffold or as hydrogels for the treatment of liver disease. For instance, Vishwakarma and cols used rat dECM scaffolds seeded with human EpCAM+ cells for the treatment of rats with ALF, showing an improved survival and the maintenance of specific hepatic functions up to one month (Vishwakarma et al., 2019). On the other hand, the decellularization of whole human liver lobes was first

demonstrated in 2015 (Mazza et al., 2015). The same authors seeded human liver cubic scaffolds with three distinct cell types (HSC, HCC and hepatoblastoma) and demonstrated thier biocompatibility by xenotransplantation into immunocompetent mice, although their therapeutic effect was not demonstrated (Mazza et al., 2015). In order to establish the scalability to human-sized techniques, engineered liver grafts of pig dECM repopulated with endothelial cells and primary hepatocytes were used in pigs subjected to 60% liver hepatectomy (Higashi et al., 2022). The study showed that dysfunction markers such as transaminases levels, bilirubin or inflammation markers were lower in the transplanted animals, which indicated the functionality of these bioengineered grafts at a clinical level (Higashi et al., 2022). Although dECM is a potential strategy as a tissue engineering approach for the treatment of end-stage liver disease, important issues related to possible risk of xenogeneic/allogeneic tissues, the recellularization process (cell sources, flow rate, migration, and repopulation, etc.) or the enduring stability of the decellularized/recellularized tissues should be solved before its clinical translation (Zhang et al., 2021).

Other authors have explored the use of synthetic scaffolds seeded with different types of hepatic cells, since they not only provide a 3D microenvironment, but their interconnected pore structure also provides a suitable nutrient supply (da Silva Morais et al., 2020). Some studies have used the scaffolds to improve the differentiation potential of multipotent stem cells before transplanting (Tai et al., 2010), while others employ the scaffolds as a delivery method and study the differentiation potential *in vivo* (Lin et al., 2015; Zhang et al., 2019). Alg scaffolds seeded with bone marrow MSC were shown to promote liver regeneration in rats after partial hepatectomy, and the transplanted cells (Lin et al., 2015) obtained specific hepatic functions such as glycogen production or albumin secretion and proved the ability of these cells to differentiate *in vivo* when transplanted within scaffolds (Lin et al., 2015). Although there are many studies using MSC to provide fully functional hepatic activity, other authors have used hepatocyte-laden scaffolds to treat liver disease, e.g. Alg scaffolds seeded with foetal liver cells were used to treat a Wilson's disease animal model, showing a significant therapeutic effect on the copper metabolism deficiency (Katsuda et al., 2010). Biodegradable materials offer an advantage for clinical application over other strategies such as using Alg. We recently showed that gelatin-hyaluronic acid (Gel-HA) scaffolds containing PHH improved hepatic functions in an APAP-ALF animal model compared to intrasplenic injection of single cells (Rodriguez-Fernandez et al., 2023). Other natural polymers such as dextran and pullulan were recently used for encapsulating HepaRG cells and showed improved survival in mice with ALF (Le Guilcher et al., 2023).

5. Bioprinting

3D bioprinting comprises a range of emerging technologies that allow the fabrication of cell-laden structures with a more complex architecture than other scaffolds or cell culture supports that have been traditionally used. First prototyped in the 1980's decade by Charles W. Hull, 3D printing was initially named stereolithography, in which thin layers of material were deposited layer-by-layer and further cured under UV light exposure, ultimately forming a 3D solid structure (Hull, 1986). This process is now widely applied to manufacture resin moulds for scaffolding across several industries. The development of aqueous and biocompatible materials opened the door to the application of 3D printing in the field of tissue engineering, combining advances in cell biology and materials science. In recent years it has become a versatile technology with the potential to produce biological constructs, such as bone scaffolds, organ-on-chip platforms, or organoids (Chliara et al., 2022; Datta et al., 2020; Tang et al., 2016).

The simultaneous incorporation of cells with a biomaterial has the potential to allow the proliferation of cells in a designed structure. Hence, animal-free *in vitro* platforms for drug toxicity screening or potential tissue replacement approaches are fields in which bioprinting is gaining popularity. Overall, 3D bioprinting comprises a set of additive manufacturing techniques where a pattern of biological material is deposited onto a substrate. However, novel strategies such as tomographic printing that operate under a different principle and are beyond the scope of this study.

5.1. Bioprinting technologies and main printing parameters

Three main strategies for 3D bioprinting can be distinguished: inkjet, laser-assisted, and extrusion-based printing (EBB) (Figure 4). The common component to all of them is the bioink, while each strategy differs in its deposition, speed, or resolution, and has its own properties and limitations (Moroni et al., 2018).

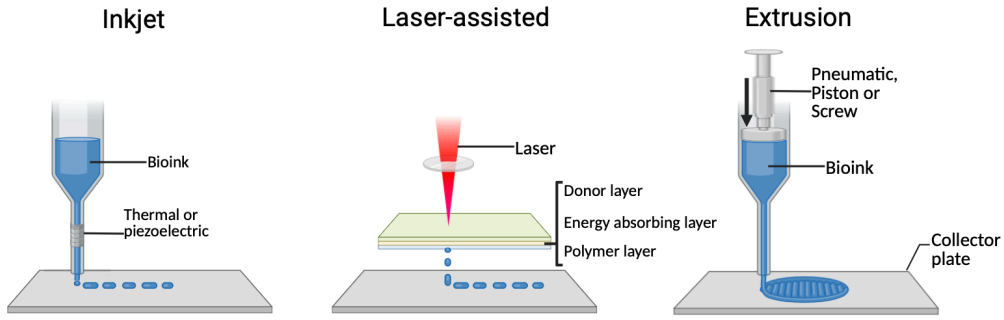

***Figure 4. General scheme of different types of bioprinting**. Image created with biorender.*

Inkjet bioprinting consists of the controlled deposition by drops of a bioink volume onto a surface, usually through piezoelectric, thermal, or electromagnetic valves to eject the drops from the cartridge. Nevertheless, the inks used must be rather liquid since it is susceptible to clogging of the nozzle (ca. 50 μm diameter), which can be a limitation when a solid and uniform 3D structure is desired upon deposition. Overall, it remains a fast and relatively cheap technique. Despite having been used in the area of tissue engineering, the cell densities achieved are generally low (Li et al., 2020; Murphy et al., 2014), since cells can hardly be homogeneously suspended in a low viscosity bioink as required. It has been applied to produce cell-laden cartilage implants (Cui et al., 2012) or liver cell culture models (Arai et al., 2017; da Silva Morais et al., 2020; Parsa et al., 2010), however, its most wide application in this area is the fabrication of organ-on-chip platforms, combined with other technologies. (Moya et al., 2018)

Laser-assisted bioprinting allows high-velocity (10 m/s) deposition of cell solutions with high cell concentrations. A donor surface with a light-absorbing layer on top of a bio-ink layer, a substrate, and a pulsed laser source are the typical components of a laser-assisted bioprinting system. When exposed to light, the light-absorbing layer locally absorbs it, causing it to vaporize and create a strong gas pressure that induces the ejection of droplets of bio-ink toward the substrate. The complexity of this mechanism is influenced by the amount of light, the length of the laser pulse, the size of the laser spot, the separation between the absorbing layer and the substrate, and the thickness of the bio-ink layer. Using this method, bio-ink droplets may be printed with high resolution and good cell viability (Murphy et al., 2014). Cells, however, can be negatively impacted by the laser's heat, and its numerous parameters make it more difficult to tune and set up while requiring bigger volumes of bioink. Additionally, this equipment has a higher cost than other bioprinting methods. There exist other types of light-assisted technologies that evolve from stereolithography techniques, such as

digital light processing (DLP), in which a specific wavelength is projected as a planar pattern and along the z-axis towards a bioink bed, activating photopolymerization. Similar to laser-assisted bioprinting, these techniques compromise cell viability via phototoxicity (Williams et al., 2005).

Generally, the most widely used as well as affordable type of bioprinters rely on bioink extrusion (or microextrusion). These usually consist of a dispensing system over a printing bed, with either one or both components capable of moving in the x, y, and z axes. The dispensing system may have one or more printheads, in which the bioink-containing cartridges are placed. Several printheads allow the deposition of several bioinks, with varying compositions or cell types. Oftentimes, these printers allow the temperature control of both the printhead and the print bed, as it may be desired to keep cell-laden inks at physiological temperature or prevent a certain polymer from reaching its crystallization temperature. Compared to other strategies, EBB performs well with a wide ran (Ilispie et al., 2020; Murphy et al., 2014). The extrusion can be actuated pneumatic or mechanically (screw or piston). In general, mechanical systems are more suitable for highly viscous inks, but incorporate smaller and more complex components. In contrast, pneumatically driven systems can be suitable for a wider range of viscosities, despite being limited to the pressure capacity of the pump. The cartridge is coupled to a tip or nozzle, with a cone-like or needle form, with varying gauges.

In EBB, bioink viscosity is one of the main parameters to be controlled for successful printing (Xie et al., 2023), which depends on characteristics such as the polymer concentration, polymer molecular weight, polydispersity index, cell density and processing temperature. Highly viscous materials produce stable structures after leaving the nozzle, although they can also produce high shear stresses in the print head, limiting cell survival. Low viscosity materials are gentle on cells, but printing pressure and filament shape are difficult to control. Shear thinning materials can be used to obtain a balance between cell survival and shape fidelity. These materials reduce their viscosity in the presence of shear forces and facilitate bioink deposition without compromising the cells. Shape fidelity is guaranteed in this type of material because filament viscosity is recovered after exiting the nozzle (Xie et al., 2023). Khati et al. developed a shear thinning bioink based on liver dECM, Gel and PEG that enabled the extrusion of dECM at body temperature (Khati et al., 2022). Hydrogel crosslinking needs to be fast enough to avoid the hydrogels spreading out so that the filament keeps its shape. In this way, better shape fidelity is obtained than in long crosslinking time hydrogels. Shape fidelity also depends on the

hydrogels' swelling properties after printing. A low degree of swelling, which can be regulated by the crosslinking degree of the hydrogel, is required to keep the shape of the filament.

The ideal structure to print to recreate the liver microenvironment is the liver lobule and most studies dedicated to build this structure have used EBB because the resulting constructs are more viable than when using the other techniques (Wang et al., 2023). The designs have a central hollow zone with printed endothelial cells, radiating endothelial cells separated from radiating hepatocytes and a final surrounding structure with endothelial cells (Wang et al., 2023). These structures combine the ECM comprising the ink together with the cells and no heterogeneity of them is desired, to better mimic the *in vivo* situation.

5.2. Bioprinting parameters for cell culture

Bioink definition not only referred for the biological origin of the components, also included the key point for bioprinting, the cells. There are parameters such as the tips or nozzle employed, or the pressure required to extrude the bioink that must be thoroughly optimized not only for the resolution or shape fidelity of the 3D bioprinted structures, also as to preserve the cell survival during the printing process.

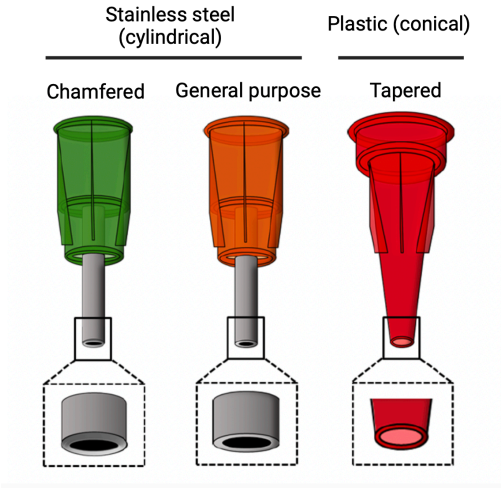

Figure 5. Types of nozzles for extrusion bioprinting. *Figure created with Biorender.*

There are a variety of tips and nozzles that can be used for bioprinting, from cylindrical tips to conical nozzles (Figure 5). Also, it can be made of different materials such as plastic or stainless steel. However, the focus on this aspect has been the stress distribution along the different tips. While conical tips always

display the highest stress point on the end of the tip, cylindrical nozzles experience that on the walls of the tip (Figure 6) (Reina-Romo et al., 2021). In addition, a study conducted by Billiet *et al.* revealed the complex relationship between the type of nozzle, the inlet pressure and the shear stress applied to HepG2 cells. Whilst low-medium inlet pressures exhibited higher cell viabilities with conical shaped-needles compared to cylindrical, it changes completely when higher inlet pressures are required. Conical needles have a short section where cells sense huge shear stress, however cylindrical needles distribute better the shear stress and work better under higher pressures (Billiet et al., 2014).

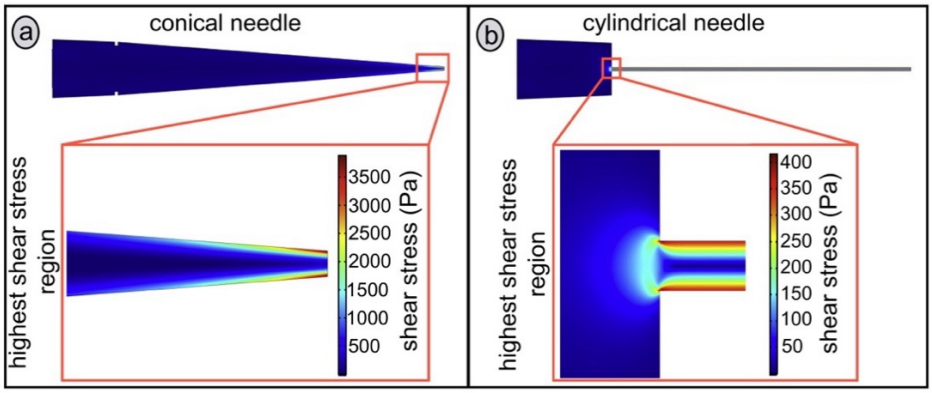

Figure 6. Stress distribution simulation on different types of nozzles: conical (left) and cylindrical (right). *Image extracted from (Billiet et al., 2014)*

The nozzle diameter also influences cell viability; large diameters require lower pressure to produce the filament than small diameters and the cells are submitted to lower shear stresses with good viability (Unagolla et al., 2020). Pressure is another factor that is set up according to the nozzle type and diameter, all of them are connected, and varying one of them will change the other.

5.3. Design and bioprinting of platforms for liver tissue engineering.

Bioprinting allows the automatic deposition of hydrogels and cells onto platforms with a precise and desired shape in a very short time, it has allowed the design of advanced 3D hepatotoxicity platforms to test the effect of multiple drugs in 3D cultured hepatic cells. This field has been extended to the automatic preparation of 3D platforms to simulate *in vitro* liver diseases for mechanistically understanding them and developing new drugs for their treatment.

5.3.1. Bioprinting for studying drug-induced liver injury

Studies generally combine different materials optimized for bioprinting, as pure components are difficult to print, as in the case of Pluronic (Gori et al., 2020), a material widely used for EBB due to its good printability and shape fidelity, although, despite these advantages, it has rather poor mechanical properties that compromise its applicability. A combination of Pluronic with Alg enhances the mechanical properties of the mixture, a method used by the authors to compare the material in supporting HepG2 cell line viability and metabolic activity with monolayer cultures, using the platform for high-throughput screening of hepatotoxic compounds. Compared to monolayer culture, cell viability was significantly reduced when the 3D liver models were incubated with APAP, demonstrating the printed model's prediction of hepatotoxicity. In the case of Col, there were some difficulties in bioprinting. This is a low-viscous liquid when dissolved in acid conditions, however when neutralized it begins to assemble into fibers, forming a physical hydrogel that compromises its bioprinting (Mazzocchi et al., 2018). The combination of methacrylate Col with thiolated HA produced a printable material with relevant components in liver ECM. When PHH were bioprinted, they maintained functionality, which declined when incubated with APAP, demonstrating the adequate response to hepatotoxic drugs (Mazzocchi et al., 2018). Another approach used a combination of Alg and Gel as bioink to construct a hepatic tissue model based on encapsulated HLC derived from iPSC. The cells within the 3D-printed model had significantly better hepatic functionality, proliferation than the monolayer cultures and non-printed sandwich-cultured models (He et al., 2022).

On the other hand, a three-component mixture is sometimes necessary to increase printability, retain shape after printing, and improve cell viability, as in the case of the 3D liver model proposed by Schmidt *et al*. in which Alg, Gel and Matrigel were mixed to print scaffolds containing HepaRG cells (Schmidt et al., 2020). The system allowed the culture of HepaRG cells for long periods, which would allow chronic treatments with toxic compounds such as albumin, suggesting that these hydrogels are suitable for repeated-dose assays.

Microfluidic systems have the advantage of the cells being physiologically stimulated under a continuous flow of cell culture media. In (Bhise et al., 2016), the authors interfaced a microfluidic bioreactor with a bioprinter to fabricate 3D hepatic constructs of spheroids encapsulated in photocrosslinkable GelMA hydrogel. The cultured spheroids were viable and active for 30 days and similarly responded to APAP-treatment to those described in other published studies on animal or *in vitro* models.

Bioprinting can be used to build complex 3D structures that mimic the liver lobule microarchitecture for drug toxicity experiments. In (Janani et al., 2022), the authors propose a physiologically relevant *in vitro* liver model formed by hepatic sinusoids with alternate cords of hepatocytes and non-parenchymal cells obtained by EBB. The bioink used was a mixture of Gel, silk fibroin, and liver ECM. The authors demonstrated that the co-culture of hepatocytes and non-parenchymal cells is more accurate than hepatocyte monoculture in predicting hepatotoxicity.

5.3.2. Bioprinting for liver disease modelling

Bioprinting can be used to develop precise liver disease models to study the underlying mechanisms and test the potential of drugs under development. Bioprinted Gel-Alg hydrogels were used to culture primary HCC cells obtained from 6 different patients. The cells retained the expression of specific HCC biomarkers as well as the genetic alterations and expression profiles of their original tumors. The model was used to evaluate the efficacy of candidate drugs for HCC (Xie et al., 2021). HCC models were also developed with photocrosslinkable liver dECM bioprinted through a rapid light-based process to tune the mechanical properties of the hydrogels (Ma et al., 2018). The dECM was mixed with photocrosslinkable GelMA to produce the bioink. By changing the light exposure time, the mechanical properties of the hydrogel increased from healthy liver values (0.5 kPa) to those of cirrhotic liver (15 kPa). HepG2 cells were less viable in the stiff scaffolds and had a significantly reduced expression of liver-specific markers, indicating that the cirrhotic mechanical environment plays a significant role in liver function.

Gel-Ma was used to model liver fibrosis for the co-culture of HepaRG and LX-2 cells (Cuvellier et al., 2021). The shear storage modulus of the hydrogels was controlled by the Gel concentration, from values ranging from 0.05 kPa to 2.12 kPa for 2.5% and 15% solutions, respectively. The printed structures were viable for one month and HepaRG cells were able to differentiate in 3D in the absence of dimethylsulfoxide. HSC were activated in response to TGF-β, depositing fibrillar collagen, suggesting the system's suitability for modelling liver fibrosis.

5.4. Current limitations on extrusion-based bioprinting

Although 3D bioprinting has allowed the cost-effective rapid manufacture of 3D models, there are still limitations and challenges to address before they can be applied to clinical applications.

Attending the definition of EBB, bioinks suffer shearing during the extrusion process limiting the lowest resolution that ensures cell survival. 3D structures below 150 μm of thickness are not possible for EBB (Miri et al., 2019; Zandrini et al., 2023). The limited resolution of EBB does not reproduce the hierarchical organization of the hepatic tissue that includes abundant vascularization and precise cell deposition to ensure long-term hepatotoxic experiments or research on liver diseases (Ma et al., 2020; Xiang et al., 2022). Vascularization is needed to ensure enough oxygen and nutrient supply, the maximum distance between vessels and cells to safely carry out cell culture is 400 μm. In fact, the integration of a fully functional vascular system is described as a strategy, which could solve the problem of maintaining long term cell culture successfully. However, current EBB methods cannot fabricate it due to the tissue complexity (Kang et al., 2016; Lovett et al., 2009). On the other hand, liver hierarchy has been described as crucial to support normal hepatic functionality and PHH survival. Liver sinusoids are structures with sizes of less than 10 μm, which display singular cell arrangement by sinusoidal endothelial cells in a radial disposition (Miri et al., 2019). Unfortunately, EBB does not offer resolutions down to 10 μm that could reproduce tissue microarchitecture and at the same time place cells as they would be in the native tissue.

Novel bioprinting technologies have tried to address the resolution problems by designing refined methods that allowed to print 3D structures smaller than 100 μm: stereolithography (SLA), DLP and volumetric bioprinting (VP). Despite these novel bioprinting techniques, resolution is still behind of what is expected to precisely recreate the tissue microarquitecture. SLA and DPL have obtained good results creating structures between 10-50 μm. Silk methacrylate hydrogels have been successfully bioprinted with cells, to reconstruct a trachea, with successfully transplantation in an animal model (Kim et al., 2020). Other natural polymers such as methacrylated chitosan have been bioprinted by DLP to study the effect of different photoinitiators and UV light on cell viability. In fact, it was demonstrated that HUVEC were safely bioprinted and suitable for DLP methods (Shen et al., 2020). Some hydrogels and resins have been reported with sizes close to the cell size but were cell-free or required a posterior cell seeding step and cannot be referred as bioinks or bioprinting (Bhusal et al., 2022; Regehly et al., 2020). Other approaches such us VP offer no shear stress, which made it attractive and feasible for bioprinting hepatic organoids. GelMA was used as bioink for hepatic organoids derived from liver healthy tissue to print them by VP into different patterns. Firstly, it was demonstrated that VP offered better cell metabolic activity and organoid size after 10 days compared to EBB, GelMA and Matrigel dooms. In addition, it was found a relationship between the pattern

printed and different hepatic basic functions such as ammonia detoxification and albumin synthesis (Bernal et al., 2022).

However, the bioink characteristics still need to be improved to allow the survival, and maintenance of the original cell functionality and morphology, an actual challenge for the current bioinks (Ma et al., 2020). Synthetic formulations have offered great mechanical properties or biocompatibility, despite this PEG hydrogels in particular did not show cell adhesion (Zhang et al., 1998). Other synthetic alternative such as Pluronic® yet displaying great 3D resolution present poor structural and biological properties (Kang et al., 2021; Smith et al., 2004; Wu et al., 2011). Natural hydrogels have tried to improve the outcomes of synthetic hydrogel blends by adding biological cues into the 3D environment. Despite the improvements that polymers such as Col, HA, Gel or chitosan have offered in terms of cell adhesion and cell survival, they still not fulfil the expectations of an optimal bioink. Col type I has been widely used as hydrogel or scaffold, currently EBB takes advantage of the crosslinking which occurs physiological conditions of temperature and pH. Additionally, Col has obtained sustained cell adhesion and survival along great cell functionality but poor mechanical properties due to an acute sensibility to MMP (Helary et al., 2010; Park et al., 2014). HA, Gel and chitosan have also the same drawbacks as mentioned for the collagen, low mechanical properties, fast degradation under physiological conditions and relatively long crosslinking times, which makes them difficult to apply in EBB (Hao et al., 2010; Jeon et al., 2007; Xing et al., 2014). Currently, Col, HA, Gel and chitosan have been blended with other polymers or modified by diverse methods to enhance their mechanical properties, delay their degradation and improve their crosslinking times (Billiet et al., 2014; Skardal et al., 2010, 2012).

In summary, additional research is needed before the optimal bioprinting method, bioink composition, and crosslinking mechanism are selected to drive the bioprinting into clinical practise (Sigaux et al., 2019).

Hypothesis

2D monolayer cell cultures do not truly reflect the actual liver microenvironment. New approaches aim to improve the behaviour of hepatic cells by reproducing the native tissue. The 3D platforms required are crosslinked polymers forming hydrogels which mimic the liver ECM, able to retain water and cells.

The hypothesis of the Doctoral Thesis is that by providing liver cells with a 3D environment *in vitro* very similar to what they find *in vivo*, we will maintain and improve their functionality for their use for studying and treating liver disease. Additionally, using injectable hydrogels that mimic liver ECM will upgrade the performance of the cells and will optimize both the delivery and retention of cells in the host liver that would likely increase the clinical efficacy of liver cell transplantation.

Objectives

The main objective of this PhD thesis is to determine the suitability of Gel and HA as biomaterials for liver tissue engineering. For this purpose, in addition to the characterization of the biomaterials, the fitness of these combinations for different *in vitro* and *in vivo* applications were explored. The specific objectives were:

1. To determine the physicochemical properties of injectable Gel and HA hydrogels that better mimic liver properties.

2. To evaluate the suitability of Gel-HA hydrogels for hepatic cell culture by analysing viability and key hepatic functions in HepG2 cells.

3. To study the suitability of Gel-HA scaffolds for culturing PHH. To this purpose, we evaluate the performance of the cells by means of urea and albumin synthesis, and phase I and II enzymes activity levels, and protein expression.

4. To analyse the effectiveness of hepatocyte-laden Gel-HA scaffolds *in vivo* using an animal model of acute liver failure.

5. To unravel the mechanisms implicated in APAP-induced liver injury and the response to cell transplantation.

6. To convert injectable Gel-HA hydrogels to bioinks in order to increase the throughput of the developed systems and create more complex models.

7. To determine the appropriateness of the developed bioinks for hepatic cell culture.

Materials

Gel-HA hydrogel synthesis required porcine gelatin type A, gel strength 300 (ref. G2500), hyaluronic acid from streptococcus equi (ref. 53747-10G), horseradish peroxidase (HRP) type IV (ref. P8375-1KU), hydrogen peroxide (30% w/w in H_2O_2, ref. H1009-100mL), tyramine hydrochloride (Tyr-98%, ref. T2879-25G), 2-(N-morpholino)ethanesulfonic acid (MES - 99%, ref. M3671-50G), N-hydroxysuccinimide (NHS - 98%, ref. 130672-25G), dialysis membranes 12.400 (ref. D0530-100FT) molecular weight cut off (MWCO) and 3500 MWCO (ref. SPEC132724), hydrochloric acid, sodium hydroxide, potassium chloride, sodium dihydrogen phosphate, HEPES salt, sodium chloride, glucose solution 1 M, bovine serum albumin (BSA), Hoescht 33342 and propidium iodide; were all purchased from Sigma-Aldrich (Spain). N-(3-Dimethylaminopropyl)-N′-ethylcarbodiimide (EDC, ref. RL-1022.0025) was obtained from Iris Biotech GmbH (Germany).

On the other hand, cell culture media and supplements as well as Dulbecco's phosphate buffered saline (dPBS) and penicillin-streptomycin-fungizone (PSS) were purchased from Gibco, (USA). Treated or non-treated well plates were bought from VWR (Spain). L-Glutamine and fetal bovine serum (FBS) were acquired from Biochrome AG (Germany). Bicarbonate 1 M was obtained from Grifols (Spain).

In vitro assays required the following reagents. Live dead fluorescent probes hoechst 33342 (ref. B2261) and propidium iodide (ref. P4170) both from Merck (USA). Urea QuantiChrom kit (ref. DUR2-100) was obtained from Bioassay System (USA). ELISA human albumin kit was obtained from Bethyl Laboratories Inc. (USA). AST/ALT colorimetric kits (refs. MAK055-1KT and MAK052-1KT respectively) were purchased from Sigma-Aldrich (Spain). Cytokine determination required a Luminex custom-designed multiplex cytokine magnetic bead panel from Merck-Millipore (MHSTCMAG-70K). Immunofluorescence for all eperiments employed the following primary antibodies; human albumin (ref. A80-229A) from Bethyl Labotatories Inc (USA), HNF4α (ref. 3113S) from Cell Signalling (USA) and alpha fetoprotein (ref. 203A-15) from Cell Marque (USA). The secondary antibodies were donkey anti-goat alexa 488 (ref. A11055), donkey anti-mouse Alexa 488 (ref. A21202) and donkey anti-rabbit Alexa 555 (ref. A31572) all from Thermo Scientific (USA)

Hydrogel degradation for DNA quantification required a variety of reagents. Quant.iT PicoGreen dsDNA Assay Kit (ref. 10545213) purchased from

Invitrogen (USA). Papain from papaya latex (ref. P4762-50MG), hyaluronidase type IV-S from bovine testes (ref- H3884-100MG) and L-cysteine (ref. 168149-100G) purchased from Merck Life Science SLU (Germany).

Miscibility experiments employed the fluorescent conjugated probes Texas Red™ (ref. A2665) and Oregon Green™ (ref. A6374), both purchased from Invitrogen-Thermo Fisher (USA).

Methods

1. Synthesis of tyramine conjugates

1.1. Gelatin tyramine conjugate (Gel-tyr)

The grafting of tyramine in the Gel is produced by the reaction of the carboxyl groups (-COOH) in the Gel chains and the amine groups ($-NH_2$) of the tyramine, as observed in Figure 7. The procedure was adapted from Kurisawa *et al.* (Kurisawa et al., 2005). We used the same molar ratios as Poveda-Reyes *et al.* (Poveda-Reyes et al., 2016), 2:1 for Tyr:COOH, 2:1 for EDC:COOH, 1:1 for EDC:Tyr and 1:10 for NHS:EDC.

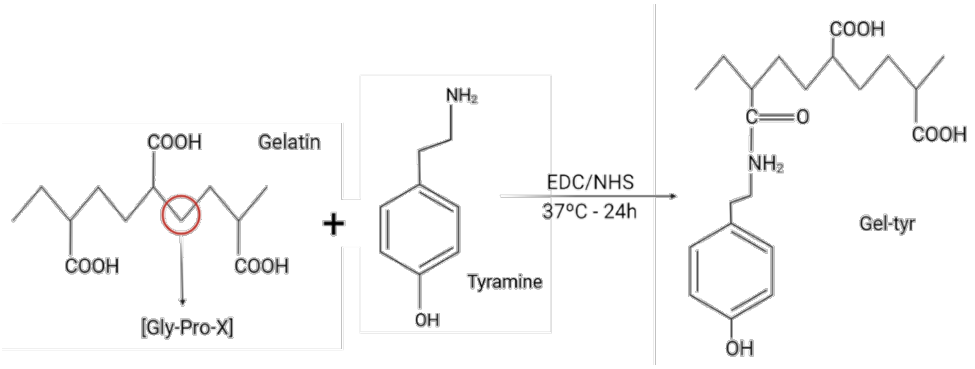

Figure 7. Tyramine grafting on Gel chains through EDC/NHS chemistry. *Image created by Biorender.*

First, 0.4 g of Gel were dissolved into 20 mL of mQ water (20 mg/mL) and then 195.24 mg of MES were added to stabilize the pH. The solution was stirred for 30 min at 60 ºC. After that, 113.13 mg of tyramine hydrochloride were added and stirred for 20 min at room temperature. The pH was adjusted to 6 by adding drops of a 0.1 M solution of NaOH. Subsequently, 7.36 mg of NHS were added and stirred for 30 min, before adding 122.8 mg of EDC. This solution was left 24 h at 37 ºC under stirring.

After the tyramine grafting was completed, the product was purified by dialysis against deionized water with a membrane of 12400 MWCO for 2 days and changing the water 3 times per day. Finally, the tyramine conjugate of Gel (Gel-tyr) was frozen during 24 h at -80 ºC and then freeze-dried for 3 days for further use.

1.2. Hyaluronic acid tyramine conjugate (HA-tyr)

The procedure to obtain tyramine grafted HA was described by Sakai *et al* (Sakai et al., 2014), based on the chemistry that Kurisawa *et al.* applied for tyramine grafts onto Gel (Kurisawa et al., 2005). During the reaction, the carboxylic groups (-COOH) of the HA are activated and linked to the amine groups ($-NH_2$) of the tyramine, forming amide bonds, as observed in Figure 8. Tyramine grafting can be performed in HA of different molecular weights. In this thesis high molecular weight (HMW) (1.5-1.8 x 10^6 Da) and low molecular weight (300 kDa) were grafted for different purposes (Poveda-Reyes et al., 2016). Low molecular weight HA required a first step of acidic degradation (Shu et al., 2002).

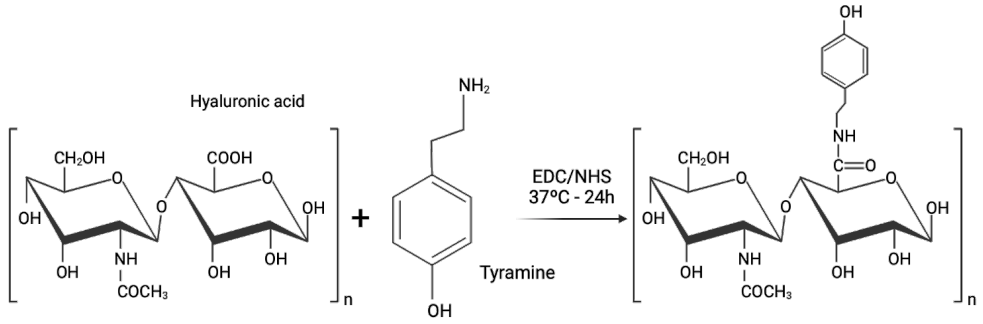

Figure 8. Tyramine grafting on HA chains through EDC/NHS chemistry. *Image created with Biorender.*

When required, and before starting the reaction, the molecular weight of pristine HA was reduced by acidic degradation. For this, a solution of HA was firstly prepared by dissolving 500 mg of HA in 50 mL of miliQ water, stirring for 24 h at 4 ºC. Then, the pH was adjusted to 0.5 by the addition of HCl, and acidic degradation took place for 24 h at 37 ºC. In this step, the molecular weight was reduced from 1.5-1.8 x 10^6 Da to 300 kDa (Poveda-Reyes et al., 2016). After this, the pH was adjusted to 7 by adding NaOH and the product was purified by dialysing against deionized water for 3 days with a membrane of 3,500 MWCO. Water was changed 3 times per day. At that point, low molecular weight HA solution was frozen at -80 ºC for 24 h and then freeze-dried for 3-4 days.

20 mL of a solution of either low or high molecular weight (pristine) HA was performed by adding 100 mg of HA in a mQ water solution containing 175.3 mg of sodium chloride (NaCl), 1.08 mg of MES (acting as a pH stabilizer) and 0.3 mL of NaOH, adjusted to pH 5.75 before adding HA. The solution was kept in agitation at room temperature for 4 h. Once dissolved, 85.64 mg of HCl-tyr were

added, stirring at room temperature for 20 min, and the solution was again adjusted to a pH of 5.75. After this, 47.77 mg of EDC and 2.87 mg of NHS were added, with agitation at 37 ºC for 24 h. In this step the grafting of tyramine molecules onto the HA chains took place. The amounts of reagents were selected respecting the same molar ratios as in (Poveda-Reyes et al., 2016); 2:1 for Tyr:COOH, 1:1 for EDC:COOH, 1:2 for EDC:Tyr and 1:10 for NHS:EDC

The solution was purified for 2 days using a 3500 MWCO dialysis membrane. The first day against a 150 mM NaCl solution and the second day against distilled water. The solution was then frozen at -80ºC and subsequently freeze-dried for 4 days. The particularity of the HA tyramine grafting is that all the processes must be carried out with the containers covered with aluminium foil since it is photosensitive.

1.3. UV-spectrophotometry for quantitative tyramine grafting evaluation.

Tyramine substitution degree determines hydrogel properties such as gelation time, crosslinking density, swelling, mechanical properties, etc. UV-spectrophotometry allows the quantification of the grafted tyramine onto the polymers by an absorbance peak at 275 nm (Darr et al., 2009; Loebel et al., 2015), characteristic wavelength of phenol groups of the tyramine, in measured solutions. Every batch of tyramine conjugated polymer was assessed to ensure that all experimentation was performed with an almost similar polymer. Absorbance measurements were made on solutions of products (Gel-tyr and HA-tyr) at 0.1% wt/v in water mQ with a *Cary 60 UV-vis* spectrophotometer (Agilent Technologies). Quartz cuvettes were filled with 450 µL of the dissolution and measured 3 times per batch. These measurements allow to determine the concentration of tyramine grafted on Gel and HA in mg/mL by using a calibration curve of HCL-tyr solutions (450 µL) of known concentrations (0.0125, 0.025, 0.05, 0.1 and 0.125 mg/mL, measured in the spectrometer). The calibration line together with the molecular weight of tyramine (137.18 g/mol) provides the experimental concentration (in mol/mL) of tyramine present within the polymers (Gel-tyr and HA-tyr). Then, the volume of the measured dissolution and the concentration allow to calculate the number of mol of tyramine in Gel-tyr and HA-tyr. Every mol of grafted tyramine corresponds to a substituted carboxylic (-COOH) group within the chains of the polymers. Then, knowing the number of -COOH of pristine Gel and HA the substitution degree of tyramine (effectively substituted -COOH groups / total number of -COOH groups in pristine polymers) could be calculated. For this we take into account that Gel has 80 mM of -COOH

per 100 mg of polymer (manufacturer's data) and HA has one -COOH per each disaccharide unit (of 401 g/mol molecular weight).

1.4. Attenuated total reflectance Fourier transformed infrared (ATR-FTIR) spectroscopy for qualitative evaluation of tyramine grafting and hydrogel forming.

Complementary to the quantitative evaluation explained at section 1.3, we qualitatively ensured the presence of tyramine molecules by (Bruker Optics ATR-FTIR Alpha II) ATR-FTIR. Unmodified Gel and HA controls were employed to compare with modified polymers, Gel-tyr and HA-tyr. Hydrogels crosslinking by HRP/H_2O_2 can create two different types of chemical bonds: C-C bond between two phenolic carbons of the tyramine molecule or C-O ester bonds between one phenolic carbon and the terminal -OH group of tyramine molecule (Kurisawa et al., 2005). Thereby, Gel-HA dried hydrogels were measured to have a qualitative overview of the bonds created when preparing the hydrogels based on their characteristic FTIR peaks.

Dry sample of each polymer (Gel, HA, Gel-tyr and HA-tyr) or Gel-HA hydrogels were obtained by freeze drying samples at least for 24 h. In addition, samples were dried in vacuum at 60 ºC to ensure that all the water was removed from the hydrogels. Measurements were preceded by a blank measurement that determined the environmental noise, which was subtracted to normalize the spectra of each sample. ATR-FTIR spectra were obtained in transmittance mode from 800 cm^{-1} to 4000 cm^{-1}, at a wavelength resolution of 4 cm^{-1}. ATR-FTIR spectra were performed after 64 scans for each sample.

1.5. Gel-HA hydrogel preparation

Hydrogels were obtained with different proportions of 2% wt/vol Gel-HA freeze-dried solutions (100-0, 80-20, 50-50, 20-80 and 0-100 vol/vol) in F12 medium at 37 ºC. Gel solution was prepared at 37 ºC for 30 min. HA solution was prepared at 4 °C for 24 h and heated to 37 °C for hydrogel preparation. Hydrogels were obtained by mixing 80 vol% of the Gel-HA mixtures in different proportions, 10 vol% of 12.5 U/mL HRP (1.25 U/mL in the final volume) and 20 mM H_2O_2 (2 mM in the final volume).

1.6. Gel-HA scaffold preparation

Tyramine derivatives of Gel and HA (Gel-tyr and HA-tyr) were dissolved in Calcium Free Krebs Ringer Buffer (CFKRB) at 2% wt/vol. The Gel-HA 20-80 hydrogel mixture was prepared in handmade cylindrical silicon moulds of 10 mm diameter with a solution volume of 250 µL. After 30 min of crosslinking at 37 °C, samples were soaked in dPBS for 24 h until equilibrium. Then, they were cleaned 3 times with milliQ water, frozen with liquid nitrogen for 2 min and lyophilized to obtain the scaffolds. The upper layer of the samples was peeled with a scalpel to show the pores of the scaffolds. Scaffolds were stored in a dry environment until use.

2. Physicochemical properties of Gel-HA hydrogels

2.1. Rheology.

2.1.1. Mechanical properties and viscosity of Gel-HA hydrogels.

Measurements were made in a Discovery HR-2 Hybrid (*TA Instruments*) rheometer and processed with TRIOS software (*TA Instruments).* Environmental conditions were set at 37 °C and a solvent trap geometry was used to reduce water loss during the experiment. Parallel plates of 20 mm diameter with a gap between them of 1100 µm were used for the hydrogels.

Gelation kinetics was recorded *in situ* by the addition of H_2O_2 to the mixture of polymer and HRP, previously placed in the lower plate of the device. The experiments had three steps: a time sweep for 45 min (strain and frequency fixed at 1% and 1 Hz, respectively) to determine gelation time, an amplitude sweep from 0.01% to 20% (frequency at 1 Hz) to fix the linear viscoelastic region and a frequency sweep to characterize crosslinked hydrogels from 0.1 Hz to 10 Hz (strain at 1%).

Rheological experiments provided the shear storage (G') and loss (G'') moduli of the samples Tan δ, is the ratio between G'' and G', also known as "loss factor" or phase angle (equation 1). It indicates the relationship between the energy dissipated and stored by the samples in a cycle of deformation and is connected with their viscoelasticity.

$$tan\,\delta = \frac{G''}{G'}$$

Equation 1. *Definition of tanδ.*

In addition, the viscosity of the Gel-tyr and HA-tyr hydrogel precursor solutions was evaluated. The solvent trap and the 20 mm diameter geometries were used. Viscosity analysis was performed in a single step of flow sweep from 0.001 to 1000 s^{-1} at 37 ºC.

2.1.2. Mechanical properties of Gel-HA scaffolds by rheology evaluation.

Rheology of Gel-HA scaffolds followed a similar experimental set up as mentioned in section 2.1.1 for Gel-HA hydrogels. Scaffolds, after crosslinking, were equilibrated in PBS for 24 h. Then, rheology analysis was performed with parallel plates of 12 mm diameter and adjusting the gap between plates manually for each replicate, fixing an axial force of approximately 0.1 N. The same amplitude and frequency sweeps used for the hydrogel's measurements were used.

2.1.3. Viscosity of Gel-HA inks and mechanical properties of printed hydrogels.

Viscosity measurements followed the protocol and environmental conditions mentioned in the section 2.1.1. The inks to be measured were placed on the lower plate of the rheometer and the upper plate gap was adjusted for the adequate filling of the space between plates. All the solutions characterized contained grafted tyramine and were composed of HA HMW and Gel-HA HMW mixtures.

For the Gel-HA HMW mixtures, the pure materials were dissolved separately and mixed in a ratio (20-80) using a syringe-to-syringe method to homogenize. CELLINK START is a standard ink provided by Cellink (Sweden) and was used as control for optimal viscosity due to its excellent extrudability. The viscosity (Pa·s) was represented against the shear rate (1/s) applied in the rheometer.

Mechanical properties of the printed hydrogels were also determined. In this case, only the Gel-HA HMW mixtures were evaluated, as they resulted optimal

for the cell culture experiments. Printed hydrogels with or without encapsulated cells were measured following the protocol described for the Gel-HA scaffolds of section 2.1.2.

2.2. Equilibrium water content

The equilibrium swelling of the hydrogels was characterized by using cylindrical samples prepared in moulds of 10 mm diameter with precursor solutions of 250 µL. Once crosslinked, hydrogels were swollen until equilibrium for 24 h in dPBS 1x at 37 °C. The hydrogels were rinsed three times with mQ water to remove salts from the dPBS and weighed to obtain the swollen mass (m_w). Then, they were lyophilized to obtain the dry mass (m_d). Equilibrium water content (w) was calculated referred to the dry mass by equation 2:

$$w = \frac{m_w - m_d}{m_d}$$

Equation 2. *Equilibrium water content formula for hydrogels and scaffolds.*

The volumetric swelling ratio (Q_v) was calculated with the data of w as previously described (Poveda-Reyes et al., 2016). The swelling capacity of the scaffold was also determined by swelling 3 different replicates of dry scaffolds in the same conditions as for the hydrogels.

2.3. Crosslinking density of Gel-HA hydrogels

Crosslinking density (ρ_x) (mol of chains per unit volume of polymer) determines relevant properties of hydrogels such as mechanical properties or the swelling. For this purpose, it was calculated as in (Poveda-Reyes et al., 2016), but considering that the hydrogels were crosslinked in aqueous medium (relaxed state (Richbourg et al., 2020) (Equation 3):

$$\rho_x = \frac{-ln(1-\phi_p) - \phi_p - \chi \cdot \phi_p^2}{v_w \phi_{p,r}^{2/3} \phi_p^{1/3}}$$

Equation 3. *Crosslinking density formula of hydrogels.*

Being ϕ_p and $\phi_{p,r}$ the volume fraction of polymer in the swollen and relaxed states, respectively, χ the Flory Huggins interaction parameter (0.49 for Gel (Leach et al., 2003) and 0.473 for HA (Bohidar, 1998) and v_w the molar volume of water.

2.4. Scaffold porosity

Morphology of the scaffold microstructure was characterized by observing cross-sections of lyophilized Gel-HA 20-80 scaffolds. Field emission scanning electron microscope (FESEM) (Ultra 55, Zeiss) was employed at an acceleration voltage of 2 kV. Sample sections were obtained with a blade cutting a thin transversal section from each scaffold. Samples were sputter coated with platinum previously to the observation. Images were treated with ImageJ software (FIJI) to obtain the mean pore size and area of the scaffold.

2.5. Estimation of Young's moduli of hydrogels in the swollen state.

The relationship between the shear storage modulus (G') of a material and its Young's modulus (E') has been widely described by the following equation 4, in which ν corresponds to the Poisson's ratio of the material (Subramani et al., 2020).

$$G' = \frac{E'}{2(1+\nu)}$$

Equation 4. *Relationship between the shear storage modulus (G') and the Young's modulus (E') of a material through its Poisson's ratio (ν).*

In many cases, hydrogels behave as elastomers, which at constant temperature deform at constant volume and energy. Pure elastomers have a Poisson's ratio of 0.5 which means that the relationship between the shear storage modulus of a hydrogel and its Young's modulus follows the equation 5 (Oppermann et al., 1985).

$$G' = \frac{E'}{3}$$

Equation 5. *Relationship between G' and E' after considering that hydrogels behave like elastomers (ν = 0.5).*

When hydrogels are crosslinked in the presence of a certain amount of water, the state just after crosslinking has been described by Peppas and Merrill as the hydrogel relaxed state (*r*) (Peppas et al., 1977). In the relaxed state one can assume that the volume fraction of the hydrogel remains constant during the crosslinking process, which means that the polymer chains do not stretch or accumulate elastic energy. By assuming this, the theoretical approximations of rubber elasticity and equilibrium swelling theories remain valid and can be

applied to hydrogels that are crosslinked in the presence of a solvent (Richbourg et al., 2020).

The values of G' and E' not only depend on the crosslinking density, but also change with the amount of water within the hydrogel (dry state, relaxed state after crosslinking with water or swollen state after equilibrating it in a certain environment). As in our study we characterized our hydrogels in the relaxed state, we can have an estimation of the elastic modulus after swelling them for 24 h in PBS, if we apply the rubber elasticity theory.

The Young's modulus of the hydrogel network in the dry state (that ideally only depends on the crosslinking density (ρ_x), perfect gas constant (R – J/molK) and temperature (T – K), as indicated in Equation 6 (Richbourg et al., 2020).

$$E'_{dry} = 3\rho_x RT$$

Equation 6. *Young's modulus for a dry ideal network.*

This equation is modified when the hydrogel network is equilibrated in a certain environment and absorbs an equilibrium water content (Equation 7), by the previously defined parameters ϕ_p and $\phi_{p,r}$ described in section 2.3, allowing the estimation of the Young's modulus of the hydrogel in the swollen state (Richbourg et al, 2020):

$$E'_{swollen} = 3\rho_x RT\phi_p^{1/3}\phi_{p,r}^{2/3}$$

Equation 7. *Estimation of the Young's modulus of a swollen hydrogel*

3. *In vitro* cell culture with HepG2 cells

3.1. Culture of HepG2 cells in Gel-HA hydrogels

HepG2 cells are a cell line isolated from a HCC, widely used in Hepatology. HepG2 cells (ECACC No.85011430) were cultured in Ham´s F-12/Leibovitz L-15 (1:1 v/v) media supplemented with 7% newborn calf serum, 50 U penicillin/mL and 50 µg streptomycin/mL. Solutions of different proportions of Gel+HRP and HA+HRP (100-0, 80-20, 50-50, 20-80 and 0-100 vol/vol) were prepared as previously described.

For subculturing purposes, medium was removed from the flasks and cells were washed with dPBS. Cells were detached by treatment with 1 mL of (0.25%) trypsin/ (0.02%) Ethylenediaminetetraacetic acid (EDTA) at 37 °C for 3-4 min.

Then, the trypsin was inactivated by adding 10 mL of HepG2 cell culture media, and the whole volume centrifuged in a falcon tube at 1500 rpm during 3 min. The supernatant was removed, and the pellet was resuspended in 10 mL of culture media. 10 μL of the cell suspension were loaded onto a Neubauer chamber to estimate cell density.

Hydrogels were seeded with 200.000 cells. For this, the desired number of cells was initially resuspended in 90 μL of the Gel-HA+HRP previously mixed and then dropped into each cell culture well and crosslinked with 10 μL of 20 mM H_2O_2 onto each hydrogel without placing the tip inside the drop, resulting Gel-HA hydrogels of 100 μL.

3.2. Live-dead staining

Viability was determined by incubating the cultures with Hoechst 33342 (1.5 μg/mL) and propidium iodide (PI) (1.5 μg/mL) for 30 min. Then, the culture medium was removed, and the samples observed under a fluorescence microscope using the appropriate filters (INCELL6000 Analyzer, GE Healthcare). Cell viability was determined by PI exclusion. Non-viable cells with compromised membrane permeability were identified by their positive red fluorescence in the nuclei. The collected images were analysed using the INCELL Workstation module. Background correction was applied to all the images before being quantified. Cell count was assessed from the Hoechst 33342 staining. The nucleus was defined as the main object using an edge detection algorithm. To separate individual cells, segmentation was applied. Cell viability was determined by PI exclusion in the main object.

3.3. Hepatic functionality of HepG2 cells

3.3.1. Urea synthesis

The ureogenic capacity was assessed by the incubation of HepG2 cells with NH_4^+ and analysing the amount of urea produced. After, cell culture the culture media was removed and 300 μL of a Hepes saline solution supplemented with 1 mM of calcium chloride and 2 mM of ammonium chloride were added to each well. Cells were maintained in the presence of ammonium for a total of 3 h 30 min, 120 μL of the supernatant were collected after 30 minutes, and the remaining 180 μL were collected after 3h and 30 min. Thus, the calculation of the increase in urea production was obtained by subtracting the values after 3h and 30 min and those from the 30 min, leaving the urea production after 3 h of treatment. All the supernatant removed was centrifuged for 5 minutes at 5000

rpm to discard aggregates. Then, the remaining supernatant was transferred to another Eppendorf and frozen at -20 ºC till the evaluation.

A standard curve was prepared, following manufacturer's instructions. Final concentrations of this curve ranged between 0.00 and 4.00 mg/mL in (Table 2).

Table 2. *Calibration curve for urea synthesis evaluation*

Urea (0.1 mg/mL)	0 µL	5 µL	10 µL	20 µL	30 µL	40 µL
Deionized water	50 µL	45 µL	40 µL	30 µL	20 µL	10 µL
Urea concentration	0.0 µg/mL	0.5 µg/mL	1 µg/mL	2 µg/mL	3 µg/mL	4 µg/mL

The samples were thawed and centrifuged at 8000 rpm for 3 min and 50 µL of the supernatant were pipetted into a well of a 96-well plate. For the blanks, the same volume was pipetted in other wells, consisting of NH_4Cl in saline Hepes that is the solution previously used for the incubation of the cultured hydrogels. Two reagents A and B, non-specified composition, were used to produce a colorimetric change on the solution, by the reaction of the o-phthaladehyde/primaquine with urea (Jung et al., 1975; Zawada et al., 2009). A 1:1 solution of the reagents was prepared, considering that there is a 20 min window of stability of the mixture. 200 µL of this solution were added to each well, and kept at room temperature for 30 min, protecting the plate from light to avoid interference.

Absorbance of the samples was measured at 520 nm. The ureogenic capacity was expressed as µg/µg DNA/min.

3.3.2. Albumin secretion by ELISA assay

Albumin synthesis and secretion into the culture media was measured as a specific hepatic function by ELISA (Enzyme-Linked ImmunoSorbent Assay) following manufacturer's protocol. A simplified scheme of ELISA sandwich is shown in Figure 9.

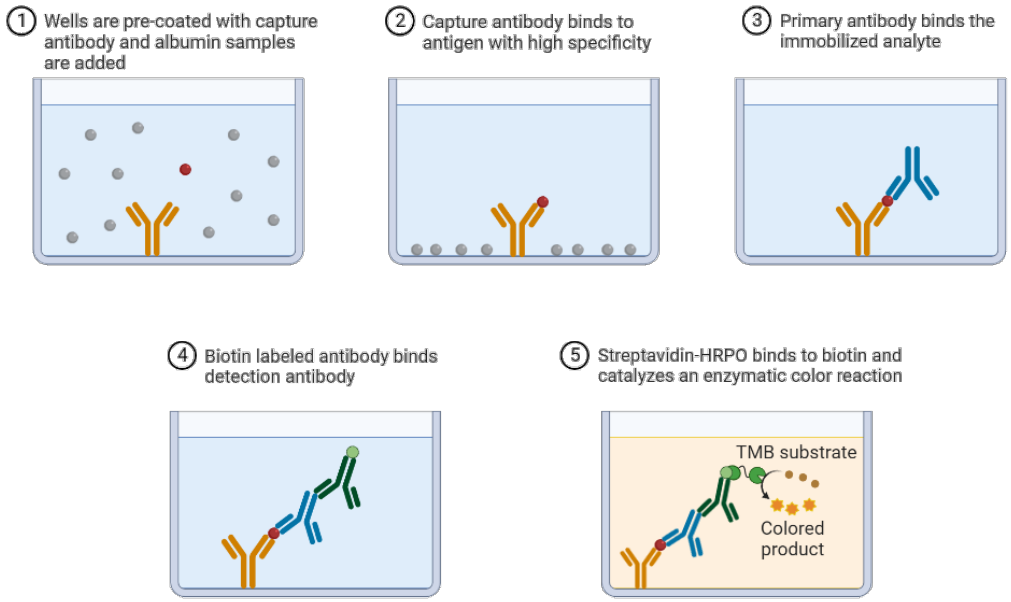

Figure 9. ELISA sandwich scheme for albumin quantification. *Image created with Biorender.*

First, 100 µL of the blank (dilution buffer) and the samples (PHH culture medium) were added to the wells (run in duplicate). To prepare the standard solution and standard curve (Table 3), 500 ng hAlbumin was reconstituted with 1 mL of 1X Dilution Buffer C, provided in the kit and was prepared according to the concentrations of the Table 3. Then, the plate was covered and incubated at room temperature for 1 h allowing the albumin to bind with capture antibodies.

***Table 3**. Calibration curve proportions for human albumin assay*

hAlbumin concentration	Dilution buffer C (1x)	hAlbumin
500 ng/mL	1 mL	500 mg (lyophilized)
167 ng/mL	300 µL	150 µL (DNA 500 ng/mL)
55.6 ng/mL	300 µL	150 µL (DNA 167 ng/mL)
18.5 ng/mL	300 µL	150 µL (DNA 55.6 ng/mL)
6.17 ng/mL	300 µL	150 µL (DNA 18.5 ng/mL)
2.06 ng/mL	300 µL	150 µL (DNA 6.17 ng/mL)
0.69 ng/mL	300 µL	150 µL (DNA 2.06 ng/mL)
0 ng/mL	300 µL	0 µL

Then, anti-albumin detection antibody was added to each well, properly mixed by tapping the well plate, covered again, and incubated at RT for 1 h. After this, wells were washed four times with 1X Wash Buffer. Then, HRP solution A was added to samples and blank, covered and incubated for 30 min at RT, and then, washed with 1X Wash Buffer. Subsequently, 3,3',5,5'-Tetramethylbenzidine (TMB) substrate was added, and the enzymatic reaction was incubated at room temperature and for 30 min in the dark, turning the solution into blue. The plate was not covered during the incubation. To stop the reaction, Stop Solution was poured in each well and the plate tapped to mix, the blue colour changed from blue to yellow. After this, and within the next 30 min the absorbance was measured on a plate reader at 450 nm.

Finally, the albumin secreted by the cells was quantified according to the standard curve in µg of albumin/min. Albumin was also normalised with DNA from each sample in the same way as the ureogenic capacity assay. Hence resulting in the albumin synthesis expressed in µg/µg DNA/h.

3.3.3. Hydrogel enzymatic degradation for DNA extraction

Gel-HA hydrogels were enzymatically degraded for DNA extraction. Gel was firstly degraded with papain and HA was then degraded with hyaluronidase.

Each enzyme was prepared in a specific buffer which fulfils the requirements for a correct enzyme activity. Papain was prepared in a phosphate salt-based buffer, adding NA_2HPO_4 (4.5 mM), NaH_2PO_4 (5.5 mM) and EDTA (5 mM). In addition, papain buffer had to contain L-cysteine (1.57 mg/mL) which helps to the enzyme stability preventing the activity lose. On the other hand, hyaluronidase needed $CaCl_2$ (140 mg/L), $MgCl_2$ (100 mg/L), $MgSO_4$ (100 mg /L), KCl (400 mg/L), KH_2PO_4 (60 mg/L), $NaHCO_3$ (350 mg/mL), NaCl (8000 mg/L) and NA_2HPO_4 (48 mg/L). Both were adjusted to the optimal pH 6.5 and 7 for papain and hyaluronidase respectively.

After the enzyme preparation, Gel-HA samples were thawed and 500 µL of papain were added to each sample and mixed with the vortex. Gel degradation took place during the following 18 h at 60 ºC. Afterwards, the samples were cooled down to room temperature and 25 µL of hyaluronidase were added for 3 h at 37 ºC. Finally, sample's DNA was kept at -20 ºC upon quantification.

3.3.4. DNA quantification by PicoGreen assay

PicoGreen assay consists of the quantification of DNA extracted from cell cultures. The technique is based on the interaction of a fluorescent molecule (PicoGreen) with the cellular DNA. The protocol followed manufacturer's instructions.

Each well contained 30 µL sample + 70 µL Pico-Green (diluted) + 100 µL TE 1X buffer (TE 20X diluted in mQ water), corresponding to a total of 200 µL per well. Afterwards, Pico-Green was added to the 1X TE solution, already considering the 70 µL of PicoGreen diluted and the TE 1X necessary for each sample. The standard curve was prepared according to the recommendations of the distributor following a 1:3 dilution from a λ-DNA standard stock 100 µg/mL (Table 4). Finally, after the addition of PicoGreen the samples were left for 5 min at RT and the absorbance of the samples was read at 485 nm.

Table 4. *PicoGreen standard curve preparation from a λ-DNA standard*

Standard curve concentration	Phosphate buffer volume	Volume DNA (Stock)
2500 ng/mL	146.25 µL	3.75 µL
833.33 ng/mL	100 µL	50 µL (DNA 2500 ng/mL)
277.78 ng/mL	100 µL	50 µL (DNA 833.33 ng/mL)
92.59 ng/mL	100 µL	50 µL (DNA 277.78 ng/mL)
30.86 ng/mL	100 µL	50 µL (DNA 92.59 ng/mL)
10.28 ng/mL	100 µL	50 µL (DNA 30.86 ng/mL)
3.42 ng/mL	100 µL	50 µL (DNA 10.28 ng/mL)

4. *In vitro* assays with primary human hepatocytes

4.1. Gel-HA scaffold sterilization

The Gel-HA 20-80 scaffold was sterilized with ethanol. The procedure required the following steps. First, 3 washes of 45 min with ethanol 70%, 1 wash of 30 min with ethanol 50%, 1 wash of 20 min with ethanol 30% and lastly 4 washes of 10 min with mQ water. Then, sterile Gel-HA scaffolds were maintained in F12 medium for 24 h as a preconditioning step prior to PHH seeding.

4.2. Isolation and culture of primary human hepatocytes

Liver samples were obtained in agreement with the rules of the hospital's Ethics Committee (2019/00111/PI) and the study was conducted in accordance with the principles of the Declaration of Helsinki. Informed consent was obtained from all subjects involved in the study. PHH were isolated from whole cadaveric livers using a two-step collagenase perfusion technique. Perfusion of collagenase was performed by a peristaltic pump at a flow rate of 200 mL/min. Free suspended PHH were obtained after tissue disruption, they were filtered and washed three

times by centrifugation 500xg for 5 min (Bonora-Centelles et al., 2010). Cellular viability was assessed by the dye exclusion test with 0.4% trypan blue. PHH were cryopreserved in ice-cold Cell Banker medium as previously described (Donato et al., 2020) at a density of 10^7 viable cells/mL. Cells were thawed (after being stored in liquid nitrogen for at least 2 weeks) in the Hepatocyte cell culture medium and were centrifuged at 100g for 3 min.

Culture medium for PHH was prepared by mixing Ham's F-12/Williams medium (1:1) supplemented with glutamine (2.5 mM), glucose (17 mM), transferrin (25 μg/mL), ascorbic acid (0.62 mM), ethanolamine (68.8 μM), linoleic acid (7.7 μM), N-omega-nitro-L-arginine methyl ester (0.64 mM), penicillin (50 U/mL), streptomycin (50 μg/mL), newborn calf serum (2%) and BSA (1 g/L) (Gómez-Lechón et al., 2006). Cell culture was removed from the wells and two million viable cryopreserved/thawed PHH were added within the scaffold by pipetting 30 μL of the cell suspension onto the top part of the scaffold. Monolayer culture served as reference for cell viability and hepatic functionality. PHH were seeded on a fibronectin/collagen type I-coated wells at a density of 2×10^5 cells (Bonora-Centelles et al., 2010; Tolosa et al., 2014). After 1 h, culture medium was added. Firstly, PHH cell viability was evaluated after 24 h of culture (method described in section 3.2.5).

Additionally, hepatic functions such as urea synthesis, albumin secretion, activity of CYP (phase I enzyme) and UDP-glucuronosyltransferase (phase II enzymes) activities were evaluated after 24 h of cell culture.

4.3. Primary human hepatocyte functionality

4.3.1. Phase I enzyme (Cytochrome P450) activity

The metabolism of different specific substrates was evaluated in PHH seeded on 96-well plates using the high-performance liquid chromatography/mass spectrometry (HPLC–MS/MS) system. For each individual CYP activity assay, a specific probe was used (Table 5). The cocktail of substrates was prepared according to the concentrations presented in the protocol made by Lahoz (Lahoz et al., 2007).

Table 5. *Cocktail of substrates to evaluate metabolic activity of the CYP.*

CYP	Substrate	Final concentration	Metabolite
1A2	Phenacetin	10 µM	Acetaminophen
2A6	Coumarin	5 µM	7-H0-Coumarin
2B6	Bupropion	10 µM	H0-Bupropion
2C19	Mephenytoin	50 µM	4´-H0-Mephenytoin
2C9	Diclofenac	10 µM	4´-H0-Diclofenac
2D6	Bufararol	10 µM	Hydroxybufuralol
2E1	Chlorzoxazone	50 µM	6-H0-Closzoxazone
3A4	Midazolam	5 µM	1´-H0-Midazolam

Activity assays were performed by the direct incubation of cell cultures with the substrates for 120 minutes. Then, supernatant was collected and centrifuged for 3 min at 5000 rpm. Finally, the samples were transferred to an Eppendorf and frozen at -80 ºC until evaluation. The final evaluation was carried by the Analytic Service from the IISLAFE, which used the Ultra Performance Liquid Chromatography-Mass Spectrometer (UPLC-MS/MS) methodology to assess the hydroxylation of the substrates, which indicates the activity of Phase I enzymes. The activity for each specific isoform was referred as pmol of the metabolites produced in the period of incubation.

4.3.2. Phase II enzyme (UDP-glucuronosyltransferase) activity

UDP-glucuronosyltransferase (UGT) activities were assayed by incubating cultured cryopreserved/thawed PHH with the corresponding selective substrates: 15 µM β-estradiol (UGT1A1), or 250 µM naloxone (UGT2B7) as previously described (Donato et al., 2010). The formation of the corresponding metabolites was measured HPLC/MS, as previously described in detail (Donato et al., 2010; Donato et al., 1993).

4.4. Immunofluorescence

After 24 h in culture, samples were fixed with 4% formaldehyde for 20 min and washed 3 times with dPBS. Fixed samples were soaked in 30% wt/vol sucrose in dPBS overnight and included in OCT. Then, samples were cut at 40 µm with the cryostat Leica CM 1860 UV.

Cryosections were permeabilized with 0.1% Triton X100 in PBS for 20 min at room temperature, washed with PBS, blocked with dPBS containing 3% BSA for 1 h at room temperature. Then, the sections were incubated overnight at 4 °C with an albumin primary antibody diluted (1:100) in 1% BSA-dPBS. Sections were washed (three times) and incubated for 1 h with the appropriate secondary antibody anti-goat Alexa 488 (1:200) diluted in 1% BSA-dPBS. Sections were then washed (three times), incubated with Hoechst 33342 (2 µg/mL) for the detection of nuclei and then mounted using Gelmount solution. Specificity controls, performed by omitting the primary antibody, resulted in the abolition of immunostaining. Images were obtained under a confocal microscope (Leica, DMI8).

5. *In vivo* experimentation on ALF model with SCID rodents

5.1. Animals and induction of ALF by APAP overdose.

Animals were housed at the animal facilities of the Instituto de Investigación Sanitaria La Fe. All animals had free access to food and water in a temperature-controlled room with a 12-hour dark/light cycle. All the animals received human care and all the experimental protocols were approved by the Institutional Animal Ethics Committee of La Fe Hospital and performed in accordance with Spanish national and institutional regulations and following EU Directive 2010/63/EU for animal experiments. All animal experiments complied with the ARRIVE guidelines. Male NOD/SCID mice (4–6 weeks) were treated with 300 mg paracetamol/kg body weight to induce ALF 16 hours prior to cell transplantation. ALF was evaluated by means of histological staining and determination of transaminases in the sera of treated animals.

5.2. Intraperitoneal transplantation of Gel-HA scaffolds containing hepatocytes into mice with ALF

Scaffolds were transplanted into the peritoneal cavity of ALF animals 16 h after APAP injection. The animals were allocated into four experimental groups (Figure 10): group 1 (Control: non-treated animals), group 2 (APAP: animals with ALF infused only with 200 µL of infusion medium), group 3 (APAP+C: transplanted with 2×10^6 PHH intrasplenically), and group 4 (APAP+SC: transplanted with Gel-HA scaffolds containing 2×10^6 PHH). Animal number was initially set for 8 animals per experimental group.

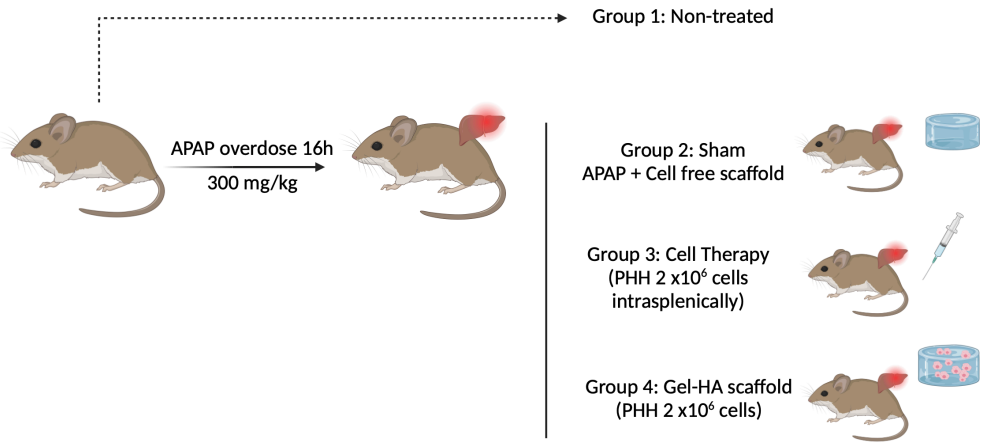

Figure 10. Schematic representation of animal groups on ALF animal model experiments. *Image created with Biorender.*

Mice were anesthetized with a sevorane/O_2 mixture. All the animals were closely monitored until recovery and were allowed free access to food and water. At 1, 3 and 7 days after transplantation, mice were sacrificed, and the liver removed for further analyses. Liver samples were frozen for oxidative stress analyses or stored in 4% paraformaldehyde for pathologic and immunofluorescence analyses. Blood samples were collected, centrifuged and serum samples stored at -20 °C for quantification of human albumin by ELISA, transaminase levels and cytokine production.

5.3. Transaminases levels (ALT/AST) determination

Serum levels of alanine aminotransferase (ALT) and aspartate aminotransferase (AST) are the most sensitive indicators of liver function. Both, AST and ALT, were measured using a commercial colorimetric kit. In the AST kit, the transfer

of an amino group from aspartate to α-ketoglutarate results in the generation of glutamate, resulting in the production of a colorimetric (450 nm) product proportional to the AST enzymatic activity present. ALT activity is determined by a coupled enzyme assay, which results in a colorimetric (570 nm)/ fluorometric (λ_{ex} = 535/λ_{em} = 587 nm) product, proportional to the pyruvate generated. Both assays contained a standard curve. The samples were prepared and analysed following manufacturer's instructions. The value taken as the activity of the sample was obtained as the latest value prior the activity exceeds the standard curve. ALT and AST activities were reported as nmol/min/mL (milliunit/mL).

5.4. Histology of liver tissue by haematoxylin-eosin staining

Liver samples were embedded in paraffin and sectioned with a 7 μm thickness. After deparaffinization, the tissue samples were stained by haematoxylin and eosin. Firstly, liver samples were exposed to haematoxylin for 50 s and thoroughly washed with water till no residual stain was observed. Then, hydrochloric alcohol, ammonia water and tap water were respectively used to wash the samples before exposing them to alcoholic eosin for 15-20 s. Finally, tap water, ethanol 96% and absolute ethanol were employed to wash the sample prior xylol treatment, thus the samples were mounted with mounting media and were dried for 24 h. Images were obtained under a transmission light microscope in Brightfield mode (Leica DMI 4000 B), with 10x magnification and 4 images per sample.

5.5. Determination of ophthalmic acid levels by mass spectrometry

Ophthalmic acid (OA) levels were determined in the liver tissue and sera by UPLC-MS/MS analysis as previously described in detail (Carretero et al., 2014).

For liver samples, frozen tissues (50–100 mg) were placed in 2-mL tubes containing CK14 ceramic beads from Precellys. Six volumes of PBS (m/v) containing 50 mM N-ethylmaleimide (NEM) were added to each tissue sample. Then, homogenization for 25 s at 6,000×g at 4 °C was repeated twice in a Precellys 24 Dual system equipped with a Cryolys cooler, also from Precellys. Tubes were centrifuged at 10,000×g for 5 min at 4 °C and supernatants were transferred to clean tubes. A second consecutive tissue extraction was performed by using four volumes of PBS containing 50 mM of NEM. Finally, both supernatants were pooled and stored at −80 °C until the analysis. For serum, 10 μL were thawed on wet ice prior to sample preparation. The levels of OA were analysed using an UPLC-MS/MS that consisted in an Acquity UPLC System from Waters (Manchester, UK), which was interfaced to a Waters Xevo TQ-S

mass spectrometer, also from Waters. The data were processed using the Waters MassLynx 4.1 software for quantitative analysis as previously described (Carretero et al., 2014).

5.6. Cytokine determination by magnetic multiplex assay

The inflammation cytokines interleukin-6 (IL-6), chemokine ligand 1 (CXCL-1), tumour necrosis factor alpha (TNF-α) and interferon gamma (IF-γ) were chosen to analyse in depth the inflammatory effects after APAP-induced ALF. Selected cytokines were analysed in mouse serum samples by Luminex following the manufacturer's guidelines. The MILLIPLEX® Mouse High Sensitivity T Cell Magnetic Bead Panel is a multiplex fluorometric assay that allow to study low-level cytokine expression but also to quantify multiple cytokine secretion levels simultaneously and in a biologically relevant context.

Serum samples (25 µL) were prepared according to the manufacturer's instructions. The standard employed for this assay is a Mouse High Sensitivity T Cell standard, with two quality controls provided by the kit. Absolute cytokine concentrations were determined using a 5-parameter logistic curve fits, with a sensitivity expressed in pg/mL. The sensitivity for each cytokine was different IL-6 (0.98-4000 pg/mL), CXCL-1 (0.73 - 3000 pg/mL, TNF-α (0.49 - 2000 pg/mL) and IFN-γ (0.49 - 2000 pg/mL).

6. Generation of 3D models for bioprinting.

FreeCAD 0.20.2 software was chosen to design all 3D models employed for the bioprinting experiments. The models after thoroughly and precise sketch were exported as *.stl* files to be rendered by *DNAStudio 3* slicer software (Cellink, Sweden) which transforms 3D models into G-code, programming language made for 3D printers. Three different models were designed: grid models, single ring models and concentric ring models (Figure 11). Each one was manually modified to follow the requirements to perform the enzymatic crosslink triggered by HRP and H_2O_2 and have the designed structures.

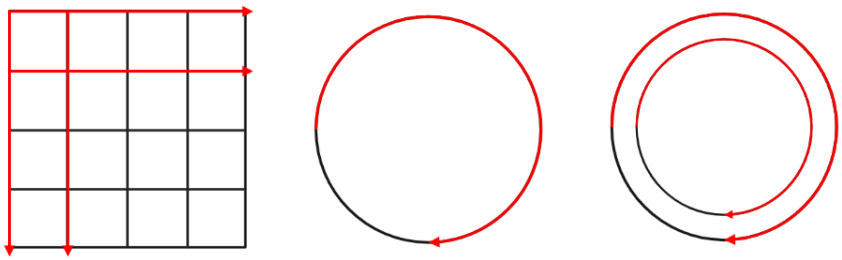

***Figure 11. 3D models used for bioprinting**. Grid model, single ring model and two-ring model. Red arrows indicate the printhead movements.*

Grid models needed that horizontal and vertical lines were exported separately to be recognized by the slicer as single line trajectory patterns. Other models designed for cell culture and miscibility assays were single and concentric circles. Concentric circles were designed, processed, and printed separately, unlike the grid model where vertical and horizontal patterns were combined into a single G-code file post-processing.

To achieve in demand crosslinking, the combined use of a bioink (polymer, HRP, and cells) and the crosslinking agent (H_2O_2) in separate printheads was programmed in the G-code. The slicer processing only accounts for one printhead. Thus, the output G-code was modified (Figure 12) to double and insert a layer of the second printhead, following the same path as the previous layer.

```
1. ;BIOX_ALTERNATING_PERIMETER_LAYER_0
2. T0 ; use printhead in first position 0
3. G1 Z0.580 F4800.000 ; move to next layer (0)
4. G1 F1200.000
5. G1 X3 Y0 E1 ;horizontal line
6. ;BIOX_ALTERNATING_PERIMETER_LAYER_1
7. T0
8. G1 Z1.160 F4800.000 ; move to next layer (1)
9. G1 F1200.000
10.G1 X0 Y3 E1 ; vertical line
11.;BIOX_ALTERNATING_PERIMETER_LAYER_2
12.T0
13.G1 Z1.740 F4800.000 ; move to next layer (2)
14.G1 F1200.000
15.G1 X1 Y3 E1
```

```
1. ;BIOX_ALTERNATING_PERIMETER_LAYER_0
2. T0 ; use first printhead
3. G1 Z0.580 F4800.000 ; move to next layer (0)
4. G1 F1200.000
5. G1 X3 Y0 E1 ;horizontal line
6. ;BIOX_ALTERNATING_PERIMETER_LAYER_0
7. T1 ; use printhead in second position 1 (EMD)
8. G1 Z0.000 F4800.000 ; move to next layer (0)
9. G1 F1200.000
10.G1 X1 Y3 E1
11.;BIOX_ALTERNATING_PERIMETER_LAYER_1
12.T0
13.G1 Z1.160 F4800.000 ; move to next layer (1)
14.G1 F1200.000
15.G1 X3 Y0 E1
16.; NEXT LAYERS BELOW
```

***Figure 12. Modification example of G-code.** Left, G-code as exported from slicer software. Right, manually inserted sections (green) to define printhead change from T0 to T1 and fix the Z position (red). The trajectory followed by T1 printhead is the same as the previous layer by T0. All text after ";" are comments for ease of understanding by the user.*

As shown in Figure 12, the line of command before the coordinates is modified from T0 (first printhead) to T2 (second printhead). G1 are extrusion commands,

in which first the Z parameter determines the height of extrusion for each layer, X and Y the relative distances to move while extruding in the x/y plane. On the other hand, F and E commands indicate the feed rate and mm of material extruded respectively, and these are not modified after processing. Ultimately, the speed and extrusion pressure were directly controlled in the printer's console. Another parameter modified when implementing both printheads was to set the electro-magnetic droplet (EMD) printhead (T1) to a fixed relative height of Z0 for all layers. Thus, the EMD printhead remained always at the height defined when calibrated, above the wells of the plate.

Another point considered for the CAD design of the models was that the model strands had to be 0.01 mm below the desired gauge to avoid an issue with the processing software. Thus, models for 20G (inner diameter 0.60 mm) and 22G (inner diameter 0.41 mm) were designed with a strand thickness of 0.59 mm and 0.40 mm, respectively.

The number of layers of the final structure was defined by the processing software, considering the *stl* model height (e.g., 3 mm) and the desired gauge. For a 3 mm tall structure, using a 20G gauge (0.60 mm), five layers of polymer were printed (3 mm/0.60 mm = 5 layers), while for 22G gauge (0.41 mm), seven layers of polymer were printed (3 mm/0.41 mm ≈ 7 layers).

7. Printability and uniformity

Printability refers to the capacity to form and maintain a reproducible 3D structure, according to a CAD-designed model. Printability was evaluated here based on extrudability, strand uniformity, and pore factor. Briefly, extrudability was assessed by testing whether it was possible to eject material through the nozzle (20G) at a certain pressure up to the maximum pressure achievable (200 kPa) by the *Cellink BIOX* printer. Both uniformity and pore factor were evaluated with a 4 x 4 (30 x 30 x 3 mm) square grid design, with a 0.60 mm strand thickness to fit a 20G nozzle. The inner squares are designed to be 7 x 7 mm (49 mm^2). Pictures of the grid were taken using a simple magnification microscope (RS Pro Portable Stand-Alone Microscope) and images analysed with *ImageJ*. Grids printed with CELLINK START were used as a control for its excellent extrudability and apparent resolution of the structures printed.

Uniformity (U) was measured as a ratio of average strand width ($\bar{X}$) measurements (n = 25) and the average of the strand thickness of the control grids (Figure 13). Thus, values above 1 represent thicker strands than the control, and closer values to 1 would be considered more uniform (Equation 8).

$$U = \frac{\overline{X}(strand\ width)_{SAMPLE}}{\overline{X}(strand\ width)_{CONTROL}}$$

Equation 8. *Uniformity formula for grid 3D models made of Gel-HA bioinks.*

The pore factor (PF) was measured as a ratio of the average pore area ($\overline{X}$) i.e., grid inner squares (n = 4) and the average pore area of the control grids (Figure 13). In this case, values below 1 imply reduced pore area compared to the control (Equation 9).

$$PF = \frac{\overline{X}(area)_{SAMPLE}}{\overline{X}(area)_{CONTROL}}$$

Equation 9. *Pore factor formula for grid 3D models made of Gel-HA bioinks.*

Printability was evaluated for all HA HMW and its mixtures with Gel, Gel-HA. The grids were printed on glass plates, with a controlled printhead and print bed temperature of 37 °C. The CELLINK START controls were printed from the cartridge as is. During the extrudability evaluation, the minimum pressure required for each mixture was also evaluated. For HA-based inks, the HA was directly dissolved in the 3 mL cartridges in F12 media. Gel was dissolved in Eppendorf separately. For the mixtures, Gel and HRP (12.5 U/mL) were introduced altogether to the cartridge and homogenized with the HA. The cartridges contained 90% of polymer solution (HA or Gel-HA) and 10% of HRP 12.5 U/mL. The EMD printhead (Electro-Magnetic Droplet) was setup at 37 °C and loaded with a H_2O_2 20 mM cartridge (diluted in F12 culture media), and after every layer of ink, this printhead deposited the peroxide on the printed pattern. The EMD valve deposited drops by opening the valve 1 ms every 80 ms.

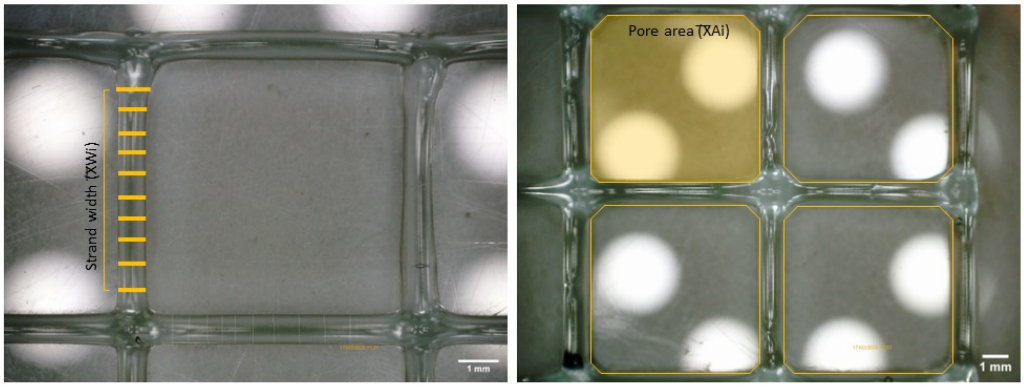

Figure 13. Scheme of uniformity and pore factor analysis. *Example of the method employed for uniformity and pore factor analysis in Cellink's control bioink respectively.*

8. *In vitro* experiments with extruded HepG2 within Gel-HA bioinks

HepG2 were encapsulated by bioprinting technique using Gel-HA bioinks: Gel-HA HMW 4% 20/80 and Gel-HA HMW 5% 20-80. Lyophilized HA HMW was let to dissolve for 3 to 5 days at 4°C in F12 cell culture media in separate cartridges for each concentration of 4% and 5%. Lyophilized non-sterile Gel was first dissolved in a falcon tube at the specified concentration, during 1 h at 37 °C. Once dissolved, it was filtered through 0.22 μm polyethylene sulfone (PES) syringe filters.

Therefore, considering our 3 mL cartridges were completely filled, 6×10^6 cells were required per cartridge. The volume of cell suspension corresponding to these of cells was centrifuged, and the pellet resuspended in the filtered Gel solution and HRP 12.5 U/mL. Thus, the mixture of cells, Gel and HRP was ready to be homogenized together with the HA HMW in the cartridge.

The bioprinter inner chamber was sterilized using its own UV program, and the laminar flow fan was on during the whole printing process. The printheads and print bed were pre-heated at 37 °C.

Table 6. *Pressure applied during bioprinting for each bioink.*

Nozzle gauge	Gel-HA (20-80) HMW 4%	Gel-HA (20-80) HMW 5%	Gel-HA (50-50) HMW 5%
20G	40-50 kPa	80-100 kPa	35-50 kPa

For each composition, the cartridge containing Gel-HA/HRP/HepG2 was loaded in the first position printhead, and a sterile solution of H_2O_2 in F12 culture media was loaded in the second printhead (EMD type). Cylindrical models of 15 mm diameter and 3 mm in height were printed in several P24 plates, at least 3 samples per condition. The printing pressure was the main parameter varying among conditions, as shown in Table 6. For all constructs, a pre-flow of 300 ms was set (e.g., time in which the extrusion starts ahead of the model). After printing, bioprinted cells were incubated at 37 °C for 15 to 30 min to let the hydrogels to properly crosslink. Next, 4 mL of HepG2 culture media were added to each well and maintained at 37 °C. Cell survival evaluation was carried out at day 0 (post-printing), day 1, day 3 and day 7 of cell culture by live-dead assay, previously detailed in section 3.2.5. In addition, urea synthesis and albumin secretion for each time point were assessed as previously described.

Lastly, immunohistochemistry was performed as mentioned in section 4.4 (Methods) but targeting other hepatic proteins. For this purpose, alpha fetoprotein primary antibody and HNF4-α primary antibody both diluted (1:100) in 1% BSA-dPBS. After the dPBS washes, cryosections of the bioprinted constructs were incubated for 1 h with anti-mouse Alexa 488 and anti-rabbit Alexa 555 respectively, diluted (1:200) in 1% BSA-dPBS.

9. Miscibility of Gel-HA hydrogels formed by the enzymatic inks Gel and HA for co-culture experiments.

To test whether bioink candidates could be printed in close contact while maintaining separate stable structures, concentric circles with a varying distance gap were printed. Considering that our bioinks form hydrogel networks, swelling of the printed structures when immersed in culture media is also expected, potentially increasing the contact area between two structures. For this assay, two blends of the Gel-HA mixtures were used: Gel-HA HMW 4% 20-80 and Gel-HA HMW 5% 20-80. The bioinks were mixed with two distinct fluorophores, Texas Red™ and Oregon Green™ and dispersed in the solution at a concentration of 200 µg/mL. The fluorophores provided by the supplier were dissolved in PBS/azide 0.05% to a concentration of 1 mg/mL and kept frozen in aliquots.

Table 7. *Gel-HA bioink detailed compositions for miscibility assay with conjugated fluorophores.*

	Gel-HA HMW (20-80) 4%	**Gel-HA HMW (20-80) 5%**	**Gel-HA HMW (50-50) 5%**
HA HMW	500 µL	500 µL	312.5 µL
Gel	125 µL	125 µL	312.5 µL
HRP	62.5 µL	62.5 µL	62.5 µL
Fluorophore (1 mg/mL)	137.4 µL	137.4 µL	137.4 µL

The cartridges were prepared as described in Table 7. The HA HMW was previously let to dissolve with F12 culture media in the cartridge for 3 days at 4 °C, at the concentration desired (4% or 5%). Gel was dissolved in F12 at each concentration separately in Eppendorf during 30 min at 37 °C. The EMD cartridge was freshly prepared with H_2O_2 20 mM in F12 media. The dissolved HA was homogenized with Gel, HRP 12.5 U/mL solution and fluorophore. The printing process was performed in the dark, and at a controlled temperature of 37 °C in printheads and print bed. A 20G (0.60 mm) nozzle was used and the CAD models were designed consistently, so that the strand thickness modelled was 0.59 mm, and each gap would be a multiple strand thickness (Figure 14).

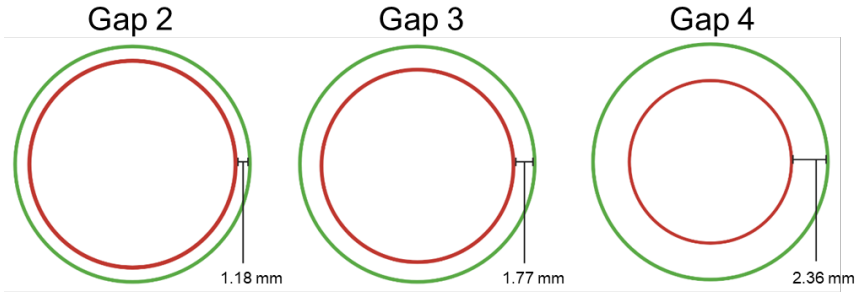

Figure 14. CAD models used for miscibility assay. *Outer circles had 13.23 mm diameter fixed, while inner circles varied the gap compared to the outer one. The gap was proportional to the thickness of the strand defined by the nozzle gauge, chosen 20G for two-ring model.*

The constructs had a modelled height of 3 mm (5 layers of bioink). The outer and inner circles were two independent models fully printed independently. Three replicas of concentric circles for each gap were printed on a P12 plate and

imaged under Leica DMI8 inverted microscope (Leica microsystems, Germany) after printing, and after incubation during 24 h in F12 culture media at 37 °C.

10. Statistical analysis

Data are expressed as the mean ± SD and represent at least triplicate measurements. A Student's t-test was used for statistically evaluating pairs of groups whereas one-way ANOVA followed by Tuckey's multiple comparison test was used when comparing 3 or more groups. The level of significance was chosen as $p<0.05$ and calculated with GraphPad Prism v8. The graphs of this thesis were also performed with GraphPad Prim v8.

Chapter 1. Physicochemical properties of injectable Gel-HA hydrogels and scaffolds.

1. Quantitative tyramine grafting evaluation by UV

Gel and HA were grafted with tyramine to be enzymatically crosslinked with HRP and form hydrogels (Figure 15). Red-ox reactions between HRP and H_2O_2 allow to transform H_2O_2 into a more reactive specie which randomly interact with the tyramine by the -OH terminal group or a phenolic carbon from the aromatic ring (Figure 15A). The result of this process were the Gel-HA hydrogels, whose physicochemical properties changed depending on the ratio of Gel to HA. Figure 15B shows the macroscopic view of the formed hydrogels, demonstrating that they were satisfactorily formed when catalysed with the enzyme and the peroxide.

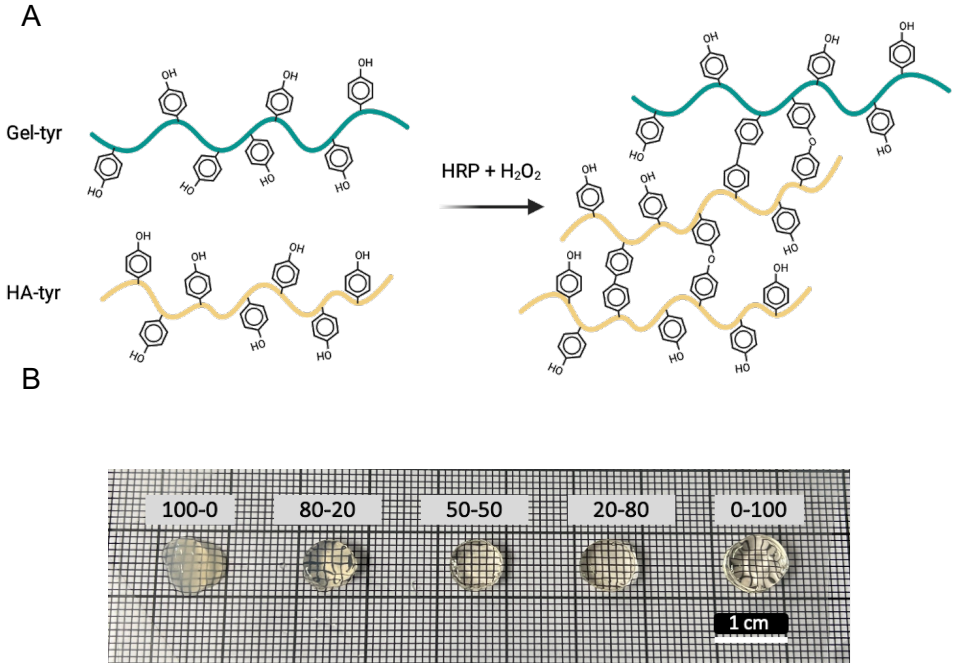

***Figure 15. Chemical structure and macroscopic morphology of Gel-HA hydrogels**. A) Molecular structure obtained after grafting tyramine to Gel and HA to form the conjugates Gel-tyr and HA-tyr and the subsequent enzymatic crosslinking of the hydrogels catalysed by HRP/H_2O_2. The hydrogels can be formed by connections between Gel-Gel, HA-HA and Gel-HA chains. B) Macroscopic image of the Gel-HA hydrogels just after crosslinking in moulds. All hydrogels are equal in size because they are not swollen into equilibrium.*

It is worth noting that Gel was whitish, while HA was transparent, having the mixtures an intermediate aspect that we could characterize as translucent (Figure 15B). Gel's opacity could be associated to a physical crosslinking of the Gel's triple helix formed at room temperature (Kripotou et al., 2019). This crosslinking process is compatible with the chemical crosslinking that was taking place at the same time.

Tyramine grafting on the hydrogel precursor macromolecules was confirmed by UV spectrophotometry by the absorbance peak at 275 nm (Figure 16A). Tyramine degree of substitution resulted similar in both polymers, 1.68×10^{-7} mol tyr/mg for Gel-tyr and 1.64×10^{-7} mol for tyr/mg HA, which in percentage of -COOH groups within the chains grafted to tyramine groups normalized by the initial -COOH groups of the chains, resulted to be 22% and 7%, for Gel-tyr and HA-tyr, respectively (Figure 16B). The substitution degree was similar to previous data published by Sanmartín-Masiá *et al*. (Sanmartín-Masiá et al., 2017)

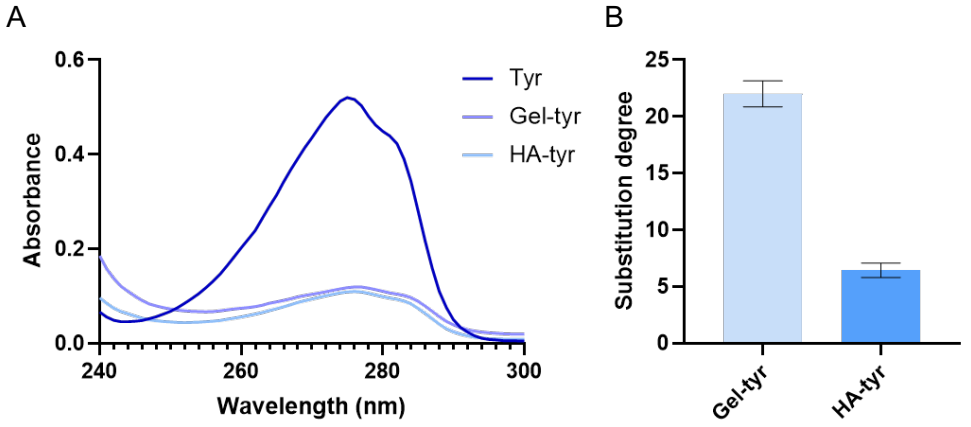

Figure 16. Tyramine grafting onto Gel and HA. *A) UV spectra of the hydrogel precursor macromolecule. Tyramine control (tyr), tyramine grafted Gel (Gel-tyr) and tyramine grafted HA (HA-tyr). B) Substitution degree of Gel-tyr and HA-tyr (n=9).*

Tyramine quantification was made for each batch as a quality control to keep tracking of the polymer synthesized and establishing standards for their use. Gel required to have at least 20% of tyramine grafted onto its chains and HA required a minimum of 5.5%, to pass the quality control test, in order to use similar polymers thoroughly the present thesis and for all the experiments.

2. Qualitative tyramine grafting evaluation by ATR-FTIR

Gel and HA are different molecules which led into different FTIR spectra, meanwhile there were peaks that share as at 3300 cm^{-1} representing phenolic and -OH groups (A) and at 2950 cm^{-1} the aromatic C-H bonds (B). Other peaks were inherent to each molecule due its nature, but not exclusive. Gel is a protein characterized by peptide bonds which were reflected at 1610 cm^{-1} the C=O bond of amide bonds (C) and at 1550 cm^{-1} the N-H bound of amide bonds (D). On the other hand, HA is a GAG with high content of carboxylic groups, represented at 1050 cm^{-1} the C-O bond of the carboxylic groups (E). Finally, the peak found at 600 cm^{-1} is related with the vibration of C-C, C-O and C-N bonds (F). Each letter assigned for each wavenumber is meant to simplify the graphs and the results of this section.

Efficient grafting of tyramine within the Gel and HA chains was confirmed by ATR-FTIR spectra (Figure 17). The spectra of Gel-tyr and HA-tyr show the B peak as described in the literature (Egbu et al., 2018; Firouzi et al., 2020) that was more pronounced in the tyramine conjugates than in pristine samples. The difference on the F peak on grafted polymers has not been described in the literature, but it could be attributed to the effect of the grafting on the vibration of the C-C, C-O and C-N bonds of the polymers.

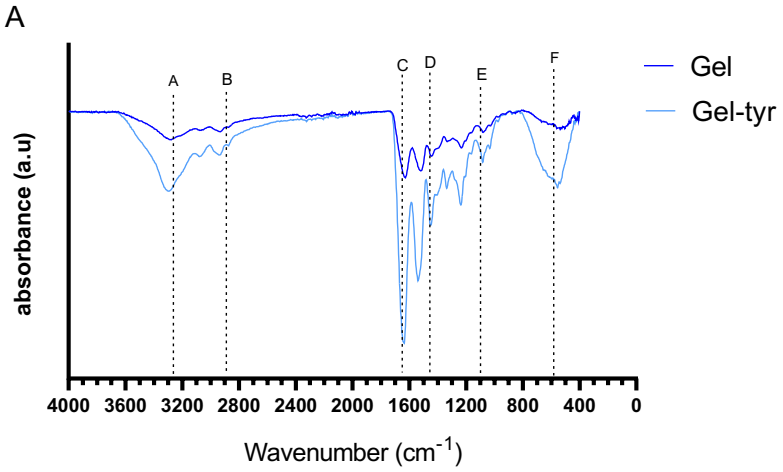

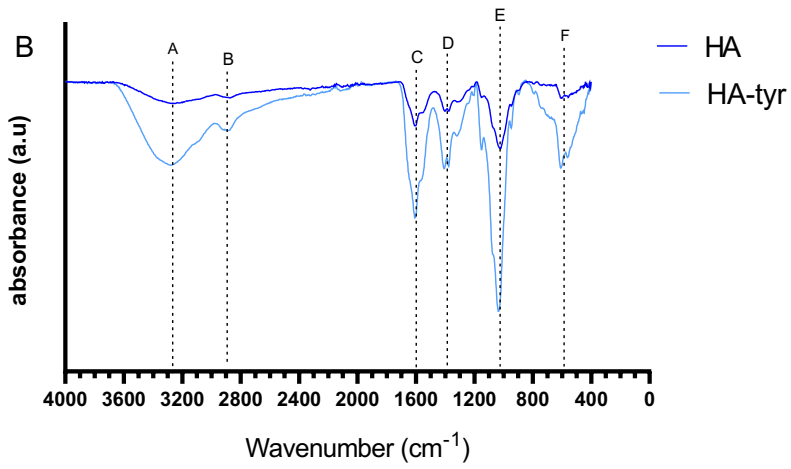

Figure 17. Fourier Transformed infrared spectra (FTIR) of hydrogel precursor macromolecules. *A) Dry unmodified Gel (Gel) and lyophilized tyramine modified Gel (Gel-tyr); B) dry unmodified HA and lyophilized tyramine modified HA (HA-tyr).*

The ATR-FTIR spectra of all hydrogels after crosslinking (dried samples) are shown in Figure 18. The characteristic peaks of each polymer Gel and HA appear in the graph and their intensity and location are connected with the amount of component in each mixture.

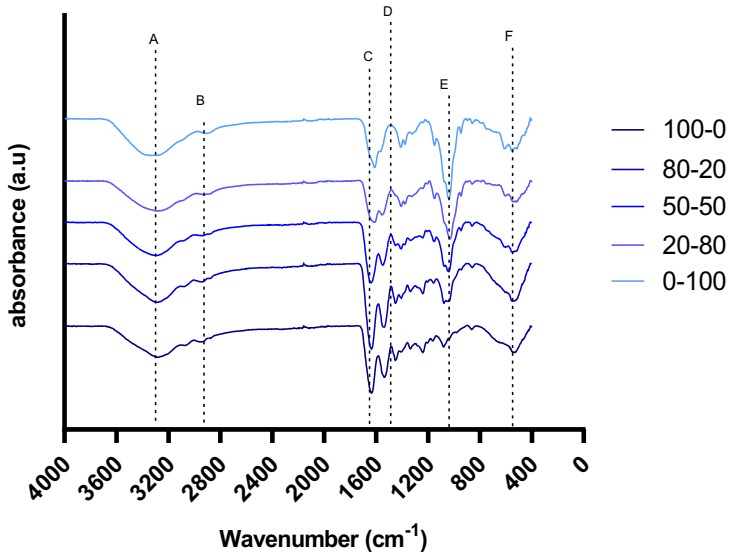

Figure 18. Fourier Transformed infrared spectra (FTIR) of dried Gel-HA hydrogels. *Dry hydrogels after crosslinking from the compositions selected.*

Gel and HA mixtures exhibited peaks of each polymer. Differences between A and B peaks were not found, crosslinked hydrogels had similar phenolic peaks and -OH group content. In addition, the F peak also showed no difference among the compositions. The footprint of the mixed polymers started to differ in their characteristic peaks. Gel-HA 80-20 showed a less pronounced C peak compared to Gel but more intense compared with the rest of Gel-HA mixtures and HA. Gel-HA 20-80 as expected displayed the other way around, E peak intensity was slightly lower compared to HA but still higher compared with the other compositions. Finally, Gel-HA 50-50 showed a balanced peak profile with intensities in all peaks half of the found in each polymer.

3. Rheology of Gel-HA hydrogels

Gelation times of the different hydrogels, determined from the evolution of the shear storage moduli (G') with the crosslinking time of Figure 19A, are listed in Table 8. Gel crosslinked significantly faster (6 min) than HA (20 min). The mixtures presented intermediate gelation times that increased with the content of HA in them. As the degree of tyramine grafting and the amount of HRP and H_2O_2 were the same for Gel and HA, the differences between the crosslinking times were probably due to the different viscosities of the polymeric solutions (Figure 19B).

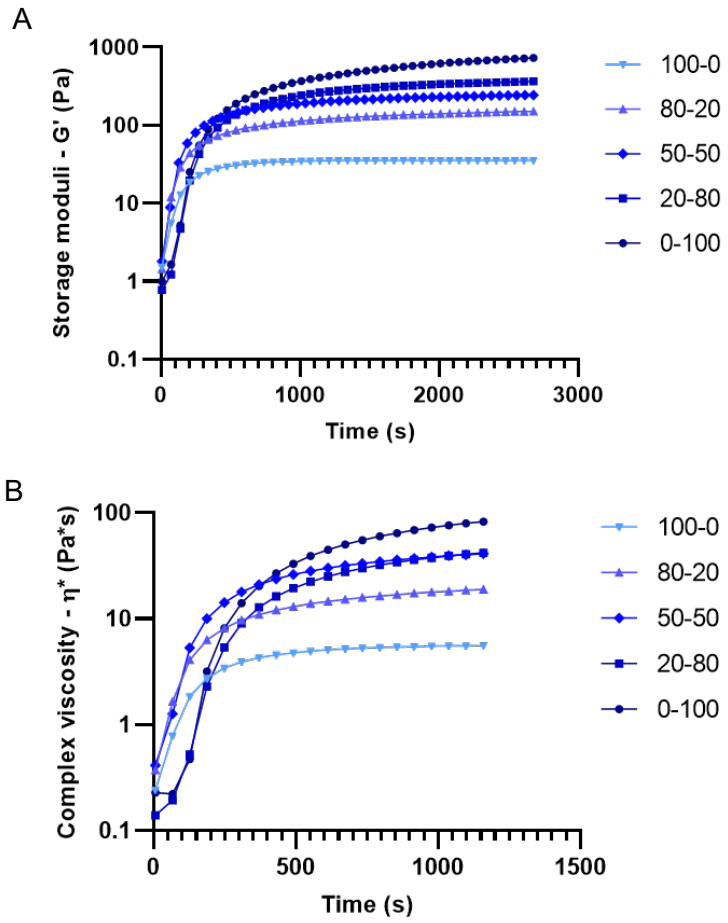

Figure 19. Mechanical properties of in situ Gel-HA hydrogels by rheology. *A) Evolution of the shear storage modulus during the crosslinking the Gel-tyr and HA-tyr mixtures in the rheometer at 1 Hz and 1% strain to form Gel-HA hydrogels (n=3). B) Complex viscosity during crosslinking of the Gel-tyr and HA-tyr mixtures to form the Gel-HA hydrogels (n=3). The measurements were performed in the rheometer at 1% strain and 1 Hz of frequency.*

Table 8. *Physicochemical properties of Gel-HA hydrogels*

	Gelation time (min)	Equilibrium water content	Crosslinking density (mol/m^3)
100-0	6 ± 1	48 ± 1	22 ± 2
80-20	9 ± 1	56 ± 2	20 ± 1
50-50	13 ± 4*	64 ± 6*	21 ± 3
20-80	16 ± 3*#	65 ± 3*	23 ± 3
0-100	20 ± 1*#&	70 ± 3*#	22 ± 2

*At least p≤0.01 (compared to 100-0); #p≤0.001 (compared to 80-20); &p≤0.01 (compared to 50-50); (n=3; ANOVA followed by Tuckey's multiple comparisons test).

Rheological properties of crosslinked hydrogels as a function of the frequency demonstrated that the storage modulus G' (Figure 20A) was much higher than the loss modulus G'' (Figure 20B), indicating that hydrogels are elastic (Moulisová et al., 2017). No significant variation of the values of G' with the frequency was observed for the HA and the mixtures. A slight increase was observed for Gel above 2 Hz, which could be indicative of a relaxation process (Kadri et al., 2016). A constant strain of 1% situated within the linear viscoelastic region was chosen for the measurements in which the complex modulus does not change with the strain (Figure 20C).

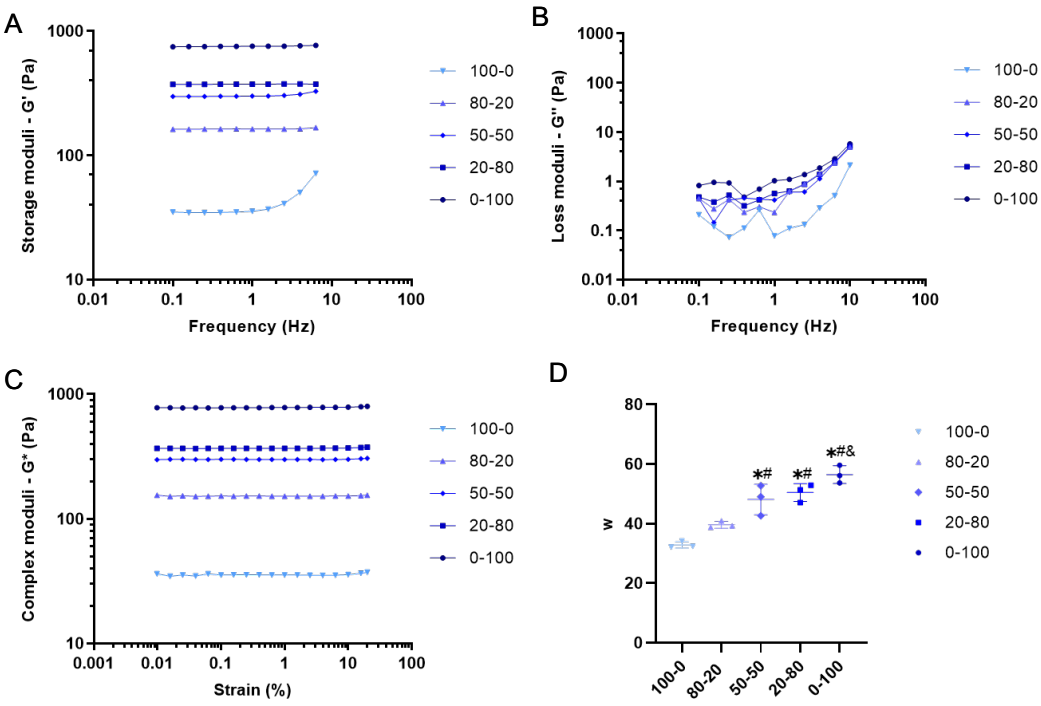

Figure 20. **Frequency and strain analysis of *in situ* Gel-HA hydrogels by rheology and water kinetics after swelling of Gel-HA hydrogels.** *A) Storage (G') and B) loss (G'') moduli after crosslinking at 1% strain as a function of the frequency of Gel-HA hydrogels. C) Complex shear modulus after crosslinking of Gel-HA hydrogels. Measurements were performed in the rheometer at 1 Hz of frequency. D) Equilibrium water content (w) of Gel-HA hydrogels after 24 h in dPBS. *At least p≤ 0.01 (compared to 100-0); $^{\#}$p≤ 0.001 (compared to 80-20); $^{\&}$p≤ 0.01 (compared to 50-50); (n=3; ANOVA followed by Tukey's multiple comparisons test)*

Gel absorbed the lower amount of water in equilibrium and HA the highest (32 g and 56 g of water per g of dry polymer, respectively) (Figure 20D) (Table 8). The amount of water within the mixtures increased with the amount of HA in them, as similarly observed by crosslinking with CF-KRB (Poveda-Reyes et al., 2016). Despite the different swelling capacity, all the samples resulted in a similar crosslinking density (Table 8), consistently with the similar degree of tyramine grafting of Gel and HA. Therefore, the higher ability of HA to absorb water compared to Gel was due to its higher hydrophilicity (Poveda-Reyes et al., 2016), expressed by the lower value of the Flory-Huggins parameter (Bohidar, 1998; Leach et al., 2003).

G' values of the hydrogels after crosslinking (*in situ* relaxed state) and at a fixed frequency of 1 Hz (Figure 21A) showed that Gel is very soft, with a G' value of 36 Pa. However, as the content of HA in the mixtures increased, the modulus significantly increased for the samples 80-20 and 50-50, with values 163 Pa and

245 Pa, respectively. A value of 375 Pa was obtained for the 20-80 sample. HA hydrogel presented the highest value, of 755 Pa, with statistically significant difference among the rest of samples.

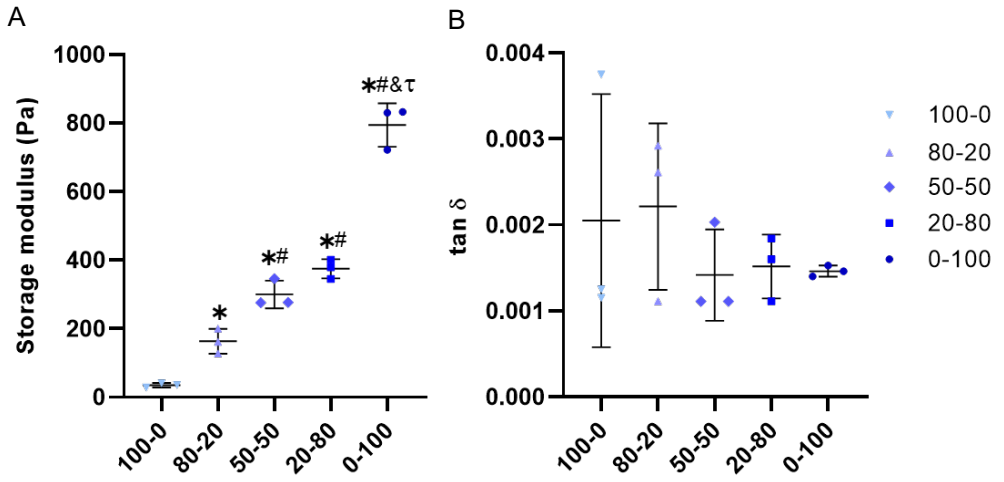

Figure 21. Mechanical properties of in situ Gel-HA hydrogels. *A) Storage moduli (G') and B) tan δ at 1 Hz of the in situ crosslinked Gel-HA hydrogels. Statistical analysis of all rheological evaluation was performed with GraphPad v8 software. *At least p≤0.01 (compared to 100-0); #p≤0.001 (compared to 80-20); &p≤0.01 (compared to 50-50); τp≤0.001 (compared to 20-80); (n=3; ANOVA followed by Tuckey's multiple comparisons test).*

Tan δ values for Gel-HA hydrogels were very low, between [0.00 – 0.004], as expected for elastic hydrogels. There was a high variability in the values of Gel-HA hydrogels 100-0 and 80-20 probably due to their softness (Figure 21B). The variability decreased with the content of HA in the mixtures. No statistical differences were found between the different Gel-HA hydrogels for tan δ values (Figure 21B).

4. Estimation of Young's moduli of hydrogels in the swollen state.

Hydrogels can be in different states depending on their amount of water: dry, relaxed (just after the crosslinking with water) and swollen at equilibrium.

The rubber elasticity theory provided an estimation of the Young's moduli of hydrogels in the swollen state, Equation 7 can be used to calculate the Young's modulus of the swollen hydrogels ($E'_{swollen}$), with the experimental data of those after crosslinking (relaxed state of Figure 16) and the data of the equilibrium water content of the hydrogels.

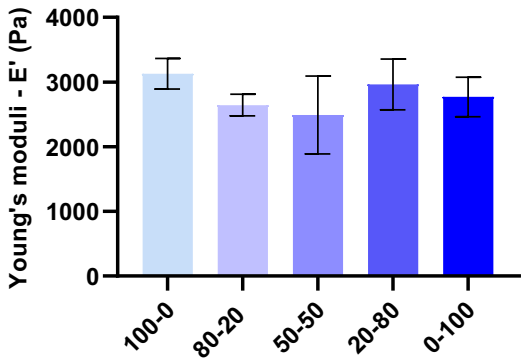

Figure 22. Estimation of Young's moduli of hydrogels in the swollen state.

Results can be seen in Figure 22. Surprisingly, no statistical differences were observed among the Gel-HA compositions and the increasing tendency of the values seen in Figure 20 with the content of HA in the hydrogels disappeared. This is a consequence of the evolution of the equilibrium water content observed in Figure 20D, which increased with the content of HA in the mixture.

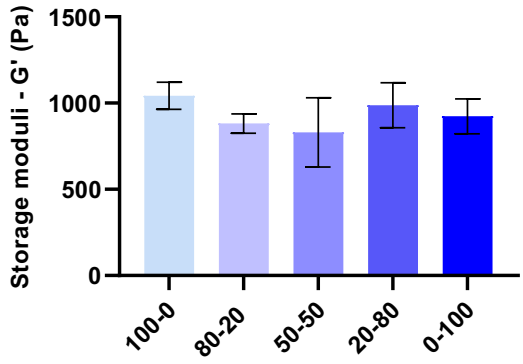

Figure 23. Estimation of storage moduli of Gel-HA hydrogels in the swollen state.

Finally, G' in the swollen state can be calculated after applying Equation 5, ranging between 680 Pa and 1200 Pa (Figure 23), again with no statistical differences among samples.

5. Rheology and swelling properties of Gel-HA (20-80) scaffolds.

Gel-HA hydrogels have been the subject of the previous experiments due to their potential to embed cells, their good mechanical properties and ability to diffuse nutrients to the cells thanks to their swelling capacity (Moulisová et al., 2017;

Poveda-Reyes et al., 2016). Even though injectable hydrogels have a good potential for liver tissue engineering, their difficult handling for *in vivo* implantation, led us to manufacture and characterize scaffolds of the optimal composition for a regenerative medicine approach.

Scaffolds were obtained by crosslinking Gel-tyr and HA-tyr in CF-KRB instead of F12 buffer because the crosslinking process is more effective. As they would be swelled, washed, sterilized, and peeled, the cells would be seeded on top of the scaffold and penetrate in their pores. Thus, Gel-HA scaffolds were obtained by lyophilizing Gel-HA 20-80 hydrogels after equilibrating them in dPBS. Figure 24A shows the evolution of the shear storage modulus with the frequency, compared with the hydrogel of the same composition (20-80). At 1 Hz G' of the scaffold, 752 Pa, is higher than that of the hydrogel in the relaxed state, 375 Pa, still close to the upper range of the modulus of human liver (Desai et al., 2016; Yeh et al., 2002). Tan δ values at 1 Hz for hydrogel were around 0.004 and for scaffold around 0.1 (Figure 24B).

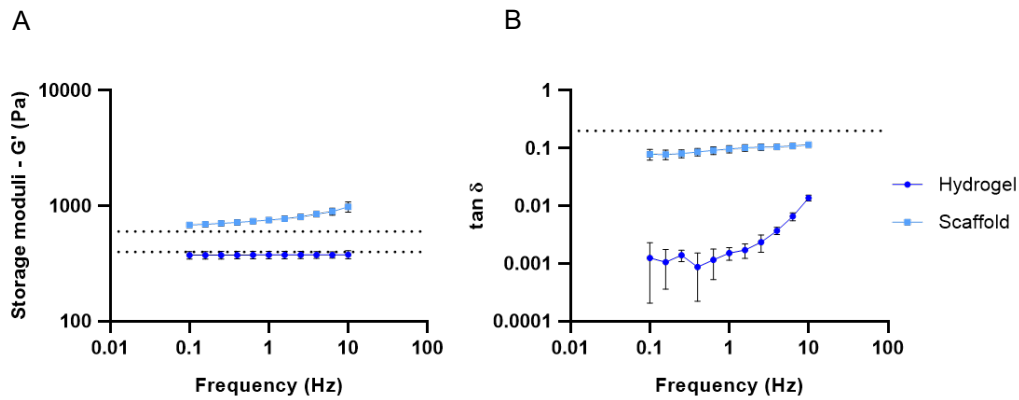

Figure 24. Characterisation of Gel-HA scaffold compared to Gel-HA hydrogel. *A) Shear storage modulus G' and B) tanδ as a function of the frequency measured in the rheometer at 1% strain of Gel-HA (20-80) hydrogel (at the relaxed state) and scaffold (after equilibrating in dPBS). Dotted lines for A) correspond to rheological G' of healthy human liver values between 400-600 Pa* (Desai et al., 2016). *Dotted line for B) correspond to fresh human liver measured by oscillatory rheology tanδ =0.2* (Estermann et al., 2021).

The morphological analysis of the scaffolds from FESEM images unveiled differences between external and internal structures. Freeze-dry process created a veil produced by the water pushing out of the polymer during the sublimation (non-peeled). The morphology of the internal structure of the scaffold was revealed by cutting a fine section of the scaffold (peeled). The internal structure was an interconnected honeycomb-like porous structure typical of hydrogels made of natural origin polymers, in which the pores were formed by the crystallization of water when freezing before drying (De France et

al., 2018). The mean pores size was 102 ± 36 μm and the mean pore area 5211 ± 3910 μm^2 (Figure 25).

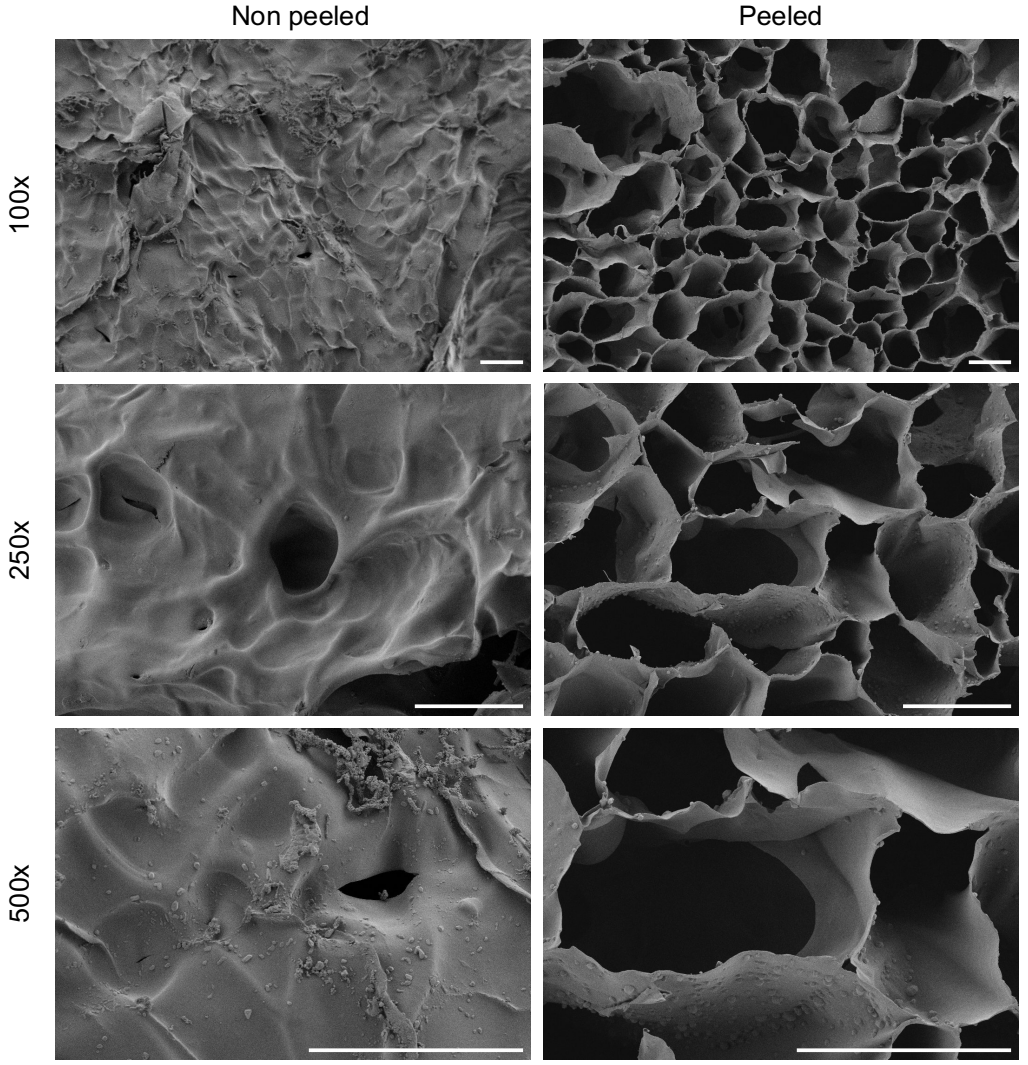

Figure 25. FESEM representative images of non-peeled and peeled honeycomb-like porous structure on lyophilized Gel-HA (20-80) scaffolds. *Images obtained at 100x, 250x and 500x magnification. Scale bar applies to all images (100 μm).*

The equilibrium water content of the scaffold was significantly lower than of the hydrogel (Figure 26), probably due to the more efficient crosslinking in CF-KRB, which also explains the increase in the mechanical properties.

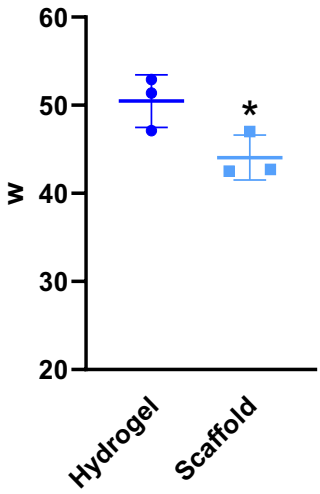

Figure 26. Equilibrium water content (w) of Gel-HA (20-80) hydrogel and scaffold. *Comparison of the water uptake after 24 h of swelling in F12 cell culture media. (n=3). *At least p≤0.05 (compared to hydrogel; Student's t-test).*

Discussion

Different kinds of biomaterials that provide the suitable microarchitecture, composition, and stiffness, among others, have been proposed for liver tissue engineering (da Silva Morais et al., 2020). The liver ECM plays a relevant role in cell behavior, enabling cell-cell and cell-ECM interactions, as well as promoting migration, proliferation, and differentiation (Baiocchini et al., 2016). Liver ECM contains a considerable number of components, including proteins such as collagen type I, II and IV, glycoproteins such as laminin and fibronectin and GAGs such as chondroitin sulfate, heparan sulfate and HA. In this thesis, we explored the use of Gel-HA hydrogels and scaffolds as a platform for liver cell culture. HA is the main component of the perisinusoidal space and has been proposed as a biocompatible material either alone or in combination with other materials such as collagen or laminin for liver regenerative medicine purposes (Ali et al, 2021; Turner et al., 2013). On the other hand, Gel is a natural component of the ECM derived from denatured collagen type I and is a biodegradable and inexpensive material that has also been proposed for hepatocyte culture (Kumari et al. 2016). Although Gel is a highly promising material, it lacks mechanical properties. Mechanical properties have been improved by mixing with HA, with excellent results in other tissue engineering applications (Moulisová et al., 2017; Vaca-González et al., 2020), which opened the way for the 3D culture of PHH. Thus, although the final goal of the thesis was to explore the suitability for hepatic cell culture, we deeply characterize different Gel-HA compositions trying to find the conditions closer to native tissue. Tyramine conjugates have been a breakthrough for tissue engineering since a non-cytotoxic reaction catalysed by HRP and H_2O_2 allows to generate hydrogels with tuneable properties. The pioneer on the modification of polymers with tyramine molecules was Kurisawa, showing tyramine conjugated HA hydrogels with great mechanical properties and degradability for tissue engineering and drug delivery purposes (Kurisawa et al., 2005). Based on this line of research, other authors have proposed these to be tuneable and for protein delivery systems (Lee et al., 2008, 2009).

The system is injectable, and the crosslinking reaction was described as non-cytotoxic in the literature (Khanmohammadi et al., 2018; Lee et al., 2015). This characteristic made it possible to use these polymers to generate hydrogels which can crosslink in the presence of cells without harmful effects derived from the crosslinking chemistry. This chemical modification has already been used by other authors in tissues other than liver, such as muscle tissue (Moulisová et al., 2017; Poveda-Reyes et al., 2016) and cartilage (Moreira Teixeira et al., 2012;

Moulisová et al., 2017). Also, by applying electrostimulation to the system it was possible to promote chondrogenic differentiation, describing the diverse applications of the very same system to different target tissues and strategies. The tyramine substitution onto Gel and HA obtained in the present study is in the range that other authors have described as optimal for the proper crosslinking in the presence of cells, with values of 24% and 7% for Gel and HA, respectively (Moulisová et al., 2017; Poveda-Reyes et al., 2016; Sanmartín-Masiá et al., 2017).

Although gelation was successfully produced, crosslinking time of Gel in F12 medium was about 6 min, whereas for HA it was about 20 min (Table 8), which are longer times than those obtained when crosslinking is produced in CF-KRB (Poveda-Reyes et al., 2016). This is probably due to the presence of antioxidant substances in the F12 medium that delays the action of the H_2O_2.

HA, as previously described, is a molecule with high affinity to H_2O molecules, explained by the higher value of the Flory-Huggins's parameter compared to the Gel and the mixtures. Thus, the equilibrium water content in HA gave values of swelling of 70 compared to the value of 48 for Gel or the 64 for Gel-HA 50-50 mixture. This has been described in similar systems with HA and collagen forming microgels, where pure collagen exhibited negligible swelling whereas HA had huge PBS uptake (Lai et al., 2016). Regarding the mechanical properties, the G' values resulted to be lower than when crosslinking in CF-KRB (Moulisová et al., 2017), probably due to the lower oxidation degree of the phenol groups of tyramine. Being HA the hydrogel that absorbs the higher amount of water and having all the hydrogels a similar crosslinking density, the higher stiffness of HA compared to Gel could then be attributed to the higher rigidity of the HA chains (Kvam et al., 1992) and the lower water permeability coefficient of HA (Kalyanam et al., 2009), as previously discussed when crosslinking in CF-KRB (Poveda-Reyes et al., 2016).

Rheological measurements of bulk human liver have shown that the storage modulus of the tissue ranges from 400 to 600 Pa (Desai et al., 2016; Yeh et al., 2002). It is in this range of matrix rigidities where hepatocytes should show optimal liver-specific functionalities. However, the mechanical properties of the hydrogels are not only defined by the molecules themselves, but the type of crosslinking also plays a relevant role on the hydrogel stiffness, and from the same polymer very different mechanical properties can be observed. Gel derivatives based on methacrylated hydrogels display G' values around 13 kPa which are not adequate for liver tissue (Carpentier et al., 2023), but varying the UV exposure time and pH lower G' values around 3200 Pa can be achieved to

better mimic the liver tissue properties (Moniruzzaman et al., 2021). Other crosslinking chemistries based on chemical or enzymatic crosslinking tune the properties to be more precise. Previous studies in HA hydrogels containing liver ECM showed higher levels of hepatocyte gene expression and higher levels of albumin secretion in hydrogels of shear moduli of 600 Pa and 1200 Pa, which significantly decreased in stiffer substrates of 4600 Pa (Deegan et al., 2016). Additionally, hybrid systems have always been chosen over polymeric systems with only one type, which does not represent the heterogeneity of the liver ECM. Gel-HA systems have already been described but crosslinked differently, PEGDA based crosslinking synthesized hydrogels with G' values from 180 Pa to 580 Pa or disulfide bond hydrogels with G' values from 120 Pa to 330 Pa which better mimic the liver properties compared to the previously monopolymeric systems (Vanderhooft et al., 2009). In the case of our hydrogels, the Gel-HA 20-80 mixture exhibited a G' value of 375 Pa that is close to 400 Pa and was chosen as optimal for hepatic cell culture and scaffold preparation.

Making use of the rubber elasticity theory, we calculated the Young's modulus of the hydrogels in the swollen state, which is closer to the state we found in cell culture, resulting very similar among the different samples and of the order of magnitude of thousands of Pa (Figure 22). The result is consistent with the theory, which says that the modulus of elastomers is only dependent with the crosslinking density, which in our hydrogels is very similar for all the samples (Table 8). This modulus was used to calculate the G' at the swollen state, which was also similar among samples, contradicting our previous experimental results with similar samples, where the modulus increased with the content of HA within the samples (Sanmartín-Masiá et al., 2017). The predicted G' values of swollen Gel-HA hydrogels can be valid in terms of liver-like mechanical properties, being close to the upper range of native liver tissue properties (400-600 Pa) and supporting the feasibility of Gel-HA systems as optimal for hepatic cell culture.

The use of scaffolds seeded with different types of hepatic cells has been explored by different authors since they not only provide a 3D microenvironment, but also the interconnected pores structure allows a suitable nutrient supply (da Silva Morais et al., 2020). Some studies have used the scaffolds for improving the differentiation potential of multipotent stem cells before transplanting them (Tai et al., 2010), whereas others use the scaffolds as a delivery method and study the differentiation potential *in vivo* (Lin et al., 2015; Zhang et al., 2019). For this reason, the Gel-HA scaffolds were prepared and characterized for future regenerative medicine applications.

Pore size and porosity have a significant influence on the regeneration and the function of cells. Previous reports have suggested a pore size of 50-200 μm for the culture of hepatocytes (Gao et al., 2020; Ranucci et al., 2000). In the case of freeze-dried scaffolds, optimal pore size for the culture of hepatocytes was higher than 100 μm (Fan et al., 2010). The same order of magnitude, 82 μm, was also optimal for rat hepatocytes cultured on collagen scaffolds (Ranucci et al., 2000). Similar Gel-based scaffolds but with different crosslinkers, achieved higher pore diameters suitable for hepatic cell culture, with values from 246 μm to 167 μm depending on the chemical reaction (Zhang et al., 2016). Our results show that the scaffold is composed of interconnected pores with the shape of honeycomb of 102 μm mean size that seems adequate for hepatocyte culture. Since the mechanical shear modulus of our scaffold is close to the upper range of the native liver (752 Pa) a proper stimulation of cells is expected. The hydrogel has shown a storage modulus that is lower than that of the scaffold, probably due to the more effective crosslinking reaction produced in CF-KRB. In addition, tanδ analysis supports the use of Gel-HA scaffold since its value (approximately 0.1) is close to the values obtained by oscillatory rheology of fresh human liver tissue (0.25) (Estermann et al., 2021). Other authors have reported higher tanδ values around 0.6 yet not comparable due to the methodology based on dynamic indentation on the liver surface. The measurements presumably were higher due to the influence of the liver capsule along other structures like vascular and connective tissue (Lim et al., 2009). The equilibrium water content of the scaffold resulted lower than that of the hydrogel, due to the more effective crosslinking of CF-KRB. Despite the lower swelling capacity, the resulting porosity seems adequate for the cell culture of hepatocytes, as is similar to the one observed in the literature.

In summary, synthetic hydrogels fail to fully replicate the biological complexity and cues present in native tissues, including the heterogeneity found in the ECM. In this thesis, a system was developed using Gel and HA to mimic the liver ECM, which is primarily composed of collagen and GAGs. By varying the ratio between both polymers, we were able to tune the mechanical properties of the hydrogels, in order to reproduce the liver stiffness between 400-600 Pa (Desai et al., 2016) and the viscoelastic behaviour described by tanδ around 0.2. Gel-HA hydrogels accomplished to resemble the mechanical properties of the liver, allowing to use the system for liver tissue engineering applications.

Chapter 2. Biological performance of Gel-HA hydrogels and scaffolds.

1. Optimisation of Gel-HA hydrogels for hepatic cell culture with a hepatoma cell line (HepG2)

In order to select the optimal composition of Gel-HA for hepatic cell culture, HepG2 cells were encapsulated in hydrogels with different compositions of Gel and HA. Representative images and image analysis showed no significant differences in viability between different hydrogel compositions (Figure 27). In fact, in all the conditions viability was higher than 90% (Figure 28).

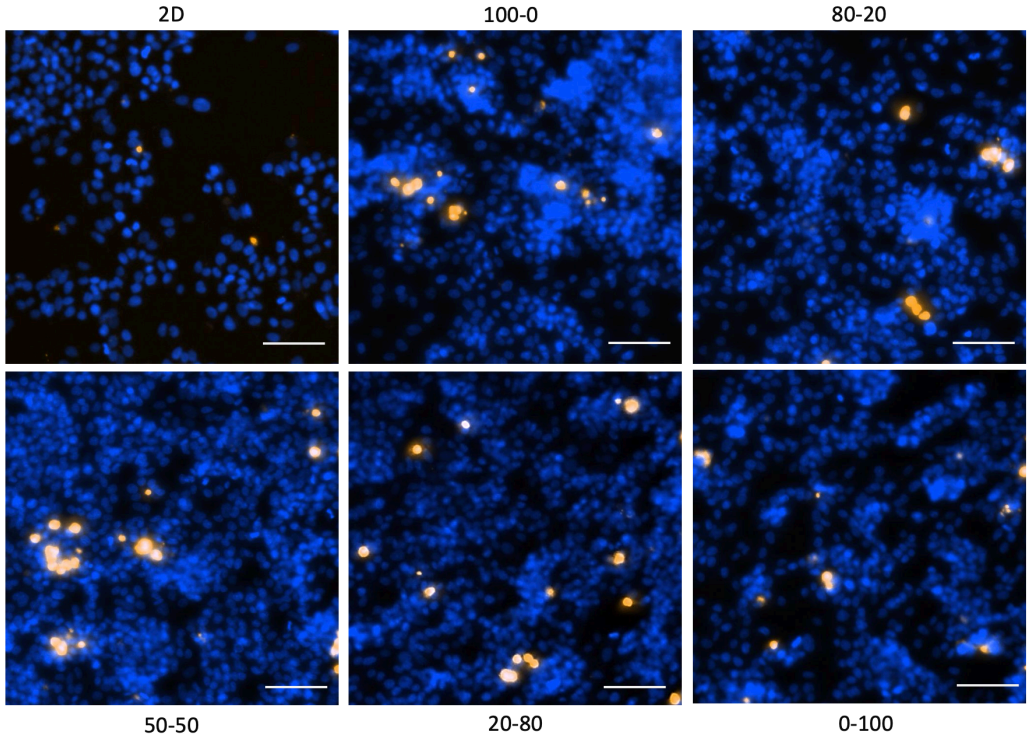

***Figure 27**. Representative images of live-dead assays of HepG2 cells in Gel-HA hydrogels after 24 h of culture. Nuclei were detected by Hoechst 33342 (blue) staining in all the images. Dead cells were identified by PI staining (orange). Scale bar 100 µm.*

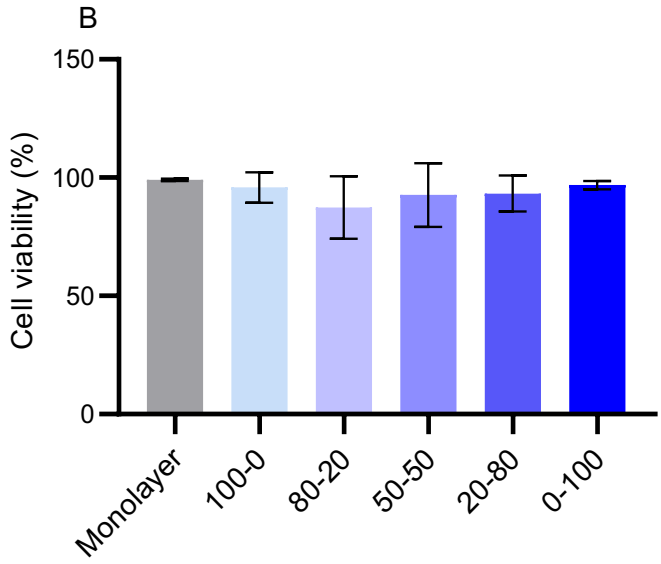

Figure 28. Quantification of cell viability of HepG2 cells cultured within Gel-HA hydrogels.

Since long crosslinking times for the HA-rich compositions had been previously observed, we analyse the distribution of the cells at different levels of the hydrogel using confocal microscopy. As shown in Figure 29, the high viscosity of the solutions prevented the cell suspension to go to the bottom of the hydrogel and a homogeneous distribution of cells within the entire volume of the hydrogels was observed.

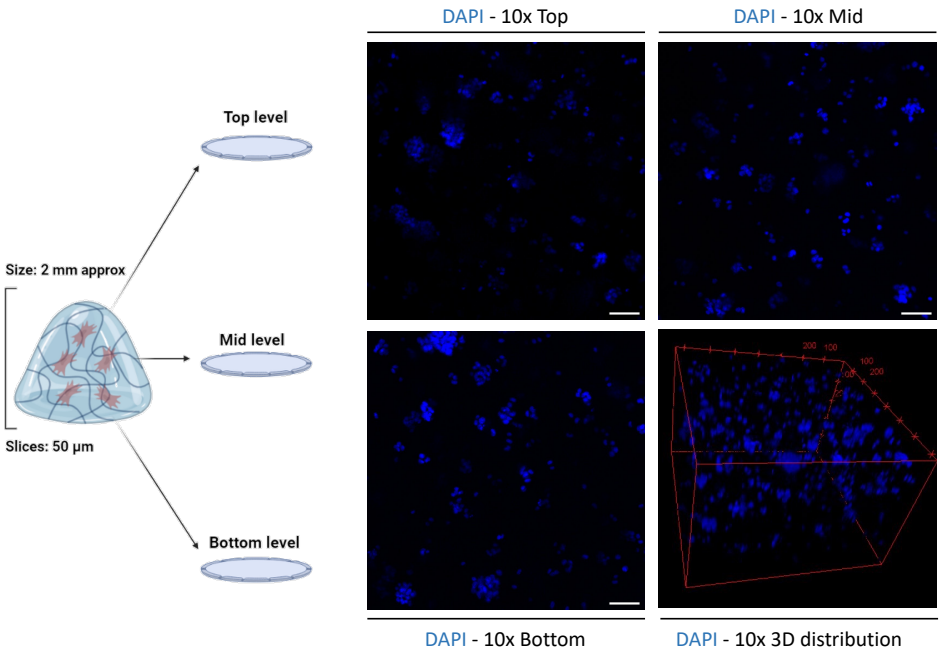

Figure 29. Distribution of HepG2 cells inside Gel-HA (20-80) hydrogels by immunohistochemistry. *Scheme of the analysis of the distribution of the cells. Slices (50 µm) from top, mid, and bottom levels of the hydrogel were obtained and stained with DAPI for nuclei staining. 3D reconstruction from 500 µm z-stack. ImageJ software employed for image analysis and 3D reconstruction. Scale bar 100 µm.*

Although no significant differences in cell viability were observed, to select an optimal composition for hepatic cell culture, other hepatic functions were also analysed. In this sense, increased ureogenic capability, a specific hepatic function, was observed in HA-rich hydrogels (Figure 30A), indicating an advantage for hepatic cell culture. Similar results were observed for albumin synthesis and secretion into the culture media of HepG2 cells encapsulated in hydrogels with different Gel-HA composition (Figure 30B).

These results, together with the analysed mechanical properties described in Chapter 1, led us to select the 20-80 Gel-HA composition as an optimal for hepatic cell culture because its storage modulus (G' = 375 Pa) is very close to the range of the human liver (from 400 to 600 Pa (Desai et al., 2016; Yeh et al., 2002)).

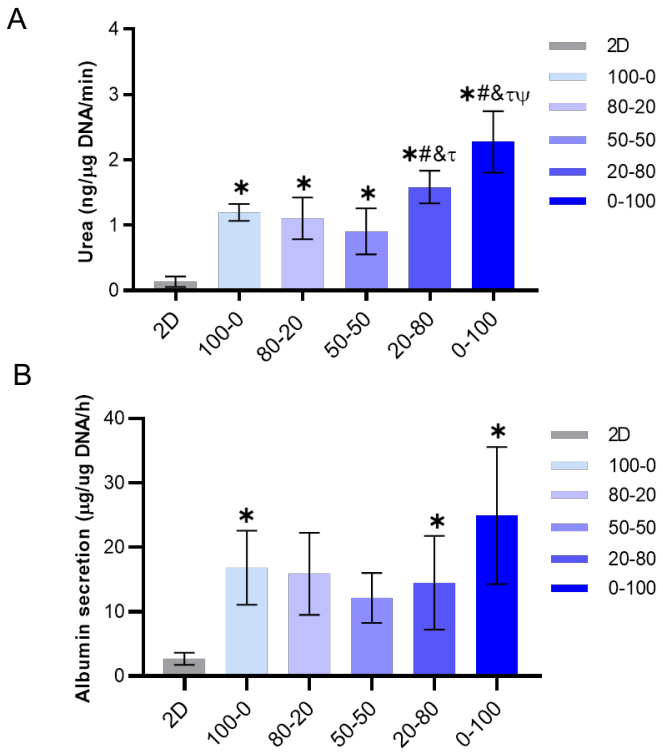

Figure 30. In vitro assessment of Gel-HA hydrogels with HepG2 cells. *A) Ureogenic capability of HepG2 encapsulated within Gel-HA. B) Albumin synthesis in different culture conditions. *At least p≤0.01 (compared to monolayer); #p≤0.001 (compared to Gel); &p≤0.01 (compared to 80-20); τp≤0.001 (compared to 50-50); Ψp≤0.001 (compared to 20-80); (n=6; ANOVA followed by Tuckey's multiple comparisons test).*

2. Gel-HA scaffolds increase the functionality of primary human hepatocytes *in vitro*.

After selecting the appropriate conditions for liver cell culture, Gel-HA 20-80 scaffolds were prepared as previously described in sections 1.6 and 4.1. Before testing the suitability of the developed scaffolds for clinical application using an animal model of disease, we explored the suitability of the Gel-HA scaffolds for hepatic cell culture, since PHH should maintain key hepatic functions such as detoxification capacity or ureogenesis. For this purpose, PHH were cultured in Gel-HA 20-80 scaffolds and cell viability and functionality were assessed and compared to monolayer cultures after 24 h of culture. The viability of cryopreserved PHH after thawing was higher than 80%. 24 h after seeding PHH in Gel-HA scaffolds, viability was maintained (78%). Immunofluorescence of scaffold sections revealed that PHH express key hepatic markers such as

albumin and that maintained cell-cell interactions that are homogeneously distributed throughout the scaffolds (Figure 31).

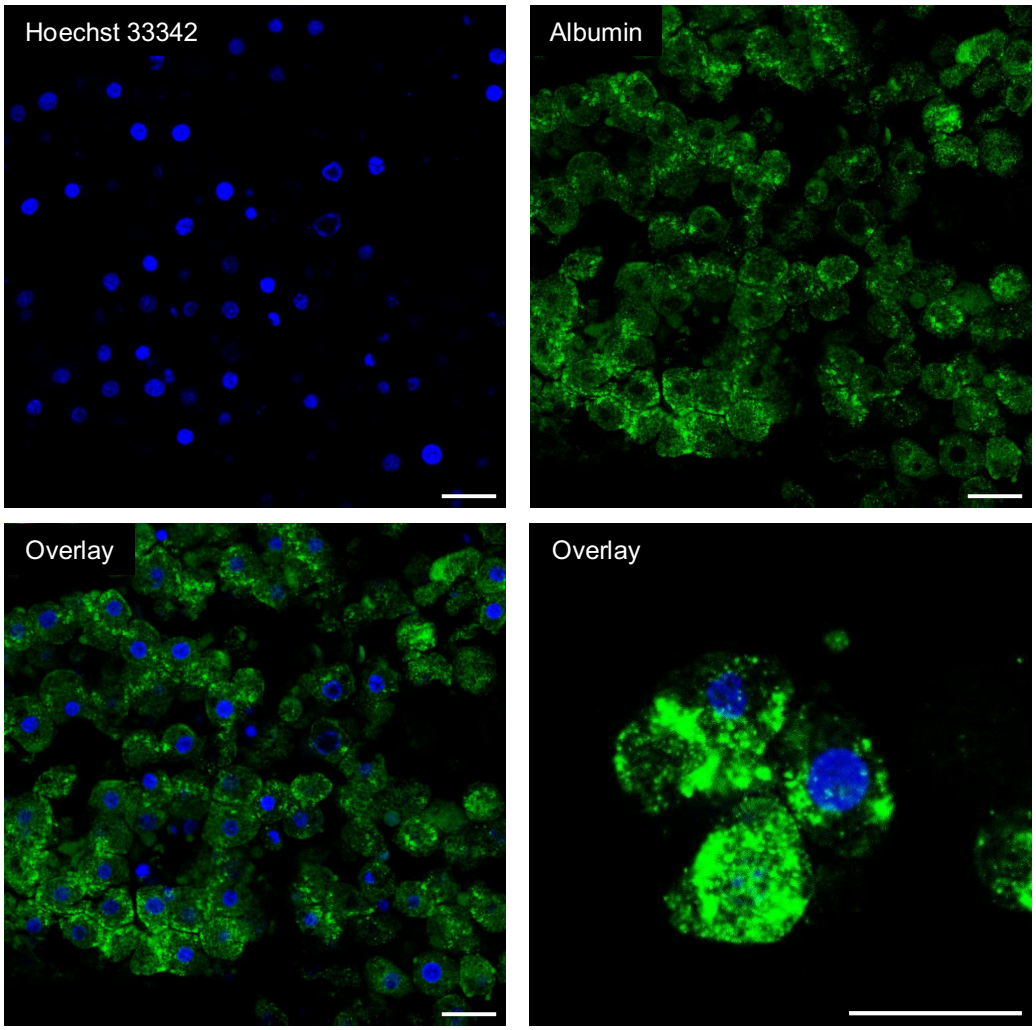

Figure 31. Expression of albumin in PHH cultured in Gel-HA scaffolds. *Immunofluorescence of human albumin (green) in PHH after 24h of culture in Gel-HA scaffolds. Nuclei were stained with Hoechst 33342 (blue). Scale bar 20 μm applies to all images.*

Drug biotransformation comprises different reactions such as oxidations, reductions or hydrolysis, that introduce new polar groups in the molecule (phase I reactions), and conjugations with hydrophilic endogenous cofactors (phase II reactions) to form water-soluble metabolites, that are finally excreted (Donato et al., 2015). These metabolism reactions mainly occur in the hepatocytes; thus, the evaluation of phase I and phase II activities is an essential indicator of the functionality of the cells. Phase I reactions are mainly mediated by CYPs, so, we

evaluated the activity of 8 major isoforms. Functional activities of CYP1A2, CYP2A6, CYP2B6, CYP2C9, CYP2C19, CYP2D6, CYP2E1 and CYP3A4 were higher in PHH-scaffolds compared to 2D cultures (Figure 33). The higher activity levels in PHH cultured in scaffolds were detected for CYP2A6, CYP2B6 and CYP2D6.

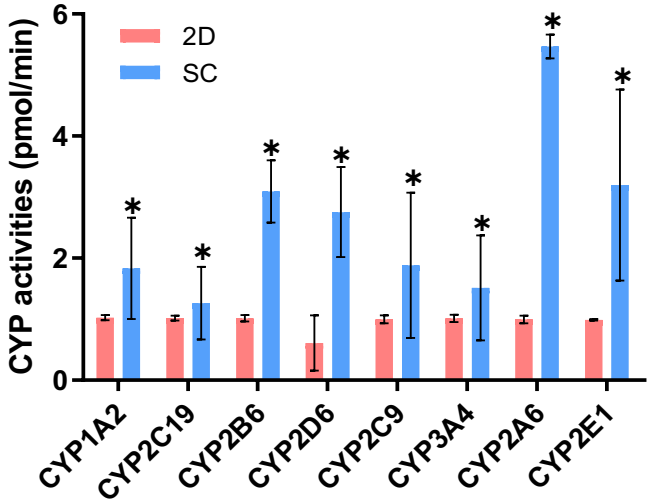

Figure 32. In vitro culture of PHH in Gel-HA scaffolds. *CYP activities levels in PHH cultured in Gel-HA scaffolds (SC) and compared to PHH cultured on monolayers (2D) after 24h of cell culture. *At least p≤0.05 (Student's t-test compared to 2D cultures).*

On the other hand, UGTs have been described as the major contributor of phase II metabolism of xenobiotics and endobiotics (Jancova et al., 2010). When phase II drug metabolizing enzymes (UGT1A1, UGT2B7) activities were analysed, we only detected enzymatic activities in PHH cultured within scaffolds, which confirms the advantage of using 3D culture over monolayers for culturing PHH (Figure 33A-B).

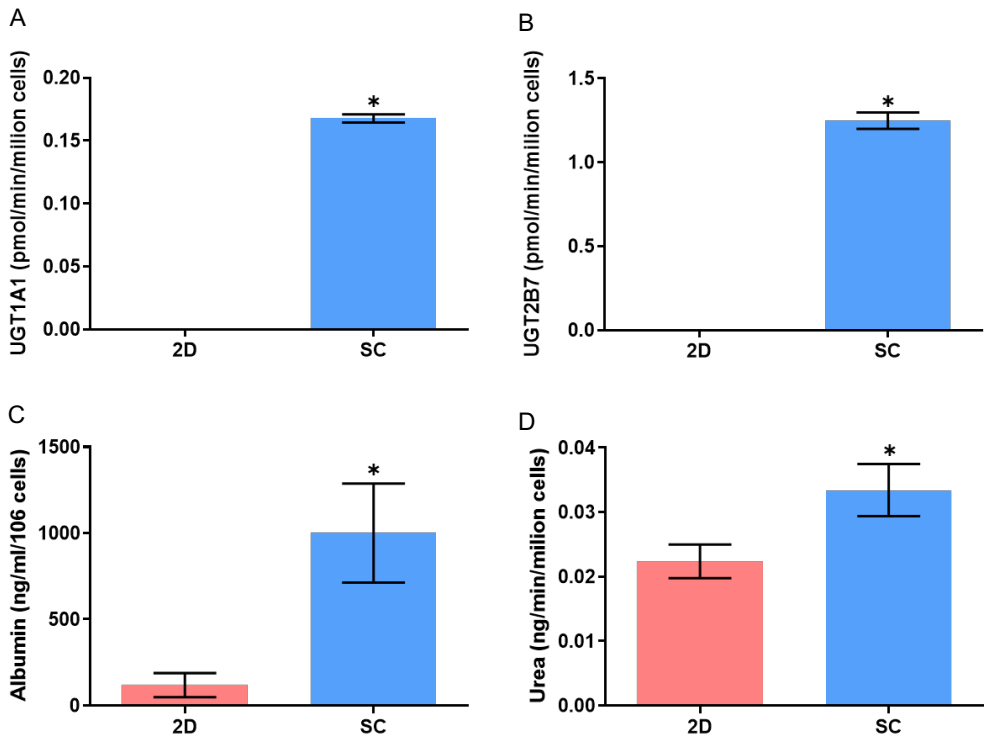

Figure 33. In vitro culture of PHH in Gel-HA scaffolds. *Comparative functionality: A) UGT1A1, B) UGT2B7 activity levels, C) secretion of albumin and D) ureogenic capacity) of PHH cultured on 2D or Gel-HA scaffolds after 1 day in culture. *At least p≤0.05 (Student's t-test compared to 2D cultures).*

Human albumin secreted into the media was measured by ELISA. Albumin production significantly increased in PHH cultured within scaffolds compared to those cultured in 2D (Figure 33C) after 24 h of culture. Additionally, PHH-scaffolds showed a significant higher ureogenic capability compared to monolayer cultures (Figure 33D).

3. Transplantation of Gel-HA scaffolds seeded with PHH rescues mice with APAP-induced liver failure.

Before the safe transfer to the clinical, it is essential to demonstrate the effectiveness or advantages of a therapy preclinically. For this reason, the tested Gel-HA scaffolds seeded with PHH in an animal model of ALF, using an overdose of APAP, the most common cause of drug induced liver injury that results in fatal ALF.

A single dose of APAP at 300 mg/kg resulted in lethality of 56% of the animals 1 week after the induction of the damage, whereas all the transplanted animals (with cells administered intrasplenically or scaffolds containing cells) survived, indicating a survival advantage for those animals receiving liver cell therapy (Figure 34A).

Human albumin was detected in the sera of transplanted mice, indicating the success of transplantation (Figure 34B). The levels of human albumin were higher in animals transplanted with PHH-scaffolds (APAP+SC) compared to those which received cells alone (APAP+C). These albumin levels were maintained up to 30 days after transplantation (data not shown). No detectable levels of human albumin were measured in non-transplanted animals (control and sham group).

Increased AST and ALT levels are indicative of PHH damage after ALF induction. As expected, APAP administration induced a significant increase in both transaminases (6-fold for ALT and 10-fold for AST) 24h after the administration. By contrast, a reduction in transaminases levels was observed in transplanted animals. Importantly, this reduction was significantly higher in animals treated with scaffolds containing PHH (APAP+SC) compared to those which received just PHH (APAP+C) intrasplenically after 1 and 3 days (Figure 34C-D).

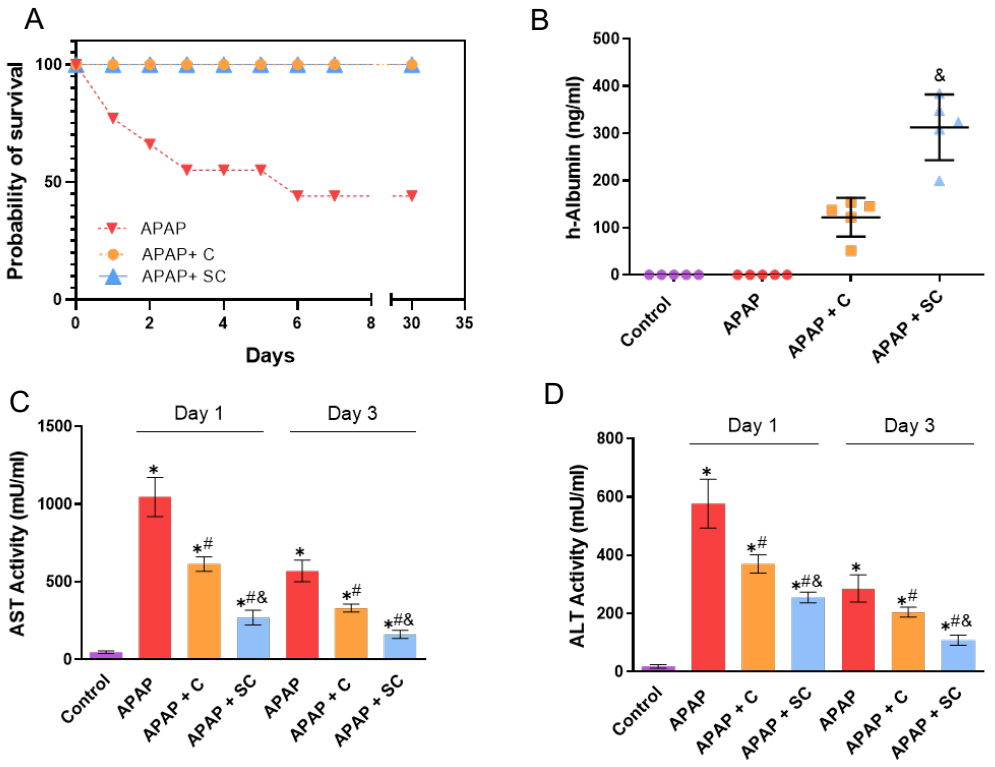

Figure 34. In vivo effects of PHH after intrasplenic transplantation or intraperitoneal administration of Gel-HA scaffolds in SCID mice with ALF. *A) Survival of transplanted animals compared to sham mice. B) Human albumin levels in the serum of transplanted animals. [&]At least p≤0.001 (compared to APAP-treated animals transplanted with PHH intrasplenically; Student's t-test). C-D) Transaminases levels (ALT and AST) in mice after ALF or mice transplanted with cells (APAP+C) or scaffolds (APAP+SC) containing PHH, 1 or 3 days after transplantation. *At least p≤0.05 (compared to control animals); #p≤0.01 (compared to APAP treated animals); &p≤0.01 (compared to APAP treated animals transplanted with PHH intrasplenically (APAP+C)) (ANOVA followed by Tuckey's multiple comparisons test).*

Histopathological analysis of liver tissue of the different animal groups revealed significant differences among them. The mice in the APAP group showed massive hepatic centrilobular necrosis, necroinflammation and degeneration. The livers of the mice in the APAP+C and APAP+SC groups exhibited a reduction of the necrotic areas and no signs of necroinflammation (Figure 35).

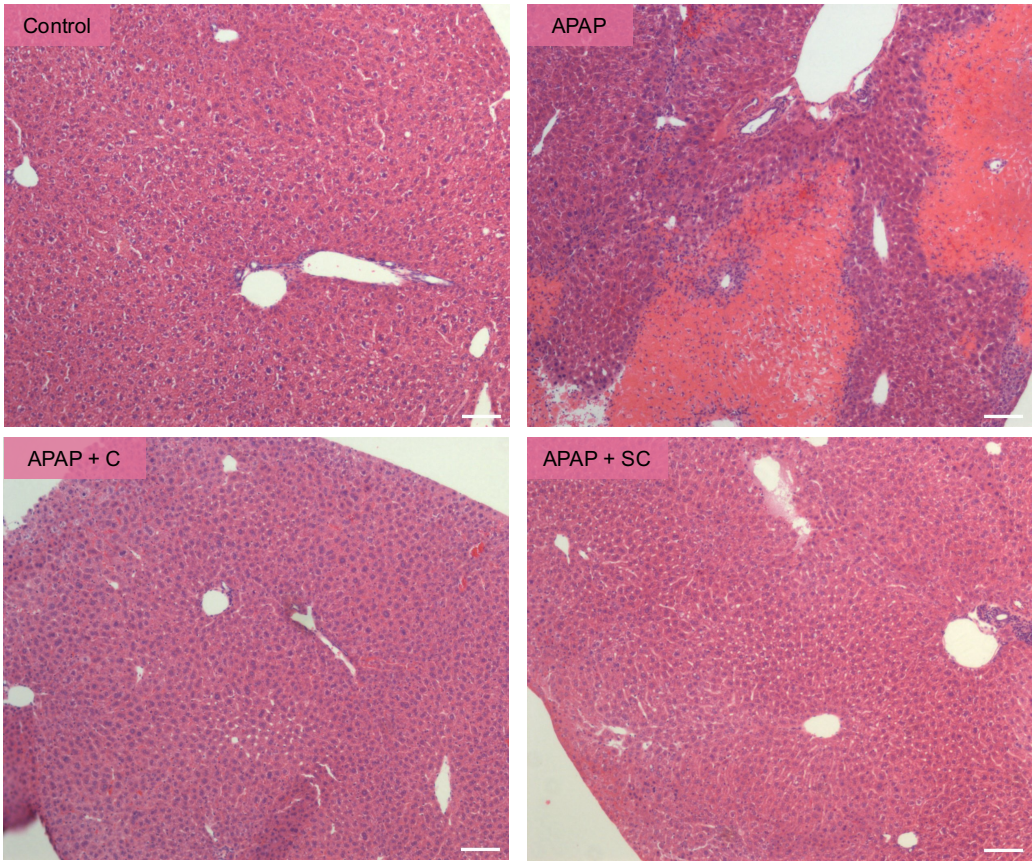

Figure 35. Histological images of liver tissue from the SCID mice during the in vivo experiment. *Representative histological images obtained from each group and stained with haematoxylin-eosin staining. APAP group presented significant inflammation and necrotic areas. Scale bar 100 μm.*

4. Transplantation of Gel-HA scaffolds with PHH results in a reduction of liver oxidative stress and decreased inflammatory response induced by APAP.

Glutathione (GSH) depletion and oxidative stress induction have been described as major mechanisms implicated in APAP-induced toxicity. Moreover, an elevation in the GSH analogue OA has been described after APAP administration (Soga et al., 2006). The differential metabolomics study revealed significantly increased levels of OA in the livers of APAP-treated mice compared to control animals, while significantly reduced levels were detected in transplanted animals (Figure 36A), with animals transplanted with PHH-scaffolds (APAP+SC) showing the lowest levels of OA. In order to look for a possible non-invasive biomarker of the success of liver cell transplantation, the

levels of OA were analysed in the sera of the different experimental groups. Increased OA levels in the serum of animals with APAP-induced ALF were detected, whereas a decrease was observed in the animals that had ALF and received the transplantation of PHH (Figure 36B). Interestingly, the reduction was significantly higher in the animals transplanted with scaffolds (APAP+SC) compared to those that were intrasplenically transplanted with PHH (APAP+C), which is in accordance with the reduction of key hepatic markers such as transaminases levels. These results indicate that levels of OA could be a potential indicator of the therapeutic efficacy of cell therapy.

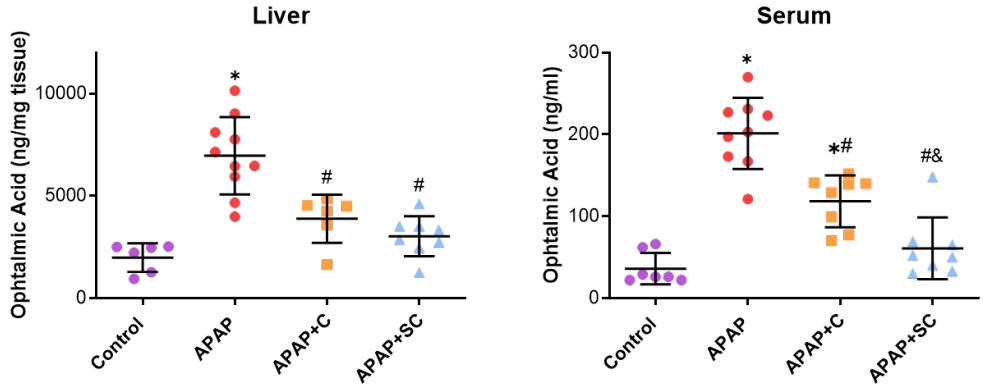

Figure 36. Transplantation of scaffolds containing PHH reduces OA levels after ALF. *A) OA levels in the liver of APAP mice receiving PHH intrasplenically (APAP+C) or transplanted intraperitoneally scaffolds with PHH (APAP+SC). B) OA levels in the serum of the different experimental groups. *At least p≤0.05 (compared to control animals); $^{\#}$p≤0.01 (compared to APAP treated animals); $^{\&}$p≤0.01 (compared to APAP treated animals transplanted with PHH intrasplenically (APAP+C)) (ANOVA followed by Tuckey's multiple comparisons test).*

Augmented levels of pro-inflammatory cytokines have been described after APAP overdose (Lawson et al., 2000). The levels of CXCL1, IL-6, TNF-α and IFN-γ in the serum of the transplanted animals were analysed. Increased cytokine levels were observed in animals after APAP administration, whereas a reduction of these levels was observed after PHH transplantation (Figure 37). The levels of CXCL1 were significantly reduced in animals transplanted with PHH-scaffolds (APAP+SC) compared to those transplanted with PHH (APAP+C). This reduction in PHH-scaffolds animals was also observed for IL-6 and TNF-α compared to APAP animals, although comparatively to PHH-mice this reduction was not significantly different. Finally, increased IFN-γ levels were observed in APAP-treated animals, but not significant changes were observed between transplanted animals.

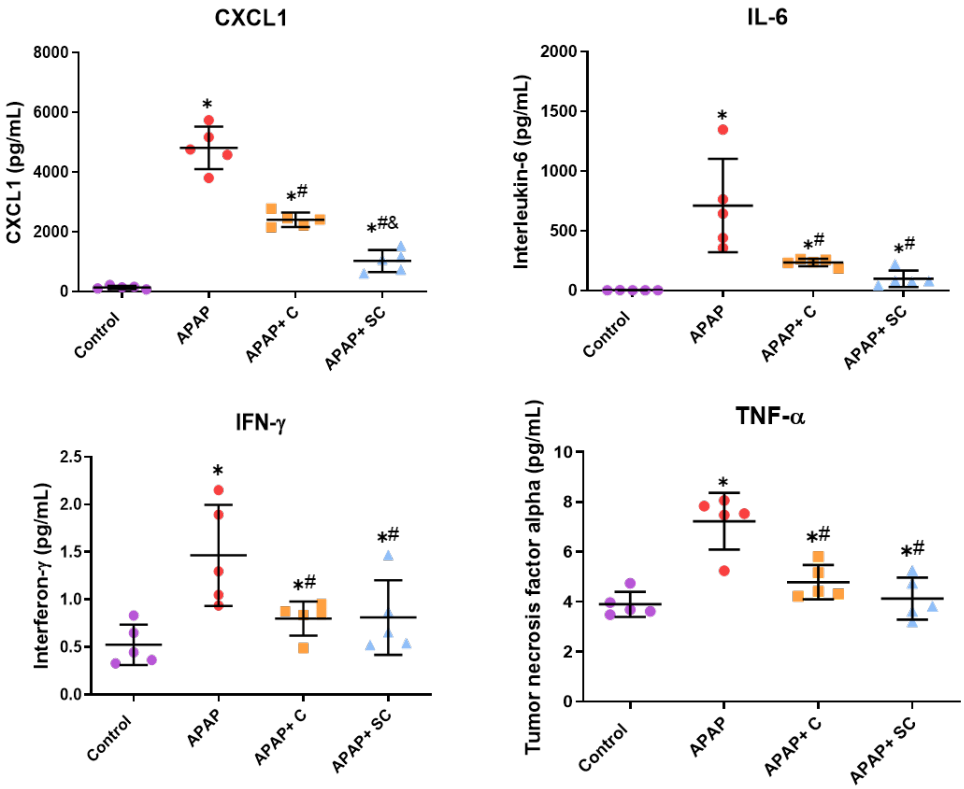

Figure 37. Transplantation of PHH-scaffolds reduces proinflammatory cytokines after ALF. *Serum concentrations of proinflammatory cytokines (CXCL1, IL-6, IFN-γ and TNF-α) were determined by Luminex in the different animal groups. *At least p≤0.05 (compared to control animals); # p≤0.01 (compared to APAP treated animals); & p≤0.01 (compared to APAP treated animals transplanted with PHH intrasplenically (APAP+C)) (ANOVA followed by Tuckey's multiple comparisons test).*

Discussion

Liver transplant is currently the only effective treatment for end-stage liver diseases, although it is limited by the scarcity of liver tissue, which has led to a search for alternative therapeutic approaches such as cell transplantation. Cell-based liver therapies based on retrieving and steadying failed metabolic function(s) for acute and chronic diseases could be a valuable substitute for organ transplantation, even though they are limited by the low engraftment capability and reduced functional quality of PHH. The ability of donor cells to access the liver and survive long enough to exert a beneficial therapeutic effect could be a significant obstacle to successful transplantation. Although cells integrate in the liver parenchyma after accessing through the sinusoids (Dwyer

et al., 2021; Gupta et al., 1999), they need appropriate signals as well as an advantage over host cells to significantly repopulate the liver (Grompe et al., 1999). In this regard, extrahepatic liver cell therapy, which provides functional assistance to the injured liver and allows vascularization, has recently been proposed as a delivery and retention method. The main objective of this thesis was to study the advantages of transplanting banked PHH seeded in Gel-HA scaffolds over intrasplenically transplanted PHH in APAP-overdosed mice, to correct hepatic disease.

Regarding the 3D culture of hepatic cells, our results agree with those that have previously demonstrated that PHH cultured in 3D constructs show better functionality than cells cultured on monolayer (Baze et al., 2018; Godoy et al., 2013). For the selection of the most suitable composition, HepG2 cells were used. Encapsulation of hepatic cells in Gel-HA hydrogels resulted in increased functionality and optimal viability for all the compositions, although HA-richer compositions with mechanical properties within the range of human liver seemed to increase the ureogenic capacity. Despite HepG2 cells show a limited metabolic capacity, their hepatic background makes them suitable for initially exploring the effects of 3D culture. Cell viability remained close to 95% after 24 h of cell culture, as well as an increased ureogenic capacity and albumin synthesis compared to the 2D cell culture. Likewise, proteins such as collagen and Gel have been used for HepG2 cells culture in 3D platforms, observing increases in ureogenic capacity and albumin synthesis (Billiet et al., 2014; Cui et al., 2019). HA also crosslinked by click chemistry displayed along HepG2 cells increased hepatic functionality compared to the forementioned 2D culture (Christoffersson et al., 2019). Altogether, HepG2 cells' performance together with the mechanical properties discussed in the Chapter 1, allowed to select the blend of Gel and HA in a ratio 20-80 as optimal to carry the experiments with PHH.

Hepatocytes are the most predominant cell type of the adult liver and perform essential functions, including plasma protein secretion, ureogenesis, metabolic homeostasis or detoxification (Chen et al., 2018). Most studies generally use the measurement of albumin and urea as indicators that transplanted cells are mature and functional, although there is a lack of standardization regarding the adequate levels for function (Ali et al, 2021). Furthermore, complete, and exhaustive characterization of cellular products is mandatory before their clinical application. It has been shown that although no significant differences in viability between 2D and 3D cultures were shown, a complete characterization of the cellular systems revealed important additional improvements of culturing hepatic

cells in Gel-HA hydrogels or scaffolds. The formation of urea is an essential hepatic function for the elimination of ammonia generated from protein catabolism in order to prevent or relieve hyper-ammonaemia in recipients, and also for the utilization of most amino acids for gluconeogenesis. It is also a good indicator of the degree of mitochondria preservation (Tolosa et al., 2014). On the other hand, detoxification, one of the liver's vital functions, involves both waste removal and xenobiotic biotransformation and is of special interest for the clinical setting of hepatocyte transplantation in which recipients receive extensive medication. Therefore, the increase in the ureogenic capacity, albumin production and the metabolic performance of the cells very likely confer to scaffolds an advantage *in vivo*.

APAP overdose is a common cause of acute liver injury and supplies a model compound for preclinical studies since the molecular mechanisms implicated in APAP-induced toxicity are well described (Starkey-Lewis et al., 2020). N-acetylcysteine treatment serves as an antidote, although this therapy is not effective if it is administered more than 10 h after the ingestion, and patients may develop ALF. Although liver transplantation is the only effective treatment for ALF, liver cell therapy could offer time for regeneration of the liver itself by recovering some liver functions. In our system, the administration of APAP produced ALF was characterized by decreased survival and increased levels of ALT, AST and proinflammatory cytokines. The administration of PHH resulted in a reduction of transaminases levels, whereas the administration of PHH-laden scaffolds resulted in better results, probably because cells better maintain functionality and were retained into the host liver. These results agree with those showed in rats with ALF induced by galactosamine, where the transplantation of hepatocytes encapsulated in Alg microbeads improved the severity of liver damage (Jitraruch et al., 2014). However, our system offers the advantage of using biodegradable materials present in the liver ECM. Moreover, Gel enables cell adhesion and HA provides stiffness and hydration.

ALF is characterized by hepatocellular necrosis and inflammation leading to liver failure. In the animal model used, we demonstrated that an overdose of APAP produces necrosis in the liver tissue that was reduced after cell therapy. It is known that APAP hepatotoxicity is initiated by the formation of N-acetyl-p-benzoquinone imine, a reactive metabolite, which depletes cellular GSH and produces the formation of protein adducts that finally lead to mitochondrial injury and oxidative stress induction (Ramachandran et al., 2017). OA is a GSH analogue where the SH group of the cysteine is replaced by 2-aminobutyrate. Significant differences in the levels of OA were observed after APAP

administration, which correlates with observations in both animal models and humans after an overdose of paracetamol (Kaur et al., 2015; Soga et al., 2006). Interestingly, after transplantation of PHH a statistically significant reduction in these levels in tissue and serum was observed, suggesting that OA could be also a valuable biomarker of the effectiveness of liver cell transplantation in ALF.

The advantages of the scaffold method, compared to intrasplenic administration, were also attributed to the difference in PHH delivery efficiency between the intrasplenic and the scaffold transplantation system, since in the intrasplenic infusion, a major percentage of the cells (more than 70%) are rapidly removed by phagocytes and macrophages (Gupta et al., 1999; Nagamoto et al., 2016). Additionally, classical cell transplantation requires cells to be transplanted either into the spleen or the liver of the animal or in the portal venous systems in humans, which would be considerably high-risk process. The use of PHH-laden scaffolds offers a safe method that allows the enhanced retention and function of PHH cultured in scaffolds, which was confirmed by biochemical and histological analysis, indicating that Gel-HA scaffolds could result in significantly improved therapeutic effect of PHH on ALF by enhancing delivery and retention and increasing long-lasting effects. Delivered Gel-HA scaffolds also decreased the inflammatory response and oxidative stress induced by APAP compared to traditional intrasplenic administration of PHH.

The scarce availability of liver tissue to isolate good-quality cells and the low engraftment capability of the cells into the host liver limit the wider application of hepatocyte transplantation. Our scaffold-based strategy allows the retention of the cells and improvement of hepatic functions; however, availability of PHH could be still a limitation (Forbes et al., 2015; Tolosa et al., 2016). Other cell sources such as human pluripotent stem cells differentiated into HLC could be used as autologous cell therapies that would avoid immune rejection and/or help to create biobanks of readily available HLC for the emergency treatment of ALF (Tolosa et al., 2015, 2016). In this case, the Gel-HA could also increase the functionality and performance of the differentiated cells, as it has been previously shown with other 3D culture systems (Godoy et al., 2013). Overall, our results open the avenue to start testing other cell types such as differentiated iPSC cultured in Gel-HA scaffolds as an alternative cell source.

Finally, it should be considered that infiltrating monocytes and other liver cell types such as KC play crucial roles in liver homeostasis and immunity and contribute to liver pathology (Zigmond et al., 2014). In this sense, alternatively activated macrophages have been shown to reduce liver injury and inflammation in APAP-treated mice (Starkey-Lewis et al., 2020); therefore, the use of other

cell types in scaffolds for treating liver disease should be also considered. Since no cell type can meet all the requirements for successful regeneration, different researchers have opted to explore the co-culture of different cell types. For instance, the use of endothelial cells has been demonstrated to not only induce vascularization but to stimulate liver organogenesis and regeneration (Ding et al., 2010; Takebe et al., 2013). Future multi-cell type strategies would help to expand the application of liver cell therapy.

To sum up, in contrast to conventional delivery techniques such intrasplenic injection, this thesis proposes a viable PHH transplant approach based on the utilization of Gel-HA scaffolds to enhance hepatic functionality in an ALF mouse model. In clinical practice, biodegradable materials like Gel and HA would be preferable to other non-biodegradable materials like alginate microbeads. Transplantation of Alg microbeads seeded with PHH to children diagnosed with ALF showed great results in terms of improve the clinical prognosis. Part of the children become unlisted for liver transplant due to their clinical improvement; others survived 1 month before the transplant even being considered as urgent transplantation. However, after 3-6 months the retrieval of the Alg microbeads revealed patients which developed granulation tissue around them. The authors address this variability to the irregular shape of the microbeads during the fabrication and the deformation during the transplantation process (Dhawan et al., 2020). The problematic associated to the retrieval of the biomaterials would be sorted out thanks to polymers with natural origin. Gel-HA scaffolds that increased liver cell therapy's *in vivo* effectiveness as well as PHH functionality *in vitro*. Since the growth in Gel-HA improves the function of the hepatic cells, the established technique could be employed for additional applications such as disease modelling and drug screening, in addition to being a potent tool in tissue engineering and regenerative medicine.

Chapter 3. Gel-HA bioprinted 3D constructs towards scale up and automatise culture of hepatic cells.

1. Rheological characterization of Gel-HA bioinks

1.1. Viscosity of Gel-HA bioinks.

Inks for bioprinting need to accomplish certain requirements for manufacturing with a 3D bioprinter. Bioinks need to be extrudable, and then, meet criteria asked for their application in tissue engineering or other approaches. We tested a variety of bioinks with potential applications for bioprinting with variable HA concentration and incorporating Gel at different concentrations (4% and 5% w/v) and ratios (20-80 and 50-50). The original formulation of Gel-HA systems was based on low molecular weight polymers, thus allowing the pipetting of low viscosity polymers along with cells. However, bioprinting techniques and in particular EBB methods have different requirements. Bioinks are required to display higher viscosities to be able to print 3D constructs with enough resolution and to maintain the shape once printed. The Gel-HA bioink transition from hydrogel system has been based on not performing the acidic degradation of the HA before the tyramine grafting. Thus, the molecular weight used increased from 300 kDa to 1.2 MDa.

Firstly, rheological measurements were performed on the bioinks, specifically shear viscosity tests, to evaluate the shear-thinning properties of the material, and its shear behaviour, which is key for EBB. Cellink START ink was used as our control to mimic due to its excellent printability. Shear viscosity results can be differentiated in two regions in the viscosity measurements (Figure 38): zero-shear zone and shear stress zone. The region that informs us about the ink behaviour upon extrusion conditions is the shear stress zone (Cooke & Rosenzweig, 2021; Paxton et al., 2017). Therefore, differences in the zero-shear zone are a mere indicator of the ink viscosity as is, which is nevertheless an important factor to consider especially for manipulation purposes, such as pipetting difficulty or achieving a homogenous mixture with other components.

All HA-HMW inks present a shear-thinning behaviour, as seen by the descending curves in Figure 38, where the viscosity is reduced when increasing the shear stress. Non-shear thinning (i.e., shear thickening) behaviour would be difficult or even fully prevent the extrusion of the ink through the nozzle. It is worth noting that HA HMW 5% was deemed the maximum concentration to be studied given that its apparent high viscosity was already hard to work with.

Interestingly, it was observed that none of the formulations reached a zero-shear viscosity as high as the control. However, if we look at the shear stress zone, in Figure 37 we can see that the viscosity values increase and approach the control as the concentration of HA increases, to a point where HA HMW 4% and HA HMW 5% overlap and even surpass the control between 10 and 1000 s^{-1}. HA HMW 3% has the closest shear stress behaviour to the control. Given these results, we proceeded to test the blends of HA HMW 4 and 5% with Gel, which we would expect would reduce the viscosity of pure HA inks and could help tune the behaviour during extrusion.

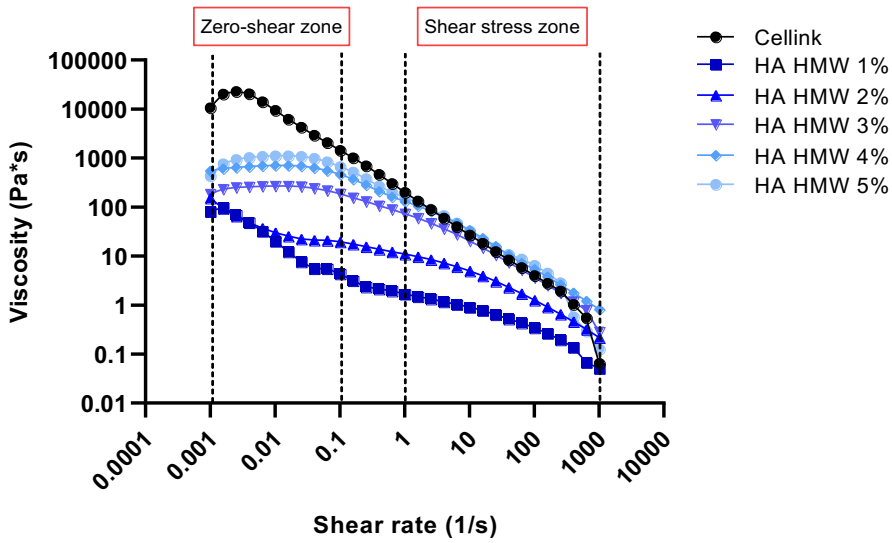

Figure 38. Shear stress analysis of non-crosslinked HA-HMW inks by rheology. *Evolution of inks viscosity as a function of the shear rate measured in the rheometer between 0.001 and 1000 s^{-1}. (n=3). Two regions that explain the behaviour and characteristics of the bioink can be differentiated: zero-shear zone and shear stress zone.*

As seen in Figure 39, with the addition of Gel to HA-HMW inks (note that from now Gel-HA bioinks always refers to HA-HMW since the transition was based on HA-HMW), the Gel-HA 4% resembles the HA-HMW 3% behaviour both in zero-shear and shear stress zones. Given that HA-HMW 3% has the closest behaviour to the Cellink control, we can infer that Gel-HA 4% will have an optimal performance in the printing process. As for Gel-HA 5%, we observe a reduced zero-shear viscosity compared to pure HA-HMW 5%, more similar to HA-HMW 4% instead. However, the shear stress curve does still overlap with the highest concentrations of HA. Based on these results, we could proceed to test whether this measured behaviour would correspond to its extrudability ability.

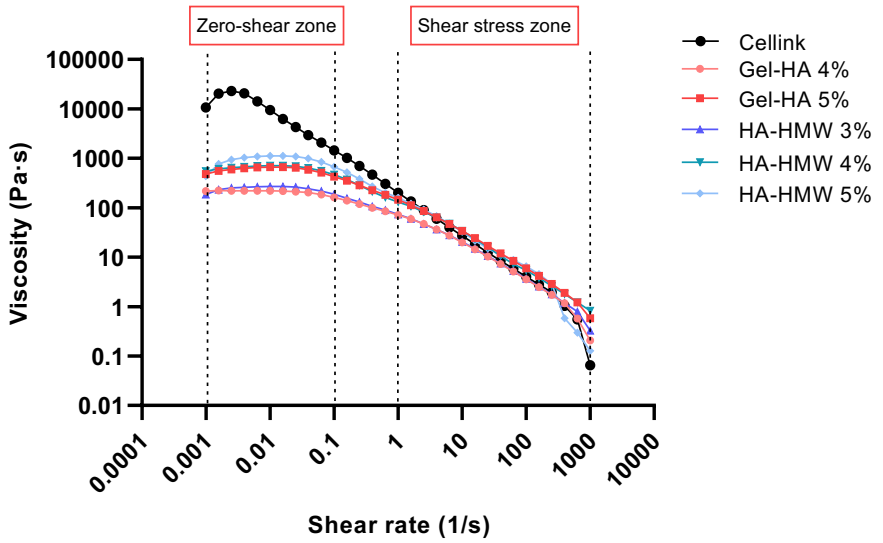

Figure 39. Shear stress analysis of non-crosslinked Gel-HA inks compared to HA-HMW inks by rheology. *Evolution of inks viscosity as a function of the shear rate measured in the rheometer between 0.001 and 1000 s-1. (n=3).*

In addition, more Gel-HA blends were explored for future applications on bioprinting with more than one bioink, adapting the bioink to the cell type used. Figure 40 compares Gel-HA 4% and 5% (20-80) with a new ratio explored Gel-HA (50-50) at 4% and 5%. Results showed that Gel-HA 4% (50-50) had a viscosity quite low compared to the others, which resulted in the rejection for further experiments. Thus, Gel-HA 5% (50-50) displayed similar behaviour compared with both Gel-HA (20-80) and was kept as an alternative within the inks chosen previously.

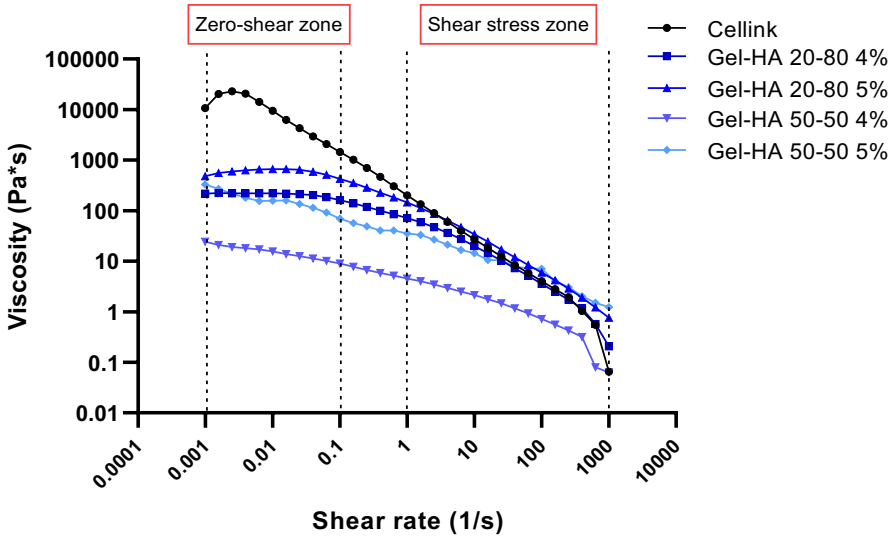

Figure 40. Shear stress analysis of non-crosslinked Gel-HA inks by rheology. *Evolution of inks viscosity as a function of the shear rate measured in the rheometer between 0.001 and 1000 s-1. (n=3).*

Furthermore, this viscosity behaviour represents the polymeric fraction of the bioink only, while the complete formulation would include a small volume of HRP for crosslinking, and cells. The incorporation of cells has been shown to decrease viscosity of the polymer-based ink. Nevertheless, some studies suggest that high concentration of cells (> 10^7 cells/mL) in suspension can increase bioink viscosity (Blaeser et al., 2016) However, this relationship will depend on the polymers used, the type of cells, and the range of viscosities.

1.2. Mechanical properties of Gel-HA bioinks.

In addition to viscosity, mechanical properties of the bioinks selected for cell culture (Gel-HA 4-5% (20-80) and Gel-HA 5% (50-50)) were also analysed.

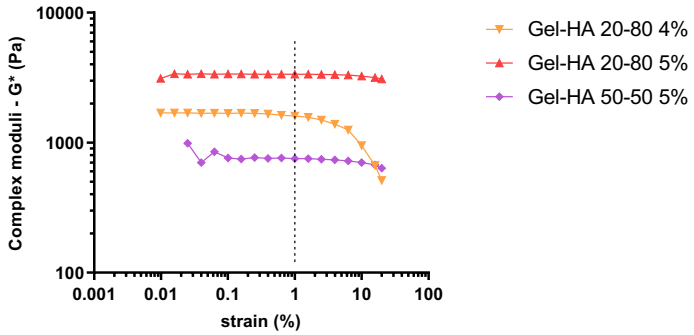

Figure 41. Strain analysis of printed Gel-HA inks by rheology. *Complex shear modulus after crosslinking of Gel-HA hydrogels. Measurements were performed in the rheometer at 1 Hz of frequency.*

Strain sweep from 0.01% to 20% was performed to each ink and as mentioned in the Chapter 1 strain analysis allowed to confirm the same parameters employed for the injectable hydrogels for the frequency sweep. Strains between 0.1% to 10% are in the linear viscoelastic region, therefore all further analysis were kept at 1% strain as previously performed (Figure 41).

After the frequency sweep, mechanical properties of the printed Gel-HA inks were analysed. G' values of the Gel-HA inks showed that high content HA inks had higher values, Gel-HA 4-5% (20-80) inks displayed G' values at 1 Hz ranging between 1610-3250 Pa and Gel-HA 5% (50-50) ink values close to 755 Pa (Figure 42A). In addition, G'' showed at 1 Hz the highest value for Gel-HA 5% (50-50) with 150 Pa, decreasing G'' when HA increased (Figure 42B). These behaviours were expected when the inks were based on a high molecular weight HA instead of a HA previously degraded.

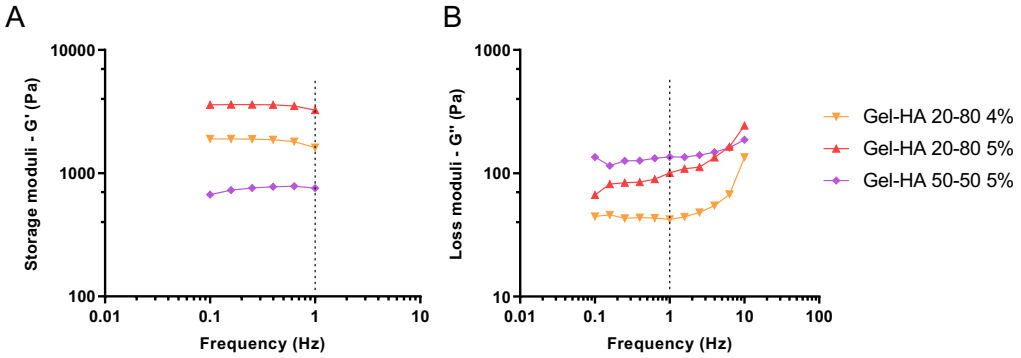

Figure 42. Frequency analysis of printed Gel-HA inks by rheology. *A) Storage (G') and B) loss (G'') moduli after crosslinking at 1% strain as a function of the frequency of crosslinked Gel-HA inks.*

The HA content influenced the mechanical properties, Gel-HA 5% (20-80) with more concentrated and a higher ratio of HA displayed the highest G' with a value of 3500 Pa, while changing the Gel-HA ratio to 50-50 decreased G' to 750 Pa (Figure 43A). Tanδ results of the inks showed that Gel-HA 5% (50-50) ink displayed the highest tanδ value with 0.2. Additionally, Gel-HA 4-5% (20-80) both displayed similar values around 0.03 (Figure 43B).

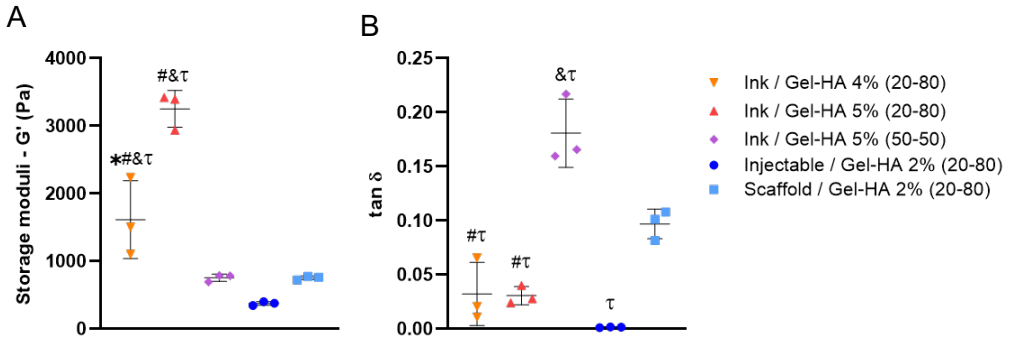

Figure 43. Mechanical properties of in situ Gel-HA inks compared with Gel-HA (20-80) injectable hydrogels and scaffold. *A) Storage moduli (G') and B) tan δ at 1 Hz of the in situ crosslinked Gel-HA bioinks, injectable hydrogel and scaffold. *At least p≤0.001 (compared to Bioink / Gel-HA 5% (20-80)); #p≤0.001 (compared to Bioink / Gel-HA 5% (50-50)); &p≤0.001 (compared to Injectable / Gel-HA 2% (20-80)); τp≤0.001 (compared to Scaffold / Gel-HA 2% (20-80)); (n=3; ANOVA followed by Tuckey's multiple comparisons test).*

Gel-HA ink mechanical properties after being characterized had to be compared with both previous systems to have an overall knowledge about how close we were to mimic the liver tissue. Regarding the G' it was clear that inks with high HA content achieved higher values compared to the ink Gel-HA 5% (50-50) due to the decrease of HA amount and compared to the injectable hydrogel and the scaffold (Figure 43A). Statistical differences were found to supporting these findings. Interestingly, tanδ showed that ink Gel-HA 5% (50-50) achieved values around 0.2 which match with the values described for the liver in the literature (Figure 43B). In fact, this ink improved the tanδ result obtained by the Gel-HA scaffold with values around 0.1, indicating a more liver-like behaviour by the Gel-HA 5% (50-50) ink (Figure 43B).

2. Printability of Gel-HA bioinks

Printability comprises a set of parameters that ultimately define the quality of the printed construct. Generally, bioinks with higher viscosity maintain its shape better; however, higher shear forces applied consequently might seriously affect the viability of the cells involved (Naghieh et al., 2021; Webb et al., 2017). The first parameter to consider is the ability of the bioink to be ejected through the nozzle, namely extrudability. Viscosity is the main feature that can be associated

to extrudability, and higher viscosities will require increased pressure or force to extrude the solution (Paxton et al., 2017). While normally, pneumatic extrusion bioprinting is suitable for viscosities ranging from $3x10^{-3}$ to $6x10^{4}$ Pa·s (Kyle et al., 2017), this will depend on the range of pressures that the printer can reach.

2.1. Extrudability of Gel-HA bioinks

The study of all bioinks was performed within the whole range of pressures achievable by Cellink BioX bioprinter (1-200 kPa) up to the minimum pressure required to observe a filament-like extrusion through the tip (20G). We could indeed notice that an increase in the HA concentration required higher pressures, which correlates with its increasing viscosity. Likewise, the incorporation of Gel to the bioink, at a 20-80 (Gel-HA) volumetric mixture, reduces the printing pressure required according to its reduced viscosity. HA 5% was not extrudable at pressures ≤ 200 kPa using a 20G nozzle and was thus not considered for further evaluation of its printability. However, the mixture of Gel-HA 5% was successfully extruded, hence HA 5% could be considered as a precursor to dilute and tune the composition (Table 9).

Table 9. *Summary of pressure and extrudability of HA HMW and Gel-HA based inks without cells and printed with a 20G nozzle.*

Composition	Pressure	Extrude
Cellink control	150 kPa	Yes
HA HMW 1%	15 kPa	Yes
HA HMW 2%	50 kPa	Yes
HA HMW 3%	100 kPa	Yes
HA HMW 4%	125 kPa	Yes
HA HMW 5%	>200 kPa	No
Gel-HA 4% (20-80)	50 kPa	Yes
Gel-HA 5% (20-80)	100 kPa	Yes
Gel-HA 5% (50-50)	60 kPa	Yes

2.2. Uniformity (U) and Pore Factor (PF) of Gel-HA bioinks.

Uniformity and pore factor were evaluated as other printability parameters of the bioink. Grid constructs (4 x 4; 30 x 30 x 3 mm) were printed for each bioink (Figure 44). Crosslinking was initiated with the presence of HRP within the bioink, and H_2O_2 (20 mM) dispensed by drops over the pattern in each layer. Uniformity is a parameter defined by the similarity of the printed strand width to the optimal strand width. Aqueous inks are going to have some dispersion of the strand compared to the model. While usually this optimal considered might be the strand width in the model (e.g., 0.41 mm), in this case we compared with the Cellink START ink as our control for its excellent printability. The width modelled was 0.60 mm (20G), while the average width of the control was 0.72 ± 0.05 mm. The area of the modelled squares was 49 mm^2, and the control was 41.90 ± 0.61 mm^2.

The average width of the printed strands was divided by the average of the control width ($\bar{X}W_i$ / $\bar{X}W_{Control}$; n = 25). From zoomed out images of the same constructs, the pore factor was computed as the ratio of areas ($\bar{X}A_i$ / $\bar{X}A_{Control}$; n = 4). In both cases, values closer to 1 were considered to have improved uniformity and pore factor, respectively. The way these measurements were done is shown in Figure 13. Both parameters are complementary and can be understood as the resolution of the final construct. Some articles define the pore factor with a ratio of perimeter/area (Naghieh et al., 2021; Sarker et al., 2018). However, we devised that this ratio can be misleading, since this ratio can give the optimal 1 when a perimeter of a printed construct is highly irregular and the area is reduced, yet the relationship between both remained close to the optimal. Other authors have used the ratio of perimeters with their theoretical optimal (e.g., 3D model) to measure the pore resolution (Ouyang et al., 2016). Other studies have also proposed that the standard deviation of the measurements is in itself an indication of uniformity (Göhl et al., 2018). Our approach was therefore a combination of the two latter ones, while considering areas instead of perimeters for the pore resolution.

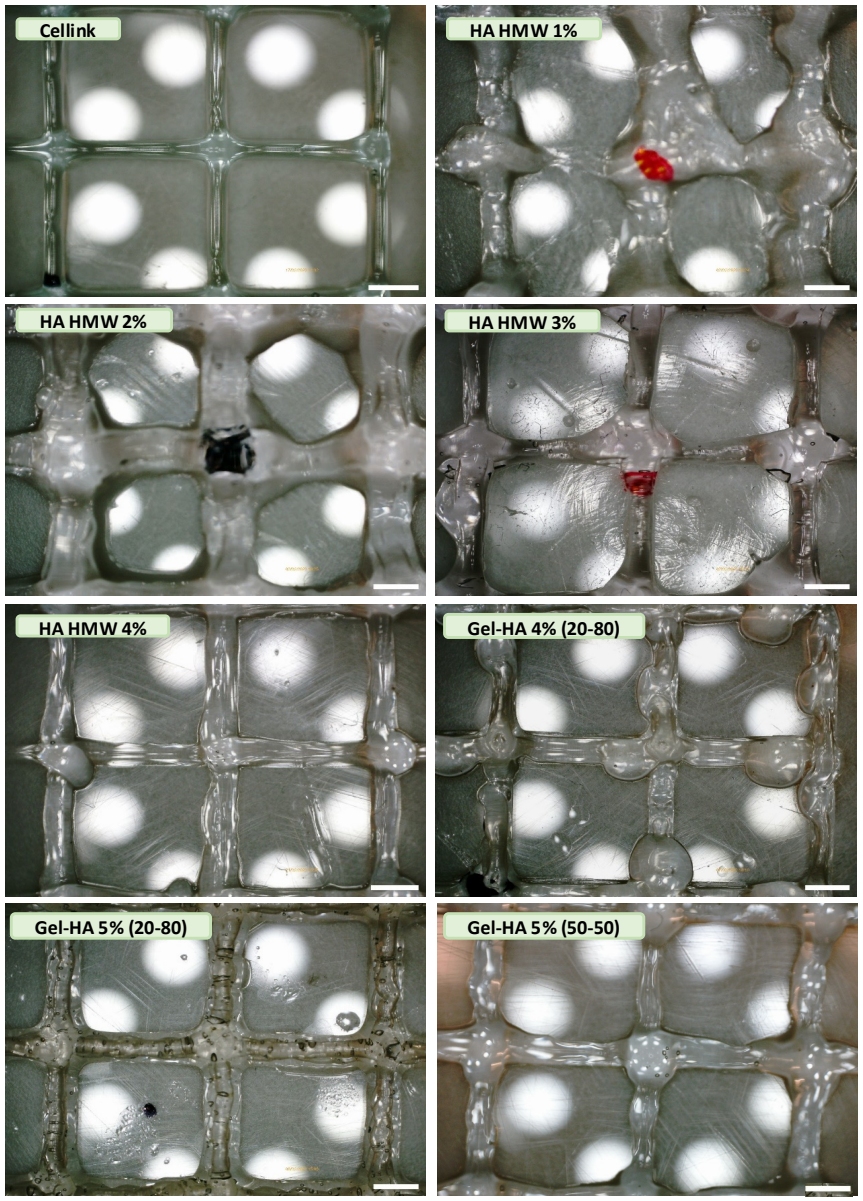

Figure 44. Macroscopic representative pictures of 3D grids printed with HA and Gel-HA inks*. Pictures were taken with a manual magnifying lens. Same sample was employed for uniformity and pore factor analysis. Scale bar 1 mm.*

As observed, an increased concentration yields more uniform constructs (Figure 45). In the case of HA 1% it seems that has a better uniformity than HA 2%, but it might be due to a finer set up of the balance of pressure/velocity. Even though both are irregular as it can be observed from the high standard deviation on these measurements when compared with the HA 3% and HA 4%. It is worth noting that HA 4%, despite displaying a higher viscosity upon shear stress

(Figure 38) than the control, almost overlapping with HA 5%, was extrudable, and HA 5% was not extrudable. HA 4% presented the highest uniformity and pore factor of all HA-based inks.

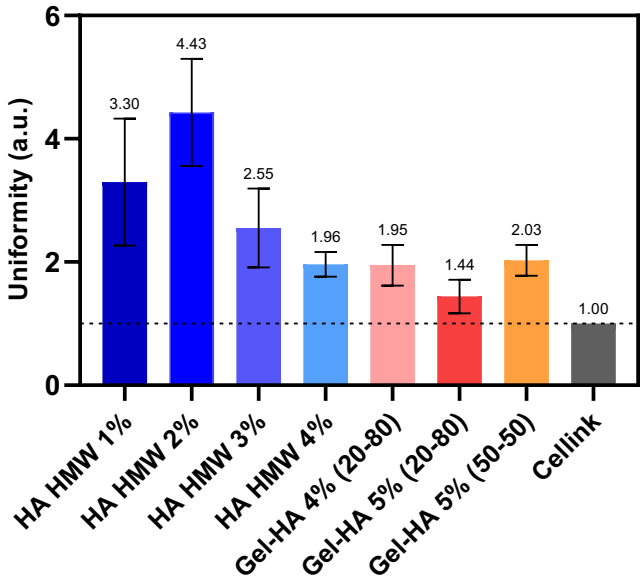

Figure 45. Printability analysis of HA and Gel-HA inks *Uniformity measurements. Sample selection were 10 lines and 10 measurements per line (n=100)*

The incorporation of Gel to the HA solutions yields constructs with higher strand uniformity. Gel-HA blends 4% and 5% have a good uniformity and pore factor, which is consistent with the fact that the viscosity of these inks is close to the control. We observe that for the Gel-HA mixtures, while strand uniformity gets closer to the control, the pore factor is reduced (Figure 46). Despite the increase of polymer concentration should improve uniformity, in the case of Gel-HA 5% a high standard deviation is obtained, which could be related to the reduction in pore factor. This result could be attributed to an irregular deposition of more viscous bioinks, where material tends to accumulate in the grid nodes reducing the overall area.

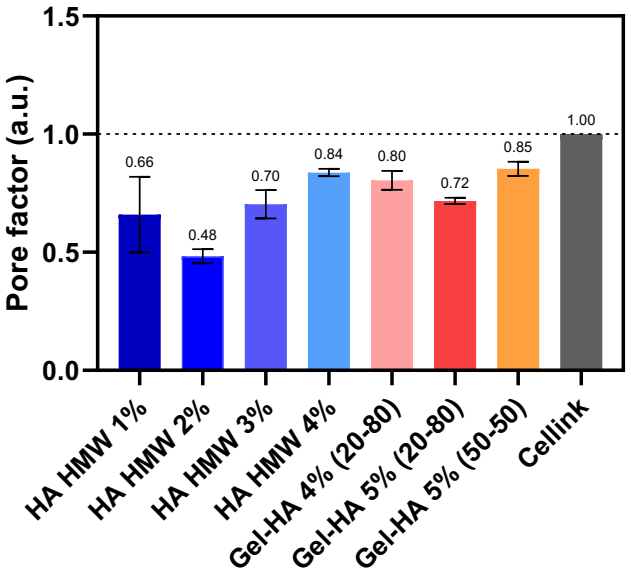

Figure 46. Printability analysis of HA and Gel-HA inks. *Pore factor measurements. Sample selection was the four central squared formed on the grid. (n=4)*

3. Bioprinting of HepG2 cells in Gel-HA bioinks

Bioinks made of Gel-HA containing HepG2 cells were printed into cylindrical-shaped hydrogels (15 mm diameter) onto the non-treated well plates using the 20G nozzle. Two different concentrations from the same bioink were tested to observe the differences on the pressure required to extrude them and the influence over the HepG2 cells. For Gel-HA 4% (20-80) the needed pressure ranged from 50 to 70 kPa, while for Gel-HA 5% (20-80) it ranged from 90 to 110 kPa. After every layer, H_2O_2 (20 mM) was dispensed on the ring to crosslink the polymers in the bioink.

The viability of cells within the constructs was evaluated at day 0 (post-printing), day 1 and day 7. HepG2 cells showed a significant difference on the cell viability after printing. Cell survival of HepG2 cells bioprinted in Gel-HA 4% (20-80) was 94%, whereas in Gel-HA 5% (20-80), it did not surpass 82% (Figure 48). Cells remained viable after 1 and 7 days, with cell survival of 86% for Gel-HA 5% (20-80) and 93% for Gel-HA 4% (20-80). Representative images of HepG2 cells cultured in both bioinks and a 2D control can be observed in Figure 47.

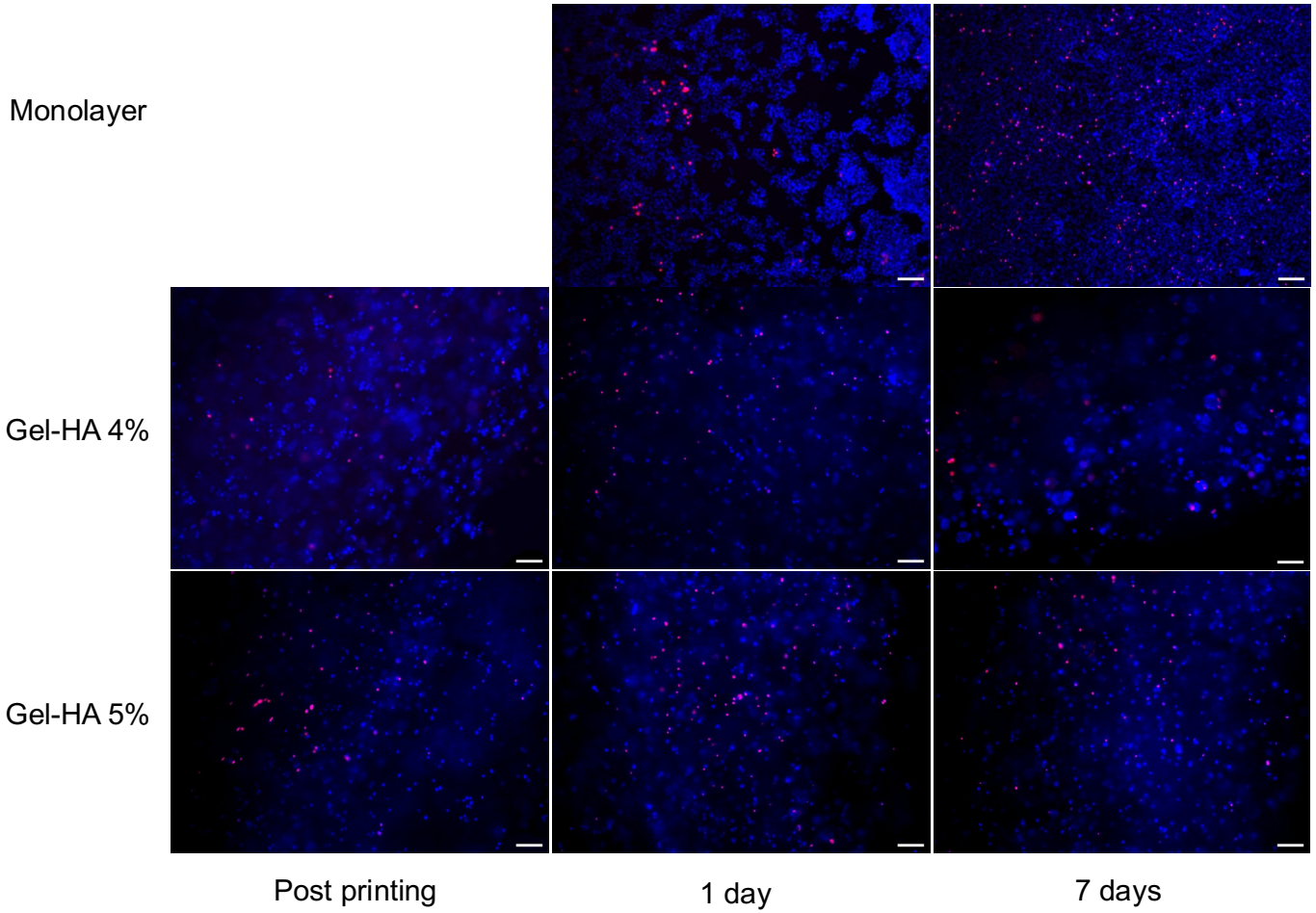

Figure 47. Representative images of HepG2 cell viability, cultured within Gel-HA bioinks. *HepG2 cells in Gel-HA bioinks after printing, 1 day and 7 days of culture. Nuclei were detected by Hoechst 33342 (blue) staining in all the images. Dead cells were identified by PI staining (orange). Scale bar 100 µm.*

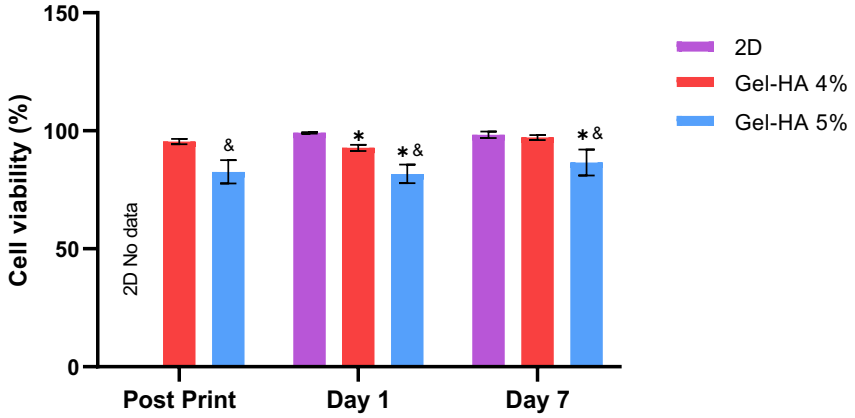

Figure 48. Quantification of cell viability of HepG2 cells cultured within Gel-HA bioinks. *Quantification of cell viability after printing, 1 day and 7 days of culture. *At least p≤0.01 (compared to monolayer) &At least p≤0.001 (compared to Gel-HA 4%) (n=6; ANOVA followed by Tuckey's multiple comparisons test).*

Since there was a significant difference in cell viability between 4% and 5%, we decided to continue the characterization of cells in 4% bioinks and discarded 5% for the next cell culture experiments.

Urea production of bioprinted HepG2 cells, revealed better outcomes compared to 2D cultures after 1 and 7 days, although only statistically significant differences were observed after 7 days (Figure 49A). On the other hand, albumin synthesis was lower in 3D after 1 day compared with the monolayer cultures, but it wasn't statistically significant. However, after 7 days, an acute increase was experienced in albumin synthesis and statistically significant compared to the 2D control (Figure 49B). Both evaluations led to consider Gel-HA 4% (20-80) as an adequate bioink for cell culture.

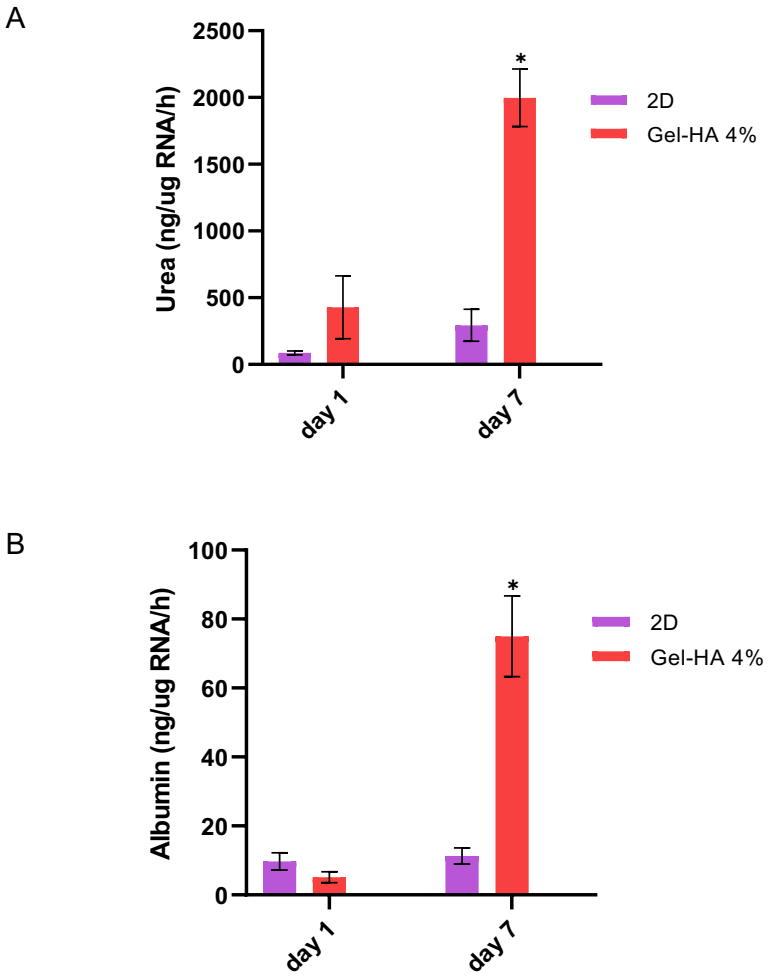

Figure 49. In vitro assessment of Gel-HA bioinks with HepG2 cells. *A) Ureogenic capability of HepG2 encapsulated within Gel-HA. B) Albumin synthesis in different culture conditions. *At least p≤0.01 (compared to monolayer) (n=3; ANOVA followed by Tuckey's multiple comparisons test).*

The expression of typical hepatic markers was also assessed by means of immunofluorescence (Figure 50). HepG2 cells cultured in bioinks expressed AFP and HNF4 after 1 and 7 days in culture and maintained cell-cell contacts.

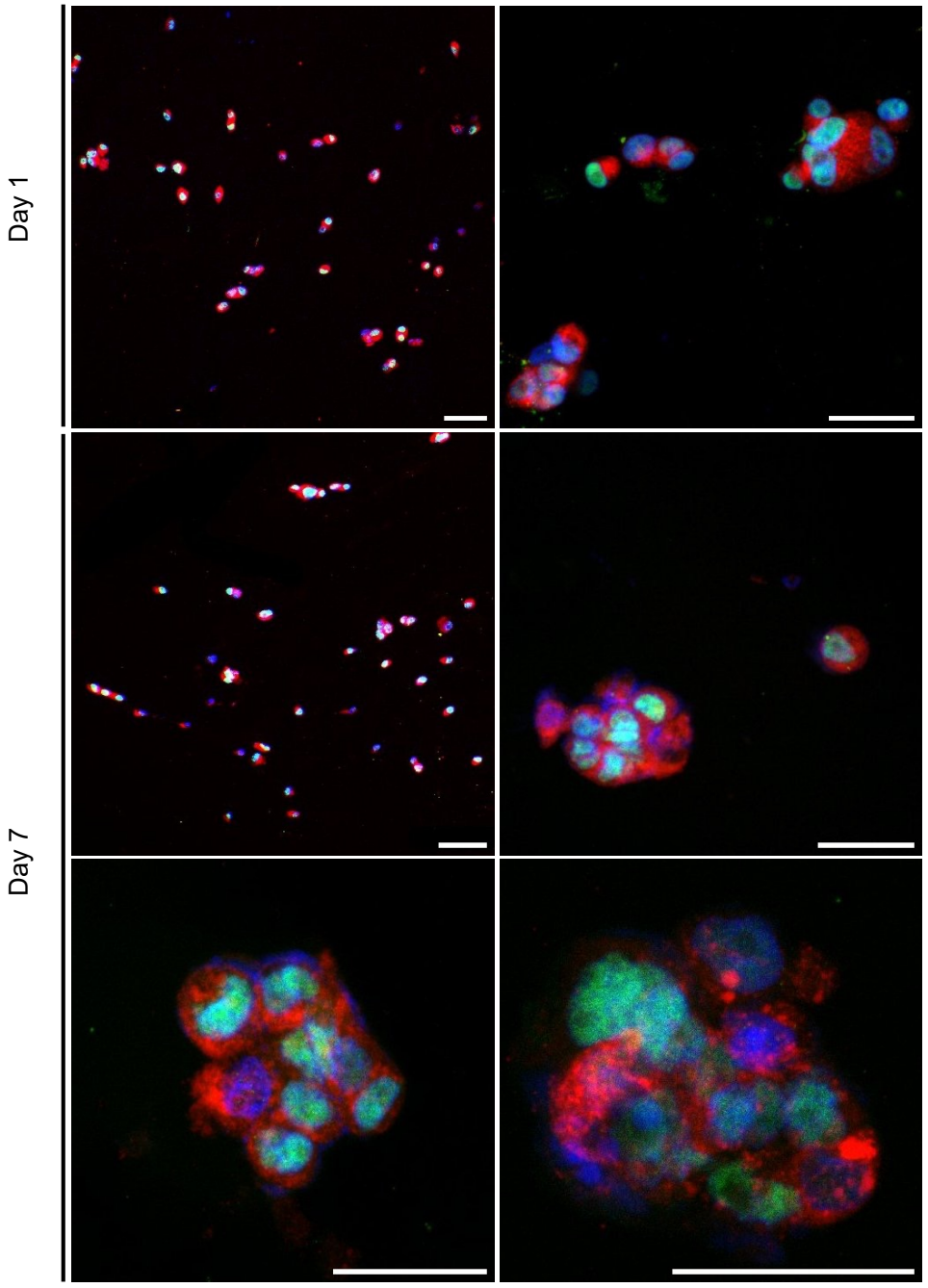

Figure 50. Expression of hepatic markers by Immunofluorescence imaging of Gel-HA 4% (20-80) bioprinted constructs after 1 and 7 days of cell culture. *Representative images (10x and 40x) from cryosections of Gel-HA bioprinted constructs with HepG2 cells were stained for the expression of two hepatic markers: Alpha fetoprotein (Alexa 555 – red) and HNF4-α (Alexa 488 – green). Day 7 images include 63x and 100x images. Scale bar 20 µm.*

4. Miscibility experiment for concentric individual compartments of Gel-HA bioinks

Several designs of concentric circles, varying the gap among them were explored for the culture of individual compartments that could be useful for future co-culture experiments. The gap was proportional to the strand thickness (0.59 mm). In Figure 14 (see Materials and Methods), the three designs tested are illustrated. Bioinks were labelled with red and green, fluorescent dyes (Invitrogen Thermo Fischer) respectively and observed the apparent overlap between the two circles under the confocal microscope (Leica Microsystems). In Figures 51 and 52, representative images of the constructs, post-printing and after incubation in F12 culture media for both combination of Gel-HA bioinks are shown. The aggregates observed for the red dye were quite difficult to remove, a short centrifuge spin was performed in the dye solution before mixing with the bioinks. However, it did not remove all the small aggregates.

Analysing first the set of cylinder-shaped hydrogels made of Gel-HA 4% (20-80) and Gel-HA 5% (20-80), different states of closeness can be observed after printing. From the constructs printed with a Gap-2, we can observe that after printing the two rings are in direct contact with no apparent overlap. After swelling, the two rings show an area at the interface where overlapping of the two layers occurs (Figure 51). Despite swelling, if the two rings are overlapping, they should be detachable since the crosslinking process was completed post-printing. Nevertheless, it was not possible to physically separate the two without partially tearing apart the structure, since some overlapping had certainly occurred, and the rings had crosslinked in some sections. As for the Gap-3 constructs, we can notice a slight contact between the rings in the post-printing, while getting full contact after swelling, not seemingly overlapping (Figure 51). The increased concentration of fluorophore at the edge of the rings might result from displacement of the dye molecules by the cell culture swelling the network. Gap-4 constructs show an obvious space between the rings after printing, guaranteeing that the two constructs will crosslink independently. After swelling, the two rings are in close contact without overlapping at the interface (Figure 51).

Then, the other set of bioinks, Gel-HA 4% (20-80) and Gel-HA 5% (50-50) was evaluated. Once the cylinders were printed at first glance the difference with the previous set of bioinks was evident. Gap 2 showed after printing and after swelling smooth contact between surfaces, indicating reduced swelling behavior (Figure 52). In addition, both constructs were separated without any difficulty which means no crosslinking occurred between both cylinders. Gap 3 constructs experienced completely distant surfaces after printing and after swelling

complete contact (Figure 52). As mentioned for Gap 2, both cylinders were able to be extracted independently. However, gap 4 constructs did not achieved contact between surfaces either after printing or after swelling (Figure 52). Thus, since both constructs showed no contact after printing and swelling, both were obtained easily separated.

The differences on the outcomes observed between both pairs of bioinks, Gel-HA 4-5% (20-80) and Gel-HA 4% (20-80) with Gel-HA 5% (50-50), was easily explained by the swelling of hydrogels. Meanwhile the first set of bioinks only comprised both with a Gel-HA ratio of 20-80, the second included an increased Gel-HA ratio of 50-50 for one of the bioinks. As it was explained before, HA has a great retention and affinity for H_2O molecules, but Gel is not that hygroscopic. Therefore, sets of bioinks with higher Gel content would need a closer gap to create smooth contact between surfaces after swelling. Finally, for the set of bioinks Gel-HA 4-5% (20-80) it was set a minimum gap of 4 times the nozzle diameter to obtain contact between constructs. On the other hand, the set Gel-HA 4% (20-80) and Gel-HA 5% (50-50) needed a minimum gap of 3 to display the same smooth contact between constructs.

The results serve as the basis for a promising design for co-culture where a compartmentalized model is desired and close communication at the interface, even diffusion or migration among layers is expected, yet maintaining the advantage of separate manipulation.

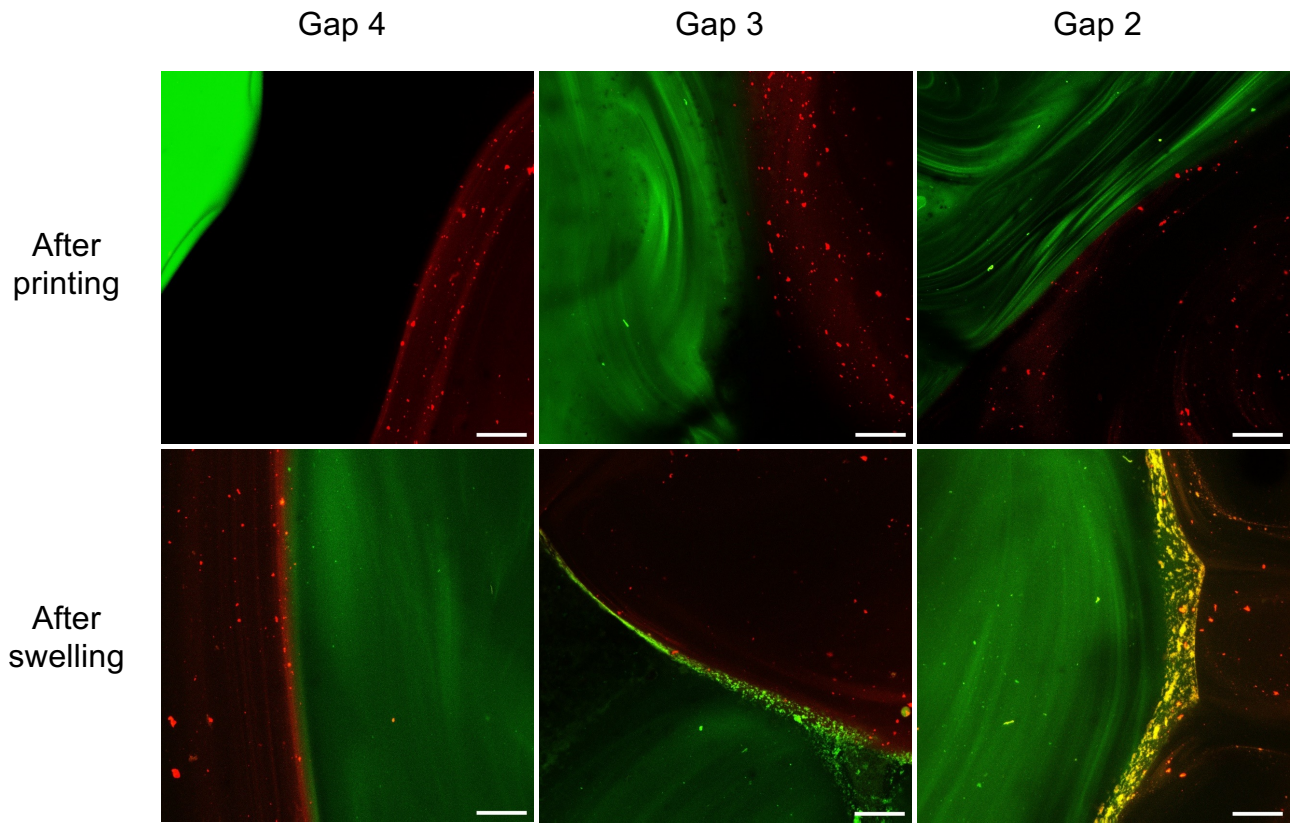

Figure 51. Representative images of Gel-HA 4-5% (20-80) ink's miscibility. *Post-printing miscibility (upper row) and after 24 h swelling in F12 culture media (bottom row) of printed concentric circles with strand gap proportional to strand thickness (0.61mm). Green fluorophore was mixed within Gel-HA 4% (20-80) and red in Gel-HA 5% (20-80). Top and bottom images do not correspond to the same point in the constructs. Images produced from stacks along Z axis. Scale bar 100 μm*

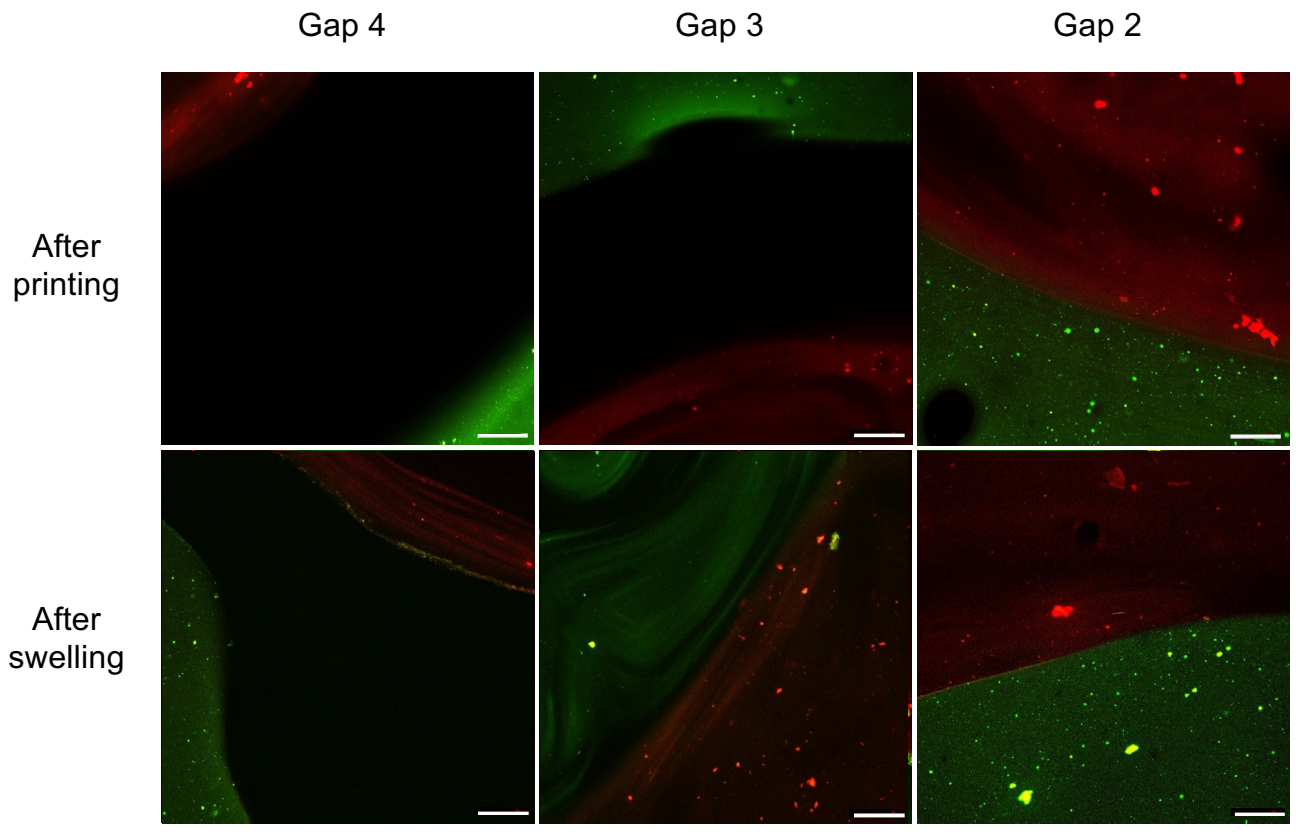

Figure 52. Representative images of Gel-HA 4% (20-80) and Gel-HA 5% (50-50) ink's miscibility. *Post-printing miscibility (upper row) and after 24 h swelling in F12 culture media (bottom row) of printed concentric circles with strand gap proportional to strand thickness (0.61 mm). Green fluorophore was mixed within Gel-HA 4% (20-80) and red in Gel-HA 5% (20-80). Top and bottom images do not correspond to the same point in the constructs Images produced from stacks along Z axis. Scale bar 100 μm.*

Discussion

3D bioprinting overcomes the limitations of monolayer cultures and better mimic the *in vivo* microenvironment complexity. In order to increase the throughput of our cell-based model and to create more complex structures, bioprinting of hepatic cells was explored and resulted to be adequate for the functionality of HepG2 cells.

In the translation of hydrogels into bioinks, several parameters should be considered. The assessment of printability indicated that HA inks with concentrations ranging from 3% to 4%, as well as Gel-HA 20-80 4-5%, exhibited extrudability and displayed great strand uniformity and pore factor. Increased polymer concentration enhanced these attributes in both cases. However, the introduction of Gel reduced the extrusion pressure required and may result in a reduction of pore factor, potentially due to the presence of bubbles and ink dispersion at the nodes. While HA served as the primary component, contributing to the high viscosity and stiffness of the printed hydrogels, Gel acted as a component to fine-tune the viscosity of the inks and, consequently, the stiffness of HA-based hydrogels. Furthermore, Gel facilitates cell adhesion (Poveda-Reyes et al., 2016; Sanmartín-Masiá et al., 2017).

At that point, it was worth to compare the mechanical properties of all Gel-HA systems utilized in chapters 1 and 2 with the Gel-HA inks developed. Generally, the inks Gel-HA 4-5% (20-80) exhibited higher G' values ranging (1610-3250 Pa) compared to the ink Gel-HA 5% (50-50) (755 Pa), the injectable hydrogel (375 Pa) and the scaffold (752 Pa). As discussed earlier, both the hydrogel and the scaffold approached to the lower and upper limits of the liver mechanical properties (400-600Pa) (Desai et al., 2016). These disparities were attributed to the increase of the molecular weight of the HA and the polymer concentration. Additionally, the ink Gel-HA 5% (50-50) displayed tanδ values (0.2) consistent with those reported in the literature for fresh human liver (0,2), as measured by rheology (Estermann et al., 2021). Despite, the Gel-HA 4-5% (20-80) inks exhibiting higher G' and lower tanδ values compared to the tissue, they were chosen for cell culture experiments to ensure similarity to Gel-HA injectable hydrogels and scaffold. Moreover, the ink Gel-HA 5% (50-50) was later included as a candidate for optimal bioink due to its close resemblance to the liver tissue.

After the characterization of our bioinks in terms of printability, cells were encapsulated, and viability was assessed in order to determine the biocompatibility after applying the required pressures. Other studies that

bioprinted HepG2 cells in different polymer bioinks used cell densities ranging from 1.5×10^6 to 5×10^6 cells/mL (Billiet et al., 2014; Sun et al., 2020; Taymour et al., 2022), which is in the range of our selected density (2×10^6 cells). It is worth noting that the addition of cells can change the viscosity of the bioink, hence influencing the parameters for the printing process. Blaeser *et al*. showed that cell concentrations over 1×10^6 cells/mL have a significant impact on Alg-based bioinks, where higher cell numbers increased viscosity and amplified the shear thinning effect (Blaeser et al., 2016). In this study, the impact of the cells on the bioink properties was not evaluated. However, the pressure required to extrude inks alone was reduced once cells were introduced to the inks. Nevertheless, no additional volume was added with the cells since they were re-suspended to the desired concentration in a Gel and HRP solution. Therefore, we hypothesize that the printing pressure difference might be due to a more sustained maintenance of the bioinks at 37 °C, since this was critical to ensure cell viability, while during the extrudability experiments, the cartridges were not kept under controlled temperature outside of the printheads. Bioprinting of Gel-HA based bioinks required to apply not a fixed pressure, small adjustments during the printing process (±10 kPa) were necessary to compensate the non-homogenous fractions in the bioink mixture. Despite of its optimum printability, pure HA bioinks were not considered for cell culture since optimally Gel would provide adhesion sites through RGD domains (Poveda-Reyes et al., 2016)

The use of Gel-HA bioinks allowed to have suitable bioinks able to host cells and maintain them alive. However, the pressure required to print each one was different, and this could be one of the reasons that affected cell viability. While Gel-HA 4% (20-80) kept a 93% of viable cells (40-50 kPa) along the 7 days of cell culture from the beginning, the formulation increasing the polymer concentration up to 5% (80-100 kPa) had affected the viability with lower values of 82%. Therefore, Gel-HA (20-80) 5% was no longer considered as suitable for cell culture. Urea synthesis was improved on HepG2 cells since day 1 of culture, increasing the outcome even more at day 7. Regarding albumin production, although no significant differences were shown after 1 day in HepG2 culture, significant increased values were detected after 7 days in bioprinted constructs, confirming the suitability for hepatic cell culture. Our results are in agreement with other groups that have shown increased functionality of bioprinted hepatic cells. For instance, Alg blends with Pluronic were the base of the bioprinting described by Gori *et al.* which compared their 3D constructs against adhered HepG2/C3A cells onto a 2D substrate, and urea synthesis improved significantly after 7 days (Gori et al., 2020). Similarly, Gel-based bioinks crosslinked by UV-light employed by Wu *et al.* and Khati *et al.* manufactured bioprinted platforms where the co-culture of HepG2 cells with NIH/3T3 cells exhibited improvements

in albumin synthesis, with an acute increase after 7 days of cell culture, which describes a similar behaviour compared to the forementioned results (Wu et al., 2020). Moreover, dECM bioinks described improvements as well for HepG2 cell culture which exhibited an increased albumin secretion after 7 days, indicating a similar trend between different systems (Khati et al., 2022).

In order to assess the possibility of bioprinting different cell types in different concentric circles, the miscibility was assessed using two different bioinks containing fluorescent dyes as previously described by other groups (Sanchez-Rubio et al., 2023). The main goal was to identify the optimal gap between the circles during construct design since variations in strand thickness from the theoretical design prompted were observed after the printing process. Introducing a gap between the circles could facilitate the printing of two distinct structures at close distance that are not crosslinked yet, enabling cell interactions. Given the anticipated swelling of the constructs post-bioprinting, the constructs are immersed in cell culture media to supply essential nutrients for the embedded cells.

Hence, we could hypothesize that constructs with a noticeable gap among them post-printing, could be in close contact after incubation in culture media and swelling of the hydrogel networks. The use of our 3D co-culture will eventually open the possibility to evolve the co-culture with transwell membranes. These types of cultures are based on the crosstalk of two different types of cells in the same culture separated by a membrane. The set-up described by Kang *et al.* allowed to simulate the configuration of a bile duct by culturing rat hepatocytes and endothelial cells, separated by a transwell membrane. Describing a synergistic effect of both cell types to each other, maintaining the cell organisation, viability, phenotype, and urea levels up to 48 days (Kang et al., 2013). In addition, the understanding achieved by this strategy was extended also to study mechanistically the role of HSC and hepatocytes in metabolic associated steatohepatitis. Where the activation of HSC was induced by cell proximity and therefore the fatty acid accumulation (Barbero-Becerra et al., 2015).

However, it still lacks the 3D component given by hydrogels or scaffolds. In the future, we aim to reproduce the crosstalk of two cell populations but adding two independent hydrogel-based printed constructs in contact to reproduce the transwell behaviour. Thus, it will allow to have the advantage of co-cultures, 3D hydrogels and transwell membranes altogether, being able to analyse the influence of each cell type to the other individually.

General discussion

The liver is the biggest gland in the human body and is in charge of several vital biological processes, such as detoxification, bile generation, and the metabolism of lipids, proteins, and carbohydrates. Although the liver has a robust capacity for regeneration, this capacity can be diminished or altered due to different pathologies such as liver fibrosis, viral infections or DILI. Therefore, the production of complex liver tissues with sufficient functionality has become especially crucial because of the increasing need for organ transplants and the incapacity to replace the *in vitro* models needed for research on liver disease and drug development (Lv et al., 2022).

Liver tissue engineering emerged as a promising alternative for liver implantation that could simulate liver microstructure and maintain key hepatic functions, as well as *in vitro* systems that could be more accurate and reliable since they can reproduce complex cell structures and cell-matrix interactions. Despite the key advances in the liver tissue engineering field, some major challenges must be overcome before they can be widely applied in both preclinical and clinical settings. First approaches tried to fabricate synthetic hydrogels and scaffolds mimicking the mechanical properties of the liver. Most of the developed hydrogels were based on PEG and their derivatives and showed an improvement of *in vitro* hepatic functionality. On the other hand, the co-culture with non-parenchymal cells also has been shown to help to maintain the hepatic phenotype (Lin et al., 2014; Stevens et al., 2015; Underhill et al., 2007). However, synthetic hydrogels lack the biological cues expected from an environment which try to mimic the native ECM. On the other hand, although, the crosslinking chemistry of the system is also relevant, non-cytotoxic reactions have been considered an advantage due to the possibility to host cells during the crosslinking process. Biomimetic environments based on HA-Col with a hybrid crosslinking based on UV light and physical crosslinking of the collagen allowed to reproduce the viscoelastic properties of the liver while allowing HepG2 cells' culture (Jiang et al., 2021). Malinen *et al.* developed a similar bioink system by substituting collagen by gelatin. Either HA or Gel were modified with thiol groups and crosslinked with PEGDA allowing HepaRG cell culture and differentiation into a hepatic phenotype (Malinen et al., 2014). Moreover, the use of dECM as a hydrogel pretended to solve the limitations of the use of other polymers or concentrations different from the native tissue. There are authors that described hydrogel systems with dECM for ICOs culture with no differences in viability onto extracts from the basement membrane (Willemse et al., 2022).

However, the system developed in this thesis introduces a non-cytotoxic crosslinking able to host HepG2 cells and mimic the mechanical properties of the liver tissue with G' values between 400-600Pa (Desai et al., 2016). In addition, HepG2 cells encapsulated in Gel-HA hydrogels showed improved ureogenic capacity and albumin production compared to monolayer cultures.

One of the major limitations of liver tissue engineering approaches remains in the cell sources used, since, although PHH are the gold standard, the shortage of liver tissue for isolating hepatocytes, their variability and instability, and the short length when in culture, restrict their application. For this reason, for the setting up and selection of the optimal composition of Gel-HA hydrogels, we used HepG2 cells, a cell line widely used for liver cell-based assays (Arzumanian et al., 2021). While HepG2 cells have been extensively employed, a significant drawback is their low phase I activity levels, which do not accurately replicate *in vivo* physiology and limit their applicability to the assessment of non-bioactivable pharmaceuticals. However, their hepatic background, easy-handling and the maintenance of key hepatic functions (Aden et al., 1979; Donato et al., 2015; Westerink et al., 2007) make them suitable for studying the suitability of new materials for hepatic cell culture. On the other hand, many studies focus on maintaining the hepatocyte phenotype without considering the liver's multicellularity. In this sense, we have shown the suitability of PHH-laden Gel-HA scaffolds for the treatment of an animal model of ALF; however, the development of an angiogenic response for regenerative medicine applications would be essential to achieve long-term effects. Thus, future developments in this field, will include the co-culture with endothelial cells to get the angiogenic component. On the other hand, despite the fact that the co-culture of hepatocytes and other non-parenchymal cells in 3D configuration has been described as an optimum method that could better recapitulate liver physiology, the random distribution of the cells, their limited expansion capability and the problems associated with maintaining functionality for longer periods remain as important challenges to be solved (Segovia-Zafra et al. 2021).

In this PhD thesis, compared to more conventional delivery techniques such as intrasplenic injection, we have presented a viable PHH transplant approach based on the utilization of Gel-HA scaffolds to improve hepatic functionality in an ALF animal model. In clinical practice, biodegradable materials like Gel and HA would be preferable to other approaches such as Alg microbeads (Dhawan et al. 2020; Jitraruch et al. 2014). Gel-HA scaffolds were effectively created to boost the effectiveness of liver cell transplantation as well as to increase the functionality of human hepatocytes when cultured *in vitro*. The developed strategy would not only be a powerful tool in tissue engineering and regenerative

medicine but could also be used for other applications such as disease modeling and drug screening since the culture in Gel-HA enhances the performance of the hepatic cells.

Lastly, the bioprinting methods pretend to overcome the low reproducibility, slow manufacturing processes, and solve the difficulties to create complex 3D structures with high resolution that show traditional methods. In order to increase the throughput of the developed Gel-HA hydrogels, we aimed transforming the hydrogels in bioinks by increasing the molecular weight of HA, obtaining optimum results in extrudability and printability, as well as promising results for hepatic cell culture on bioprinted constructs. On the other hand, we developed a new system that kept the essence of dispensing drop-by drop the crosslinker as we did with injectable hydrogels. The advantage to use this strategy compared to other methods is the low amount of crosslinker, not requiring the submersion of the bioink into the compound or rely in the shape retention of the bioink to crosslink it afterwards. We developed a novel bioprinting protocol which blends a fast crosslinking while the printing process takes place.

In order to consider liver's multicellularity, we developed a bioprintable system that would allow the simultaneous co-culture of different cell types, but that would also permit differentiating distinct cellular responses after different stimulus, what would be an advantage over direct co-culture systems while maintaining the three-dimensionality.

Finally, other liver tissue engineering approaches include dynamic culture in bioreactors or in microfluidic chip devices with micro-physiological stimulation. This will play a key role in drug screening and liver disease modelling and could open the door to the clinical application of the developments (da Silva Morais et al., 2020).

Conclusions

The present thesis has described a new versatile system based on Gel-HA suitable for hepatic cell culture. Gel-HA hydrogels, possessing liver-like mechanical properties, have successfully enhanced hepatic functionality of different hepatic cells compared to traditional cell culture. Furthermore, the use of Gel-HA scaffolds for the treatment of animals with chemically-induced liver failure has demonstrated its efficacy *in vivo*. Finally, we successfully transitioned from using injectable hydrogels and scaffolds to developing bioinks and establishing a novel bioprinting protocol that maintains the same crosslinking procedure. Additionally, Gel-HA bioinks demonstrated the ability to host cells during the printing process and showcased improvements over 2D cell cultures. Thus, we have successfully adapted conventional applications of hydrogels and scaffolds into a novel technology expected to be the base for the advances in the field of tissue engineering.

The work of the present thesis can be summarized in the following conclusions by chapter order.

- Gel and HA were correctly modified substituting activated COOH groups with tyramine molecules by EDC/NHS chemistry. Substitution degree was qualitative assessed by ATR-FTIR and quantitatively obtained by UV-spectroscopy, allowing a non-cytotoxic crosslinking for *in situ* hydrogel synthesis.

- HA hydrogels achieved the highest storage modulus value, explained by the stiffness of the molecule and water retention capacity under deformation compared to the gelatin. Hybrid hydrogels were able to simulate liver-like mechanical properties to mimic the hepatic tissue.

- Gel-HA (20-80) scaffolds have similar mechanical properties compared to injectable hydrogels and still in the upper range of the native tissue.

- HepG2 cells were successfully encapsulated in Gel-HA hydrogels and exhibited increased functionality. HA-rich compositions exhibited higher production of urea and albumin, which would implicate an advantage for hepatic cell culture.

- The mechanical characterization of the hydrogels together with the *in vitro* results with HepG2 cells, led us to select 20-80 Gel-HA hydrogels as optimum for 3D hepatic cell culture.

- PHH cultured in Gel-HA scaffolds showed an increase in urea synthesis, albumin secretion, and activity levels of phase I enzymes and phase II enzymes compared to 2D cultures, which implies an improved functionality closer to *in vivo* systems.

- We established a feasible PHH transplantation technology based on the use of Gel-HA scaffolds that increases hepatic functions in an animal model of ALF compared to traditional delivery methods such as intrasplenic injection.

- Mechanistically, PHH-laden scaffolds attenuated hepatocyte necrosis by reducing oxidative stress and production of cytokines in mouse liver failure, thus increasing survival.

- Cytokines and ophthalmic acid could be used as non-invasive biomarkers for the effectiveness of liver cell transplantation in the treatment of acute liver failure.

- We successfully transitioned to Gel-HA inks by increasing the molecular weight of the HA, thus enabling a viscous hydrogel which was considered as an ink.

- Viscosity, uniformity, and pore factor properties of the different HA-HMW and Gel-HA inks helped to choose Gel-HA 4-5% (ratio 20-80) and Gel-HA 5% (ratio 50-50) as optimal printable inks, by comparing with a commercial ink.

- Gel-HA 4% (ratio 20-80) was the optimal bioink to host cells during the printing process and maintain great cell viability for 7 days. Hepatic functionality was improved, considering our bioink as suitable for long term bioprinting cell culture.

- Feasible 3D co-culture model based on Gel-HA bioinks was successfully developed, the approach using two different printheads and bioinks led to non-miscible ring constructs which were in contact but kept independent.

Future perspectives

Co-culture by bioprinting: Continuing double ring 3D constructs.

Different studies have already described outstanding results based on co-culture models and specifically novel 3D bioprinted models for co-culture (Fan et al., 2023; Janani et al., 2022; Skardal et al., 2015; Taymour et al., 2021, 2022). However, almost all systems are based on UV-light crosslinking with methacrylated polymers or temperature-sensitive crosslinking. UV-crosslinked systems are considered not the optimal method due to the secondary effects of this type of radiation to the cells or the low mechanical properties presented, respectively. A system that modified the cartridges with different compartments allowed to print different bioinks as strands with a hexagonal pattern on the centre. Collagen-based bioinks were printed along HepG2 cells mimicking the hexagonal morphology of the liver lobules (Kang et al., 2020). Hong *et al.* used a similar method by a co-axial bioprinting of an aqueous phase and an oil phase, achieving similar 3D strands with a different bioink core and liver spheroids (Hong et al., 2021). Other authors relied onto constructs which replicated the lobule microarchitecture by co-culturing HUVEC, HSC and HLC and using bioinks that mixed Gel, silk fibroin and microparticles made from liver ECM (Janani et al., 2022). In addition, bioprinting not only has focused on just create 3D constructs that supported cell viability, hepatic functionality or gene expression of the different cells cultured. As previously mentioned, bioprinting has already been employed for hepatotoxicity studies, but few studies reported co-culture for that purpose. Fan *et al.* evaluated the potential of bioprinted HepG2-HUVEC in dots hexagonally arranged mimicking the liver lobule as a platform to replicate a DILI model (Fan et al., 2023).

Ultimately, the creation of a realistic liver model would be improved by the synergy between the multicellularity of co-cultures and the automated processes and reproducibility of bioprinting. However, there are certain fields that remain now unexplored. Variations in bioprinter configuration (i.e multiple printheads, sacrifice material, EMD deposition) and introducing additional design complexities will improve the reproduction of the *in vivo* microarchitecture. In the case of the system of this Thesis, the tuneable stiffness of the hydrogels, influenced by the varying Gel-HA ratio, could be instrumental in addressing specific liver diseases characterized by distinct stiffening in native tissue (Bomo et al., 2016; Serras et al., 2021; Ye et al., 2019). Also, focusing on the integration of immune cells, such as Kupffer-like cells, could provide insight into mimicking and studying inflammatory responses through cytokine expression. Moreover,

comprehensive analysis of hepatic cells such as HepG2 or PHH functionality through assessments like albumin secretion and CYP activity, by culturing with not only two different types of cells, may enhance the understanding of how this 3D bioprinted model compares and improves the conventional 2D platforms.

Contributions

The present thesis has produced relevant results that have been diffused on different publications, international and national conferences. In addition, we received the yESAO exchange award by the young European Society for Artificial Organs that every year allows the exchange of PhDs of two institutions. We performed a small project between the University of Compiegne in France through the PhD student Lisa Moriseau and me from the Centre for Biomaterials and Tissue Engineering of the Universitat Politècnica de València. The two stages had a duration of 15 days in each laboratory and the resulting project was invited to be presented during the ESAO 2023 congress in Bergamo in September 2023.

1. Publications in scientific journals

Publications as first author:

1. Primary human hepatocyte-laden scaffolds for the treatment of acute liver failure. **Julio Rodríguez-Fernández**, Emma García-Legler, Estela Villanueva-Bádenas, M. Teresa Donato, José Luis Gómez-Ribelles, Manuel Salmerón-Sánchez, Gloria Gallego-Ferrer and Laia Tolosa. Biomaterials Advances, 153, 213576 **(2023)**. Doi: 10.1016/j.bioadv.2023.213576
2. Challenges and perspectives of liver tissue engineering: from cell therapy to bioprinting. **Julio Rodríguez-Fernández**, M. Teresa Donato, Gloria Gallego-Ferrer and Laia Tolosa. International Journal of Bioprinting **(2024)**. Doi: 10.36922/ijb.2706

Other publications:

1. Synthesis and Characterization of Oxidized Polysaccharides for In Situ Forming Hydrogels. Muhammad Muhammad, Christian Willems, **Julio Rodríguez-Fernández**, Gloria Gallego-Ferrer, Thomas Groth, Biomolecules (2020), 10, 1185. Doi: 10.3390/biom10081185.

2. International conferences

1. Hepatic cell culture in hyaluronic acid/gelatin biosponges.
   Conference: Cloud-yESAO 2020 Congress
   City, Country / Year: Online / 2020
   Format: Oral presentation
   Authors: Emma García-Legler, Estela Sánchez-González, **Julio Rodríguez-Fernández**, Sandra Clara-Trujillo, Maria Teresa Donato, Gloria Gallego-Ferrer, Laia Tolosa

2. 3D Hydrogel microenvironments of gelatin and hyaluronic acid for liver tissue engineering.
   Conference: 6th world congress of the Tissue Engineering and Regenerative Medicine International Society (TERMIS2021)
   City, Country / Year: Rotterdam, The Netherlands (Online) / 2020
   Format: Oral presentation
   Authors: Gloria Gallego-Ferrer, **Julio Rodríguez-Fernández**, Emma García-Legler, Sandra Clara-Trujillo, Maria Teresa Donato, Manuel Salmeron-Sanchez, Laia Tolosa.

3. 3D Hydrogels of Tyramine-Modified Gelatin and Hyaluronic Acid for Liver Tissue Engineering: Physicochemical, *In Vitro* and *In Vivo* Experimentation
   Conference: 48th Annual ESAO Congress
   City, Country / Year: Vienna, Austria / 2022
   Format: Oral presentation
   Authors: **Julio Rodríguez-Fernández,** Estela Villanueva-Bádenas, Emma García-Legler, Maria Teresa Donato, Manuel Salmeron-Sanchez, Gloria Gallego-Ferrer, Laia Tolosa.

4. 3D printable hydrogels of hyaluronic acid and gelatin based on enzymatic crosslinking.
   Conference: 49th ESAO-IFAO Congress
   City, Country / Year: Bergamo, Italy / 2023
   Format: Poster
   Authors: **Julio Rodríguez-Fernández,** Teresa Diaz-Jordá, Maria Teresa Donato, Manuel Salmeron-Sanchez, Gloria Gallego-Ferrer, Laia Tolosa.

5. Gelatin-hyaluronic acid scaffolds for the treatment of acute liver failure.
   Conference: 49th ESAO-IFAO Congress
   City, Country / Year: Bergamo, Italy / 2023
   Format: Poster

Authors: **Julio Rodríguez-Fernández,** Emma García-Legler, Estela Villanueva-Bádenas, Maria Teresa Donato, Jose Luis Gómez-Ribelles Manuel Salmeron-Sanchez, Gloria Gallego-Ferrer, Laia Tolosa.

3. National conferences

1. Primary hepatocytes embedded in hybrid hydrogels of hyaluronic acid and gelatin for liver tissue engineering.
   Conference: IV Congreso Nacional de Jóvenes Investigadores en Biomedicina
   City, Country / Year: Online / 2020
   Format: Oral presentation
   Authors: **Julio Rodríguez-Fernández**, Estela Sánchez-González, Emma García-Legler, Sandra Clara-Trujillo, Maria Teresa Donato, Gloria Gallego-Ferrer, Laia Tolosa

4. Other contributions.

4.1. R&D Competitive Projects.

1. Hidrogeles biomiméticos imprimibles con presentación de factores de crecimiento eficiente para estudios de hepatotoxicidad de alto rendimiento.
   Contribution: Predoctoral researcher
   Funding entity: Agencia Estatal de Investigación, Ministerio de Ciencia e Innovación (PID2019-106000RB-C21)
   Duration: 01-06-2020 / 31-12-2023
   Budget: 242.000 €
   PI: Gallego Ferrer, Gloria and Salmerón Sánchez, Manuel

4.2. Awards

1. yESAO exchange award 2023
   Title: Modelling Non-Alcoholic Fatty Liver Disease by culturing HepG2C3A cells using a microfluidic biochip combined with a biomimetic hydrogel.
   Funding entity: yESAO
   Budget: 750 €
   Duration: 2 weeks
   Authors: Lisa Morisseau, **Julio Rodriguez-Fernandez**, Gloria Gallego-Ferrer, Laia Tolosa, Cécile Legallais, Rachid Jellali, Yasuyuki Sakai, Manuel Salmeron-Sanchez, Eric Leclerc

2. 1st Prize "Best poster" award 49th ESAO-IFAO 2023
   3D printable hydrogels of hyaluronic acid and gelatin based on enzymatic crosslinking.
   City, Country / Year: Bergamo, Italy / 2023
   Format: Poster
   Authors: **Julio Rodríguez-Fernández,** Teresa Diaz-Jordá, Maria Teresa Donato, Manuel Salmeron-Sanchez, Gloria Gallego-Ferrer, Laia Tolosa.

4.3. Supervision of bachelor and master thesis.

1. Estudio de optimización de la síntesis y gelificación de hidrogeles inyectables y su aplicación como sistemas de liberación de factores de crecimiento hepático.
   Student: Sofía Mares Bou (Bachelor thesis)
   Supervisors: Gloria Gallego Ferrer and **Julio Rodriguez Fernandez**.

2. Bioprinting of enzymatically crosslinked hyaluronic acid-gelatin hydrogels
   Student: Teresa Díaz Jordá (Master thesis)
   Supervisors: Gloria Gallego Ferrer and **Julio Rodriguez Fernandez**.

References

Adam, R., Karam, V., Delvart, V., O'Grady, J., Mirza, D., Klempnauer, J., Castaing, D., Neuhaus, P., Jamieson, N., Salizzoni, M., Pollard, S., Lerut, J., Paul, A., Garcia-Valdecasas, J. C., Rodríguez, F. S. J., & Burroughs, A. (2012). Evolution of indications and results of liver transplantation in Europe. A report from the European Liver Transplant Registry (ELTR). *Journal of Hepatology*, *57*(3), 675–688. https://doi.org/10.1016/j.jhep.2012.04.015

Aden, D. P., Fogel, A., Plotkin, S., Damjanov, I., & Knowles, B. B. (1979). Controlled synthesis of HBsAg in a differentiated human liver carcinoma-derived cell line. *Nature*, *282*(5739), 615–616. https://doi.org/10.1038/282615a0

Agarwal, T., Subramanian, B., & Maiti, T. K. (2019). Liver Tissue Engineering: Challenges and Opportunities. *ACS Biomaterials Science & Engineering*, *5*(9), 4167–4182. https://doi.org/10.1021/acsbiomaterials.9b00745

Aizarani, N., Saviano, A., Sagar, Mailly, L., Durand, S., Herman, J. S., Pessaux, P., Baumert, T. F., & Grün, D. (2019). A human liver cell atlas reveals heterogeneity and epithelial progenitors. *Nature*, *572*(7768), 199–204. https://doi.org/10.1038/s41586-019-1373-2

Ali, M., & Payne, S. L. (2021). Biomaterial-based cell delivery strategies to promote liver regeneration. In *Biomaterials Research* (Vol. 25, Issue 1). BioMed Central Ltd. https://doi.org/10.1186/s40824-021-00206-w

Allu, I., Sahi, A. K., Koppadi, M., Gundu, S., & Sionkowska, A. (2023). Decellularization Techniques for Tissue Engineering: Towards Replicating Native Extracellular Matrix Architecture in Liver Regeneration. In *Journal of Functional Biomaterials* (Vol. 14, Issue 10). Multidisciplinary Digital Publishing Institute (MDPI). https://doi.org/10.3390/jfb14100518

An, S., Choi, S., Min, S., & Cho, S.-W. (2021). Hyaluronic Acid-based Biomimetic Hydrogels for Tissue Engineering and Medical Applications. *Biotechnology and Bioprocess Engineering*, *26*(4), 503–516. https://doi.org/10.1007/s12257-020-0343-8

Anand, S. K., Caputo, M., Xia, Y., Andersson, E., Cansby, E., Kumari, S., Henricsson, M., Porosk, R., Keuenhof, K. S., Höög, J. L., Nair, S., Marschall, H.-U., Blüher, M., & Mahlapuu, M. (2022). Inhibition of MAP4K4 signaling initiates metabolic reprogramming to protect hepatocytes from

lipotoxic damage. *Journal of Lipid Research*, *63*(7), 100238. https://doi.org/10.1016/j.jlr.2022.100238

Annabi, N., Tamayol, A., Uquillas, J. A., Akbari, M., Bertassoni, L. E., Cha, C., Camci-Unal, G., Dokmeci, M. R., Peppas, N. A., & Khademhosseini, A. (2014). 25th Anniversary Article: Rational Design and Applications of Hydrogels in Regenerative Medicine. *Advanced Materials*, *26*(1), 85–124. https://doi.org/10.1002/adma.201303233

Arai, K., Yoshida, T., Okabe, M., Goto, M., Mir, T. A., Soko, C., Tsukamoto, Y., Akaike, T., Nikaido, T., Zhou, K., & Nakamura, M. (2017). Fabrication of 3D-culture platform with sandwich architecture for preserving liver-specific functions of hepatocytes using 3D bioprinter. *Journal of Biomedical Materials Research Part A*, *105*(6), 1583–1592. https://doi.org/https://doi.org/10.1002/jbm.a.35905

Arriazu, E., Ruiz de Galarreta, M., Cubero, F. J., Varela-Rey, M., Pérez de Obanos, M. P., Leung, T. M., Lopategi, A., Benedicto, A., Abraham-Enachescu, I., & Nieto, N. (2014). Extracellular Matrix and Liver Disease. *Antioxidants & Redox Signaling*, *21*(7), 1078–1097. https://doi.org/10.1089/ars.2013.5697

Arzumanian, V. A., Kiseleva, O. I., & Poverennaya, E. V. (2021). The curious case of the HepG2 cell line: 40 years of expertise. In *International Journal of Molecular Sciences* (Vol. 22, Issue 23). MDPI. https://doi.org/10.3390/ijms222313135

Arzumanyan, A., Reis, H. M. G. P. V., & Feitelson, M. A. (2013). Pathogenic mechanisms in HBV- and HCV-associated hepatocellular carcinoma. *Nature Reviews Cancer*, *13*(2), 123–135. https://doi.org/10.1038/nrc3449

Asrani, S. K., Devarbhavi, H., Eaton, J., & Kamath, P. S. (2019). Burden of liver diseases in the world. *Journal of Hepatology*, *70*(1), 151–171. https://doi.org/10.1016/j.jhep.2018.09.014

Au, S. H., Chamberlain, M. D., Mahesh, S., Sefton, M. V., & Wheeler, A. R. (2014). Hepatic organoids for microfluidic drug screening. *Lab on a Chip*, *14*(17), 3290–3299. https://doi.org/10.1039/c4lc00531g

Baiocchini, A., Montaldo, C., Conigliaro, A., Grimaldi, A., Correani, V., Mura, F., Ciccosanti, F., Rotiroti, N., Brenna, A., Montalbano, M., D'Offizi, G., Capobianchi, M. R., Alessandro, R., Piacentini, M., Schininà, M. E., Maras, B., Del Nonno, F., Tripodi, M., & Mancone, C. (2016). Extracellular matrix

molecular remodeling in human liver fibrosis evolution. *PLoS ONE*, *11*(3). https://doi.org/10.1371/journal.pone.0151736

Barbero-Becerra, V. J., Giraudi, P. J., Chávez-Tapia, N. C., Uribe, M., Tiribelli, C., & Rosso, N. (2015). The interplay between hepatic stellate cells and hepatocytes in an in vitro model of NASH. *Toxicology in Vitro*, *29*(7), 1753–1758. https://doi.org/10.1016/j.tiv.2015.07.010

Bataller, R., Cabezas, J., Aller, R., Ventura-Cots, M., Abad, J., Albillos, A., Altamirano, J., Arias-Loste, M. T., Bañares, R., Caballería, J., Caballería, L., Carrión, J. A., Diago, M., Fernández Rodríguez, C., Gallego, R., García-Cortes, M., García-Monzón, C., Genescà, J., Ginés, P., … Romero-Gómez, M. (2019). Enfermedad hepática por alcohol. Guías de práctica clínica. Documento de consenso auspiciado por la AEEH. *Gastroenterología y Hepatología*, *42*(10), 657–676. https://doi.org/10.1016/j.gastrohep.2019.09.006

Baze, A., Parmentier, C., Hendriks, D. F. G., Hurrell, T., Heyd, B., Bachellier, P., Schuster, C., Ingelman-Sundberg, M., & Richert, L. (2018). Three-Dimensional Spheroid Primary Human Hepatocytes in Monoculture and Coculture with Nonparenchymal Cells. *Tissue Engineering - Part C: Methods*, *24*(9), 534–545. https://doi.org/10.1089/ten.tec.2018.0134

Bedossa, P., & Paradis, V. (2003). Liver extracellular matrix in health and disease. *The Journal of Pathology*, *200*(4), 504–515. https://doi.org/10.1002/path.1397

Bell, C. C., Dankers, A. C. A., Lauschke, V. M., Sison-Young, R., Jenkins, R., Rowe, C., Goldring, C. E., Park, K., Regan, S. L., Walker, T., Schofield, C., Baze, A., Foster, A. J., Williams, D. P., van de Ven, A. W. M., Jacobs, F., van Houdt, J., Lähteenmäki, T., Snoeys, J., … Ingelman-Sundberg, M. (2018). Comparison of hepatic 2D sandwich cultures and 3d spheroids for long-term toxicity applications: A multicenter study. *Toxicological Sciences*, *162*(2), 655–666. https://doi.org/10.1093/toxsci/kfx289

Bernal, P. N., Bouwmeester, M., Madrid-Wolff, J., Falandt, M., Florczak, S., Rodriguez, N. G., Li, Y., Größbacher, G., Samsom, R., van Wolferen, M., van der Laan, L. J. W., Delrot, P., Loterie, D., Malda, J., Moser, C., Spee, B., & Levato, R. (2022). Volumetric Bioprinting of Organoids and Optically Tuned Hydrogels to Build Liver-Like Metabolic Biofactories. *Advanced Materials*, *34*(15). https://doi.org/10.1002/adma.202110054

Bhatia, S. N., Underhill, G. H., Zaret, K. S., & Fox, I. J. (2014). Cell and tissue engineering for liver disease. *Science Translational Medicine*, *6*(245). https://doi.org/10.1126/scitranslmed.3005975

Bhise, N. S., Manoharan, V., Massa, S., Tamayol, A., Ghaderi, M., Miscuglio, M., Lang, Q., Zhang, Y. S., Shin, S. R., Calzone, G., Annabi, N., Shupe, T. D., Bishop, C. E., Atala, A., Dokmeci, M. R., & Khademhosseini, A. (2016). A liver-on-a-chip platform with bioprinted hepatic spheroids. *Biofabrication*, *8*(1). https://doi.org/10.1088/1758-5090/8/1/014101

Bhusal, A., Dogan, E., Nguyen, H.-A., Labutina, O., Nieto, D., Khademhosseini, A., & Miri, A. K. (2022). Multi-material digital light processing bioprinting of hydrogel-based microfluidic chips. *Biofabrication*, *14*(1), 014103. https://doi.org/10.1088/1758-5090/ac2d78

Billiet, T., Gevaert, E., De Schryver, T., Cornelissen, M., & Dubruel, P. (2014). The 3D printing of gelatin methacrylamide cell-laden tissue-engineered constructs with high cell viability. *Biomaterials*, *35*(1), 49–62. https://doi.org/10.1016/j.biomaterials.2013.09.078

Bissell, D. M., & Choun, M. O. (1988). The Role of Extracellular Matrix in Normal Liver. *Scandinavian Journal of Gastroenterology*, *23*(sup151), 1–7. https://doi.org/10.3109/00365528809095908

Bizzaro, Russo, & Burra. (2019). New Perspectives in Liver Transplantation: From Regeneration to Bioengineering. *Bioengineering*, *6*(3), 81. https://doi.org/10.3390/bioengineering6030081

Björnsson, E. S., Gunnarsson, B. I., Gröndal, G., Jonasson, J. G., Einarsdottir, R., Ludviksson, B. R., Gudbjörnsson, B., & Olafsson, S. (2015). Risk of drug-induced liver injury from tumor necrosis factor antagonists. *Clinical Gastroenterology and Hepatology*, *13*(3), 602–608. https://doi.org/10.1016/j.cgh.2014.07.062

Blaeser, A., Duarte Campos, D. F., Puster, U., Richtering, W., Stevens, M. M., & Fischer, H. (2016). Controlling Shear Stress in 3D Bioprinting is a Key Factor to Balance Printing Resolution and Stem Cell Integrity. *Advanced Healthcare Materials*, *5*(3), 326–333. https://doi.org/10.1002/adhm.201500677

Bohidar, H. B. (1998). Hydrodynamic properties of gelatin in dilute solutions. *International Journal of Biological Macromolecules*, *23*(1), 1–6. https://doi.org/10.1016/S0141-8130(98)00003-8

Bomo, J., Ezan, F., Tiaho, F., Bellamri, M., Langouët, S., Theret, N., & Baffet, G. (2016). Increasing 3D Matrix Rigidity Strengthens Proliferation and Spheroid Development of Human Liver Cells in a Constant Growth Factor Environment. *Journal of Cellular Biochemistry*, *117*(3), 708–720. https://doi.org/10.1002/jcb.25356

Bonora-Centelles, A., Donato, M. T., Lahoz, A., Pareja, E., Mir, J., Castell, J. V., & Gómez-Lechón, M. J. (2010). Functional Characterization of Hepatocytes for Cell Transplantation: Customized Cell Preparation for Each Receptor. *Cell Transplantation*, *19*(1), 21–28. https://doi.org/10.3727/096368909X474267

Broutier, L., Mastrogiovanni, G., Verstegen, M. M., Francies, H. E., Gavarró, L. M., Bradshaw, C. R., Allen, G. E., Arnes-Benito, R., Sidorova, O., Gaspersz, M. P., Georgakopoulos, N., Koo, B.-K., Dietmann, S., Davies, S. E., Praseedom, R. K., Lieshout, R., IJzermans, J. N. M., Wigmore, S. J., Saeb-Parsy, K., … Huch, M. (2017). Human primary liver cancer–derived organoid cultures for disease modeling and drug screening. *Nature Medicine*, *23*(12), 1424–1435. https://doi.org/10.1038/nm.4438

Burton, R., Henn, C., Lavoie, D., O'Connor, R., Perkins, C., Sweeney, K., Greaves, F., Ferguson, B., Beynon, C., Belloni, A., Musto, V., Marsden, J., & Sheron, N. (2017). A rapid evidence review of the effectiveness and cost-effectiveness of alcohol control policies: an English perspective. *The Lancet*, *389*(10078), 1558–1580. https://doi.org/10.1016/S0140-6736(16)32420-5

Cantini, M., Donnelly, H., Dalby, M. J., & Salmeron-Sanchez, M. (2020). The Plot Thickens: The Emerging Role of Matrix Viscosity in Cell Mechanotransduction. *Advanced Healthcare Materials*, *9*(8). https://doi.org/10.1002/adhm.201901259

Carpentier, N., Van der Meeren, L., Skirtach, A. G., Devisscher, L., Van Vlierberghe, H., Dubruel, P., & Van Vlierberghe, S. (2023). Gelatin-Based Hybrid Hydrogel Scaffolds: Toward Physicochemical Liver Mimicry. *Biomacromolecules*, *24*(10), 4333–4347. https://doi.org/10.1021/acs.biomac.2c00643

Carretero, A., León, Z., García-Cañaveras, J. C., Zaragoza, Á., Gómez-Lechón, M. J., Donato, M. T., & Lahoz, A. (2014). In vitro/in vivo screening of oxidative homeostasis and damage to DNA, protein, and lipids using UPLC/MS-MS. *Analytical and Bioanalytical Chemistry*, *406*(22), 5465–5476. https://doi.org/10.1007/s00216-014-7983-5

Chawla, S., & Das, A. (2023). Preclinical-to-clinical innovations in stem cell therapies for liver regeneration. *Current Research in Translational Medicine*, *71*(1), 103365. https://doi.org/10.1016/j.retram.2022.103365

Chen, C., Soto-Gutierrez, A., Baptista, P. M., & Spee, B. (2018). Biotechnology Challenges to In Vitro Maturation of Hepatic Stem Cells. *Gastroenterology*, *154*(5), 1258–1272. https://doi.org/10.1053/j.gastro.2018.01.066

Chen, S., Liu, A., Wu, C., Chen, Y., Liu, C., Zhang, Y., Wu, K., Wei, D., Sun, J., Zhou, L., & Fan, H. (2021). Static–Dynamic Profited Viscoelastic Hydrogels for Motor-Clutch-Regulated Neurogenesis. *ACS Applied Materials & Interfaces*, *13*(21), 24463–24476. https://doi.org/10.1021/acsami.1c03821

Chiang, C. H., Wu, W. W., Li, H. Y., Chien, Y., Sun, C. C., Peng, C. H., Lin, A. T. L., Huang, C. S., Lai, Y. H., Chiou, S. H., Hung, S. I., Chang, Y. L., Lan, Y. T., Liu, D. M., Chien, C. S., Huo, T. I., Lee, S. D., & Wang, C. Y. (2015). Enhanced antioxidant capacity of dental pulp-derived iPSC-differentiated hepatocytes and liver regeneration by injectable HGF-releasing hydrogel in fulminant hepatic failure. *Cell Transplantation*, *24*(3), 541–559. https://doi.org/10.3727/096368915X686986

Chliara, M. A., Elezoglou, S., & Zergioti, I. (2022). Bioprinting on Organ-on-Chip: Development and Applications. In *Biosensors* (Vol. 12, Issue 12). https://doi.org/10.3390/bios12121135

Chowdhary, V., Teng, K., Thakral, S., Zhang, B., Lin, C., Wani, N., Bruschweiler-Li, L., Zhang, X., James, L., Yang, D., Junge, N., Brüschweiler, R., Lee, W. M., & Ghoshal, K. (2017). miRNA-122 Protects Mice and Human Hepatocytes from Acetaminophen Toxicity by Regulating Cytochrome P450 Family 1 Subfamily A Member 2 and Family 2 Subfamily E Member 1 Expression. *The American Journal of Pathology*, *187*(12), 2758–2774. https://doi.org/10.1016/j.ajpath.2017.08.026

Christoffersson, J., Aronsson, C., Jury, M., Selegård, R., Aili, D., & Mandenius, C. F. (2019). Fabrication of modular hyaluronan-PEG hydrogels to support 3D cultures of hepatocytes in a perfused liver-on-a-chip device. *Biofabrication*, *11*(1). https://doi.org/10.1088/1758-5090/aaf657

Clancy, A., Chen, D., Bruns, J., Nadella, J., Stealey, S., Zhang, Y., Timperman, A., & Zustiak, S. P. (2022). Hydrogel-based microfluidic device with multiplexed 3D in vitro cell culture. *Scientific Reports*, *12*(1). https://doi.org/10.1038/s41598-022-22439-y

Cooke, M. E., & Rosenzweig, D. H. (2021). The rheology of direct and suspended extrusion bioprinting. In *APL Bioengineering* (Vol. 5, Issue 1). American Institute of Physics Inc. https://doi.org/10.1063/5.0031475

Cui, J., Wang, H., Shi, Q., Sun, T., Huang, Q., & Fukuda, T. (2019). Multicellular co-culture in three-dimensional gelatin methacryloyl hydrogels for liver tissue engineering. *Molecules*, *24*(9). https://doi.org/10.3390/molecules24091762

Cui, X., Breitenkamp, K., Finn, M. G., Lotz, M., & D'Lima, D. D. (2012). Direct human cartilage repair using three-dimensional bioprinting technology. *Tissue Engineering. Part A*, *18*(11–12), 1304–1312. https://doi.org/10.1089/ten.TEA.2011.0543

Cuvellier, M., Ezan, F., Oliveira, H., Rose, S., Fricain, J.-C., Langouët, S., Legagneux, V., & Baffet, G. (2021). 3D culture of HepaRG cells in GelMa and its application to bioprinting of a multicellular hepatic model. *Biomaterials*, *269*, 120611. https://doi.org/10.1016/j.biomaterials.2020.120611

da Silva Morais, A., Vieira, S., Zhao, X., Mao, Z., Gao, C., Oliveira, J. M., & Reis, R. L. (2020). Advanced Biomaterials and Processing Methods for Liver Regeneration: State-of-the-Art and Future Trends. *Advanced Healthcare Materials*, *9*(5). https://doi.org/10.1002/adhm.201901435

Darr, A., & Calabro, A. (2009). Synthesis and characterization of tyramine-based hyaluronan hydrogels. *Journal of Materials Science: Materials in Medicine*, *20*(1), 33–44. https://doi.org/10.1007/s10856-008-3540-0

Datta, P., Dey, M., Ataie, Z., Unutmaz, D., & Ozbolat, I. T. (2020). 3D bioprinting for reconstituting the cancer microenvironment. *Npj Precision Oncology*, *4*(1), 18. https://doi.org/10.1038/s41698-020-0121-2

Davidson, M. D., Pickrell, J., & Khetani, S. R. (2021). Physiologically inspired culture medium prolongs the lifetime and insulin sensitivity of human hepatocytes in micropatterned co-cultures. *Toxicology*, *449*. https://doi.org/10.1016/j.tox.2020.152662

De France, K. J., Xu, F., & Hoare, T. (2018). Structured Macroporous Hydrogels: Progress, Challenges, and Opportunities. *Advanced Healthcare Materials*, *7*(1), 1–17. https://doi.org/10.1002/adhm.201700927

Deegan, D. B., Zimmerman, C., Skardal, A., Atala, A., & Shupe, T. D. (2016). Stiffness of hyaluronic acid gels containing liver extracellular matrix

supports human hepatocyte function and alters cell morphology. *Journal of the Mechanical Behavior of Biomedical Materials*, *55*, 87–103. https://doi.org/10.1016/j.jmbbm.2015.10.016

Deguchi, S., Tsuda, M., Kosugi, K., Sakamoto, A., Mimura, N., Negoro, R., Sano, E., Nobe, T., Maeda, K., Kusuhara, H., Mizuguchi, H., Yamashita, F., Torisawa, Y. S., & Takayama, K. (2021). Usability of Polydimethylsiloxane-Based Microfluidic Devices in Pharmaceutical Research Using Human Hepatocytes. *ACS Biomaterials Science and Engineering*, *7*(8), 3648–3657. https://doi.org/10.1021/acsbiomaterials.1c00642

Desai, S. S., Tung, J. C., Zhou, V. X., Grenert, J. P., Malato, Y., Rezvani, M., Español-Suñer, R., Willenbring, H., Weaver, V. M., & Chang, T. T. (2016). Physiological ranges of matrix rigidity modulate primary mouse hepatocyte function in part through hepatocyte nuclear factor 4 alpha. *Hepatology*, *64*(1), 261–275. https://doi.org/10.1002/hep.28450

Desimone, M. F., Hélary, C., Rietveld, I. B., Bataille, I., Mosser, G., Giraud-Guille, M. M., Livage, J., & Coradin, T. (2010). Silica-collagen bionanocomposites as three-dimensional scaffolds for fibroblast immobilization. *Acta Biomaterialia*, *6*(10), 3998–4004. https://doi.org/10.1016/j.actbio.2010.05.014

Dhanasekaran, R., Bandoh, S., & Roberts, L. R. (2016). Molecular pathogenesis of hepatocellular carcinoma and impact of therapeutic advances. *F1000Research*, *5*, 879. https://doi.org/10.12688/f1000research.6946.1

Dhawan, A., Chaijitraruch, N., Fitzpatrick, E., Bansal, S., Filippi, C., Lehec, S. C., Heaton, N. D., Kane, P., Verma, A., Hughes, R. D., & Mitry, R. R. (2020). Alginate microencapsulated human hepatocytes for the treatment of acute liver failure in children. *Journal of Hepatology*, *72*(5), 877–884. https://doi.org/10.1016/j.jhep.2019.12.002

Dhawan, A., Mitry, R. R., Hughes, R. D., Lehec, S., Terry, C., Bansal, S., Arya, R., Wade, J. J., Verma, A., Heaton, N. D., Rela, M., & Mieli-Vergani, G. (2004). Hepatocyte transplantation for inherited factor VII deficiency. *Transplantation*, *78*(12), 1812–1814. https://doi.org/10.1097/01.TP.0000146386.77076.47

Dianat, N., Dubois-Pot-Schneider, H., Steichen, C., Desterke, C., Leclerc, P., Raveux, A., Combettes, L., Weber, A., Corlu, A., & Dubart-Kupperschmitt, A. (2014). Generation of functional cholangiocyte-like cells from human pluripotent stem cells and HepaRG cells. *Hepatology*, *60*(2), 700–714. https://doi.org/10.1002/hep.27165

Diehl, A. M., & Day, C. (2017). Cause, Pathogenesis, and Treatment of Nonalcoholic Steatohepatitis. *New England Journal of Medicine*, *377*(21), 2063–2072. https://doi.org/10.1056/NEJMra1503519

Ding, B. Sen, Cao, Z., Lis, R., Nolan, D. J., Guo, P., Simons, M., Penfold, M. E., Shido, K., Rabbany, S. Y., & Rafii, S. (2014). Divergent angiocrine signals from vascular niche balance liver regeneration and fibrosis. *Nature*, *505*(7481), 97–102. https://doi.org/10.1038/nature12681

Ding, B. Sen, Nolan, D. J., Butler, J. M., James, D., Babazadeh, A. O., Rosenwaks, Z., Mittal, V., Kobayashi, H., Shido, K., Lyden, D., Sato, T. N., Rabbany, S. Y., & Rafii, S. (2010). Inductive angiocrine signals from sinusoidal endothelium are required for liver regeneration. *Nature*, *468*(7321), 310–315. https://doi.org/10.1038/nature09493

Dixon, L. J., Barnes, M., Tang, H., Pritchard, M. T., & Nagy, L. E. (2013). Kupffer Cells in the Liver. In *Comprehensive Physiology* (Vol. 3, Issue 2, pp. 785–797). Wiley. https://doi.org/10.1002/cphy.c120026

Donato, M. T., Bolonio, M., Cabezas, E., Pelechá, M., Pareja, E., Domènech, A., Castell, J. V., Gómez-Lechón, M. J., & Tolosa, L. (2020). Improved in vivo efficacy of clinical-grade cryopreserved human hepatocytes in mice with acute liver failure. *Cytotherapy*, *22*(2), 114–121. https://doi.org/10.1016/j.jcyt.2019.12.005

Donato, M. T., Gomezlechon, M. J., & Castell, J. V. (1993). A Microassay for Measuring Cytochrome P450IA1 and Cytochrome P450IIB1 Activities in Intact Human and Rat Hepatocytes Cultured on 96-Well Plates. *Analytical Biochemistry*, *213*(1), 29–33. https://doi.org/10.1006/abio.1993.1381

Donato, M. T., Montero, S., Castell, J. V., Gómez-Lechón, M. J., & Lahoz, A. (2010). Validated assay for studying activity profiles of human liver UGTs after drug exposure: Inhibition and induction studies. *Analytical and Bioanalytical Chemistry*, *396*(6), 2251–2263. https://doi.org/10.1007/s00216-009-3441-1

Donato, M. T., Tolosa, L., & Gómez-Lechón, M. J. (2015). Culture and Functional Characterization of Human Hepatoma HepG2 Cells. In *Protocols in In Vitro Hepatocyte Research* (pp. 77–93). Springer New York. https://doi.org/10.1007/978-1-4939-2074-7_5

Dutkowski, P., Linecker, M., DeOliveira, M. L., Müllhaupt, B., & Clavien, P.-A. (2015). Challenges to Liver Transplantation and Strategies to Improve

Outcomes. *Gastroenterology*, *148*(2), 307–323. https://doi.org/10.1053/j.gastro.2014.08.045

Dwyer, B. J., Macmillan, M. T., Brennan, P. N., & Forbes, S. J. (2021). Cell therapy for advanced liver diseases: Repair or rebuild. *Journal of Hepatology*, *74*(1), 185–199. https://doi.org/10.1016/j.jhep.2020.09.014

EASL. (2016). EASL-EASD-EASO Clinical Practice Guidelines for the Management of Non-Alcoholic Fatty Liver Disease. *Obesity Facts*, *9*(2), 65–90. https://doi.org/10.1159/000443344

EASL. (2019). EASL Clinical Practice Guidelines: Drug-induced liver injury. *Journal of Hepatology*, *70*(6), 1222–1261. https://doi.org/10.1016/j.jhep.2019.02.014

Egbu, R., Brocchini, S., Khaw, P. T., & Awwad, S. (2018). Antibody loaded collapsible hyaluronic acid hydrogels for intraocular delivery. *European Journal of Pharmaceutics and Biopharmaceutics*, *124*, 95–103. https://doi.org/10.1016/j.ejpb.2017.12.019

Estermann, S. J., Förster-Streffleur, S., Hirtler, L., Streicher, J., Pahr, D. H., & Reisinger, A. (2021). Comparison of Thiel preserved, fresh human, and animal liver tissue in terms of mechanical properties. *Annals of Anatomy*, *236*. https://doi.org/10.1016/j.aanat.2021.151717

Fan, J., Shang, Y., Yuan, Y., & Yang, J. (2010). Preparation and characterization of chitosan/galactosylated hyaluronic acid scaffolds for primary hepatocytes culture. *Journal of Materials Science: Materials in Medicine*, *21*(1), 319–327. https://doi.org/10.1007/s10856-009-3833-y

Fan, Z., Wei, X., Chen, K., Wang, L., & Xu, M. (2023). 3D Bioprinting of an Endothelialized Liver Lobule-like Construct as a Tumor-Scale Drug Screening Platform. *Micromachines*, *14*(4). https://doi.org/10.3390/mi14040878

Firouzi, N., Baradar Khoshfetrat, A., & Kazemi, D. (2020). Enzymatically gellable gelatin improves nano-hydroxyapatite-alginate microcapsule characteristics for modular bone tissue formation. *Journal of Biomedical Materials Research - Part A*, *108*(2), 340–350. https://doi.org/10.1002/jbm.a.36820

Forbes, S. J., Gupta, S., & Dhawan, A. (2015). Cell therapy for liver disease: From liver transplantation to cell factory. *Journal of Hepatology*, *62*(1), S157–S169. https://doi.org/10.1016/j.jhep.2015.02.040

Ford, A. J., & Rajagopalan, P. (2018). Extracellular matrix remodeling in 3D: implications in tissue homeostasis and disease progression. *Wiley Interdisciplinary Reviews: Nanomedicine and Nanobiotechnology*, *10*(4). https://doi.org/10.1002/wnan.1503

FOX. (2004). Hepatocyte transplantation. *Journal of Hepatology*, *40*(6), 878–886. https://doi.org/10.1016/j.jhep.2004.04.009

Frantz, C., Stewart, K. M., & Weaver, V. M. (2010). The extracellular matrix at a glance. *Journal of Cell Science*, *123*(24), 4195–4200. https://doi.org/10.1242/jcs.023820

Gao, C., Yang, Y., Zhang, Y., Qian, M., & Yang, J. (2020). HGF Gene Delivering Alginate/Galactosylated Chitosan Sponge Scaffold for Three-Dimensional Coculture of Hepatocytes/3T3 Cells. *DNA and Cell Biology*, *39*(3), 451–458. https://doi.org/10.1089/dna.2019.5136

Gebhardt, R., & Matz-Soja, M. (2014). Liver zonation: Novel aspects of its regulation and its impact on homeostasis. *World Journal of Gastroenterology*, *20*(26), 8491. https://doi.org/10.3748/wjg.v20.i26.8491

Gillispie, G., Prim, P., Copus, J., Fisher, J., Mikos, A. G., Yoo, J. J., Atala, A., & Lee, S. J. (2020). Assessment methodologies for extrusion-based bioink printability. *Biofabrication*, *12*(2), 22003. https://doi.org/10.1088/1758-5090/ab6f0d

Godoy, P., Hewitt, N. J., Albrecht, U., Andersen, M. E., Ansari, N., Bhattacharya, S., Bode, J. G., Bolleyn, J., Borner, C., Böttger, J., Braeuning, A., Budinsky, R. A., Burkhardt, B., Cameron, N. R., Camussi, G., Cho, C.-S., Choi, Y.-J., Craig Rowlands, J., Dahmen, U., … Hengstler, J. G. (2013). Recent advances in 2D and 3D in vitro systems using primary hepatocytes, alternative hepatocyte sources and non-parenchymal liver cells and their use in investigating mechanisms of hepatotoxicity, cell signaling and ADME. *Archives of Toxicology*, *87*(8), 1315–1530. https://doi.org/10.1007/s00204-013-1078-5

Gómez-Lechón, M. J., Donato, M. T., Castell, J. V, & Jover, R. (2004). Human Hepatocytes in Primary Culture: The Choice to Investigate Drug Metabolism in Man. In *Current Drug Metabolism* (Vol. 5).

Gómez-Lechón, M. J., Lahoz, A., Jiménez, N., Vicente Castell, J., & Donato, M. T. (2006). Cryopreservation of rat, dog and human hepatocytes: Influence of preculture and cryoprotectants on recovery, cytochrome P450 activities

and induction upon thawing. *Xenobiotica*, *36*(6), 457–472. https://doi.org/10.1080/00498250600674352

Gómez-Lechón, M. J., Tolosa, L., Conde, I., & Donato, M. T. (2014). Competency of different cell models to predict human hepatotoxic drugs. In *Expert Opinion on Drug Metabolism and Toxicology* (Vol. 10, Issue 11, pp. 1553–1568). Informa Healthcare. https://doi.org/10.1517/17425255.2014.967680

Gómez-Mariano, G., Matamala, N., Martínez, S., Justo, I., Marcacuzco, A., Jimenez, C., Monzón, S., Cuesta, I., Garfia, C., Martínez, M. T., Huch, M., Pérez de Castro, I., Posada, M., Janciauskiene, S., & Martínez-Delgado, B. (2020). Liver organoids reproduce alpha-1 antitrypsin deficiency-related liver disease. *Hepatology International*, *14*(1), 127–137. https://doi.org/10.1007/s12072-019-10007-y

Gori, M., Giannitelli, S. M., Torre, M., Mozetic, P., Abbruzzese, F., Trombetta, M., Traversa, E., Moroni, L., & Rainer, A. (2020). Biofabrication of Hepatic Constructs by 3D Bioprinting of a Cell-Laden Thermogel: An Effective Tool to Assess Drug-Induced Hepatotoxic Response. *Advanced Healthcare Materials*, *9*(21). https://doi.org/10.1002/adhm.202001163

Gori, M., Simonelli, M. C., Giannitelli, S. M., Businaro, L., Trombetta, M., & Rainer, A. (2016). Investigating nonalcoholic fatty liver disease in a liver-on-a-chip microfluidic device. *PLoS ONE*, *11*(7). https://doi.org/10.1371/journal.pone.0159729

Grompe, M., Laconi, E., & Shafritz, D. (1999). Principles of Therapeutic Liver Repopulation. *Seminars in Liver Disease*, *19*(01), 7–14. https://doi.org/10.1055/s-2007-1007093

Guan, Y., Enejder, A., Wang, M., Fang, Z., Cui, L., Chen, S. Y., Wang, J., Tan, Y., Wu, M., Chen, X., Johansson, P. K., Osman, I., Kunimoto, K., Russo, P., Heilshorn, S. C., & Peltz, G. (2021). A human multi-lineage hepatic organoid model for liver fibrosis. *Nature Communications*, *12*(1). https://doi.org/10.1038/s41467-021-26410-9

Gupta, S., Rajvanshi, P., Sokhi, R., Slehria, S., Yam, A., Kerr, A., & Novikoff, P. M. (1999). Entry and integration of transplanted hepatocytes in rat liver plates occur by disruption of hepatic sinusoidal endothelium. *Hepatology*, *29*(2), 509–519. https://doi.org/10.1002/hep.510290213

Halpern, K. B., Shenhav, R., Massalha, H., Toth, B., Egozi, A., Massasa, E. E., Medgalia, C., David, E., Giladi, A., Moor, A. E., Porat, Z., Amit, I., & Itzkovitz,

S. (2018). Paired-cell sequencing enables spatial gene expression mapping of liver endothelial cells. *Nature Biotechnology*, *36*(10), 962. https://doi.org/10.1038/nbt.4231

Hammond, J. S., Beckingham, I. J., & Shakesheff, K. M. (2006). Scaffolds for liver tissue engineering. *Expert Review of Medical Devices*, *3*(1), 21–27. https://doi.org/10.1586/17434440.3.1.21

Han, J., & Ulevitch, R. J. (2005). Limiting inflammatory responses during activation of innate immunity. *Nature Immunology*, *6*(12), 1198–1205. https://doi.org/10.1038/ni1274

Hannan, N. R. F., Segeritz, C. P., Touboul, T., & Vallier, L. (2013). Production of hepatocyte-like cells from human pluripotent stem cells. *Nature Protocols*, *8*(2), 430–437. https://doi.org/10.1038/nprot.2012.153

Hansel, M. C., Gramignoli, R., Skvorak, K. J., Dorko, K., Marongiu, F., Blake, W., Davila, J., & Strom, S. C. (2014). The history and use of human hepatocytes for the treatment of liver diseases: The first 100 patients. *Current Protocols in Toxicology*, *2014*(November), 14.12.1-14.12.23. https://doi.org/10.1002/0471140856.tx1412s62

Hao, T., Wen, N., Cao, J. K., Wang, H. B., Lü, S. H., Liu, T., Lin, Q. X., Duan, C. M., & Wang, C. Y. (2010). The support of matrix accumulation and the promotion of sheep articular cartilage defects repair in vivo by chitosan hydrogels. *Osteoarthritis and Cartilage*, *18*(2), 257–265. https://doi.org/10.1016/j.joca.2009.08.007

HARKNESS, R. D. (1961). BIOLOGICAL FUNCTIONS OF COLLAGEN. *Biological Reviews*, *36*(4), 399–455. https://doi.org/10.1111/j.1469-185X.1961.tb01596.x

Hart, C. L., Morrison, D. S., Batty, G. D., Mitchell, R. J., & Smith, G. D. (2010). Effect of body mass index and alcohol consumption on liver disease: Analysis of data from two prospective cohort studies. *BMJ (Online)*, *340*(7747), 634. https://doi.org/10.1136/bmj.c1240

He, J., Wang, J., Pang, Y., Yu, H., Qin, X., Su, K., Xu, T., & Ren, H. (2022). Bioprinting of a Hepatic Tissue Model Using HumanInduced Pluripotent Stem Cell-derived Hepatocytes for Drug-Induced Hepatotoxicity Evaluation. *International Journal of Bioprinting*, *8*(3), 581. https://doi.org/10.18063/ijb.v8i3.581

Helary, C., Bataille, I., Abed, A., Illoul, C., Anglo, A., Louedec, L., Letourneur, D., Meddahi-Pellé, A., & Giraud-Guille, M. M. (2010). Concentrated collagen hydrogels as dermal substitutes. *Biomaterials*, *31*(3), 481–490. https://doi.org/10.1016/j.biomaterials.2009.09.073

Hewitt, N. J., Gómez Lechón, M. J., Houston, J. B., Hallifax, D., Brown, H. S., Maurel, P., Kenna, J. G., Gustavsson, L., Lohmann, C., Skonberg, C., Guillouzo, A., Tuschl, G., Li, A. P., LeCluyse, E., Groothuis, G. M. M., & Hengstler, J. G. (2007). Primary Hepatocytes: Current Understanding of the Regulation of Metabolic Enzymes and Transporter Proteins, and Pharmaceutical Practice for the Use of Hepatocytes in Metabolism, Enzyme Induction, Transporter, Clearance, and Hepatotoxicity Studies. *Drug Metabolism Reviews*, *39*(1), 159–234. https://doi.org/10.1080/03602530601093489

Higashi, H., Yagi, H., Kuroda, K., Tajima, K., Kojima, H., Nishi, K., Morisaku, T., Hirukawa, K., Fukuda, K., Matsubara, K., Kitago, M., Shinoda, M., Obara, H., Adachi, S., Nishimura, K., Natsume, T., Tomi, M., Soto-Gutierrez, A., & Kitagawa, Y. (2022). Transplantation of bioengineered liver capable of extended function in a preclinical liver failure model. *American Journal of Transplantation*, *22*(3), 731–744. https://doi.org/10.1111/ajt.16928

Hoebe, K. H. N., Witkamp, R. F., Fink-Gremmels, J., Van Miert, A. S. J. P. A. M., Monshouwer, M., & Miert, A. S. J. P. A. M. Van. (2001). *Direct cell-to-cell contact between Kupffer cells and hepatocytes augments endotoxin-induced hepatic injury*. http://www.ajpgi.org

Huang, D. (Danielle), Gibeley, S. B., Xu, C., Xiao, Y., Celik, O., Ginsberg, H. N., & Leong, K. W. (2020). Engineering Liver Microtissues for Disease Modeling and Regenerative Medicine. *Advanced Functional Materials*, *30*(44). https://doi.org/10.1002/adfm.201909553

Huch, M., & Koo, B. K. (2015). Modeling mouse and human development using organoid cultures. In *Development (Cambridge)* (Vol. 142, Issue 18, pp. 3113–3125). Company of Biologists Ltd. https://doi.org/10.1242/dev.118570

Hull, C. W. (1986). *Apparatus for production of three-dimensional objects by stereolitography* (Patent US4575330A). https://ppubs.uspto.gov/pubwebapp/static/pages/ppubsbasic.html

Iansante, V., Mitry, R. R., Filippi, C., Fitzpatrick, E., & Dhawan, A. (2018). Human hepatocyte transplantation for liver disease: current status and future

perspectives. *Pediatric Research*, *83*(1–2), 232–240. https://doi.org/10.1038/pr.2017.284

Janani, G., Priya, S., Dey, S., & Mandal, B. B. (2022). Mimicking Native Liver Lobule Microarchitecture In Vitro with Parenchymal and Non-parenchymal Cells Using 3D Bioprinting for Drug Toxicity and Drug Screening Applications. *ACS Applied Materials and Interfaces*, *14*(8), 10167–10186. https://doi.org/10.1021/acsami.2c00312

Jancova, P., Anzenbacher, P., & Anzenbacherova, E. (2010). PHASE II DRUG METABOLIZING ENZYMES. *Biomedical Papers*, *154*(2), 103–116. https://doi.org/10.5507/bp.2010.017

Jenne, C. N., & Kubes, P. (2013). Immune surveillance by the liver. *Nature Immunology*, *14*(10), 996–1006. https://doi.org/10.1038/ni.2691

Jeon, O., Song, S. J., Lee, K. J., Park, M. H., Lee, S. H., Hahn, S. K., Kim, S., & Kim, B. S. (2007). Mechanical properties and degradation behaviors of hyaluronic acid hydrogels cross-linked at various cross-linking densities. *Carbohydrate Polymers*, *70*(3), 251–257. https://doi.org/10.1016/j.carbpol.2007.04.002

Jiang, J., Tan, Y., Liu, A., Yan, R., Ma, Y., Guo, L., Sun, J., Guo, Z., & Fan, H. (2021). Tissue engineered artificial liver model based on viscoelastic hyaluronan-collagen hydrogel and the effect of EGCG intervention on ALD. *Colloids and Surfaces B: Biointerfaces*, *206*. https://doi.org/10.1016/j.colsurfb.2021.111980

Jitraruch, S., Dhawan, A., Hughes, R. D., Filippi, C., Soong, D., Philippeos, C., Lehec, S. C., Heaton, N. D., Longhi, M. S., & Mitry, R. R. (2014). Alginate microencapsulated hepatocytes optimised for transplantation in acute liver failure. *PLoS ONE*, *9*(12), 1–23. https://doi.org/10.1371/journal.pone.0113609

José Gómez-Lechón, M., Castell, J. V, María, &, & Donato, T. (2008). An update on metabolism studies using human hepatocytes in primary culture. *Expert Opin. Drug Metab. Toxicol*, *4*(7), 837–854. https://doi.org/10.1517/17425250802159015

Ju, S. M., Jang, H. J., Kim, K. B., & Kim, J. (2015). High-Throughput Cytotoxicity Testing System of Acetaminophen Using a Microfluidic Device (MFD) in HepG2 Cells. *Journal of Toxicology and Environmental Health - Part A: Current Issues*, *78*(16), 1063–1072. https://doi.org/10.1080/15287394.2015.1068650

Kadri, R., Ben Messaoud, G., Tamayol, A., Aliakbarian, B., Zhang, H. Y., Hasan, M., Sánchez-González, L., & Arab-Tehrany, E. (2016). Preparation and characterization of nanofunctionalized alginate/methacrylated gelatin hybrid hydrogels. *RSC Advances*, *6*(33), 27879–27884. https://doi.org/10.1039/c6ra03699f

Kalyanam, S., Yapp, R. D., & Insana, M. F. (2009). Poro-viscoelastic behavior of gelatin hydrogels under compression- implications for bioelasticity imaging. *Journal of Biomechanical Engineering*, *131*(8), 1–13. https://doi.org/10.1115/1.3127250

Kang, D., Hong, G., An, S., Jang, I., Yun, W. S., Shim, J. H., & Jin, S. (2020). Bioprinting of Multiscaled Hepatic Lobules within a Highly Vascularized Construct. *Small*, *16*(13). https://doi.org/10.1002/smll.201905505

Kang, H. K., Sarsenova, M., Kim, D. H., Kim, M. S., Lee, J. Y., Sung, E. A., Kook, M. G., Kim, N. G., Choi, S. W., Ogay, V., & Kang, K. S. (2021). Establishing a 3d in vitro hepatic model mimicking physiologically relevant to in vivo state. *Cells*, *10*(5). https://doi.org/10.3390/cells10051268

Kang, H.-W., Lee, S. J., Ko, I. K., Kengla, C., Yoo, J. J., & Atala, A. (2016). A 3D bioprinting system to produce human-scale tissue constructs with structural integrity. *Nature Biotechnology*, *34*(3), 312–319. https://doi.org/10.1038/nbt.3413

Kang, Y. B., Rawat, S., Cirillo, J., Bouchard, M., & Noh, H. (2013). Layered long-term co-culture of hepatocytes and endothelial cells on a transwell membrane: Toward engineering the liver sinusoid. *Biofabrication*, *5*(4). https://doi.org/10.1088/1758-5082/5/4/045008

Kaplowitz, N. (2005). Idiosyncratic drug hepatotoxicity. *Nature Reviews Drug Discovery*, *4*(6), 489–499. https://doi.org/10.1038/nrd1750

Katsuda, T., Teratani, T., Ochiya, T., & Sakai, Y. (2010). Transplantation of a fetal liver cell-loaded hyaluronic acid sponge onto the mesentery recovers a Wilson's disease model rat. *Journal of Biochemistry*, *148*(3), 281–288. https://doi.org/10.1093/jb/mvq063

Kaur, G., Leslie, E. M., Tillman, H., Lee, W. M., Swanlund, D. P., Karvellas, C. J., Larson, A. M., Liou, I., Fix, O., Schilsky, M., Ganger, D., Han, S. H. B., Fontana, R., McGuire, B., Reuben, A., Koch, D., Reddy, R., Stravitz, R. T., Hanje, J., … Gottfried, M. (2015). Detection of ophthalmic acid in serum from acetaminophen-induced acute liver failure patients is more frequent in

non-survivors. *PLoS ONE*, *10*(9), 1–10. https://doi.org/10.1371/journal.pone.0139299

Khanmohammadi, M., Dastjerdi, M. B., Ai, A., Ahmadi, A., Godarzi, A., Rahimi, A., & Ai, J. (2018). Horseradish peroxidase-catalyzed hydrogelation for biomedical applications. In *Biomaterials Science* (Vol. 6, Issue 6, pp. 1286–1298). Royal Society of Chemistry. https://doi.org/10.1039/c8bm00056e

Khati, V., Ramachandraiah, H., Pati, F., Svahn, H. A., Gaudenzi, G., & Russom, A. (2022). 3D Bioprinting of Multi-Material Decellularized Liver Matrix Hydrogel at Physiological Temperatures. *Biosensors*, *12*(7), 521. https://doi.org/10.3390/bios12070521

Kholodenko, I. V., & Yarygin, K. N. (2017). Cellular Mechanisms of Liver Regeneration and Cell-Based Therapies of Liver Diseases. *BioMed Research International*, *2017*, 1–17. https://doi.org/10.1155/2017/8910821

Kim, M., Lee, J. Y., Jones, C. N., Revzin, A., & Tae, G. (2010). Heparin-based hydrogel as a matrix for encapsulation and cultivation of primary hepatocytes. *Biomaterials*, *31*(13), 3596–3603. https://doi.org/10.1016/j.biomaterials.2010.01.068

Kim, S. H., Seo, Y. B., Yeon, Y. K., Lee, Y. J., Park, H. S., Sultan, Md. T., Lee, J. M., Lee, J. S., Lee, O. J., Hong, H., Lee, H., Ajiteru, O., Suh, Y. J., Song, S.-H., Lee, K.-H., & Park, C. H. (2020). 4D-bioprinted silk hydrogels for tissue engineering. *Biomaterials*, *260*, 120281. https://doi.org/10.1016/j.biomaterials.2020.120281

Kripotou, S., Stefanopoulou, E., Culebras-Martínez, M., Morales-Román, R. M., Gallego Ferrer, G., & Kyritsis, A. (2019). Water dynamics and thermal properties of tyramine-modified hyaluronic acid - Gelatin hydrogels. *Polymer*, *178*. https://doi.org/10.1016/j.polymer.2019.121598

Kurisawa, M., Chung, J. E., Yang, Y. Y., Gao, S. J., & Uyama, H. (2005). Injectable biodegradable hydrogels composed of hyaluronic acid-tyramine conjugates for drug delivery and tissue engineering. *Chemical Communications*, *34*, 4312–4314. https://doi.org/10.1039/b506989k

Kvam, B. J., Atzori, M., Toffanin, R., Paoletti, S., & Biviano, F. (1992). 1H- and 13C-NMR studies of solutions of hyaluronic acid esters and salts in methyl sulfoxide: comparison of hydrogen-bond patterns and conformational behaviour. *Carbohydrate Research*, *230*(1), 1–13. https://doi.org/10.1016/S0008-6215(00)90509-3

Kyle, S., Jessop, Z. M., Al-Sabah, A., & Whitaker, I. S. (2017). 'Printability'' of Candidate Biomaterials for Extrusion Based 3D Printing: State-of-the-Art.' *Advanced Healthcare Materials*, *6*(16), 1700264. https://doi.org/https://doi.org/10.1002/adhm.201700264

Lahoz, A., Donato, M. T., Picazo, L., Gómez-Lechón, M. J., & Castell, J. V. (2007). Determination of major human cytochrome P450s activities in 96-well plates using liquid chromatography tandem mass spectrometry. *Toxicology in Vitro*, *21*(7), 1247–1252. https://doi.org/10.1016/j.tiv.2007.03.022

Lai, J. Y. (2010). Biocompatibility of chemically cross-linked gelatin hydrogels for ophthalmic use. *Journal of Materials Science: Materials in Medicine*, *21*(6), 1899–1911. https://doi.org/10.1007/s10856-010-4035-3

Lai, V. K., Nedrelow, D. S., Lake, S. P., Kim, B., Weiss, E. M., Tranquillo, R. T., & Barocas, V. H. (2016). Swelling of Collagen-Hyaluronic Acid Co-Gels: An In Vitro Residual Stress Model. *Annals of Biomedical Engineering*, *44*(10), 2984–2993. https://doi.org/10.1007/s10439-016-1636-0

Lamberg, S. I., & Stoolmiller, A. C. (1974). Glycosaminoglycans. A Biochemical and Clinical Review. *Journal of Investigative Dermatology*, *63*(6), 433–449. https://doi.org/10.1111/1523-1747.ep12680346

Lan, S.-F., Safiejko-Mroczka, B., & Starly, B. (2010). Long-term cultivation of HepG2 liver cells encapsulated in alginate hydrogels: A study of cell viability, morphology and drug metabolism. *Toxicology in Vitro*, *24*(4), 1314–1323. https://doi.org/10.1016/j.tiv.2010.02.015

Lancaster, M. A., & Knoblich, J. A. (2014). Generation of cerebral organoids from human pluripotent stem cells. *Nature Protocols*, *9*(10), 2329–2340. https://doi.org/10.1038/nprot.2014.158

Lawson, J. A., Farhood, A., Hopper, R. D., Bajt, M. L., & Jaeschke, H. (2000). The hepatic inflammatory response after acetaminophen overdose: Role of neutrophils. *Toxicological Sciences*, *54*(2), 509–516. https://doi.org/10.1093/toxsci/54.2.509

Le Guilcher, C., Merlen, G., Dellaquila, A., Labour, M.-N., Aid, R., Tordjmann, T., Letourneur, D., & Simon-Yarza, T. (2023). Engineered human liver based on pullulan-dextran hydrogel promotes mice survival after liver failure. *Materials Today Bio*, *19*, 100554. https://doi.org/10.1016/j.mtbio.2023.100554

Leach, J. B., Bivens, K. A., Patrick, C. W., & Schmidt, C. E. (2003). Photocrosslinked hyaluronic acid hydrogels: Natural, biodegradable tissue engineering scaffolds. *Biotechnology and Bioengineering*, *82*(5), 578–589. https://doi.org/10.1002/bit.10605

Lee, C. H., Singla, A., & Lee, Y. (2001). Biomedical applications of collagen. In *International Journal of Pharmaceutics* (Vol. 221). www.elsevier.com/locate/ijpharm

Lee, F., Bae, K. H., & Kurisawa, M. (2015). Injectable hydrogel systems crosslinked by horseradish peroxidase. *Biomedical Materials (Bristol)*, *11*(1). https://doi.org/10.1088/1748-6041/11/1/014101

Lee, F., Chung, J. E., & Kurisawa, M. (2008). An injectable enzymatically crosslinked hyaluronic acid-tyramine hydrogel system with independent tuning of mechanical strength and gelation rate. *Soft Matter*, *4*(4), 880–887. https://doi.org/10.1039/b719557e

Lee, F., Chung, J. E., & Kurisawa, M. (2009). An injectable hyaluronic acid-tyramine hydrogel system for protein delivery. *Journal of Controlled Release*, *134*(3), 186–193. https://doi.org/10.1016/j.jconrel.2008.11.028

Lee, H., Ahn, J., Jung, C., Jeung, Y., Cho, H., Son, M. J., & Chung, K. (2020). Optimization of 3D hydrogel microenvironment for enhanced hepatic functionality of primary human hepatocytes. *Biotechnology and Bioengineering*, *117*(6), 1864–1876. https://doi.org/10.1002/bit.27328

Lee, J. W., Choi, Y.-J., Yong, W.-J., Pati, F., Shim, J.-H., Kang, K. S., Kang, I.-H., Park, J., & Cho, D.-W. (2016). Development of a 3D cell printed construct considering angiogenesis for liver tissue engineering. *Biofabrication*, *8*(1), 015007. https://doi.org/10.1088/1758-5090/8/1/015007

Lee, J. Y., Han, H. J., Lee, S. J., Cho, E. H., Lee, H. B., Seok, J. H., Lim, H. S., & Son, W. C. (2020). Use of 3D human liver organoids to predict drug-induced phospholipidosis. *International Journal of Molecular Sciences*, *21*(8). https://doi.org/10.3390/ijms21082982

Leite, S. B., Roosens, T., El Taghdouini, A., Mannaerts, I., Smout, A. J., Najimi, M., Sokal, E., Noor, F., Chesne, C., & van Grunsven, L. A. (2016). Novel human hepatic organoid model enables testing of drug-induced liver fibrosis in vitro. *Biomaterials*, *78*, 1–10. https://doi.org/10.1016/j.biomaterials.2015.11.026

Lemos, F. de O., Florentino, R. M., Filho, A. C. M. L., Santos, M. L. dos, & Leite, M. de F. (2019). Inositol 1,4,5-trisphosphate receptor in the liver: Expression and function. *World Journal of Gastroenterology*, *25*(44), 6483–6494. https://doi.org/10.3748/wjg.v25.i44.6483

Leroy, V., Monier, F., Bottari, S., Trocme, C., Sturm, N., Hilleret, M.-N., Morel, F., & Zarski, J.-P. (2004). Circulating Matrix Metalloproteinases 1, 2, 9 and Their Inhibitors TIMP-1 and TIMP-2 as Serum Markers of Liver Fibrosis in Patients With Chronic Hepatitis C: Comparison With PIIINP and Hyaluronic Acid. *American Journal of Gastroenterology*, *99*(2), 271–279. https://doi.org/10.1111/j.1572-0241.2004.04055.x

Li, X., Liu, B., Pei, B., Chen, J., Zhou, D., Peng, J., Zhang, X., Jia, W., & Xu, T. (2020). Inkjet Bioprinting of Biomaterials. *Chemical Reviews*, *120*(19), 10793–10833. https://doi.org/10.1021/acs.chemrev.0c00008

Lim, Y. J., Deo, D., Singh, T. P., Jones, D. B., & De, S. (2009). In situ measurement and modeling of biomechanical response of human cadaveric soft tissues for physics-based surgical simulation. *Surgical Endoscopy*, *23*(6), 1298–1307. https://doi.org/10.1007/s00464-008-0154-z

Lin, J., Meng, L., Yao, Z., Chen, S., Yang, J., Tang, Z., Lin, N., & Xu, R. (2015). Use an alginate scaffold-bone marrow stromal cell (BMSC) complex for the treatment of acute liver failure in rats. *International Journal of Clinical and Experimental Medicine*, *8*(8), 12593–12600. http://www.ncbi.nlm.nih.gov/pubmed/26550170

Lin, T. Y., Ki, C. S., & Lin, C. C. (2014). Manipulating hepatocellular carcinoma cell fate in orthogonally cross-linked hydrogels. *Biomaterials*, *35*(25), 6898–6906. https://doi.org/10.1016/j.biomaterials.2014.04.118

Loebel, C., D'Este, M., Alini, M., Zenobi-Wong, M., & Eglin, D. (2015). Precise tailoring of tyramine-based hyaluronan hydrogel properties using DMTMM conjugation. *Carbohydrate Polymers*, *115*, 325–333. https://doi.org/10.1016/j.carbpol.2014.08.097

Lovett, M., Lee, K., Edwards, A., & Kaplan, D. L. (2009). Vascularization Strategies for Tissue Engineering. *Tissue Engineering Part B: Reviews*, *15*(3), 353–370. https://doi.org/10.1089/ten.teb.2009.0085

Lv, W., Zhou, H., Aazmi, A., Yu, M., Xu, X., Yang, H., Huang, Y. Y. S., & Ma, L. (2022). Constructing biomimetic liver models through biomaterials and vasculature engineering. In *Regenerative Biomaterials* (Vol. 9). Oxford University Press. https://doi.org/10.1093/rb/rbac079

Lysy, P. A., Najimi, M., Stéphenne, X., Bourgois, A., Smets, F., & Sokal, E. M. (2008). Liver cell transplantation for Crigler-Najjar syndrome type I: Update and perspectives. *World Journal of Gastroenterology*, *14*(22), 3464. https://doi.org/10.3748/wjg.14.3464

Ma, L., Wu, Y., Li, Y., Aazmi, A., Zhou, H., Zhang, B., & Yang, H. (2020). Current Advances on 3D-Bioprinted Liver Tissue Models. *Advanced Healthcare Materials*, *9*(24). https://doi.org/10.1002/adhm.202001517

Ma, X., Yu, C., Wang, P., Xu, W., Wan, X., Lai, C. S. E., Liu, J., Koroleva-Maharajh, A., & Chen, S. (2018). Rapid 3D bioprinting of decellularized extracellular matrix with regionally varied mechanical properties and biomimetic microarchitecture. *Biomaterials*, *185*, 310–321. https://doi.org/10.1016/j.biomaterials.2018.09.026

Malinen, M. M., Kanninen, L. K., Corlu, A., Isoniemi, H. M., Lou, Y.-R., Yliperttula, M. L., & Urtti, A. O. (2014). Differentiation of liver progenitor cell line to functional organotypic cultures in 3D nanofibrillar cellulose and hyaluronan-gelatin hydrogels. *Biomaterials*, *35*(19), 5110–5121. https://doi.org/10.1016/j.biomaterials.2014.03.020

Mao, S., Gao, D., Liu, W., Wei, H., & Lin, J. M. (2012). Imitation of drug metabolism in human liver and cytotoxicity assay using a microfluidic device coupled to mass spectrometric detection. *Lab on a Chip*, *12*(1), 219–226. https://doi.org/10.1039/c1lc20678h

Mazza, G., Rombouts, K., Rennie Hall, A., Urbani, L., Vinh Luong, T., Al-Akkad, W., Longato, L., Brown, D., Maghsoudlou, P., Dhillon, A. P., Fuller, B., Davidson, B., Moore, K., Dhar, D., De Coppi, P., Malago, M., & Pinzani, M. (2015). Decellularized human liver as a natural 3D-scaffold for liver bioengineering and transplantation. *Scientific Reports*, *5*(1), 13079. https://doi.org/10.1038/srep13079

Mazzocchi, A., Devarasetty, M., Huntwork, R., Soker, S., & Skardal, A. (2018). Optimization of collagen type I-hyaluronan hybrid bioink for 3D bioprinted liver microenvironments. *Biofabrication*, *11*(1), 015003. https://doi.org/10.1088/1758-5090/aae543

McKiernan, P. J., & Squires, R. H. (2020). Bridging transplantation with beads in paediatric acute liver failure. *Nature Reviews Gastroenterology & Hepatology*, *17*(4), 197–198. https://doi.org/10.1038/s41575-020-0281-0

Mejias, M., Gallego, J., Naranjo-Suarez, S., Ramirez, M., Pell, N., Manzano, A., Suñer, C., Bartrons, R., Mendez, R., & Fernandez, M. (2020). CPEB4

Increases Expression of PFKFB3 to Induce Glycolysis and Activate Mouse and Human Hepatic Stellate Cells, Promoting Liver Fibrosis. *Gastroenterology*, *159*(1), 273–288. https://doi.org/10.1053/j.gastro.2020.03.008

Messelmani, T., Le Goff, A., Souguir, Z., Maes, V., Roudaut, M., Vandenhaute, E., Maubon, N., Legallais, C., Leclerc, E., & Jellali, R. (2022). Development of Liver-on-Chip Integrating a Hydroscaffold Mimicking the Liver's Extracellular Matrix. *Bioengineering*, *9*(9). https://doi.org/10.3390/bioengineering9090443

Meyburg, J., Das, A. M., Hoerster, F., Lindner, M., Kriegbaum, H., Engelmann, G., Schmidt, J., Ott, M., Pettenazzo, A., Luecke, T., Bertram, H., Hoffmann, G. F., & Burlina, A. (2009). One Liver for Four Children: First Clinical Series of Liver Cell Transplantation for Severe Neonatal Urea Cycle Defects. *Transplantation*, *87*(5), 636–641. https://doi.org/10.1097/TP.0b013e318199936a

Michalopoulos, G. K., & DeFrances, M. C. (1997). Liver Regeneration. *Science*, *276*(5309), 60–66. https://doi.org/10.1126/science.276.5309.60

Miri, A. K., Mirzaee, I., Hassan, S., Mesbah Oskui, S., Nieto, D., Khademhosseini, A., & Zhang, Y. S. (2019). Effective bioprinting resolution in tissue model fabrication. *Lab on a Chip*, *19*(11), 2019–2037. https://doi.org/10.1039/c8lc01037d

Moniruzzaman, S., Das, P., Panwar, A., & Tan, L. P. (2021). Synthesis and characterization of site selective photo-crosslinkable glycidyl methacrylate functionalized gelatin-based 3D hydrogel scaffold for liver tissue engineering. *Materials Science and Engineering C*, *123*. https://doi.org/10.1016/j.msec.2020.111694

Moreira Teixeira, L. S., Bijl, S., Pully, V. V., Otto, C., Jin, R., Feijen, J., van Blitterswijk, C. A., Dijkstra, P. J., & Karperien, M. (2012). Self-attaching and cell-attracting in-situ forming dextran-tyramine conjugates hydrogels for arthroscopic cartilage repair. *Biomaterials*, *33*(11), 3164–3174. https://doi.org/10.1016/j.biomaterials.2012.01.001

Moroni, L., Boland, T., Burdick, J. A., De Maria, C., Derby, B., Forgacs, G., Groll, J., Li, Q., Malda, J., Mironov, V. A., Mota, C., Nakamura, M., Shu, W., Takeuchi, S., Woodfield, T. B. F., Xu, T., Yoo, J. J., & Vozzi, G. (2018). Biofabrication: A Guide to Technology and Terminology. *Trends in Biotechnology*, *36*(4), 384–402. https://doi.org/https://doi.org/10.1016/j.tibtech.2017.10.015

Moulisová, V., Poveda-Reyes, S., Sanmartín-Masiá, E., Quintanilla-Sierra, L., Salmerón-Sánchez, M., & Gallego Ferrer, G. (2017). Hybrid Protein-Glycosaminoglycan Hydrogels Promote Chondrogenic Stem Cell Differentiation. *ACS Omega*, *2*(11), 7609–7620. https://doi.org/10.1021/acsomega.7b01303

Moya, A., Ortega-Ribera, M., Guimerà, X., Sowade, E., Zea, M., Illa, X., Ramon, E., Villa, R., Gracia-Sancho, J., & Gabriel, G. (2018). Online oxygen monitoring using integrated inkjet-printed sensors in a liver-on-a-chip system. *Lab on a Chip*, *18*(14), 2023–2035. https://doi.org/10.1039/c8lc00456k

Murphy, S. V, & Atala, A. (2014). 3D bioprinting of tissues and organs. *Nature Biotechnology*, *32*(8), 773–785. https://doi.org/10.1038/nbt.2958

Nagamoto, Y., Takayama, K., Ohashi, K., Okamoto, R., Sakurai, F., Tachibana, M., Kawabata, K., & Mizuguchi, H. (2016). Transplantation of a human iPSC-derived hepatocyte sheet increases survival in mice with acute liver failure. *Journal of Hepatology*, *64*(5), 1068–1075. https://doi.org/10.1016/j.jhep.2016.01.004

Naghieh, S., & Chen, X. (2021). Printability–A key issue in extrusion-based bioprinting. *Journal of Pharmaceutical Analysis*, *11*(5), 564–579. https://doi.org/https://doi.org/10.1016/j.jpha.2021.02.001

Neuman, M. G., Cohen, L. B., & Nanau, R. M. (2016). Hyaluronic acid as a non-invasive biomarker of liver fibrosis. In *Clinical Biochemistry* (Vol. 49, Issue 3, pp. 302–315). Elsevier Inc. https://doi.org/10.1016/j.clinbiochem.2015.07.019

O′Brien, P. J., Chan, K., & Silber, P. M. (2004). Human and animal hepatocytes in vitro with extrapolation in vivo. *Chemico-Biological Interactions*, *150*(1), 97–114. https://doi.org/10.1016/j.cbi.2004.09.003

O'Brien, P. J., Irwin, W., Diaz, D., Howard-Cofield, E., Krejsa, C. M., Slaughter, M. R., Gao, B., Kaludercic, N., Angeline, A., Bernardi, P., Brain, P., & Hougham, C. (2006). High concordance of drug-induced human hepatotoxicity with in vitro cytotoxicity measured in a novel cell-based model using high content screening. *Archives of Toxicology*, *80*(9), 580–604. https://doi.org/10.1007/s00204-006-0091-3

Ohkura, T., Ohta, K., Nagao, T., Kusumoto, K., Koeda, A., Ueda, T., Jomura, T., Ikeya, T., Ozeki, E., Wada, K., Naitoh, K., Inoue, Y., Takahashi, N., Iwai, H., Arakawa, H., & Ogihara, T. (2014). Evaluation of human hepatocytes

cultured by three-dimensional spheroid systems for drug metabolism. *Drug Metabolism and Pharmacokinetics*, *29*(5), 373–378. https://doi.org/10.2133/dmpk.DMPK-13-RG-105

Oppermann, W., Rose, S., & Rehage, G. (1985). ELASTIC BEHAVIOUR OF HYDROGELS. *British Polymer Journal*, *17*(2), 175–180. https://doi.org/10.1002/pi.4980170216

Panday, R., Monckton, C. P., & Khetani, S. R. (2022). The Role of Liver Zonation in Physiology, Regeneration, and Disease. *Seminars in Liver Disease*, *42*(01), 001–016. https://doi.org/10.1055/s-0041-1742279

Pareja, E., Gómez-Lechón, M. J., & Tolosa, L. (2020). Induced pluripotent stem cells for the treatment of liver diseases: challenges and perspectives from a clinical viewpoint. *Annals of Translational Medicine*, *8*(8), 566–566. https://doi.org/10.21037/atm.2020.02.164

Park, J. Y., Choi, J. C., Shim, J. H., Lee, J. S., Park, H., Kim, S. W., Doh, J., & Cho, D. W. (2014). A comparative study on collagen type i and hyaluronic acid dependent cell behavior for osteochondral tissue bioprinting. *Biofabrication*, *6*(3). https://doi.org/10.1088/1758-5082/6/3/035004

Parsa, S., Gupta, M., Loizeau, F., & Cheung, K. C. (2010). Effects of surfactant and gentle agitation on inkjet dispensing of living cells. *Biofabrication*, *2*(2), 25003. https://doi.org/10.1088/1758-5082/2/2/025003

Paxton, N., Smolan, W., Böck, T., Melchels, F., Groll, J., & Jungst, T. (2017). Proposal to assess printability of bioinks for extrusion-based bioprinting and evaluation of rheological properties governing bioprintability. *Biofabrication*, *9*(4). https://doi.org/10.1088/1758-5090/aa8dd8

Pelechá, M., Villanueva-Bádenas, E., Timor-López, E., Donato, M. T., & Tolosa, L. (2021). Cell Models and Omics Techniques for the Study of Nonalcoholic Fatty Liver Disease: Focusing on Stem Cell-Derived Cell Models. *Antioxidants*, *11*(1), 86. https://doi.org/10.3390/antiox11010086

Peppas, N. A., & Merrill, E. W. (1977). Crosslinked poly(vinyl alcohol) hydrogels as swollen elastic networks. *Journal of Applied Polymer Science*, *21*(7), 1763–1770. https://doi.org/10.1002/app.1977.070210704

Peter Guengerich, F. (2019). Cytochrome P450 research and The Journal of Biological Chemistry. *Journal of Biological Chemistry*, *294*(5), 1671–1680. https://doi.org/10.1074/jbc.TM118.004144

Peters, J. T., Wechsler, M. E., & Peppas, N. A. (2021). Advanced biomedical hydrogels: molecular architecture and its impact on medical applications. *Regenerative Biomaterials*, *8*(6). https://doi.org/10.1093/rb/rbab060

Pimpin, L., Cortez-Pinto, H., Negro, F., Corbould, E., Lazarus, J. V., Webber, L., & Sheron, N. (2018). Burden of liver disease in Europe: Epidemiology and analysis of risk factors to identify prevention policies. *Journal of Hepatology*, *69*(3), 718–735. https://doi.org/10.1016/j.jhep.2018.05.011

Poveda-Reyes, S., Moulisova, V., Sanmartín-Masiá, E., Quintanilla-Sierra, L., Salmerón-Sánchez, M., & Ferrer, G. G. (2016). Gelatin—Hyaluronic Acid Hydrogels with Tuned Stiffness to Counterbalance Cellular Forces and Promote Cell Differentiation. *Macromolecular Bioscience*, 1311–1324. https://doi.org/10.1002/mabi.201500469

Prior, N., Inacio, P., & Huch, M. (2019). Liver organoids: From basic research to therapeutic applications. In *Gut* (Vol. 68, Issue 12, pp. 2228–2237). BMJ Publishing Group. https://doi.org/10.1136/gutjnl-2019-319256

Prodanov, L., Jindal, R., Bale, S. S., Hegde, M., Mccarty, W. J., Golberg, I., Bhushan, A., Yarmush, M. L., & Usta, O. B. (2016). Long-Term Maintenance of a Microfluidic 3D Human Liver Sinusoid. *Biotechnol. Bioeng*, *113*, 241–246. https://doi.org/10.1002/bit.25700/abstract

Puche, J. E., Saiman, Y., & Friedman, S. L. (2013). Hepatic Stellate Cells and Liver Fibrosis. In *Comprehensive Physiology* (Vol. 3, Issue 4, pp. 1473–1492). Wiley. https://doi.org/10.1002/cphy.c120035

Raghuwanshi, V. S., & Garnier, G. (2019). Characterisation of hydrogels: Linking the nano to the microscale. *Advances in Colloid and Interface Science*, *274*, 102044. https://doi.org/10.1016/j.cis.2019.102044

Ramachandran, A., & Jaeschke, H. (2017). Mechanisms of acetaminophen hepatotoxicity and their translation to the human pathophysiology. *Journal of Clinical and Translational Research*, *3*, 157–169. https://doi.org/10.18053/jctres.03.2017s1.002

Ramachandran, P., Dobie, R., Wilson-Kanamori, J. R., Dora, E. F., Henderson, B. E. P., Luu, N. T., Portman, J. R., Matchett, K. P., Brice, M., Marwick, J. A., Taylor, R. S., Efremova, M., Vento-Tormo, R., Carragher, N. O., Kendall, T. J., Fallowfield, J. A., Harrison, E. M., Mole, D. J., Wigmore, S. J., … Henderson, N. C. (2019). Resolving the fibrotic niche of human liver cirrhosis at single-cell level. *Nature*, *575*(7783), 512–518. https://doi.org/10.1038/s41586-019-1631-3

Ramachandran, P., Matchett, K. P., Dobie, R., Wilson-Kanamori, J. R., & Henderson, N. C. (2020). Single-cell technologies in hepatology: new insights into liver biology and disease pathogenesis. *Nature Reviews Gastroenterology & Hepatology*, *17*(8), 457–472. https://doi.org/10.1038/s41575-020-0304-x

Ramiah, P., du Toit, L. C., Choonara, Y. E., Kondiah, P. P. D., & Pillay, V. (2020). Hydrogel-Based Bioinks for 3D Bioprinting in Tissue Regeneration. *Frontiers in Materials*, *7*. https://doi.org/10.3389/fmats.2020.00076

Ranucci, C. S., Kumar, A., Batra, S. P., & Moghe, P. V. (2000). Control of hepatocyte function on collagen foams: Sizing matrix pores toward selective induction of 2-D and 3-D cellular morphogenesis. *Biomaterials*, *21*(8), 783–793. https://doi.org/10.1016/S0142-9612(99)00238-0

Ray, G. (2022). Management of liver diseases: Current perspectives. *World Journal of Gastroenterology*, *28*(40), 5818–5826. https://doi.org/10.3748/wjg.v28.i40.5818

Regehly, M., Garmshausen, Y., Reuter, M., König, N. F., Israel, E., Kelly, D. P., Chou, C.-Y., Koch, K., Asfari, B., & Hecht, S. (2020). Xolography for linear volumetric 3D printing. *Nature*, *588*(7839), 620–624. https://doi.org/10.1038/s41586-020-3029-7

Reid, L. M., Fiorino, A. S., Sigal, S. H., Brill, S., & Holst, P. A. (1992). Extracellular matrix gradients in the space of disse: Relevance to liver biology. *Hepatology*, *15*(6), 1198–1203. https://doi.org/10.1002/hep.1840150635

Reina-Romo, E., Mandal, S., Amorim, P., Bloemen, V., Ferraris, E., & Geris, L. (2021). Towards the Experimentally-Informed In Silico Nozzle Design Optimization for Extrusion-Based Bioprinting of Shear-Thinning Hydrogels. *Frontiers in Bioengineering and Biotechnology*, *9*. https://doi.org/10.3389/fbioe.2021.701778

Ricard-Blum, S. (2011). The Collagen Family. *Cold Spring Harbor Perspectives in Biology*, *3*(1), a004978–a004978. https://doi.org/10.1101/cshperspect.a004978

Richbourg, N. R., & Peppas, N. A. (2020). The swollen polymer network hypothesis: Quantitative models of hydrogel swelling, stiffness, and solute transport. *Progress in Polymer Science*, *105*, 101243. https://doi.org/10.1016/j.progpolymsci.2020.101243

Rizwan, M., Ling, C., Guo, C., Liu, T., Jiang, J., Bear, C. E., Ogawa, S., & Shoichet, M. S. (2022). Viscoelastic Notch Signaling Hydrogel Induces Liver Bile Duct Organoid Growth and Morphogenesis. *Advanced Healthcare Materials*, *11*(23). https://doi.org/10.1002/adhm.202200880

Rodriguez-Fernandez, J., Garcia-Legler, E., Villanueva-Badenas, E., Donato, M. T., Gomez-Ribelles, J. L., Salmeron-Sanchez, M., Gallego-Ferrer, G., & Tolosa, L. (2023). Primary human hepatocytes-laden scaffolds for the treatment of acute liver failure. *Biomaterials Advances*, *153*, 213576. https://doi.org/10.1016/j.bioadv.2023.213576

Ruff, S. M., Manne, A., Cloyd, J. M., Dillhoff, M., Ejaz, A., & Pawlik, T. M. (2023). Current Landscape of Immune Checkpoint Inhibitor Therapy for Hepatocellular Carcinoma. *Current Oncology*, *30*(6), 5863–5875. https://doi.org/10.3390/curroncol30060439

Sakai, S., Ashida, T., Ogino, S., Taya, M., Rose, J. B., Pacelli, S., El Haj, A. J., Dua, H. S., Hopkinson, A., White, L. J., Rose, F. R. A. J., Sakai, S., Hirose, K., Taguchi, K., Ogushi, Y., Kawakami, K., Kurisawa, M., Chung, J. E., Yang, Y. Y., … Uyama, H. (2014). Injectable biodegradable hydrogels composed of hyaluronic acid-tyramine conjugates for drug delivery and tissue engineering. *Journal of Microencapsulation*, *7*(4), 4312–4314. https://doi.org/10.1039/b506989k

Salas-Silva, S., Simoni-Nieves, A., Chávez-Rodríguez, L., Gutiérrez-Ruiz, M. C., Bucio, L., & Quiroz, L. E. G. (2021). Mechanism of cholangiocellular damage and repair during cholestasis. *Annals of Hepatology*, *26*, 100530. https://doi.org/10.1016/j.aohep.2021.100530

Sanchez-Rubio, A., Salmeron-Sanchez, M., & Dalby, M. (2023). *Novel bioinks and bioprinted constructs for tissue engineering* [University of Glasgow]. https://doi.org/10.5525/gla.thesis.83835

Sanmartín-Masiá, E., Poveda-Reyes, S., & Gallego Ferrer, G. (2017). Extracellular matrix–inspired gelatin/hyaluronic acid injectable hydrogels. *International Journal of Polymeric Materials and Polymeric Biomaterials*, *66*(6), 280–288. https://doi.org/10.1080/00914037.2016.1201828

Sanz-García, C., Fernández-Iglesias, A., Gracia-Sancho, J., Arráez-Aybar, L. A., Nevzorova, Y. A., & Cubero, F. J. (2021). The Space of Disse: The Liver Hub in Health and Disease. *Livers*, *1*(1), 3–26. https://doi.org/10.3390/livers1010002

Schmidt, K., Berg, J., Roehrs, V., Kurreck, J., & Al-Zeer, M. A. (2020). 3D-bioprinted HepaRG cultures as a model for testing long term aflatoxin B1 toxicity in vitro. *Toxicology Reports*, *7*, 1578–1587. https://doi.org/10.1016/j.toxrep.2020.11.003

Schulze, R. J., Schott, M. B., Casey, C. A., Tuma, P. L., & McNiven, M. A. (2019). The cell biology of the hepatocyte: A membrane trafficking machine. *Journal of Cell Biology*, *218*(7), 2096–2112. https://doi.org/10.1083/jcb.201903090

Schyschka, L., Sánchez, J. J. M., Wang, Z., Burkhardt, B., Müller-Vieira, U., Zeilinger, K., Bachmann, A., Nadalin, S., Damm, G., & Nussler, A. K. (2013). Hepatic 3D cultures but not 2D cultures preserve specific transporter activity for acetaminophen-induced hepatotoxicity. *Archives of Toxicology*, *87*(8), 1581–1593. https://doi.org/10.1007/s00204-013-1080-y

Senoo, H. (2004). Structure and function of hepatic stellate cells. *Medical Electron Microscopy*, *37*(1), 3–15. https://doi.org/10.1007/s00795-003-0230-3

Serras, A. S., Rodrigues, J. S., Cipriano, M., Rodrigues, A. V., Oliveira, N. G., & Miranda, J. P. (2021). A Critical Perspective on 3D Liver Models for Drug Metabolism and Toxicology Studies. In *Frontiers in Cell and Developmental Biology* (Vol. 9). Frontiers Media S.A. https://doi.org/10.3389/fcell.2021.626805

Shagidulin, M., Onishchenko, N., Sevastianov, V., Krasheninnikov, M., Lyundup, A., Nikolskaya, A., Kryzhanovskaya, A., Voznesenskaia, S., Gorelova, M., Perova, N., Kozlov, I., Venediktov, A., Piavchenko, G., & Gautier, S. (2023). Experimental Correction and Treatment of Chronic Liver Failure Using Implantable Cell-Engineering Constructs of the Auxiliary Liver Based on a Bioactive Heterogeneous Biopolymer Hydrogel. *Gels*, *9*(6), 456. https://doi.org/10.3390/gels9060456

Shen, Y., Tang, H., Huang, X., Hang, R., Zhang, X., Wang, Y., & Yao, X. (2020). DLP printing photocurable chitosan to build bio-constructs for tissue engineering. *Carbohydrate Polymers*, *235*, 115970. https://doi.org/10.1016/j.carbpol.2020.115970

Shu, X. Z., Liu, Y., Luo, Y., Roberts, M. C., & Prestwich, G. D. (2002). Disulfide cross-linked hyaluronan hydrogels. In *Biomacromolecules* (Vol. 3, Issue 6, pp. 1304–1311). https://doi.org/10.1021/bm025603c

Sigaux, N., Pourchet, L., Breton, P., Brosset, S., Louvrier, A., & Marquette, C. A. (2019). 3D Bioprinting:principles, fantasies and prospects. In *Journal of Stomatology, Oral and Maxillofacial Surgery* (Vol. 120, Issue 2, pp. 128–132). Elsevier Masson SAS. https://doi.org/10.1016/j.jormas.2018.12.014

Skardal, A., Devarasetty, M., Kang, H. W., Mead, I., Bishop, C., Shupe, T., Lee, S. J., Jackson, J., Yoo, J., Soker, S., & Atala, A. (2015). A hydrogel bioink toolkit for mimicking native tissue biochemical and mechanical properties in bioprinted tissue constructs. *Acta Biomaterialia*, *25*, 24–34. https://doi.org/10.1016/j.actbio.2015.07.030

Skardal, A., Mack, D., Kapetanovic, E., Atala, A., Jackson, J. D., Yoo, J., & Soker, S. (2012). Bioprinted Amniotic Fluid-Derived Stem Cells Accelerate Healing of Large Skin Wounds. *Stem Cells Translational Medicine*, *1*(11), 792–802. https://doi.org/10.5966/sctm.2012-0088

Skardal, A., Zhang, J., McCoard, L., Xu, X., Oottamasathien, S., & Prestwich, G. D. (2010). Photocrosslinkable hyaluronan-gelatin hydrogels for two-step bioprinting. *Tissue Engineering - Part A*, *16*(8), 2675–2685. https://doi.org/10.1089/ten.tea.2009.0798

Smets, F., Najimi, M., & Sokal, E. M. (2008). Cell transplantation in the treatment of liver diseases. *Pediatric Transplantation*, *12*(1), 6–13. https://doi.org/10.1111/j.1399-3046.2007.00788.x

Smith, C. M., Stone, A. L., Parkhill, R. L., Stewart, R. L., Simpkins, M. W., Kachurin, A. M., Warren, W. L., & Williams, S. K. (2004). Three-Dimensional BioAssembly Tool for Generating Viable Tissue-Engineered Constructs. In *TISSUE ENGINEERING* (Vol. 10, Issue 9).

Soga, T., Baran, R., Suematsu, M., Ueno, Y., Ikeda, S., Sakurakawa, T., Kakazu, Y., Ishikawa, T., Robert, M., Nishioka, T., & Tomita, M. (2006). Differential metabolomics reveals ophthalmic acid as an oxidative stress biomarker indicating hepatic glutathione consumption. *Journal of Biological Chemistry*, *281*(24), 16768–16776. https://doi.org/10.1074/jbc.M601876200

Soldatow, V. Y., LeCluyse, E. L., Griffith, L. G., & Rusyn, I. (2013). In vitro models for liver toxicity testing. *Toxicol. Res.*, *2*(1), 23–39. https://doi.org/10.1039/C2TX20051A

Sørensen, K. K., Simon-Santamaria, J., McCuskey, R. S., & Smedsrød, B. (2015). Liver Sinusoidal Endothelial Cells. In *Comprehensive Physiology*

(Vol. 5, Issue 4, pp. 1751–1774). Wiley. https://doi.org/10.1002/cphy.c140078

Starkey Lewis, P., Campana, L., Aleksieva, N., Cartwright, J. A., Mackinnon, A., O'Duibhir, E., Kendall, T., Vermeren, M., Thomson, A., Gadd, V., Dwyer, B., Aird, R., Man, T. Y., Rossi, A. G., Forrester, L., Park, B. K., & Forbes, S. J. (2020). Alternatively activated macrophages promote resolution of necrosis following acute liver injury. *Journal of Hepatology*, *73*(2), 349–360. https://doi.org/10.1016/j.jhep.2020.02.031

Stevens, K. R., Miller, J. S., Blakely, B. L., Chen, C. S., & Bhatia, S. N. (2015). Degradable hydrogels derived from PEG-diacrylamide for hepatic tissue engineering. *Journal of Biomedical Materials Research Part A*, *103*(10), 3331–3338. https://doi.org/10.1002/jbm.a.35478

Ströbel, S., Kostadinova, R., Fiaschetti-Egli, K., Rupp, J., Bieri, M., Pawlowska, A., Busler, D., Hofstetter, T., Sanchez, K., Grepper, S., & Thoma, E. (2021). A 3D primary human cell-based in vitro model of non-alcoholic steatohepatitis for efficacy testing of clinical drug candidates. *Scientific Reports*, *11*(1), 22765. https://doi.org/10.1038/s41598-021-01951-7

Subramani, R., Izquierdo-Alvarez, A., Bhattacharya, P., Meerts, M., Moldenaers, P., Ramon, H., & Van Oosterwyck, H. (2020). The Influence of Swelling on Elastic Properties of Polyacrylamide Hydrogels. *Frontiers in Materials*, *7*. https://doi.org/10.3389/fmats.2020.00212

Sun, L., & Hui, L. (2020). Progress in human liver organoids. *Journal of Molecular Cell Biology*, *12*(8), 607–617. https://doi.org/10.1093/jmcb/mjaa013

Sun, L., Wang, Y., Cen, J., Ma, X., Cui, L., Qiu, Z., Zhang, Z., Li, H., Yang, R. Z., Wang, C., Chen, X., Wang, L., Ye, Y., Zhang, H., Pan, G., Kang, J. S., Ji, Y., Zheng, Y. W., Zheng, S., & Hui, L. (2019). Modelling liver cancer initiation with organoids derived from directly reprogrammed human hepatocytes. *Nature Cell Biology*, *21*(8), 1015–1026. https://doi.org/10.1038/s41556-019-0359-5

Sun, L., Yang, H., Wang, Y., Zhang, X., Jin, B., Xie, F., Jin, Y., Pang, Y., Zhao, H., Lu, X., Sang, X., Zhang, H., Lin, F., Sun, W., Huang, P., & Mao, Y. (2020). Application of a 3D Bioprinted Hepatocellular Carcinoma Cell Model in Antitumor Drug Research . In *Frontiers in Oncology* (Vol. 10).

Tai, B. C. U., Du, C., Gao, S., Wan, A. C. A., & Ying, J. Y. (2010). The use of a polyelectrolyte fibrous scaffold to deliver differentiated hMSCs to the liver.

Biomaterials, *31*(1), 48–57. https://doi.org/10.1016/j.biomaterials.2009.09.022

Tai, Y., Gao, J.-H., Zhao, C., Tong, H., Zheng, S.-P., Huang, Z.-Y., Liu, R., Tang, C.-W., & Li, J. (2018). SK-Hep1: not hepatocellular carcinoma cells but a cell model for liver sinusoidal endothelial cells. In *Int J Clin Exp Pathol* (Vol. 11, Issue 5). www.ijcep.com/

Takayama, K., Morisaki, Y., Kuno, S., Nagamoto, Y., Harada, K., Furukawa, N., Ohtaka, M., Nishimura, K., Imagawa, K., Sakurai, F., Tachibana, M., Sumazaki, R., Noguchi, E., Nakanishi, M., Hirata, K., Kawabata, K., & Mizuguchi, H. (2014). Prediction of interindividual differences in hepatic functions and drug sensitivity by using human iPS-derived hepatocytes. *Proceedings of the National Academy of Sciences*, *111*(47), 16772–16777. https://doi.org/10.1073/pnas.1413481111

Takebe, T., Sekine, K., Enomura, M., Koike, H., Kimura, M., Ogaeri, T., Zhang, R.-R., Ueno, Y., Zheng, Y.-W., Koike, N., Aoyama, S., Adachi, Y., & Taniguchi, H. (2013). Vascularized and functional human liver from an iPSC-derived organ bud transplant. *Nature*, *499*(7459), 481–484. https://doi.org/10.1038/nature12271

Tan, H., & Marra, K. G. (2010). Injectable, Biodegradable Hydrogels for Tissue Engineering Applications. *Materials*, *3*(3), 1746–1767. https://doi.org/10.3390/ma3031746

Tang, D., Tare, R. S., Yang, L.-Y., Williams, D. F., Ou, K.-L., & Oreffo, R. O. C. (2016). Biofabrication of bone tissue: approaches, challenges and translation for bone regeneration. *Biomaterials*, *83*, 363–382. https://doi.org/https://doi.org/10.1016/j.biomaterials.2016.01.024

Taymour, R., Chicaiza-Cabezas, N. A., Gelinsky, M., & Lode, A. (2022). Core-shell bioprinting of vascularized in vitro liver sinusoid models. *Biofabrication*, *14*(4). https://doi.org/10.1088/1758-5090/ac9019

Taymour, R., Kilian, D., Ahlfeld, T., Gelinsky, M., & Lode, A. (2021). 3D bioprinting of hepatocytes: core–shell structured co-cultures with fibroblasts for enhanced functionality. *Scientific Reports*, *11*(1). https://doi.org/10.1038/s41598-021-84384-6

Thanapirom, K., Caon, E., Papatheodoridi, M., Frenguelli, L., Al-Akkad, W., Zhenzhen, Z., Vilia, M. G., Pinzani, M., Mazza, G., & Rombouts, K. (2021). Optimization and Validation of a Novel Three-Dimensional Co-Culture System in Decellularized Human Liver Scaffold for the Study of Liver

Fibrosis and Cancer. *Cancers*, *13*(19), 4936. https://doi.org/10.3390/cancers13194936

Tolosa, L., Caron, J., Hannoun, Z., Antoni, M., López, S., Burks, D., Castell, J. V., Weber, A., Gomez-Lechon, M.-J., & Dubart-Kupperschmitt, A. (2015). Transplantation of hESC-derived hepatocytes protects mice from liver injury. *Stem Cell Research & Therapy*, *6*(1), 246. https://doi.org/10.1186/s13287-015-0227-6

Tolosa, L., Pareja, E., & Gómez-Lechón, M. J. (2016). Clinical Application of Pluripotent Stem Cells: An Alternative Cell-Based Therapy for Treating Liver Diseases? *Transplantation*, *100*(12), 2548–2557. https://doi.org/10.1097/TP.0000000000001426

Tolosa, L., Pareja-Ibars, E., Donato, M. T., Cortés, M., López, S., Jiménez, N., Mir, J., Castell, J. V., & Gómez-Lechón, M. J. (2014). Neonatal Livers: A Source for the Isolation of Good-Performing Hepatocytes for Cell Transplantation. *Cell Transplantation*, *23*(10), 1229–1242. https://doi.org/10.3727/096368913X669743

Tolosa, L., Pareja-Ibars, E., Teresa Donato, M., Cortés, M., López, S., Jiménez, N., Mir, J., Castell, J. V., & Gómez-Lechón, M. J. (2014). Neonatal livers: A source for the isolation of good-performing hepatocytes for cell transplantation. *Cell Transplantation*, *23*(10), 1229–1242. https://doi.org/10.3727/096368913X669743

Tong, X., Zhao, F., Ren, Y., Zhang, Y., Cui, Y., & Wang, Q. (2018). Injectable hydrogels based on glycyrrhizin, alginate, and calcium for three-dimensional cell culture in liver tissue engineering. *Journal of Biomedical Materials Research Part A*, *106*(12), 3292–3302. https://doi.org/10.1002/jbm.a.36528

Tostões, R. M., Leite, S. B., Serra, M., Jensen, J., Björquist, P., Carrondo, M. J. T., Brito, C., & Alves, P. M. (2012). Human liver cell spheroids in extended perfusion bioreactor culture for repeated-dose drug testing. *Hepatology*, *55*(4), 1227–1236. https://doi.org/10.1002/hep.24760

Trefts, E., Gannon, M., & Wasserman, D. H. (2017). The liver. *Current Biology*, *27*(21), R1147–R1151. https://doi.org/10.1016/j.cub.2017.09.019

Trujillo, S., Dobre, O., Dalby, M. J., & Salmeron-Sanchez, M. (2019). Mechanotransduction and Growth Factor Signaling in Hydrogel-Based Microenvironments. In *Reference Module in Biomedical Sciences* (Vols. 1–

3, pp. V1-87-V1-101). Elsevier. https://doi.org/10.1016/B978-0-12-801238-3.11141-9

Tsuchida, T., & Friedman, S. L. (2017). Mechanisms of hepatic stellate cell activation. *Nature Reviews Gastroenterology & Hepatology*, *14*(7), 397–411. https://doi.org/10.1038/nrgastro.2017.38

Turner, R. A., Wauthier, E., Lozoya, O., McClelland, R., Bowsher, J. E., Barbier, C., Prestwich, G., Hsu, E., Gerber, D. A., & Reid, L. M. (2013). Successful transplantation of human hepatic stem cells with restricted localization to liver using hyaluronan grafts. *Hepatology*, *57*(2), 775–784. https://doi.org/10.1002/hep.26065

Unagolla, J. M., & Jayasuriya, A. C. (2020). Hydrogel-based 3D bioprinting: A comprehensive review on cell-laden hydrogels, bioink formulations, and future perspectives. *Applied Materials Today*, *18*, 100479. https://doi.org/10.1016/j.apmt.2019.100479

Underhill, G. H., Chen, A. A., Albrecht, D. R., & Bhatia, S. N. (2007). Assessment of hepatocellular function within PEG hydrogels. *Biomaterials*, *28*(2), 256–270. https://doi.org/10.1016/j.biomaterials.2006.08.043

Vaca-González, J. J., Clara-Trujillo, S., Guillot-Ferriols, M., Ródenas-Rochina, J., Sanchis, M. J., Ribelles, J. L. G., Garzón-Alvarado, D. A., & Ferrer, G. G. (2020). Effect of electrical stimulation on chondrogenic differentiation of mesenchymal stem cells cultured in hyaluronic acid – Gelatin injectable hydrogels. *Bioelectrochemistry*, *134*, 107536. https://doi.org/10.1016/j.bioelechem.2020.107536

Vanderhooft, J. L., Alcoutlabi, M., Magda, J. J., & Prestwich, G. D. (2009). Rheological properties of cross-linked hyaluronan-gelatin hydrogels for tissue engineering. *Macromolecular Bioscience*, *9*(1), 20–28. https://doi.org/10.1002/mabi.200800141

Vishwakarma, S. K., Bardia, A., Lakkireddy, C., Raju, N., Paspala, S. A. B., Habeeb, Md. A., & Khan, A. A. (2019). Intraperitoneal transplantation of bioengineered humanized liver grafts supports failing liver in acute condition. *Materials Science and Engineering: C*, *98*, 861–873. https://doi.org/10.1016/j.msec.2019.01.045

Wang, Q., Liu, J., Yin, W., Wang, A., Zheng, J., Wang, Y., & Dong, J. (2023). Microscale tissue engineering of liver lobule models: advancements and applications. In *Frontiers in Bioengineering and Biotechnology* (Vol. 11). Frontiers Media SA. https://doi.org/10.3389/fbioe.2023.1303053

Webb, B., & Doyle, B. J. (2017). Parameter optimization for 3D bioprinting of hydrogels. *Bioprinting*, *8*, 8–12. https://doi.org/https://doi.org/10.1016/j.bprint.2017.09.001

Westerink, W. M. A., & Schoonen, W. G. E. J. (2007). Phase II enzyme levels in HepG2 cells and cryopreserved primary human hepatocytes and their induction in HepG2 cells. *Toxicology in Vitro*, *21*(8), 1592–1602. https://doi.org/10.1016/j.tiv.2007.06.017

Willemse, J., van Tienderen, G., van Hengel, E., Schurink, I., van der Ven, D., Kan, Y., de Ruiter, P., Rosmark, O., Westergren-Thorsson G, G., Schneeberger, K., van der Eerden, B., Roest, H., Spee, B., van der Laan, L., de Jonge, J., & Verstegen, M. (2022). Hydrogels derived from decellularized liver tissue support the growth and differentiation of cholangiocyte organoids. *Biomaterials*, *284*, 121473. https://doi.org/10.1016/j.biomaterials.2022.121473

Williams, C. G., Malik, A. N., Kim, T. K., Manson, P. N., & Elisseeff, J. H. (2005). Variable cytocompatibility of six cell lines with photoinitiators used for polymerizing hydrogels and cell encapsulation. *Biomaterials*, *26*(11), 1211–1218. https://doi.org/10.1016/j.biomaterials.2004.04.024

Wiśniewski, J. R., Vildhede, A., Norén, A., & Artursson, P. (2016). In-depth quantitative analysis and comparison of the human hepatocyte and hepatoma cell line HepG2 proteomes. *Journal of Proteomics*, *136*, 234–247. https://doi.org/10.1016/j.jprot.2016.01.016

Wu, W., Deconinck, A., & Lewis, J. A. (2011). Omnidirectional printing of 3D microvascular networks. *Advanced Materials*, *23*(24). https://doi.org/10.1002/adma.201004625

Xiang, Y., Miller, K., Guan, J., Kiratitanaporn, W., Tang, M., & Chen, S. (2022). 3D bioprinting of complex tissues in vitro: state-of-the-art and future perspectives. In *Archives of Toxicology* (Vol. 96, Issue 3, pp. 691–710). Springer Science and Business Media Deutschland GmbH. https://doi.org/10.1007/s00204-021-03212-y

Xie, F., Sun, L., Pang, Y., Xu, G., Jin, B., Xu, H., Lu, X., Xu, Y., Du, S., Wang, Y., Feng, S., Sang, X., Zhong, S., Wang, X., Sun, W., Zhao, H., Zhang, H., Yang, H., Huang, P., & Mao, Y. (2021). Three-dimensional bio-printing of primary human hepatocellular carcinoma for personalized medicine. *Biomaterials*, *265*, 120416. https://doi.org/10.1016/j.biomaterials.2020.120416

Xie, M., Su, J., Zhou, S., Li, J., & Zhang, K. (2023). Application of Hydrogels as Three-Dimensional Bioprinting Ink for Tissue Engineering. *Gels*, *9*(2), 88. https://doi.org/10.3390/gels9020088

Xing, Q., Yates, K., Vogt, C., Qian, Z., Frost, M. C., & Zhao, F. (2014). Increasing mechanical strength of gelatin hydrogels by divalent metal ion removal. *Scientific Reports*, *4*. https://doi.org/10.1038/srep04706

Xu, K., Lee, F., Gao, S. J., Chung, J. E., Yano, H., & Kurisawa, M. (2013). Injectable hyaluronic acid-tyramine hydrogels incorporating interferon-α2a for liver cancer therapy. *Journal of Controlled Release*, *166*(3), 203–210. https://doi.org/10.1016/j.jconrel.2013.01.008

Yada, T., Koide, N., & Kimata, K. (2003). Functions of Proteoglycan/Glycosaminoglycan in Liver. In *Extracellular Matrix and the Liver* (pp. 55–74). Elsevier. https://doi.org/10.1016/B978-012525251-5/50005-1

Ye, N., Qin, J., Liu, X., Shi, W., & Lin, B. (2007). Characterizing doxorubicin-induced apoptosis in HepG2 cells using an integrated microfluidic device. *Electrophoresis*, *28*(7), 1146–1153. https://doi.org/10.1002/elps.200600450

Ye, S., Boeter, J. W. B., Penning, L. C., Spee, B., & Schneeberger, K. (2019). Hydrogels for liver tissue engineering. In *Bioengineering* (Vol. 6, Issue 3). MDPI AG. https://doi.org/10.3390/bioengineering6030059

Yeh, W. C., Li, P. C., Jeng, Y. M., Hsu, H. C., Kuo, P. L., Li, M. L., Yang, P. M., & Po, H. L. (2002). Elastic modulus measurements of human liver and correlation with pathology. *Ultrasound in Medicine and Biology*, *28*(4), 467–474. https://doi.org/10.1016/S0301-5629(02)00489-1

Yeon, J. H., Na, D., & Park, J. K. (2010). Hepatotoxicity assay using human hepatocytes trapped in microholes of a microfluidic device. *Electrophoresis*, *31*(18), 3167–3174. https://doi.org/10.1002/elps.201000122

Yuan, J., Li, X., & Yu, S. (2023). Cancer organoid co-culture model system: Novel approach to guide precision medicine. *Frontiers in Immunology*, *13*. https://doi.org/10.3389/fimmu.2022.1061388

Zandrini, T., Florczak, S., Levato, R., & Ovsianikov, A. (2023). Breaking the resolution limits of 3D bioprinting: future opportunities and present challenges. In *Trends in Biotechnology* (Vol. 41, Issue 5, pp. 604–614). Elsevier Ltd. https://doi.org/10.1016/j.tibtech.2022.10.009

Zhang, L.-K., Wang, H., Yang, R., Liu, M., Ban, Q., Chen, W., Zhao, M., You, R., Jin, Y., & Guan, Y.-Q. (2019). Bone marrow stem cells combined with polycaprolactone-polylactic acid-polypropylene amine scaffolds for the treatment of acute liver failure. *Chemical Engineering Journal*, *360*, 1564–1576. https://doi.org/10.1016/j.cej.2018.10.230

Zhang, M., Desai, T., & Ferrari, M. (1998). Proteins and cells on PEG immobilized silicon surfaces. In *Biomaterials* (Vol. 19).

Zhang, W., Du, A., Liu, S., Lv, M., & Chen, S. (2021). Research progress in decellularized extracellular matrix-derived hydrogels. *Regenerative Therapy*, *18*, 88–96. https://doi.org/10.1016/j.reth.2021.04.002

Zhang, Y., Chen, H., Zhang, T., Zan, Y., Ni, T., Cao, Y., Wang, J., Liu, M., & Pei, R. (2019). Injectable hydrogels from enzyme-catalyzed crosslinking as BMSCs-laden scaffold for bone repair and regeneration. *Materials Science and Engineering: C*, *96*(December 2018), 841–849. https://doi.org/10.1016/j.msec.2018.12.014

Zhang, Y., Wang, Q. S., Yan, K., Qi, Y., Wang, G. F., & Cui, Y. L. (2016). Preparation, characterization, and evaluation of genipin crosslinked chitosan/gelatin three-dimensional scaffolds for liver tissue engineering applications. *Journal of Biomedical Materials Research - Part A*, *104*(8), 1863–1870. https://doi.org/10.1002/jbm.a.35717

Zhao, Y., Xu, B., Liang, W., Ding, Y., Li, J., Zhang, Y., Xu, F., Zhou, H., & Xu, Y. (2019). Multisite Injection of Bioengineered Hepatic Units from Collagen Hydrogel and Neonatal Liver Cells in Parenchyma Improves Liver Cirrhosis. *Tissue Engineering Part A*, *25*(15–16), 1167–1174. https://doi.org/10.1089/ten.tea.2018.0107

Zhong, C., Xie, H.-Y., Zhou, L., Xu, X., & Zheng, S.-S. (2016). Human hepatocytes loaded in 3D bioprinting generate mini-liver. *Hepatobiliary & Pancreatic Diseases International*, *15*(5), 512–518. https://doi.org/10.1016/S1499-3872(16)60119-4

Zigmond, E., Samia-Grinberg, S., Pasmanik-Chor, M., Brazowski, E., Shibolet, O., Halpern, Z., & Varol, C. (2014). Infiltrating Monocyte-Derived Macrophages and Resident Kupffer Cells Display Different Ontogeny and Functions in Acute Liver Injury. *The Journal of Immunology*, *193*(1), 344–353. https://doi.org/10.4049/jimmunol.1400574